POL-VIET
2019

full papers

POL-VIET
2019

full papers

Honorary Committee:

Vu Nang Dzung – H. E. Ambassador of Vietnam (Ambassador Extraordinary and Plenipotentiary)
Wojciech Gerwel – H. E. Ambassador of Poland (Ambassador Extraordinary and Plenipotentiary)
Prof. Le Hai An – Deputy Minister in the Ministry of Education and Training, Hanoi, Vietnam
Prof. Trần Thanh Hải– H. M. Rector of Hanoi University of Mining and Geology, Hanoi, Vietnam
Prof. Cao Việt Hiếu– H. M. Rector of Binh Duong University, Binh Duong, Vietnam
Prof. Tadeusz Słomka – H. M. Rector of AGH University of Science and Technology, Krakow, Poland
Prof. Jerzy Lis – Vice-Rector for Cooperation of AGH University of Science and Technology, Krakow, Poland
Prof. Andrzej R. Pach – Vice-Rector for Science of AGH University of Science and Technology, Krakow, Poland
Prof. Chau Van Minh – President of Vietnam Academy of Science and Technology, Hanoi, Vietnam
Józef Siwiec – President of Zakłady Magnezytowe "ROPCZYCE" S.A., Ropczyce, Poland
Henryk Stabla – President of „CARBOAUTOMATYKA" S.A., Tychy, Poland
Le Minh Chuan – President of Vinacomin, Hanoi, Vietnam
M.B.A. Pham Dang Phu – Headmaster, Vinacomin Buissnes School, Hanoi, Vietnam
Assoc. Prof. Du Thi Xuan Thao – Hanoi University of Mining and Geology, Hanoi, Vietnam

Scientific Committee:

Prof. Jadwiga Jarzyna – Chairman of the Committee, AGH UST
Prof. Marek Cała – Dean of the Faculty of Mining and Geoengineering, AGH UST
Prof. Jacek Matyszkiewicz – Dean of the Faculty of Geology, Geophysics and Environmental Protection, AGH UST
Prof. Stanisław Gruszczyński – Dean of the Faculty of Mining Surveying and Environmental Engineering, AGH UST
Prof. Włodzimierz Mozgawa – Dean of the Faculty of Materials Science and Ceramics, AGH UST
Prof. Rafał Wiśniowski – Dean of the Faculty of Drilling, Oil and Gas, AGH UST
Prof. Wojciech Suwała – Dean of the Faculty of Energy and Fuels, AGH UST
Assoc. Prof. Piotr Łebkowski – Dean of the Faculty of Management, AGH UST
Assoc. Prof. Barbara Gąciarz – Dean of the Faculty of Humanities, AGH UST
Assoc. Prof. Nguyen Quang Minh – Hanoi University of Mining and Geology, Hanoi, Vietnam
Prof. Nguyen van Giang – Vietnam Academy of Science and Technology, Hanoi, Vietnam

Organisational Committee:

Assoc. Prof. Marek Borowski – Chairman of the Committee, Faculty of Mining and Geoengineering, AGH UST
M. Sc. Marta Foryś – Vice-Chairman of the Committee, Department of International Relations, AGH UST
Assoc. Prof. Tomasz Lipecki – Vice - Dean of the Faculty of Mining Surveying and Environmental Engineering, AGH UST
M. Sc. Ho Chi Hung – Vietnam-Poland Friendship Associations, Hanoi, Vietnam
Assoc. Prof. Nguyen Thi Hoai Nga – Hanoi University of Mining and Geology, Hanoi, Vietnam
Dr. Do Ngoc Anh – Hanoi University of Mining and Geology, Hanoi, Vietnam
Dr Michał Karch - Faculty of Mining and Geoengineering, AGH UST
MA Paweł Świerk – Department of International Relations, AGH UST
M. Sc. Paweł Kućmierz – Rector's Office, AGH UST
PhD Sylwia Cygan-Korecka – Department of International Relations, AGH UST
MA Aleksandra Perkins-Oleszkowicz – Department of International Relations AGH UST
M. Sc. Mateusz Jabłoński – Faculty of Mining Surveying and Environmental Engineering, AGH UST

POL-VIET 2019

Scientific-research cooperation
between Poland and Vietnam

Book of Full Papers. Vol 1, Ed 1. Kraków, 2019

ISBN: 978-83-943772-4-3

prof. Jadwiga Jarzyna – opieka merytoryczna | organizator

Wydanie specjalne 1, Kraków 2019

redaktor wydania | Marcin Tora
redaktor techniczny | Julia Okręglicka

układ typograficzny | Julia Okręglicka
projekt | NWH

kontakt | marcin.tora@nwh.pl

AGH

Table of content

MINING

GEOLOGY GEOPHYSICS

GEODESY AND MINING SURVEYING

MISCELLANEOUS

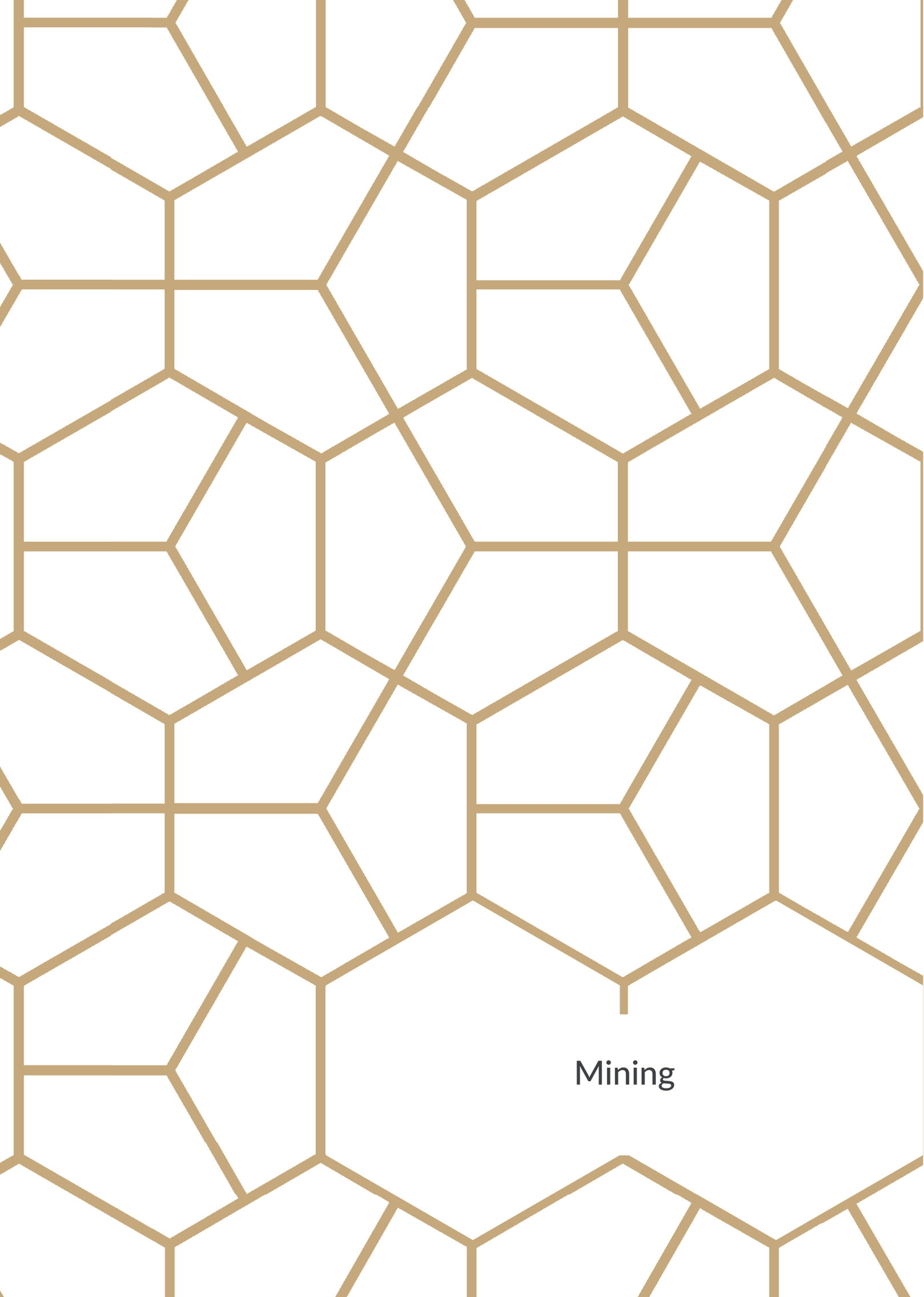
Mining

Determination of methane content at Maokhe coal mine from curent mining to -450 level in Vietnam

VanThinh NGUYEN[1,*], CaoKhai NGUYEN[1], VanQuang NGUYEN[1], CaoKhai NGUYEN[1] and XuanHa TRAN[1]

[1] HUMG Hanoi University of Mining and Geology, Faculty of Mining, Hanoi, Vietnam

Abstract. Methane gas is one of the most serious dangers of underground coal mining as its buildup can lead to methane gas explosion. In QuangNinh province- Vietnam, several coal mines such as TrangKhe II-III coal mine, Khe Cham coal mine, especially MaoKhe mine that have high methane content. At the MaoKhe coal mine,experimental data showed thatthe concentration of methane in coal seams at different depths were not similar.In order to ensure safety, this report has been undertaken to determine a pattern of changing methane contents of coal seams at different exploitation depths in MaoKhe underground coal mine.

1. Introduction to Maokhe underground coal mine

Maokhe underground coal mine is located in DongTrieu town, Quang Ninh province, Vietnam

+ The North, it borders on TrungLuong commune
+ The East, it borders on PhamHongThai commune
+ The South, it borders on 18A road
+ The West, it borders on KimSon commune

Geographical coordinates of Quang Hanh coal mine:

From $106^0 33' 44'' \div 106^0 30' 27''$ North latitude

From $21^0 02' 33'' \div 21^0 06' 15''$ East longitude

The expected output of MaoKhe underground coal mine in 2019 is 1 600 000 tons/year.

At the moment, Maokhe underground coal mine is mining at level -250 and this mine is digging tunnel vertical tilt from level +56 to level -450.

It is therefore necessary to determine the methane content of the coal seams from level -150 to level -450 of MaoKhe underground coal mine.

2. Coal sampling and methane gas analysis sequense

Take the coal sample from boreholes drilled into the coal seams at a depth of 4.5 m and put into steel containers, with tightly covered lid.

Samples of coal are fed into a vibrating shaker inMine safety center- Vinacomin's laboratory to crush the sample by the impact of steel balls. Then introduced into the

* Corresponding author: nguyenthinhtkv@gmail.com

vacuum gas separation system to separate the gas and determine the volume of gas (Fig 1). The extracted gas composition was analyzed by VARIAN gas chromatography. Analysis results from the VARIAN machine will determine the volume of methane gas from each sample of coal (Analysis results are presented in Section 3).

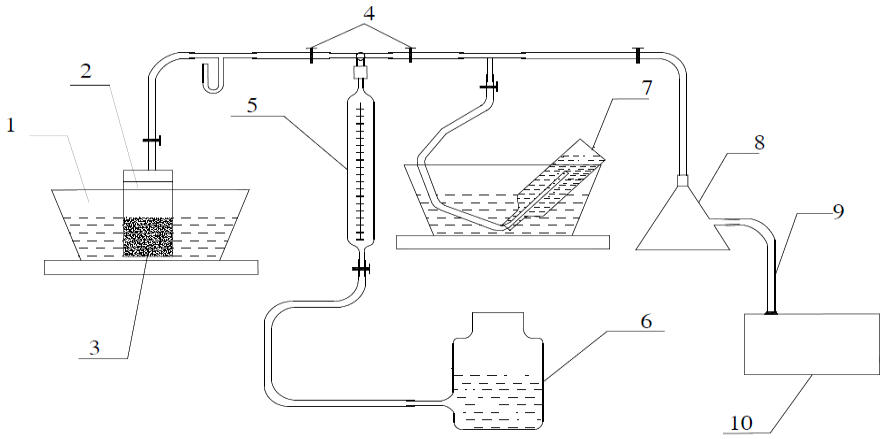

Fig.1. Gas separation diagram by vacuum heat
1.Hot water bottle; 2.Coal sample container; 3.Electric stove; 4.Regulating valve;5.Piet measured the volume; 6.Pressure vessel; 7. Bottle containing specimen separation gas; 8.Intermediate gas cylinders; 9. Tube; 10. Vacuum machine

From the results of the analysis, establish a relationship between the trend of methane density and the depth of the coal seam by using Excel software to construct methane gas prediction graph. Forecast results are presented in Section 4.

3. Results of analysis of methane content in Maokhe underground coal mine

The results of the analysis are shown in table 1 to table 4 with the corresponding coal seams of Maokhe underground coal mine.

Table1.Analysis results CH_4 at $N^0$1CB and $N^0$5 coal seam

$N^0$1CB coal seam			$N^0$5 coal seam		
TT	Depths	CH_4 density, m^3/T_{KC}	TT	Depths	CH_4 density, m^3/T_{KC}
1	50	0.01787	1	-15	0.253
2	-25	0.311	2	-59	0.467
3	-70	0.32033	3	-80	0.78
4	-120	0.462	4	-100	0.825
5	-150	0.634	5	-150	1.05

Table2.Analysis results CH_4 at $N^0$6 and $N^0$7 coal seam

$N^0$6 coal seam			$N^0$7 coal seam		
TT	Depths	CH_4 density, m^3/T_{KC}	TT	Depths	CH_4 density, m^3/T_{KC}

1	30	0.299	1	-25	0.366
2	-25	0.399	2	-50	0.938
3	-60	0.422	3	-80	1.01266
4	-80	0.456	4	-120	1.342
5	-100	0.672	5	-150	1.5785
6	-150	0.9582			

Table3.Analysis results CH_4 at $N^0$8 and $N^0$9 coal seam

$N^0$8 coal seam			$N^0$9 coal seam		
TT	Depths	CH_4 density, m^3/T_{KC}	TT	Depths	CH_4 density, m^3/T_{KC}
1	-25	0.367	1	30	0.356
2	-50	0.52639	2	-25	0.698
3	-80	1.418	3	-57	1.389
4	-135	1.83364	4	-80	2.26722
5	-150	1.988	5	-120	3.59497
			6	-150	4.217

Table4.Analysis results CH_4 at $N^0$9b and $N^0$10 coal seam

$N^0$9b coal seam			$N^0$10 coal seam		
TT	Depths	CH_4 density, m^3/T_{KC}	TT	Depths	CH_4 density, m^3/T_{KC}
1	-25	0.1479	1	70	0.21066
2	-58	0.4141	2	32	0.289
3	-68	0.8571	3	-25	0.375
4	-80	1.423	4	-38	0.661
5	-105	1.635	5	-80	0.936
6	-150	3.477	6	-95	1.029
			7	-150	1.217

4. Results of gas density forecast methane as mine continue to exploit deeper

From the methane content figures in tables 1 to tables 4, We use Excel software to graph the gas variability at different levels of coal seams.

The results of the analysis are shown in table 5 to table 8, and Fig 2 to Figure 9 with the corresponding coal seams

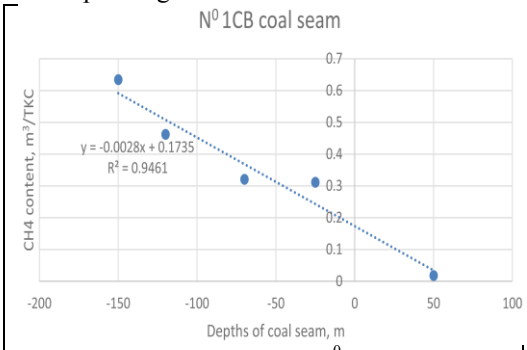

Fig.2. Forecast chart CH_4 at $N^0$1CB coal seam

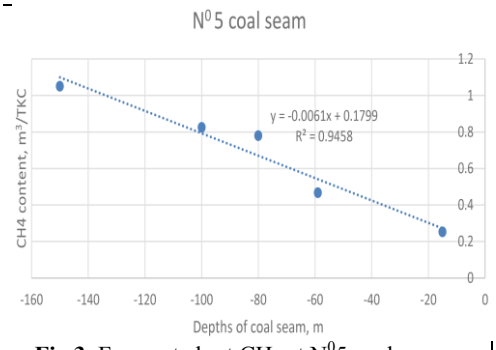

Fig.3. Forecast chart CH_4 at $N^0$5 coal seam

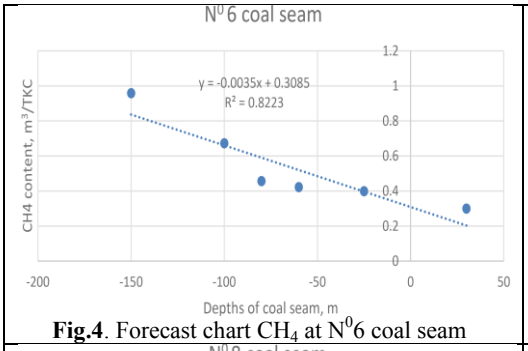

Fig.4. Forecast chart CH_4 at $N^0$6 coal seam

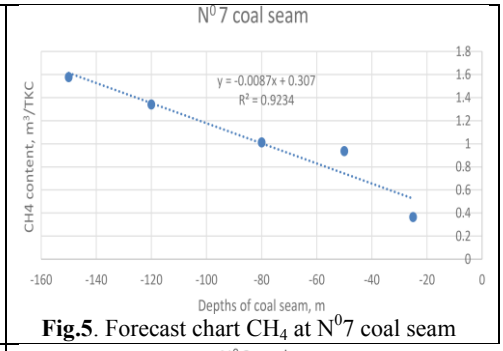

Fig.5. Forecast chart CH_4 at $N^0$7 coal seam

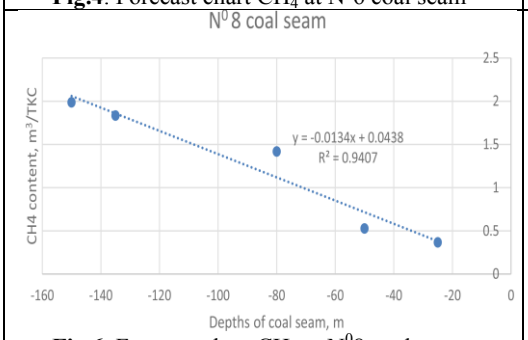

Fig.6. Forecast chart CH_4 at $N^0$8 coal seam

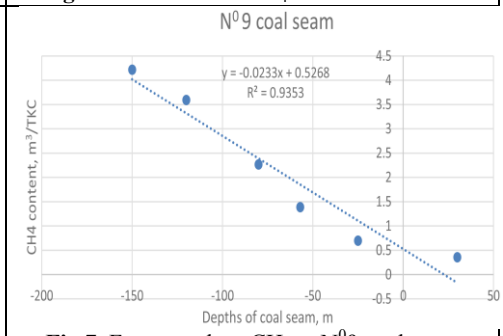

Fig.7. Forecast chart CH_4 at $N^0$9 coal seam

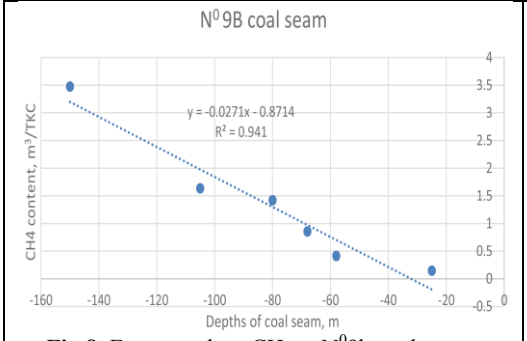

Fig.8. Forecast chart CH_4 at $N^0$9b coal seam

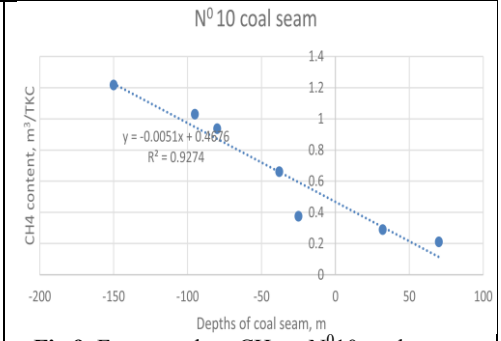

Fig.9. Forecast chart CH_4 at $N^0$10 coal seam

Table 5. Forecast results CH_4 at $N^0$1CB and $N^0$5 coal seam

$N^0$1CB coal seam			$N^0$5 coal seam		
TT	Depths	CH_4 density, m^3/T_{KC}	TT	Depths	CH_4 density, m^3/T_{KC}
1	-200	0.773	1	-200	1.379
2	-250	0.923	2	-250	1.679
3	-300	1.073	3	-300	1.979
4	-350	1.223	4	-350	2.279
5	-400	1.373	5	-400	2.579
6	-450	1.523	6	-450	2.879

Table 6. Forecast results CH_4 at $N^0$6 and $N^0$7 coal seam

$N^0$6 coal seam			$N^0$7 coal seam		
TT	Depths	CH_4 density, m^3/T_{KC}	TT	Depths	CH_4 density, m^3/T_{KC}
1	-200	1.008	1	-200	1.907

2	-250	1.183	2	-250	2.307
3	-300	1.358	3	-300	2.707
4	-350	1.533	4	-350	3.107
5	-400	1.708	5	-400	3.507
6	-450	1.883	6	-450	3.907

Table 7. Forecast results CH_4 at $N^0$8 and $N^0$9 coal seam

$N^0$8 coal seam			$N^0$9 coal seam		
TT	Depths	CH_4 density, m^3/T_{KC}	TT	Depths	CH_4 density, m^3/T_{KC}
1	-200	2.643	1	-200	5.126
2	-250	3.293	2	-250	6.276
3	-300	3.943	3	-300	7.426
4	-350	4.593	4	-350	8.576
5	-400	5.243	5	-400	9.726
6	-450	5.893	6	-450	10.876

Table 8. Forecast results CH_4 at $N^0$9b and $N^0$10 coal seam

$N^0$9b coal seam			$N^0$10 coal seam		
TT	Depths	CH_4 density, m^3/T_{KC}	TT	Depths	CH_4 density, m^3/T_{KC}
1	-200	4.477	1	-200	1.467
2	-250	5.477	2	-250	1.717
3	-300	6.477	3	-300	1.967
4	-350	7.477	4	-350	2.217
5	-400	8.477	5	-400	2.467
6	-450	9.477	6	-450	2.717

4 Conclusion

From the results of the analysis and forecast results from table 1 to tables 8 and figures 2 to figures 9 show the degree of methane storage in the coal seams of the mines with great variation. And the greater the depth, the higher the gas density. Specific for each seam as follows:

- For $N^0$1CB coal seam: From depths level +50 to depths level -450 the density of methane contained in the coal seam is determined and predicted from 0.01787 m^3/T_{KC} to 1.523m^3/T_{KC} (This coal seam is ranked I according to QCVN / 03-BCT / 2011, Vietnam) [4] .

- For $N^0$5 coal seam: From depths level -15 to depths level -350 the density of methane contained in the coal seam is determined and forecasted from 0.0731m^3/T_{KC} to 2.279m^3/T_{KC} (This coal seam is ranked I according to QCVN / 03-BCT / 2011, Vietnam). At depths below level -390 to level -450 the methane content forecasted from 2.5 m^3/T_{KC} to 2.879m^3/T_{KC} (This coal seam is ranked II according to QCVN / 03-BCT / 2011, Vietnam) [4]

- For $N^0$6 coal seam: From depths level 30 to depths level -450 the density of methane contained in the coal seam is determined and forecasted from 0.299m^3/T_{KC} to 1.883m^3/T_{KC} (This coal seam is ranked I according to QCVN / 03-BCT / 2011, Vietnam) [4]

- For $N^0$7 coal seam: From depths level -25 to depths level -250 the density of methane contained in the coal seam is determined and forecasted from 0.366m^3/T_{KC} to 2.307m^3/T_{KC} (This coal seam is ranked I according to QCVN / 03-BCT / 2011, Vietnam). At depths below level -280 to level -450 the methane content forecasted from 2.5 m^3/T_{KC} to

3.907m^3/T_{KC} (This coal seam is ranked II according to QCVN / 03-BCT / 2011, Vietnam) [4]

- For $N^0$8 coal seam: From depths level -25 to depths level -180 the density of methane contained in the coal seam is determined and forecasted from 0.367m^3/T_{KC} to 2.5m^3/T_{KC} (This coal seam is ranked I according to QCVN / 03-BCT / 2011, Vietnam). From depths level -200 to depths -450, the density of methane contained in the coal seam is forecasted from 2.643m^3/T_{KC} to 5.893m^3/T_{KC} (This coal seam is ranked II according to QCVN / 03-BCT / 2011, Vietnam) [4].

- For $N^0$9 coal seam: From depths level +30 to depths level -80 the density of methane contained in the coal seam is determined and forecasted from 0.356m^3/T_{KC} to 2.26722m^3/T_{KC} (This coal seam is ranked I according to QCVN / 03-BCT / 2011, Vietnam). From depths level -95 to depths -140, the density of methane contained in the coal seam is forecasted from 2.5m^3/T_{KC} to 4m^3/T_{KC} (This coal seam is ranked II according to QCVN / 03-BCT / 2011, Vietnam), from depths level -150 to depths -320, the density of methane contained in the coal seam is forecasted from 4.217m^3/T_{KC} to 8.0m^3/T_{KC} (This coal seam is ranked III according to QCVN / 03-BCT / 2011, Vietnam) and from depths level -350 to depths -450, the density of methane contained in the coal seam is forecasted from 8.576m^3/T_{KC} to 10.876m^3/T_{KC} (This coal seam is ranked IV according to QCVN / 03-BCT / 2011, Vietnam) [4].

- For $N^0$9b coal seam: From depths level -25 to depths level -125 the density of methane contained in the coal seam is determined and forecasted from 0.1479m^3/T_{KC} to 2.5m^3/T_{KC} (This coal seam is ranked I according to QCVN / 03-BCT / 2011, Vietnam), From depths level -125 to depths -190, the density of methane contained in the coal seam is forecasted from 2.5m^3/T_{KC} to 4m^3/T_{KC} (This coal seam is ranked II according to QCVN / 03-BCT / 2011, Vietnam), from depths level -200 to depths -380, the density of methane contained in the coal seam is forecasted from 4.477m^3/T_{KC} to 8.0m^3/T_{KC} (This coal seam is ranked III according to QCVN / 03-BCT / 2011, Vietnam) and from depths level -380 to depths -450, the density of methane contained in the coal seam is forecasted from 8.0m^3/T_{KC} to 9.477m^3/T_{KC} (This coal seam is ranked IV according to QCVN / 03-BCT / 2011, Vietnam) [4].

- For $N^0$10 coal seam: From depths level +70 to depths level -410 the density of methane contained in the coal seam is determined and forecasted from 0.21066m^3/T_{KC} to 2.5m^3/T_{KC} (This coal seam is ranked I according to QCVN / 03-BCT / 2011, Vietnam, From depths level -410 to depths level -450 the density of methane contained in the coal seam is determined and forecasted from 2.5m^3/T_{KC} to 2.717m^3/T_{KC} (This coal seam is ranked II according to QCVN / 03-BCT / 2011, Vietnam [4]).

References

1. Mining curent status of Maokhe underground coal mine in 2019. Technical Department, Maokhe coal Company, Quangninh-Vietnam (2019)
2. Report on sampling results, annual methane analysis for 2017. Mine safety center-Vinacomin, Quangninh, Vietnam (2018)
3. Report on geological exploration results of Maokhe underground coal mine, 2011. Mining geology company-TKV, Quangninh,Vietnam (2011)
4. Vietnam National Technical Regulation on safety in underground coal mining– QCVN01:2011/BCT. Ministry of Industry and Trade, Hanoi, Vietnam (2011)

A Lasso and Elastic-Net Regularized Generalized Linear Model for Predicting Blast-Induced Air Over-pressure in Open-Pit Mines

BUI Xuan Nam[1,2,*], NGUYEN Hoang[1,2,*], TRAN Quang Hieu[1,2], BUI Hoang Bac[3,4], NGUYEN Quoc Long[1,2], NGUYEN Dinh An[1,2], LE Thi Thu Hoa[1,2], PHAM Van Viet[1,2]

[1] Hanoi University of Mining and Geology, Hanoi, Vietnam
[2] Center for Mining, Electro-Mechanical research, Hanoi, Vietnam
[3] Hanoi University of Mining and Geology, Hanoi, Vietnam
[4] Center for Excellence in Analysis and Experiment, Hanoi University of Mining and Geology, Hanoi, Vietnam

Abstract: Air overpressure (AOp) is one of the products of blasting operations in open-pit mines which have a great impact on the environment and public health. It can be dangerous for the lungs, brain, hearing and the other human senses. In addition, the impact on the surrounding environment such as the vibration of buildings, break the glass door systems are also dangerous agents caused by AOp. Therefore, it should be properly controlled and forecasted to minimize the impacts on the environment and public health. In this paper, a Lasso and Elastic-Net Regularized Generalized Linear Model (GLMNET) was developed for predicting blast-induced AOp. The United States Bureau of Mines (USBM) empirical technique was also applied to estimate blast-induced AOp and compare with the developed GLMNET model. Nui Beo open-pit coal mine, Vietnam was selected as a case study. The performance indices are used to evaluate the performance of the models, including Root Mean Square Error (RMSE), Determination Coefficient (R2), and Mean Absolute Error (MAE). For this aim, 108 blasting events were investigated with the Maximum of explosive charge capacity, monitoring distance, powder factor, burden, and the length of stemming were considered as input variables for predicting AOp. As a result, a robust GLMNET model was found for predicting blast-induced AOp with an RMSE of 1.663, R2 of 0.975, and MAE of 1.413 on testing datasets. Whereas, the USBM empirical method only reached an RMSE of 2.982, R2 of 0.838, and MAE of 2.162 on testing datasets.

[1] *Corresponding author: buixuannam@humg.edu.vn*

1. Introduction

Open-pit mining projects often have a significant impact on the environment and public health, particularly in neighboring areas. The increase in environmental pollution caused by mining operations has been found in the concentrations of wastewater, emissions, radiation, and related policies [23]. The adverse effects caused by blasting operations in open-pit mine such as ground vibration, air overpressure (AOp), fly rock, and back-break are also dangerous agents for humans and the surrounding environment [12, 20, 29, 31]. Of these side effects, AOp is the most dangerous factor.

Air overpressure (AOp) is one of the side effects of blasting operations in an open-pit mine. It is caused by the vibration of the air adjacent to the explosive block or by vibration from the ground. In the case of explosions on the ground, AOp is created directly by the pressure of the explosive product into the ambient air with high destructive power. This side effect of AOp is caused by a sudden increase in air pressure that is greater than the atmospheric pressure at the passing wave. Similar to explosions caused by bombs or weapons, the blast-induced AOp in open-pit mine is responsible for brain, eyes, ears, nasopharynx, oropharynx, larynx and trachea (URT), lung, heart, abdomen, and genito-urinary [26]. At a high level, some pathologies involving the brain, lung, and heart can lead to death. Thus, accurate control and prediction of blast-induced AOp is an essential issue in order to reduce its adverse effects on the environment and the surrounding community.

Review of the literature shows that studies focused on the physiological, pathological, safety threshold and molecular mechanisms of trauma caused by AOp were performed [11]. In addition, the correlation between air overpressure, duration of the blast wave, body mass, and probability of survival was also found in a study by Bowen, Fletcher [7]. However, these studies mainly serve the mode of treatment without the ability to predict and control AOp.

For estimating blast-induced AOp, many scholars have attempted to develop empirical methods based on the relation of the explosive charge per delay (W) and monitoring distance (R) [24, 27, 28, 30, 32]. However, in some cases, experimental methods are often less accurate because the conditions applied in each region are different [15, 16, 20].

In recent years, artificial intelligence (AI) system has become popular and widely applied in many fields. In predicting blast-induced AOp, many scientists have studied and developed predictive models with promising results. Armaghani, Hajihassani [4] successfully developed an adaptive neuro-fuzzy inference system (ANFIS) model for predicting blast-induced AOp in three quarry sites in Malaysia using 128 blasting events. Several empirical methods, artificial neural networks (ANN) and multiple regression (MR) techniques were also used to predict blast-induced AOp and compared with the ANFIS model. The results revealed that the ANFIS was the best model for predicting blast-induced AOp in their study with an RMSE of 2.329 and R^2 of 0.971. In another study, Amiri, Amnieh [3] performed a blast-induced AOp predictive study based on ANN and K‑nearest neighbors (KNN), i.e., ANN-KNN. 75 blasting events were collected from the Shur river dam, Iran for their study. The United States Bureau of Mines (USBM) empirical and a single ANN model were also developed to predict blast-induced AOp. The results indicated that the developed ANN-KNN is a superior model in comparison with the ANN and USBM models with RMSE = 1.7 and R^2 = 0.95. Based on the hybrid model technique, Hasanipanah, Shahnazar [17] have also successfully developed a blast-induced AOp model using particle swarm optimization (PSO) and support vector regression (SVR) algorithms, namely PSO-SVR. Three forms of equation include linear (L), quadratic (Q) and radial basis (RBF) kernel functions were applied for PSO-SVR model. Multiple linear regression (MLR) technique was also conducted to estimate AOp and compared with PSO-SVR models. For this aim, 83 datasets were recorded at Shur river dam, Iran. However, their

results were not so good with an RMSE of 0.45 and R2 of 0.996 on the testing datasets for the most outstanding performance of PSO-SVR-RBF. In recent studies, Mahdiyar, Marto [25], AminShokravi, Eskandar [2], Alel, Upom [1], Armaghani, Hasanipanah [6], and Faradonbeh, Hasanipanah [13] have also successfully developed blast-induced AOp predictive models based on AI techniques such as Monte Carlo, PSO, genetic algorithm, ANN, and gene expression programming. They are really new powerful tools for predicting blast-induced AOp to control the effects on the environment and public health.

The literature shows that the studies of applying and development of the AI system have been studied and implemented quite well. However, the fact that they are not applied for all subjects or in everywhere. Furthermore, no artificial intelligence model can represent all models to predict blast-induced AOp for all regions. Therefore, in this study, a Lasso and Elastic-Net Regularized Generalized Linear Model (GLMNET) is developed for predicting blast-induced air overpressure to minimize impacts on the environment and public health at Nui Beo open-pit coal mine, Vietnam.

The rest of the article is organized as follows: Section 2 describes the study area and data used in this study; Section 3 gives an overview of the GLMNET algorithm; Section 4 carried out the development of blast-induced AOp predictive models; Section 5 presents the results of this work and discussion; Finally, the conclusions and remarks are drawled in section 6.

2. Materials

In this study, Nui Beo open-pit coal mine, Vietnam was selected as a case study for predicting blast-induced AOp. It is located in the central of Halong City, Quang Ninh province, Vietnam, and it lies within latitudes 20057’30”N - 20058’30”N, and longitudes 10707’55”E - 107009’00”E (Figure 1). This mine is one of the sizeable open-pit coal mines in Vietnam with a production of 1,125,000 tons/year; the capacity of overburden is 4.815.000 m3/year [9]. The fragmentation of rock is conducted by blasting method in the mine. Explosives used on the mine are ANFO, Z113 and AN13 emulsion with 250mm for blast hole diameter in rock breakage and 42mm diameter for oversize rock breakage.

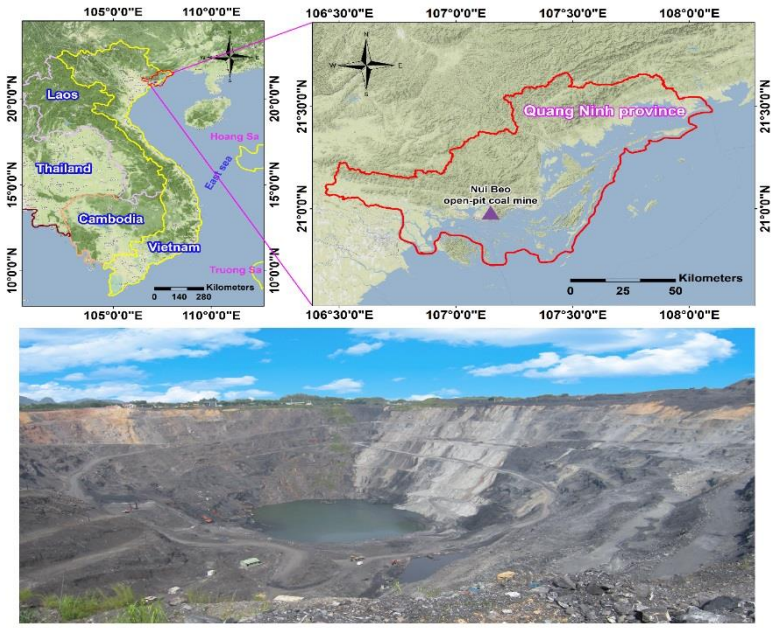

Figure 1. A view of the Nui Beo open-pit coal mine, Vietnam

The study area has complex geological conditions, including many faults and folds. The sedimentary rocks consist of conglomerate, sandstone, claystone, and sandstone with high hardness. The coal seams with average thicknesses are interspersed in clay layers. Figure 2 illustrates the examples of geological cross-sections of the study area.

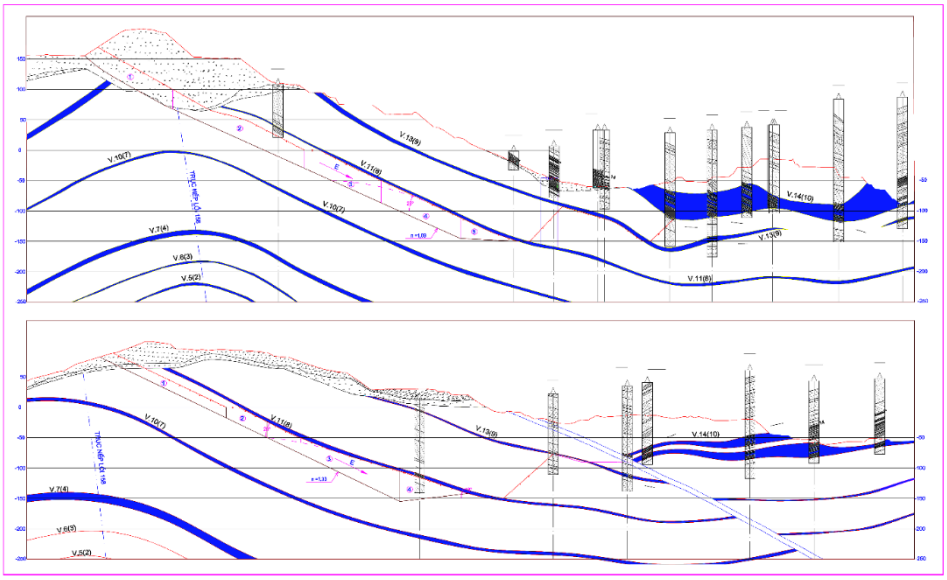

Figure 2. The representative geological cross sections of the Nui Beo open-pit coal mine

For collecting data, the maximum of explosive charge capacity (W), monitoring distance (R), powder factor (P), burden (B), and the length of stemming (T) were considered as the input variables for predicting blast-induced AOp. The Blastmate III (Instantel – Canada) was used to record the values of AOp from blasting operations (Figure 3). A handheld GPS navigation system is used to determine the monitoring distance. The remaining parameters are collected from blast design. Table 1 summarized the datasets used in this study.

Table 1. Summary of the datasets used in this study

W	**R**	**P**
Min. : 1382	Min. :104.0	Min. :0.350
1st Qu.: 4460	1st Qu.:269.5	1st Qu.:0.390
Median : 5932	Median :345.5	Median :0.430
Mean : 5844	Mean :369.0	Mean :0.426
3rd Qu.: 7250	3rd Qu.:451.8	3rd Qu.:0.460
Max. :10143	Max. :740.0	Max. :0.500
B	**T**	**AOp**
Min. :6.600	Min. :6.600	Min. : 79.96
1st Qu.:7.000	1st Qu.:6.900	1st Qu.: 90.76
Median :7.450	Median :7.300	Median : 94.76
Mean :7.442	Mean :7.288	Mean : 95.59
3rd Qu.:7.900	3rd Qu.:7.600	3rd Qu.:100.44
Max. :8.200	Max. :8.000	Max. :115.78

In this study area, the maximum of AOp value is 115.78 decibels (dB) at 104m for the monitoring distance, the mean of AOp value is 95.59 dB. Whereas, the nearest distance to the surrounding residential is 100m. The allowable noise level in the recommended occupational is 85 dB, whereas, the people and the workers in the mine must be continuously exposed to noise beyond the allowable limits caused by the blast. Hearing difficulties and other cardiovascular diseases can arise. Therefore, they need to be controlled and predicted to minimize the negative impact on public health.

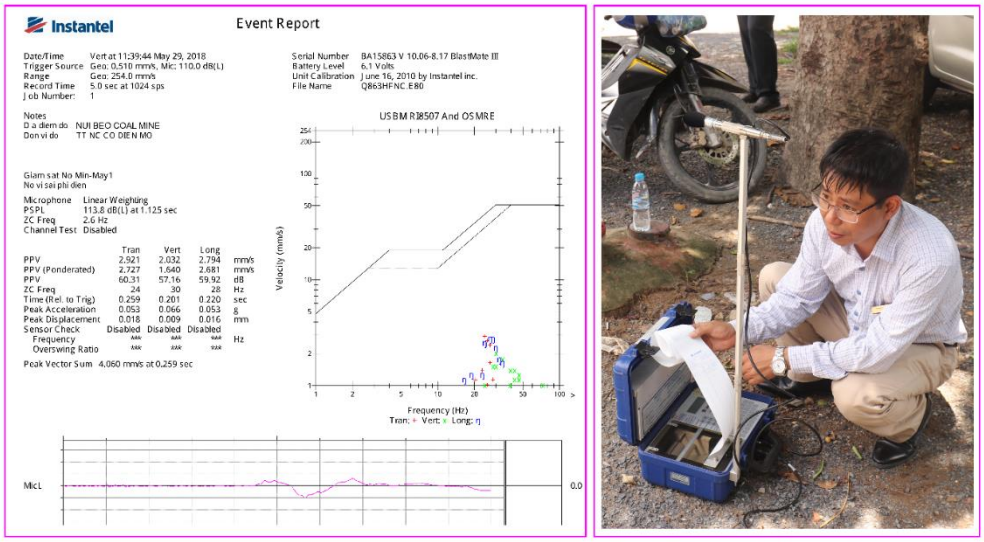

Figure 3. Collecting data by Blastmate III – Instantel

3. Details of GLMNET

The Lasso and Elastic-Net Generalized Linear Model (GLMNET) is one of the machine learning algorithms in the artificial intelligence system introduced by Friedman, Hastie [14]. The GLMNET algorithms continuously optimize the objective function on each parameter; the remaining parameters are fixed. It uses cyclical coordinate descent and executes continuously until convergence [18]. For predicting blast-induced AOp, the GLMNET can be described as follows:

Let y_i is the value to forecast, i.e., AOp; x_i is a matrix consisting of input variables such as W, R, P, B, and T; $x_i = (x_{i1}, x_{i2}, ..., x_{ij}, ..., x_{ik})^T$ with k denotes the number of descriptors. A linear model for each predicted AOp result is assumed as follows:

$$y_i = x_i^T \beta + \varepsilon_i \quad (1)$$

Where β is a coefficient, $\beta = (\beta_1, \beta_2, \ldots, \beta_j, \ldots, \beta_k)^T$; ε_i is the error between the actual and the predicted AOp values. The coefficients β are determined that ε_i is minimized. The residual sum of squares is minimized as follows:

$$E(\beta) = \sum_{i=1}^{n} (y_i - x_i^T \beta)^2 \quad (2)$$

The minimizing coefficients are defined by ordinary least squares method [10] as follows:

$$\hat{\beta} = (X^T X)^{-1} X^T y \quad (3)$$

Where $X = (x_1^T, x_2^T, \ldots, x_i^T, \ldots, x_n^T)$ and $y = (y_1, y_2, \ldots, y_i, \ldots, y_n)^T$.

Should be noted that, this equation cannot be solved in the case of $k > n$ because$X^T X$ becomes singular. Therefore, the regularized regression technique can be employed for instead. The loss function for a type of regularized regression, i.e., Elastic-Net is defined as follows:

$$E(\beta) \sum_{i=1}^{n} (y_i - x_i^T \beta)^2 + \lambda \sum_{i=1}^{k} (1 - \alpha)\beta_j^2 + \alpha|\beta_j| \quad (4)$$

By minimizing the loss function of Elastic-Net in equation (4), the coefficients β can be estimated. The factors that are not important to AOp can be eliminated, even if $k > n$. It can be seen that, α and λ are parameters that determine the performance of the forecasting model and adjusted for the purpose of the user $(0 < \alpha < 1)$. If $\alpha = 0$, this model corresponds to ridge regression [19]. In the case of $\alpha = 1$, this model corresponds to LASSO regression [33]. For each value of α, the λ and β parameters are defined so that the loss function $E(\beta)$ is minimized. The values of λ are determined by leave-one-out cross-validation method (LOOCV) [8].

By continuously optimizing the objective function on each parameter while other parameters are fixed, GLMNET has the high-speed computing power and sparse resolution in the input matrix x_i [18] for predicting blast-induced AOp.

The literature review showed that GLMNET had not been developed to predict blast-induced AOp. Therefore, it was conducted in this study to assess its applicability and accuracy level in predicting blast-induced AOp.

4. Developing the AOp predictive models

For developing the AOp predictive models, a randomized data splitting procedure is performed. Accordingly, the initial datasets with 108 blasting events are divided into two parts: 80% of the whole datasets (including 88 blasting events) are used as the training datasets for developing the predictive models; the remaining 20% (equivalent to 20 blasting events) are used as the testing datasets for evaluating the performance of the developed models. For the comparison purposes, the United States Bureau of Mines (USBM) empirical technique is also applied for estimating blast-induced AOp. Should be noted that all AOp predictive models are developed on the same set of training data.

To avoid overfitting in the development of the predictive models, a resampling technique is used, i.e., repeated k-fold cross-validation [21]. For the number of data in the training datasets are 88 observations, we chose k = 10 fold for resampling technique, namely 10-fold cross-validation with 3 repeats. The detailed of 10-fold cross-validation resampling technique can be explained in reference [34].

4.1. Empirical

Empirical is one of the methods used to estimate the blast-produced AOp in an open-pit mine. It is realized by collecting the datasets of blasting operations and using a statistical method to find out the site factors and forecasting equations. Kuzu, Fisne [22] conducted AOp predictions by identifying scaled-distanced (SD) based on the United States Bureau of Mines (USBM) empirical equation to calculate the site factors. Among the empirical methods, USBM method is the experimental technique was widely used to predict AOp in open-cast mine based on the relationship between the monitoring distance (R) and the

maximum explosive charge capacity (W), and site factors [5, 15]. The relationship between W and R is determined through the SD values as below [22]:

$$SD = RW^{-0.33} \quad (5)$$

Where R denotes the monitoring distance (m); W is the maximum explosive charge capacity (kg); SD is the scaled distance factor (m kg-0.33).

From the scaled distance, AOp can be calculated as follow [22]:

$$AOp = k(SD)^{-\beta} \quad (6)$$

Where AOp is measured in decibels (dB), k and β are site factors and computed by the regression analysis method. Depending on the specific conditions of each mine, the site factors are different.

In this study, the training datasets with 88 blasting events are used to calculate the site factors of the Nui Beo open-pit coal mine, Vietnam. Eviews software version 8.0 was used for multivariate regression analysis to determine the site factors in this study. As a result, the site factors are determined as $k=175.307$ and $\beta=0.203$ for USBM empirical equation. The USBM equation for predicting blast-induced AOp in this study is described as follows:

$$AOp = 175.307(SD)^{-0.203} \quad (7)$$

4.2. GLMNET

In GLMNET, α and λ are the parameters of the algorithm used to control the quality of the forecasting model as mentioned. It is complicated to know that which model is the best for predicting blast-induced AOp in this study. Therefore, a "trial and error" procedure was performed with 1000 different GLMNET models in the R software environment version 3.4.4. Should be noted that the values of α being in the range of 0 to 1; corresponds to each value of α, λ is defined by the LOOCV method so that the loss function was minimized. The performance of the predictive models on the training datasets is assessed based on the Root Mean Square Error (RMSE) metric. Figure 4 demonstrated the performance of 1000 GLMNET models with various of α and λ parameters in the “trial and error” procedure. Finally, a best GLMNET model was found with $\alpha=0.974$ and λ=0.117.

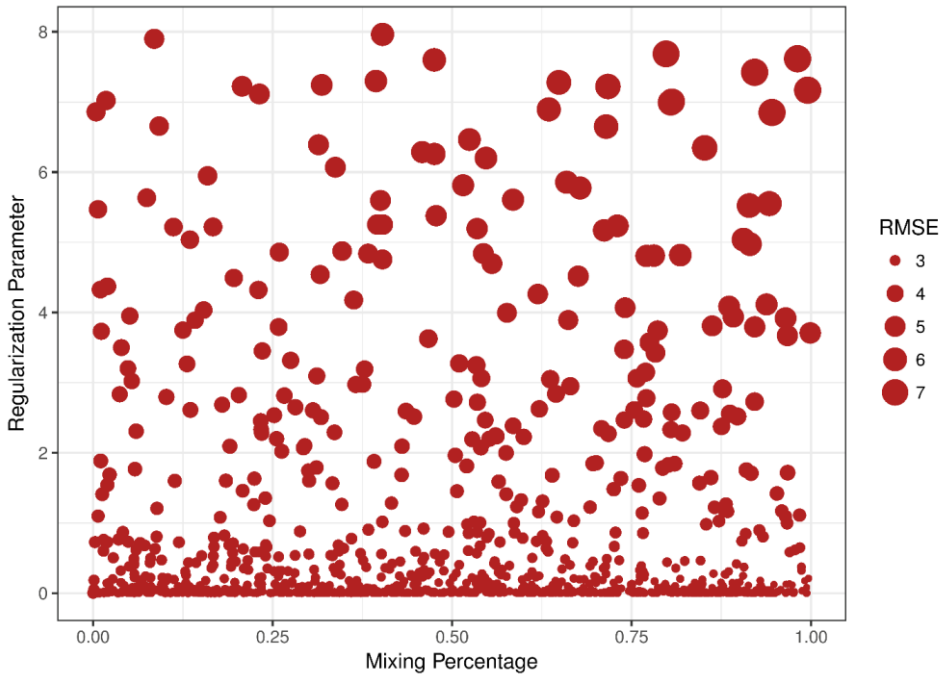

Figure 4. The performance of the GLMNET models on the training datasets

5. Results and discussion

As regarded, the performance of the blast-induced AOp predictive models was compared and evaluated on both the training datasets and the testing datasets. The performance indices include Root Mean Square Error (RMSE), Determination Coefficient (R2), and Mean Absolute Error (MAE) are used to evaluate the performance of the predictive models and computed as follow:

$$RMSE = \sqrt{\frac{1}{n}\sum_{i=1}^{n}(y_i - \hat{y}_i)^2} \quad (8)$$

$$R^2 = 1 - \frac{\sum_i (y_i - f_i)^2}{\sum_i (y_i - \overline{y})^2} \quad (9)$$

$$MAE = \frac{1}{n}\sum_{j=1}^{n} |y_i - \hat{y}_i| \quad (10)$$

Where n is the total number of data, y_i is the measured value, $\hat{y}_i$ is the predicted value, and $\overline{y}$is mean of measured values. In the most optimal model, R^2 should be equal to 1, and the RMSE and MAE should be equal to 0, respectively.

Based on the developed models and equations (8-10), the performance of the predictive models on the training and testing datasets are computed as shown in Table 2.

Table 2. Performance indices of the AOp predictive models

Model	Training datasets			Testing datasets		
	RMSE	R2	MAE	RMSE	R2	MAE
Empirical (USBM)	4.195	0.682	2.548	2.982	0.838	2.162
GLMNET	2.837	0.822	1.713	1.663	0.975	1.413

From Table 2, it can be seen that the GLMNET model outperformed the empirical model on both the training datasets and the testing datasets. The performance of the GLMNET model reached an RMSE of 2.837, R^2 of 0.822, and MAE of 1.713. Whereas, the empirical model only achieved an RMSE of 4.915, R^2 of 0.682, and MAE of 2.548 on the training datasets.

As mentioned, the testing datasets as the unseen data are used to evaluate the performance of the developed models. Accordingly, the selected GLMNET model provided very high performance with RMSE = 1.663, R^2 = 0.975, and MAE = 1.413 on the testing datasets. Whereas, the empirical model only achieved performance with RMSE = 2.982, R^2 = 0.838, and MAE = 2.612 on the testing datasets. Figure 5 interpreted the relationship between measured and predicted values on the testing datasets.

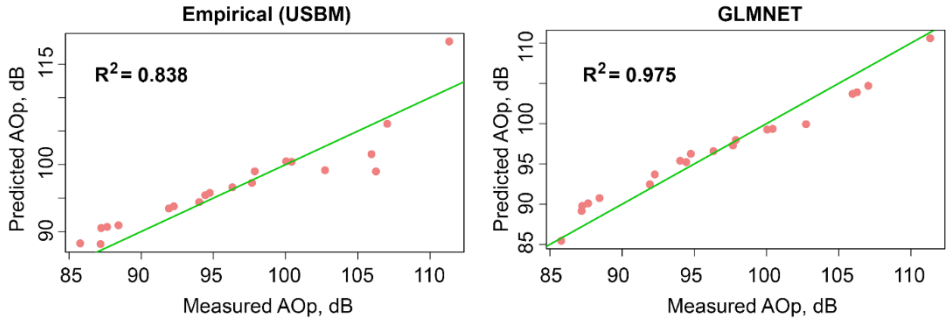

Figure 5. The relationship between measured and predicted values

As set out in this study, high levels of accuracy are needed for predicting blast-induced AOp to minimize the impact on the environment and public health. Figure 6 demonstrated that the developed GLMNET model provides very high levels of accuracy for predicting blast-induced AOp in comparison with empirical models and measured values for the testing of datasets.

It can be seen that the GLMNET model works very well in this study with the number of input variable is high (5 input variables). Whereas, the USBM empirical technique uses only two input variables for predicting blast-induced AOp. Therefore, a technique for analyzing the influence of input variables on the performance of the GLMNET model was implemented in this study. As a result, W, R, P, and T are the input variables that affect the performance of the GLMNET model with the overall effect level of W is 0.076; R is 6.269; P is 0.303; and T is 0.083. The results of the analysis also showed that B is a parameter that

does not affect the performance of the GLMNET forecasting model and should be considered for elimination during the development of the AOp forecasting model.

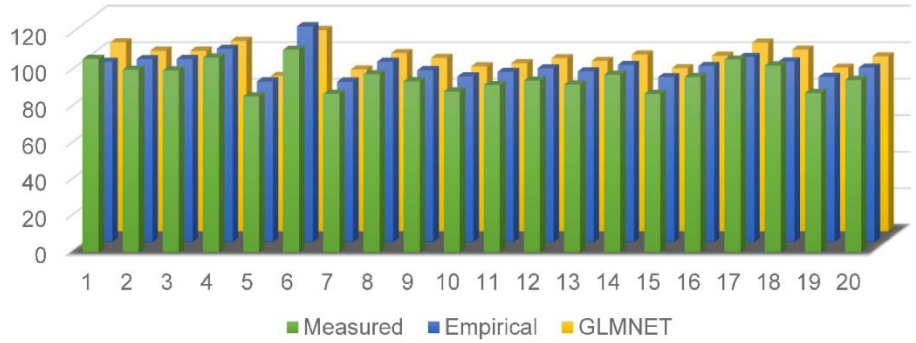

Figure 6. Comparison of predicted values by empirical and GLMNET models

6. Conclusions and remarks

Blasting is an indispensable task for rock fragmentation in an open-pit mine. However, its undesirable effects need to be controlled to minimize adverse effects on the environment and public health, especially air overpressure. Based on the results of this study, we draw some conclusions:

- GLMNET is an advanced artificial intelligence system for predicting blast-induced AOp in open-pit mine with high accuracy. It is possible to explain the linear relationship between multiple input variables that affect the performance of the AOp predictive model. However, the development of the GLMNET model is often complex and takes much time to find the optimal parameters for the model. In addition, higher input variables require more careful and thorough data collection.

- The input parameters include maximum explosion charge capacity (W), monitoring distance (R), powder factor (P), and the length of stemming (T) are the main parameters that affect the performance of the AOp predictive model. Burden (B) parameter should be considered for elimination during the development of AOp predictive models.

- The selected GLMNET model in this study is the best of the 1000 GLMNET models developed. However, some of the other GLMNET models also yielded relatively high performance. Their combination should be studied and considered to improve the accuracy of the blast-induced AOp model.

7. Acknowledgments

Paper was presented during the 5th POL – VIET International Conference Scientific-Research Cooperation between Vietnam and Poland, 08-10.07.2019, AGH UST, Krakow, Poland. This research was supported by Hanoi University of Mining and Geology (HUMG) and Center for Mining, Electro-Mechanical research of Hanoi University of Mining and Geology.

References

1. Alel, M.N.A., et al. *Optimizing Blasting's Air Overpressure Prediction Model using Swarm Intelligence*. in *Journal of Physics: Conference Series*. 2018. IOP Publishing.
2. AminShokravi, A., et al., *The potential application of particle swarm optimization algorithm for forecasting the air-overpressure induced by mine blasting.* Engineering with Computers, 2018. **34**(2): p. 277-285.
3. Amiri, M., et al., *A new combination of artificial neural network and K-nearest neighbors models to predict blast-induced ground vibration and air-overpressure.* Engineering with Computers, 2016. **32**(4): p. 631-644.
4. Armaghani, D.J., et al., *Neuro-fuzzy technique to predict air-overpressure induced by blasting.* Arabian Journal of Geosciences, 2015. **8**(12): p. 10937-10950.
5. Armaghani, D.J., M. Hasanipanah, and E.T. Mohamad, *A combination of the ICA-ANN model to predict air-overpressure resulting from blasting.* Engineering with Computers, 2016. **32**(1): p. 155-171.
6. Armaghani, D.J., et al., *Airblast prediction through a hybrid genetic algorithm-ANN model.* Neural Computing and Applications, 2018. **29**(9): p. 619-629.
7. Bowen, I.G., E.R. Fletcher, and D.R. Richmond, *Estimate of man's tolerance to the direct effects of air blast*. 1968, LOVELACE FOUNDATION FOR MEDICAL EDUCATION AND RESEARCH ALBUQUERQUE NM.
8. Cawley, G.C. *Leave-one-out cross-validation based model selection criteria for weighted LS-SVMs*. in *Neural Networks, 2006. IJCNN'06. International Joint Conference on*. 2006. IEEE.
9. company, N.B., *Summary report of production in 2010, Nui Beo (unpublish report)*. 2010.
10. Dismuke, C. and R. Lindrooth, *Ordinary least squares.* Methods and Designs for Outcomes Research, 2006. **93**: p. 93-104.
11. Elsayed, N.M., N.V. Gorbunov, and V.E. Kagan, *A proposed biochemical mechanism involving hemoglobin for blast overpressure-induced injury.* Toxicology, 1997. **121**(1): p. 81-90.
12. Faradonbeh, R.S., M. Monjezi, and D.J. Armaghani, *Genetic programing and non-linear multiple regression techniques to predict backbreak in blasting operation.* Engineering with Computers, 2016. **32**(1): p. 123-133.
13. Faradonbeh, R.S., et al., *Development of GP and GEP models to estimate an environmental issue induced by blasting operation.* Environmental monitoring and assessment, 2018. **190**(6): p. 351.
14. Friedman, J., T. Hastie, and R. Tibshirani, *Regularization paths for generalized linear models via coordinate descent.* Journal of statistical software, 2010. **33**(1): p. 1.
15. Hajihassani, M., et al., *Prediction of airblast-overpressure induced by blasting using a hybrid artificial neural network and particle swarm optimization.* Applied Acoustics, 2014. **80**: p. 57-67.
16. Hasanipanah, M., et al., *Several non-linear models in estimating air-overpressure resulting from mine blasting.* Engineering with Computers, 2016. **32**(3): p. 441-455.
17. Hasanipanah, M., et al., *Prediction of air-overpressure caused by mine blasting using a new hybrid PSO–SVR model.* Engineering with Computers, 2017. **33**(1): p. 23-31.
18. Hastie, T. and J. Qian, *Glmnet vignette.* Retrieved June, 2014. **9**(2016): p. 1-30.
19. Hoerl, A.E. and R.W. Kennard, *Ridge regression: Biased estimation for nonorthogonal problems.* Technometrics, 1970. **12**(1): p. 55-67.

20. Khandelwal, M. and P. Kankar, *Prediction of blast-induced air overpressure using support vector machine.* Arabian Journal of Geosciences, 2011. **4**(3-4): p. 427-433.
21. Kohavi, R. *A study of cross-validation and bootstrap for accuracy estimation and model selection*. in *Ijcai*. 1995. Montreal, Canada.
22. Kuzu, C., A. Fisne, and S. Ercelebi, *Operational and geological parameters in the assessing blast induced airblast-overpressure in quarries.* Applied Acoustics, 2009. **70**(3): p. 404-411.
23. Li, G., et al., *The Empirical Relationship between Mining Industry Development and Environmental Pollution in China.* International journal of environmental research and public health, 2017. **14**(3): p. 254.
24. Loder, B. *National Association of Australian State Road Authorities*. in *Australian Workshop for Senior ASEAN Transport Officials, 1985, Canberra*. 1987.
25. Mahdiyar, A., A. Marto, and S.A. Mirhosseinei, *Probabilistic air-overpressure simulation resulting from blasting operations.* Environmental Earth Sciences, 2018. **77**(4): p. 123.
26. Mayorga, M.A., *The pathology of primary blast overpressure injury.* Toxicology, 1997. **121**(1): p. 17-28.
27. McKenzie, C., *Quarry blast monitoring: technical and environmental perspectives.* Quarry Management, 1990. **17**: p. 23-4.
28. Mohamad, E.T., et al., *Estimation of air-overpressure produced by blasting operation through a neuro-genetic technique.* Environmental Earth Sciences, 2016. **75**(2): p. 174.
29. Rezaei, M., M. Monjezi, and A.Y. Varjani, *Development of a fuzzy model to predict flyrock in surface mining.* Safety science, 2011. **49**(2): p. 298-305.
30. Rosenthal, M.F. and G.L. Morlock, *Blasting guidance manual.* 1987.
31. Saadat, M., M. Khandelwal, and M. Monjezi, *An ANN-based approach to predict blast-induced ground vibration of Gol-E-Gohar iron ore mine, Iran.* Journal of Rock Mechanics and Geotechnical Engineering, 2014. **6**(1): p. 67-76.
32. Siskind, D.E., et al., *Structure response and damage produced by airblast from surface mining*. 1980: Citeseer.
33. Tibshirani, R., *Regression shrinkage and selection via the lasso.* Journal of the Royal Statistical Society. Series B (Methodological), 1996: p. 267-288.
34. Venables, W.N. and B.D. Ripley, *Tree-based methods*, in *Modern Applied Statistics with S*. 2002, Springer. p. 251-269.

Estimation of truck-shovel dispatching in Cao Son Open-Pit coal mine and the ability in applying information technology for increasing its efficiency

Van Hoa PHAM[1,*], Xuan Nam BUI[1], Van Quyen LE, Thi Thu Hoa LE[1] and Van Viet PHAM[1]

[1] HUMG Hanoi University of Mining and Geology, Faculty of Mining, Hanoi, Vietnam

Abstract. With many types of trucks and shovels for hauling large volume of waste rocks to the dump sites and coal to the storages, the truck – shovel dispatching in Cao Son open pit coal mine is the operation which needs to be improved. At present, the combination between trucks and shovel is usually assigned at the beginning of shift and adjusted during the operation at the mine. The GPS tracking system are integrated into each truck to monitor the position in real time, but applying this information to find the best destination to send the truck to satisfy the production requirements and to minimize truck operating costs is still not used. This paper presents the estimation of the information system, data, the remaining problems of truck – shovel dispatching system, from that proposes the application of available information technology for increasing the efficiency of this activities at the mine.

1. Introduction

Cao Son surface coal mine, one of the biggest surface coal mine in northeastern coast of Vietnam, is located in Quang Ninh province (Figure 1). The mine has the mining area of 4.87 km^2 and the reserve of 48.13 milion tons. At present, the coal production of the mine is from 2.8 to 3.3 milion tons/year and the waste rocks which need to be loaded and hauled is from 26 to 32 milion m^3/year. Therefore, the loading and hauling operation plays an important role in the whole mining system of the mine. The waste rock is transported to the outside waste dumps in two types: 1) directly to the waste dump by trucks and 2) combination of trucks and conveyer belt.

The combination between trucks and shovel is usually assigned at the beginning of shift and adjusted during the operation at the mine. Although the GPS tracking system are integrated into each truck to monitor the position in real time, but using this information to find the best destination for sending the truck to satisfy the production requirements and to minimize truck operating costs is still not used. The present choice of the mine is the stratery of fixed asignment of each truck at the beginning of the shift to a specific shovel and a dump point and this trucks works with that shovel for the entire shift. In the case of changing in practical operating conditions, such as breakdown of the shovel, the trucks then are reassigned to another loading position. This strategy ussualy causes more idle times due

* Corresponding author: phamvanhoa@humg.edu.vn

to the lack of trucks or the queues form near paticular shovels. Another strategy is dynamic assigment of trucks and shovel with flexible asignment of truck after dumping to a free or less busy shovel is still not applied due to the weak in technology and the large number of trucks and shovels at the mine. It is clearly that the mine should the way to improve the truck-shovel dispatching system by applying available information technology for increasing the efficiency of this activities at the mine.

Fig. 1. Location of Cao Son surface coal mine [google maps]

2 Real situation of truck-shovel dispatching at the mine

Cao Son surface coal mine is working 3 shifts/day for loading waste rocks, 2 shifts/day for loading coal and 8 hours/shift. With the diversity of 20 rope shovels and 11 excavators with bucket capacity from 3.3 m^3 to 12 m^3. The rope shovels were invested about 40 years ago and sometimes breakdown due to technical problems and maintainance. The other 11 hydraulic excavators are used for both loading waste rocks and coal at the seam. The waste rock is excavated with the bench height from 10m to 15m by rope shovels or hydraulic excavators. Coal is loaded with the subbench height from 5m to 7.5 m. As reported by Cao Son mine [1], the rope shovels mostly are out of date and ussualy damages which lead to low efficiency of the shovels. The hydraulic excavators are in good quality and meet the technical requirements of the mine, however, due to the small number, they do not replace the old rope shovels. For hauling the waste rocks and coal at the mine, there are total 148 trucks are used, which include: 121 trucks with weight from 55 tons to 98 tons for hauling waste rock and 18 trucks with weight from 32 tons to 40 tons for hauling coal and auxiliary works. Table 1 shows the types of shovels and excavators used at the mine.

Table 1. Types of shovels and excavators at Cao Son surface coal mine [1]

No.	Type	Bucket capacity, m^3	Number
1	Rope shovels ЕКГ – 4,6; ЕКГ – 5А	4.6 to 5.0	11
2	Rope shovels ЕКГ – 8И	8	8
3	Rope shovel ЕКГ – 10	10	1
4	Komatsu PC1800-6	12	1
5	Komatsu PC750-7	3.4	2
6	Komatsu PC1250	6.7	4

7	Hitachi 670	3.5	2
8	Caterpilar CAT – 356 BL	3.2	2

The transportation of waste rock from loading points to dump sites is carried out by a system of haul roads with different length and slope inside and outside the mine. The loading time depends on the bucket capacity, digability, and weight or truck capacity. The queue at the loading points ussualy happens when the trucks with different capapacity are used at each shovel or excavator. Therefore, the positioning of trucks for transporting waste rock from a particular mining area to bring profit for the mine is an important but complex issues. The efficiency of mining operations largely depend on the proper dispatching the position of truck and shovel, respectively, along the haul roads and dump sites. Type and number of trucks and shovels is one of the important factors for determining the optimal paramters of surface mining system. Besides, the running and loading time of trucks at the shovels will define the efficiency of truck-shovel system. The diversity in capacity of trucks and shovels at Cao Son clearly shows the complex in dispatching process at the mine. Any improvement on efficiency of truck-shovel system may save large amount of money in almost mining procedures at mine but with little or no investment on buying or repalce the neccesary mining quipments. Figure 2-4 show charts getting from statistical data of stopping and running time of shovels and excavator at Cao Son coal mine [2].

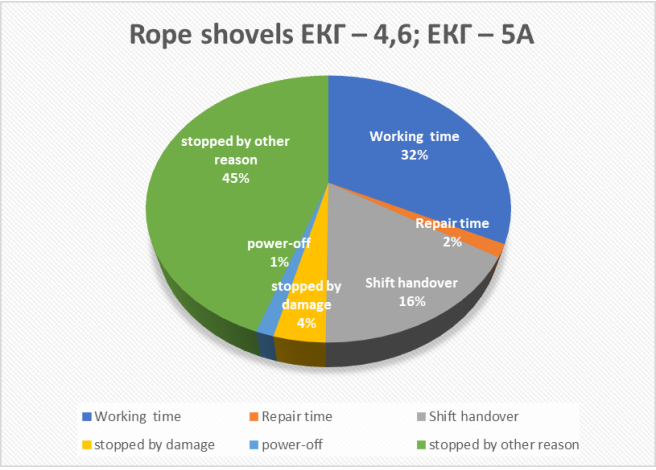

Fig. 2. Working and stopping time of Rope shovels ЕКГ – 4,6; ЕКГ – 5А [2]

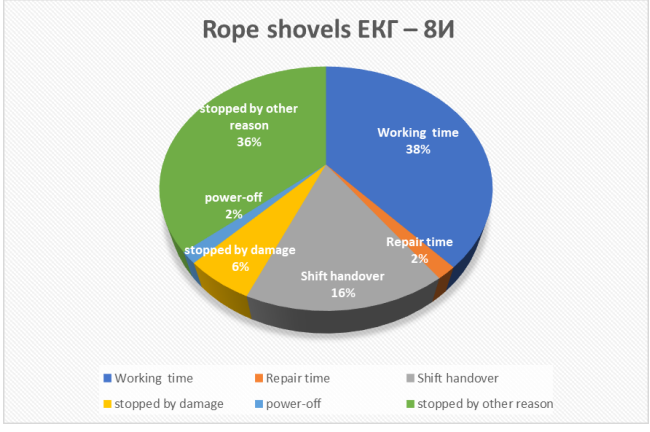

Fig. 3. Working and stopping time of Rope shovels ЕКГ – 8И [2]

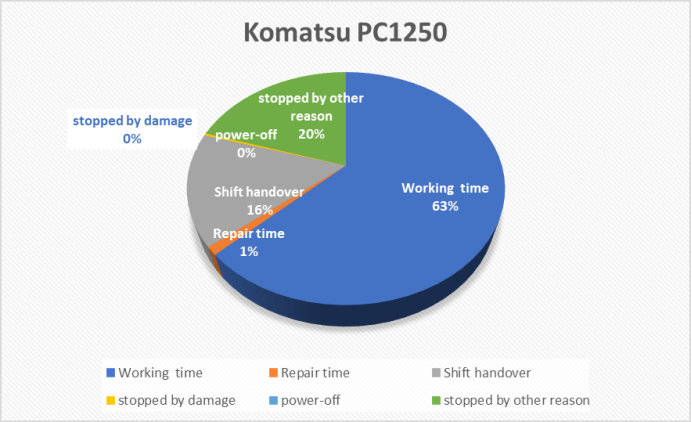

Fig. 4. Working and stopping time of hydraulic excavator PC-1250 [2]

It can be easily seen from charts in Figure 2 to 4 that the working time of the rope shovels is from 32% to 3%, while the stopping time due to damage, repair, and other reasons is nearly 50%. For hydraulic excavator, the working time is much higher, 63%, and total stopping time by all reasons is much lower, 21%. Stopping time by damage is quite high for rope shovels, from 4% to 6%, while this time in hydraulic excavator is only 0%. It clearly shows the disadvantage in the working ability of old rope shovels in comparison with new hydraulic excavators at the mine. For both types of rope shovel and hydraulic excavator, the stopping time by other reasons, that include the dispatching problems, is still high to very high and this should be strongly reduced to increase the efficiency and reducing cost from loading operation. The diversity of 8 excavator types and bucket capacity at Cao Son coal mine proposes the complex problems for truck – shovel system and it is difficult to solve with practical technical condtions of mine.

For the hauling work, the volume of waste rock is quite stable annually. With the new investment of conveyor belt system in 2017, the combination of trucks and conveyor belt prevails over dirrect transportion to the waste dump. Table 2 shows the volume of waste rocks transported at Cao Son surface coal mine in recent years.

Table 2. Types of shovels and excavators at Cao Son surface coal mine [2]

Year	Total volume, milion m^3	Transported directly by trucks, milion m^3	Combination trucks and conveyor belt, milion m^3
2014	33 210	33210	
2015	33 200	33 200	
2016	25 800	25 800	
2017	25 700	12 700	13 000 (50.58%)
2018	21 700	4 700	17 000 (78.34%)

At this time, the average hauling distance for direct transportation of waste rock to the dump site is 7.5 km, maximum hauling distance is about 10 km. There are two waste dumps for the trucks directly unloading the waste rocks and the loading lift height is from 300m to 350 m. For the combination between trucks and conveyor belt, the waste rock is transported with average distance of 2.5 km to the crushing machine on the surface and then transports by conveyor belt to the waste dump. Conveyor belt has width of 2 m, velocity from 4.0 to

6.0 m/s, length of 3550 m. Maximum fragment size providing for crusher is smaller than 1 m, maximum output fragment size from crusher to the conveyor belt is smaller than 0.4 m. As can be seen in Table 2, the volume of waste rock transported by the combination of trucks and conveyor belt increases the ratio from 50.58% to 78.34%. This proved that this type of hauling has many advantages on production and cost. According to the plan, the hauling volume by conveyer belt increases to 20 milion m^3 in year 2019.

Some difficulties with the hauling work by trucks at Cao Son coal mine such as: creating dust in dry season, rainy season makes slippery road, mist hides the vision of drivers, long hauling distance, hight road slope… These dificulties reduce the hauling capacity of the trucks. The hauling work by truck-conveyor belt requires smaller fragment size from blasting, if fragment size is large, this will reduce productivity and even causing stuck which leads to reducing of hauling productivity. Table 3 presents the working efficiency of trucks at Cao Son coal mine.

Table 3. Working efficiency of trucks at Cao Son surface coal mine [2]

No.	Truck	Number of truck			Working hours		
		Available trucks	Using number	% using	Total	Efficient time, h	% Efficient time
1	CAT 773E, 58 tons	22	18	82	72683	58883	81
2	CAT 773F, 55 tons	10	9	90	23466	19284	82.2
3	CAT 777D, 96 tons	20	16	80	59350	51945	87,5
4	HD 565-7, 58 tons	42	38	90	126542	107923	85,2
5	HD 565-7R, 58 tons	30	28	93	107074	99746	93
6	HD785, 91 tons	14	12	86	45256	40746	90
7	Volvo A35D, 32.5 tons	10	7	70	26751	24471	91.5
8	Volvo A40E, 38 tons	8	7	88	28782	28494	99
9	HM 400-2R, 36.5 tons	15	13	87	39799	28148	70,7
10	Kamaz 6520, 20 tons	10	7	70	8240		
11	Scania P340, 28 tons	10	9	90	40300		

The data from Table 3 shows that the number of trucks put into working is from 70% to 93%, that means the trucks in the ready or maintaince state but not in use are still high, from 7% to 30%, depending on particular truck type.

3 Factors influencing on dispatching strategy at the mine

For monitoring the position of trucks and shovels at mine site, the GPS positioning devices are installed for each truck and shovel or excavator at Cao Son surface coal mine. The mine operating engineers can access the information of trucks and shovels at real time. The 3G signal is covered all mining area, event at the deep bottom of the mine. However, the lack of modern technology leads to the backward in applying efficient ditspatching strategy for the mine. The integrated GPS devices only used for tracking and observing mining equipments, the positioning data is not used to make the decision in real time for dispatching the truck-shovel system more effiective.

As mention in section 1, the fixed assignment strategy is applying at the mine. The shovels or excavators with bucket capacity from 3 m^3 to 5 m^3 are ussually assigned with trucks of weight from 27 tons to 58 tons. The bigger buckets capacity of more than 5 m^3 are assigned with trucks of bigger 58 tons. The mine is working 3 shifts/day for loading waste rocks, 2 shifts/day for loading coal and 8 hours/shift. Due to the lack in compatibility of mining equipment, trucks with different types and capacity run on the same hauling road and unload on the same waste dump, it is difficult for the operating engineers in executive work, especially in effectively assigning truck and shovel, and this leads to the reduction in

productivity of each mining equipments, in particularly, and trucks-shovels system in general.

It can be realized that: some factors influence on reduction of truck-shovel system, such as: bad fragmetation from the muckpiles after blasting leads to the extention of loading time and reduction of loading productivity; the different in combination bucket capcity and truck capacity will lead to the reduction in both loading and hauling productivity of truck and shovel. This problem can be only solved when applying dynamic assigment of truck-shovel in real time. To do this, the available information technology infrastructure of the mine shoul be effectively used and modern available devices or softwares should be applied for the practical conditions of the mine.

4 Development direction for improving dispatching process at Cao Son surface coal mine

The tranditional approach focuses on effectively operating the trucks to improve the use of mining equipments in all procedures in a surface mine. Increasing the use of trucks leads to increase profit, reduce the size of fleet and increase general efficiency. To get this target, the mine can apply some solutions such as: improving the operational efficiency of trucks through increasing productivity and reliable, increasing the truck capacity, combination trucks with conveyor belt system, using truck lifting system to reduce the hauling time. The targets for reducing operational costs of a mine also can be done by effectively use the trucks and shovels with the help of information technology. The truck-shovel system operated by information technology can increase the hauling capacity with existing trucks and shovels or get the production target with less number of mining equipments. The assignment of truck and shovel is carefully considered to increase the use of existing trucks - shovels and reduce the waiting time in hauling system. The waiting time is the main reason that leads to low efficiency of mining equipments and it should be reduced to the smallest.

Many companies have developed mine fleet management system such as “VG Karier” of VistGroup, DISPATCH of Modular Mining or Link of Caterpilar,… with hardware and software system to automatically manage the truck-shovel system through GPS positioning devices [3-5]. In general, the comercial fleet management systems in the world are developed to increase the used time of mining equipments, increase work discipline, the operational engineer can reconsider and improve their efficiency. The available information technology infrastructure at Cao Son coal mine can be used for the integration such system to manage the trucks and shovels. However, the high investment cost of these commertial systems is a problem for the mine to apply. This leads to the requirements to develop a fleet management system with reasonable cost for the mine. With the fast development of GPS positioning devices, especially a smartphone can carry out this function. Therefore, the idea of using smartphone in tracking the position of trucks and shovels for managing and operating works. This device can be programed to interact with drivers of trucks and shovels to operational center for optimizating calculation.

From above analysis, it can be realized that the application of information technology is the neccesary trend for improving truck-shovel dispatching process at Cao Son surface coal mine. Only when the positioning data are managed and then are used for the autonomous asignment of truck and shovel by information technology, the efficiency of truck – shovel then can be increased to its maximum ability.

5 Conclusions

Practical conditions at the mine leads to the application of the fixed asigment strategy for trucks and shovels at Cao Son surface coal mine. Statistical data of working and stopping times of trucks and shovels shows a clear disadvantages of this dispatching strategy to the real conditions. The application of fleet managemnt system with the use of smartphone as tracking devices is the idea that should be encouraged. Due to the its resonable prices and ability to interact with driver, this device can be effectively use to develop a good and reasonable system for ditspatching process at the mine.

6 Acknowledgements

Paper was presented during the 5th POL – VIET International Conference Scientific-Research Cooperation between Vietnam and Poland, 08-10.07.2019, AGH UST, Krakow, Poland. The authors would like to thank all staffs at Cao Son surface coal mine, in general, and especially the staffs at mining department, transportation and loading factories in supporting us to collect the data.

1. Cao Son mine, *Technology report of Cao Son surface coal mine* (company document, 2018)
2. Vinacomin, *Technical data of Cao Son surface Coal mine* (company document, 2018)
3. VIST Group, VG Karier Mine Fleet Management System (online at: https://vistgroup.ru/upload/iblock/0cc/VG-Karier.pdf)
4. DISPATCHM Mine Management System (online at : https://www.modularmining.com/wp-content/uploads/2019/03/02-DISPATCH-Flyer.pdf)
5. CAT Product link, Fleet management solutions (online at : https://www.cat.com/en_GB/support/operations/technology/fleet-management-solutions/product-link.html)

Study on some solutions for enlarging the application scope of the fully mechanized longwall coal mining technology according to seam dip angle at underground coal mines in Quang Ninh coalfield

Trung NGUYEN DUC[1*], Waldemar KORZENIOWSKI[1], Krzysztof SKRZYPKOWSKI[1] and Nguyen PHAM TRUNG[2]

[1] AGH University of Science and Technology, Krakow, Poland, Faculty of Mining and Geoengineering

[2] Institute of Mining Science And Technology, Hanoi, Vietnam

Abstract: The paper summarizes the applied experience, the technical solutions to limit the adverse effects of slope angle in the mechanized longwall mining at underground mines in the world. The paper proposes some solutions for enlarging the application field of the fully mechanized longwall mining technology according to seam dip angle at underground coal mines belonging to Vinacomin.

The current, Vietnam National Coal – Mineral Industries Holding Corporation Limited (Vinacomin) is promoting the application of the mechanized coal mining technology, in order to improve capacity and labor productivity, meet the demand for the economy. In which, the process of applying mechanized technology to mining coal seams with dip angle $\alpha \leq 35^0$, solved the requirements of capacity, productivity and labor safety. However, in condition ofsome inclined seams with a dip angle $\alpha > 20^0$, the level of efficiency of the technology decreased sharply (equal to 25 to 30-percent compared to the stable period). Although the device is designed with the ability to work when the angle is up to 25^0, even to 35^0.

The results of assessment mechanization application process in coal mines in Quang Ninh in the past ten years show that: Stable working time of longwall accounts for 38% to 45% of total operating time [2]. The remaining time, the longwall often encountered trouble, in which the slope factor plays an important role (accounting for 17% of the total unstable operation time and accounting for 38.6% of the geological problems). If the dip angle is greater than 20^0, the equipment in the mechanized longwall will work with low reliability, usually occurs sliding, must stop troubleshooting, affects the durability of the device and reduce exploitation efficiency.

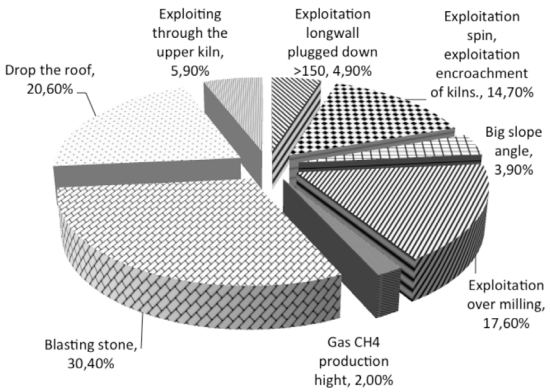

Figure 1. Proportion of factors affecting the reduction of longwall production

Therefore, study on some solutions for enlarging the application field of the fully mechanized longwall mining technology is necessary for underground coal mines in the Quang Ninh coalfield.

I. Study on some solutions for enlarging the application scope of the fully mechanized longwall mining technology at underground coal mines

In the world, to exploit coal seams of medium to thick thickness, dip angle above 20º by mechanized longwall, there are some following solution:

1. Improving the structure of the support.

This method link individual support units into clusters by the anti-topple jacks and face conveyor with power support by anti-slip device. The addition of large hydraulic jacks with thrust (or pull) along the direction of the dip angle of the longwall, linking the canapy and base of the single power support as above is quite effective in keeping the supports and face conveyor not fall over by the impact of the dip seam, thereby increasing the scope of application according to the working angle of the power supports and conveyor.

a. Anti-drift system of power support

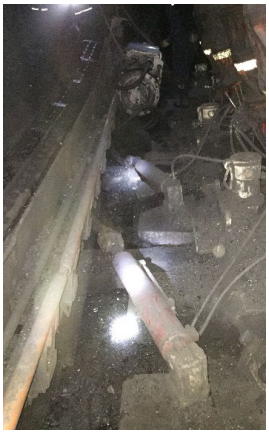

b. Anti-drift system of face-conveyor

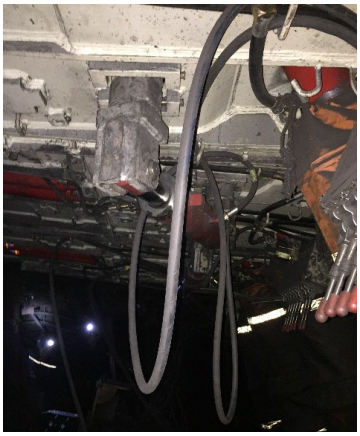

c. Anti-topple system of power support

Figure 2. Hydraulic jacks against drifting, anti-topple of face conveyor at mechanized longwall, Quang Hanh Coal Company

This solution has been practically applied and highly effective in some mechanized longwall mining at the medium thick seams in Chinese underground mines such as Doanh Coc Son and Xuong Hung of Ban district - Guizhou; Dai Hung mine - Tao Trang; mine No. 10 - Binh Dinh Son - Ha Nam Province; Tuan Duc Mine - Hac Cuong Mine - Hac Long Giang Province .... The mechanized longwall have a length of 100 ÷ 150m, have coal output of 350,000 ÷ 600,000 tons/year, some favorable cases, the longwall capacity reaches 1.5 million tons/year, labor productivity reaches 20 ÷ 50 tons/work, the exploitation coefficient reaches 90 ÷ 95% [2]. In Quang Ninh region, the longwall CGH TT-6-1 located in the coal seams 6 of the Trung Tam area, Quang Hanh coal mine has been equipped with anti-drift hydraulic jacking system, the longwall relatively stable operation in sloping conditions of about 25º.

2. Solution of longwall mining in the direction of selling oblique to reduce slope angle.

This solution set the coal face of longwall in the semi-oblique direction to reduce the dip angle of the longwall. The degree of dip angle of the longwall α_{lw} (compared to the true dip angle of coal seams α_{cs}) depends on the semi-oblique angle between coal faceand the strike of the coal seams (or the line of dip) γ.

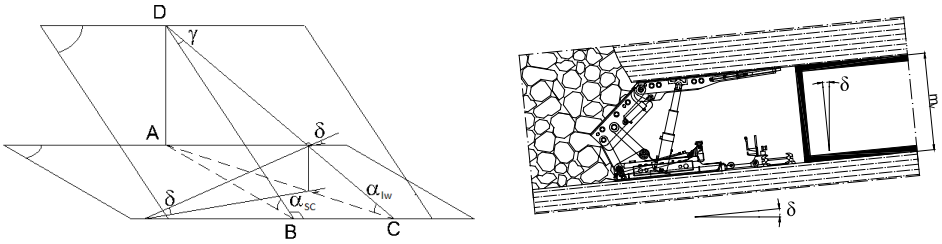

Figure 3. Diagram to calculate the dependence of the dip angle of longwall α_{lw} and the angle of the coalface into the semi-oblique angle γ

The relationship between the dip angle of the longwall α_{lw}, the true dip dip angle of the coal seam αv, inclined angle of the coal face δ with the semi-oblique angle of the coal face compared to the the line of dip -γ, is represented by the formulas:

$$\sin \alpha_{lw} = \sin \alpha v \times \cos \gamma; \sin \delta = \sin \alpha_{cs} \times \sin \gamma \quad (1)$$

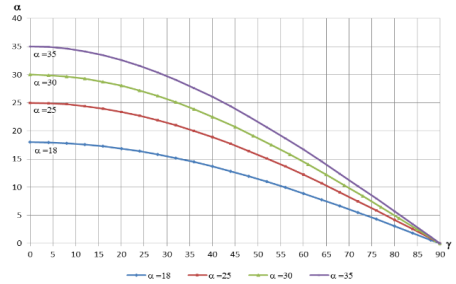

Figure 4. Chart of the dependence of the dip angle α_{lw} in the semi-oblique angle of longwall γ

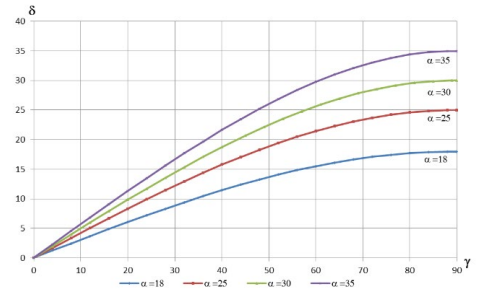

Figure 5. Chart of the dependence of the inclined angle of the coalface δ to the semi-oblique angle γ

Based on the chart in Figure 4, Figure 5 can be seen in the case of the longwall kiln perpendicular to line direction of coal seam (semi-oblique angle $\gamma = 0^o$), the slope angle of the longwall will be equal to the slope of coal seam. For example, if coal seams have dip angle $\alpha_{cs} = 25^o$ and thesemi-oblique angle $\gamma = 35^o$, the dip angle of the longwall will be 20^o, corresponding to a decrease of 5^o compared with the seam dip angle.

However, if set the conveyor gateway area of the longwall go ahead the air-return gateway area, we will create a semi-oblique angle as above, the coalface of longwall will tilt accordingly at an angle of about $\delta = 13 \div 14^o$, easy to happen risk, for example, failed roof, coal falling. Thus mining operations may stop and major reinforcement begin immediately.

To avoid this phenomenon, we can set the coal face in the opposite direction, The head area of longwallt is over the foot are of the longwall (Figure 6b) or the foot areas are still advanced ahead of the longwall but the coal face is straight (Figure 6a).

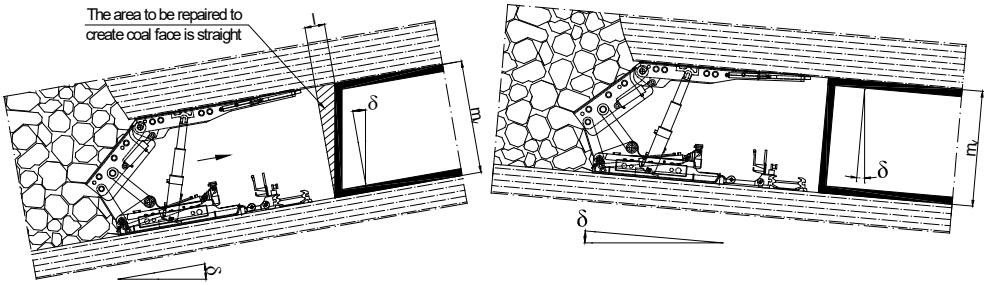

a, support case of longwall legs first *b, support case of longwall head first*

Figure 6. The type of coal face in a semi-obliqued longwall

Along with the layout of semi-obliqued longwall, the arrangement: supports - face conveyor (Figure 7a) is often preferred over the oblique form (Figure 7b) because the structure of the link between the face conveyor and the hydraulic anti-topple jacks (or hydraulic anti-slip device) is simpler, easier to fabricate and more durable, as well as the supports structure of the supports can be reduced significantly less.

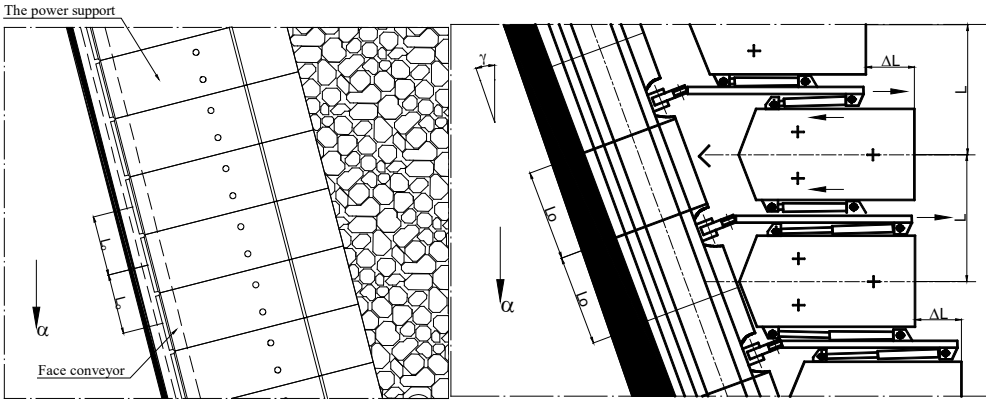

a, The power support - face conveyor are perpendicular in a semi-obliqued longwall *b, The power support - face conveyor are oblique in a semi-obliqued longwall*

Figure 7. The arrangement of the power support – face conveyor in a semi-obliqued longwall

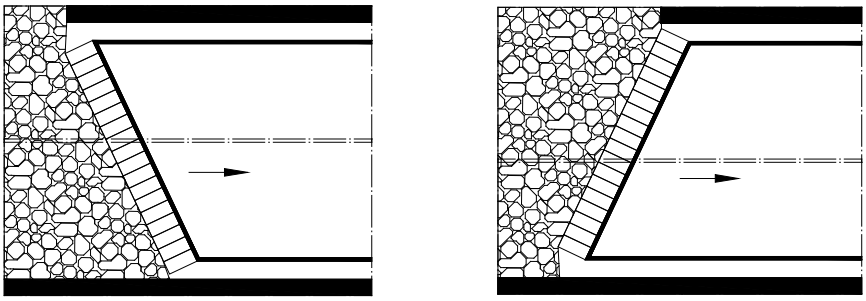

a, Longwall legs first *b, Longwall head first*

Figure 8. The arrangement of longwall on strike

However, the arrangement of mining in the form of the first part of the longwall goes ahead, the major disadvantage is that according to the mining schedule, the support system and the face conveyor will automatically move down, although it is not affected (or subjected to little) impact by the dip angle. Meanwhile, the coal face of the longwall has legs ahead, often with the opposite direction of movement, the support and the face conveyor move themselves upwards according to the progress of mining and effectively overcome the drift downwards [3, 4].

With the above arrangement, combined with the solution of using hydraulic system, anti-topple jacks and anti-drifting, the longwall has made relatively good exploitation, avoiding impacted slippery due to the influence of seam dip angle. Underground coal mine applied simultaneously with the above two solutions bring good results. For example, the Tuan Duc mine, Heilongjiang province, China used support HY-300, the KYBLK-70 scraper with combine machine KWB-3RW exploiting coal seams with average thickness of 2.75m, the 35º dip angle gives mining capacity of 350 thousand tons/year, labor productivity of 10 tons/work or Dong Vinh II mine, Hac Long Giang province using support ZZ4800 / 15/30, SGZ-764/2 × 200 and shearer MG250 / 601QWD in the longwall length of 114m to exploit coal seams with thickness 2.7m, dip angle 34º for a capacity of 1.580,000 tons/year, labor productivity reaches 45 tons/work shift [2].

3. Solution to organize diagrams of mechanized mining coal face in longwall.

This solution use a shearer in one direction from top to bottom. The movement direction of the machine from bottom to top is done in the form of no-load movement. The control of shearer in the direction from top to bottom has create the device thrust upward reduce the slippage effect of the face conveyor indirectly to reduce the slippage effect of the support because the support and the face conveyor are always linked together.

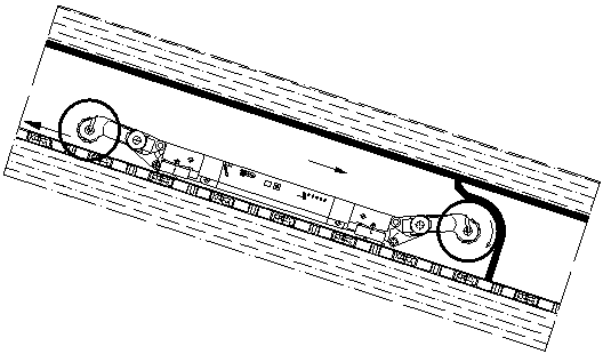

Figure 9. Diagram of shearer mining coal faceshearer

This solution has been applied at the longwall 10121, 12 mines of Lao Oc Co mine, Quy Chau province (China), exploiting seams with thickness 1.5 ÷ 5.5 m, average 3.5 m, dip angle 32 ÷ 45º. Synchronous equipment includes the ZFQ4000/15/26 power support, combine MXG-250/600QWD and the SZ730/400 face conveyor for a 190,000 tons/year capacity.

In order to reduce the influence of the seam dip angle, the coal mine has organized a mining diagram in one direction from top to bottom, the direction of the moving upwards is done in the form of no-load. Accordingly, when the coal face is cut, the previous cutting drum of the shearer cuts off the top coal, the next one cuts the flat coal, each one arranges a driver. Due to the steep angle of the longwall, during the time of coal mining, the machine operator must stand inside the column of anti-rig pillars, use the control to manipulate the control of the machine to avoid falling coal and rock. Due to the longwall dip angle is large, after cutting coal, the moving position of the support is at least 20 m from the combination of the shearer, to prevent rolling rock from causing accidents for workers at the time of moving the support apply the sequence from bottom to top.

4. Solution top coal cavingand reduce the dip angle of the conveyor gateway area of the longwall.

This solution is only applied to mechanized longwall top coal caving. Characteristics of the mechanized longwall top coal caving is that after the recovery, the exposed area of the support on the top coal is significantly reduced and under the influence of the dip angle, the rear base of power support tends to drift downwards in steep direction, making the support less stable.

In order to overcome this phenomenon, it is possible to arrange a conveyor gateway located on the side of the roof to create the scope of the foot of the longwall create a segment with a low slope angle (Figure 10). At the same time, increasing the recovery progress of coal (usually, after about 2 steps of exploiting and executing the recovery of coal down). This solution can improve the stability of the support by indirectly increasing the contact area of the support with the top coal and a part of the foot of the longwall with a low, almost non-slip slope will create a base for the support will not drift down.

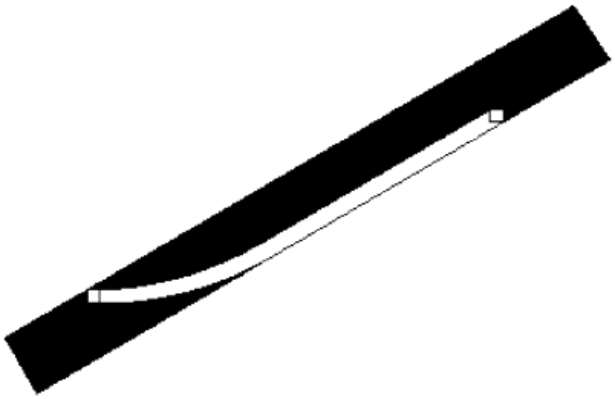

Figure 10. Preparation diagram to reduce slope angle at the foot of the longwall

This solution has been applied in the longwall 44407 at Vuong Gia Son coal mine - Noi Mong area to exploit soft coal seam (f = 1), thickness of 13.5 ÷ 23m, dip angle 38 ÷ 49º. The length of longwall is 145m, located at a depth of 260 ÷ 320m compared to the topographic surface with longwall height is 2.4m (the remaining coal is lowered to the ceiling) with a capacity of 53,000 tons/month. In addition, at the longwall 5335 U Lan mine - Noi Mong area has also applied mining mechanization technology in very soft coal seam conditions (f = 0.6 ÷ 1.2), average coal seam thickness 8.0 m, dip angle from 25 ÷ 35º. The length of the longwall according to the line of dip is 110 m, the depth of exploitation is -350 m compared to the topographic surface, the longwall output reaches 70,000 ÷ 80,000 tons/month.

II. Conclusion

Some solutions for enlarging the application scope of the fully mechanized longwall mining technology at underground coal mines as above, limiting the adverse effects of seam dip angle has been drawn from practical experience in underground mines around the world. The consideration of the application of the above solutions may help mechanized longwalls at Quangninh underground coal mines to improve the exploitation efficiency.

Reference material

1. Dr. Tran Xuan Hoa, “Nghiên cứu nâng cao mức độ cơ giới hóa và hiện đại hóa khai thác than hầm lò và định hướng ứng dụng cho các mỏ than hầm lò vùng Quảng Ninh”, Institute Of Mining Science And Technology- Vinacomin (2011).

2. Msc. Dang Thanh Hai, “Phát triển áp dụng cơ giới hóa đào lò và khai thác tại các mỏ than hầm lò vùng Quảng Ninh giai đoạn 2013 ÷ 2015, lộ trình đến 2020”, Institute Of Mining Science And Technology- Vinacomin (2016).

3. Msc. Tran Tuan Ngan, “Một số vấn đề về lựa chọn dàn chống, tổ chức khai thác và điều khiển đá vách trong khai thác vỉa dốc nghiêng, dốc đứng có chiều dày trung bình và mỏng”, Mining technology bulletin, **17** ÷ **23** (2016)

4. Коровкин Ю.А., Савченко П.Ф., Теория и практика длиннолавных систем, «Техгормаш» Москва (2004).

The possibilities of the revitalisation of post-mining areas – the Polish and Vietnamese examples

Zuzanna ŁACNY[1], Natalia KOWALSKA[1*] and Linh TRAN[1]

[1] AGH University of Science and Technology, Faculty of Mining and Geoengineering, Krakow, Poland

Abstract: Mining activity plays a significant role in the national economies of Poland and Vietnam. For centuries they have been determined by traditional industries, and now have to face restructuring processes after discontinuing mining operations. This article presents examples of post-mining sites in Poland and Vietnam, which require special revitalisation projects, because of their surroundings. The discussed examples show that post-mining areas have the potential for developing tourism, recreation and nature functions. The article indicates that it is necessary to balance the interests of the beneficiaries of revitalisation processes and, therefore, to keep in mind the overriding principle of planning - sustainable development. The authors emphasise that revitalisation projects lend a new quality to post-mining sites, which can become landmarks of entire regions, and build their new identity. Polish and Vietnamese experiences, supported by numerous examples, can provide both countries with inspiration for revitalisation projects while also serving as a warning against making similar mistakes in their implementation.

Introduction

Tourism plays an important role in the development of many regions around the world [1, 2]. The World Tourism Organization (UNWTO) has estimated that in 2020 revenues from tourism will reach the level of approximately 2 billion dollars. National and local-level sites and objects of exceptional (cultural and natural) value can be protected on the basis of internal regulations. The most valuable ones can receive a distinction by being included on the UNESCO World Heritage List (hereinafter referred to as the UNESCO List). Moreover, such inclusion, in addition to the guarantee of global recognition and significant financial revenues from tourism, has also some negative consequences. The most often cited one is an increase in its popularity resulting in excessive tourist traffic [3, 4]. Mass tourism which is based on the objects of world heritage is heading towards a negative impact on the cultural environment and contributes to natural resource degradation [5, 6]. Furthermore, one can also observe an increase in the prices of services and property, which to leads the depopulation of historic districts and changes in their function. Therefore, it emergences of artificial enclaves, thus resulting in the area losing its historical character [5]. Such a situation can be observed, for example in Venice, Florence, Barcelona, Rome, Prague and Kazimierz. The often results

* Corresponding author: nkowalska@agh.edu.pl

of aggressive commercialization are the local communities protests against the excessive development of tourist functions [7]. Decreasing tourist traffic involves the introduction of restrictions on visitor admission. Some cities have resources which allow them to apply alternative solutions, and thereby utilise areas previously regarded as unattractive. By utilising the potential of urban post-industrial areas, they are able to unload tourist traffic in cities (or parts of cities) included in the UNESCO list.

The aim of this paper is to present the possibilities for adapting (post)industrial areas in Kraków and Ha Long. The cities are party included on the UNESCO list and inextricably connected with mining activity. The paper indicates that the attractive development of post-mining areas may create an opportunity for reducing the intensity of tourist traffic by reorienting the direction of sightseeing from main attractions to the post-mining revitalised areas. Such an approach presents one of the possibilities of developing tourism in large agglomerations in a sustainable way. The methodology of the study relies on case studies. The Kraków and Ha Long cities were analyzed, respectively, where in addition to tourist sites included on the UNESCO World Heritage List, there are (post-)mining sites with potential for development.

1 The Cities of Kraków and Ha Long as the beneficiaries of the UNESCO list

The Global Destination Cities Index (2018) shows that historic cities with valuable sites and a rich past are the most often visited cities in the world. They constitute the top destinations in terms of cultural tourism [8]. This is also the case with Kraków. In 1978, the Old Town, including Wawel, Kazimierz and Stradom, making a unique urban and architectural complex, were included on the UNESCO World Heritage List. Other things which attract great numbers of visitors are museums, galleries, celebrations, customs (Lajkonik, Wianki), cultural events (Jewish Culture Festival), etc. [9].

The Quang Ninh Province with the city of Ha Long is an area with many unique geomorphological features and sites of historical importance (mainly archaeological) [10]. In 1994 and 2000 Ha Long Bay was included on the UNESCO list due to its exceptional landscape and geological values.

Tourist traffic intensifies every year in Kraków and Ha Long. In 2018, Kraków was visited by 13.5 million tourists [11], while the Quang Ninh Province by 12.2 million people (including 6.93 million visiting Ha Long in 2017) (Figures 1-4). The growing number of visitors poses a problem for the functioning of these cities.

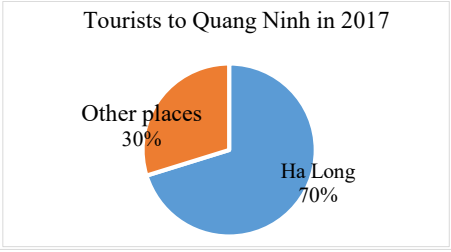

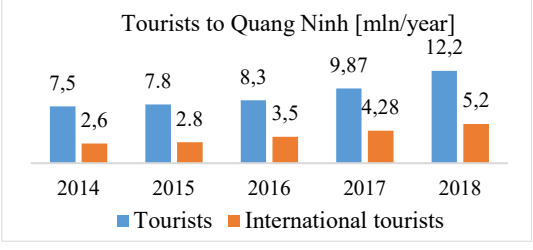

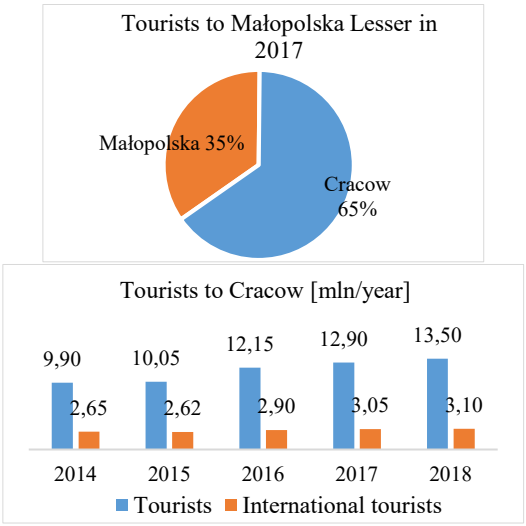

Fig. 1-4. Tourists in Quang Ninh Province, Małopolska Region and Kraków [11-12]

2 The potential of urban post-industrial sites to create tourist attractions

Kraków and Ha Long would benefit from a policy facilitating the control of tourist traffic and sustainable tourism management, i.e. one which minimises the negative impact of the attractions on the environment (natural and cultural values and local community). The necessity to develop tourism based on the principles of sustainable development is highlighted in the Strategy for Tourism Development in Kraków 2014-2020 [13] and the Environmental Report for the Quang Ninh Province [14]. Nowadays, it can observe more intense efforts to utilise post-industrial sites for tourist purposes on a global scale [15]. The study carried out by Kaczmarska et al. [16] has shown that industrial relics used for tourist purposes are enjoying the interest of visitors and tourists. Traditional tourist traffic is increasingly often being complemented by niche forms of tourism, which penetrate into all spheres and levels of landscape in a way that is difficult to control [17]. There are many known cases of post-industrial sites which enjoy such interest, e.g. Kadzielnia in Kielce [18], Park Buttes Chaumont in Paris [19], etc. The literature highlights the importance of developing post-industrial areas in city centers due to their location and transport accessibility [20, 21]. The use of former mining sites for new investments translates into a number of benefits, such as counteracting the excessive replacement of urban green areas with buildings, protecting animate and inanimate nature, protecting material goods (including cultural landscape) as heritage sites, creating jobs, etc. The authors would like to especially emphasise that undeveloped post-mining sites often cause accidents (falls, drowning, etc.) which forms another reason for their revitalisation.

Appropriate landscape management is one of the priorities of the spatial policy in the European Union. Goal 11 of the Agenda for Sustainable Development refers to access to safe green areas which foster social integration in urban areas, strengthening efforts to protect and safeguard cultural and natural heritage, and sustainable urbanization conducive to social inclusion and participation [22]. The New Charter of Athens underlines the necessity to rehabilitate the degraded urban fabric [23]. The development of tourism has a crucial role in the processes of spatial planning and strategic development [17].

In view of the above, it appears justified to combine the two increasingly popular trends of managing closed mine pits for tourist purposes and balancing tourist traffic, as its excess has a negative impact on the (natural and human) environment. Kraków and Ha Long are facing the problem of intensified tourist traffic but have an opportunity to tap into the potential of post-mining sites to regulate this traffic. This issue will be discussed in more detail later in the article.

3 The history of the Liban Quarry and the present situation at the post-industrial site

The Liban Quarry (Figure 5), which is the subject of our discussion, is part of the Krzemionki Podgórskie, fault-block hills located in the southern part of Kraków, mined from the 14 century for carbonate raw materials used for construction purposes (Ostręga, 2004 as cited in Kotewicz, 1981) [21, 24]. 7 open pit mines has operated in the Krzemionki area. The Liban Quarry is located at a distance of 3 km to the Main Square, in the Podgórze district (which was previously a town).

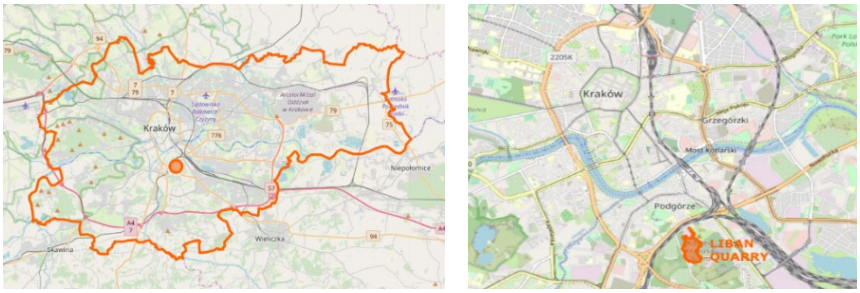

Fig. 5. Liban Quarry location in Poland and Kraków (Source: Own work based on OpenStreetMap)

The Liban limestone quarry (Figure 6) was established in 1873. During World War 2 (1942 – 1944) the Nazi-German Baudienst Camp operated the pit. Mining ended in 1986 due to the significant environmental burden associated with it (air pollution caused by lime burning). In 1987, the "Krzemionki" mining area was dissolved. Between 1988 and 2004, the quarry was used as a storage site for construction materials and housed offices of Public Services Companies [21]. At present (March 2019), the quarry is managed by the Public Utility and Transportation Infrastructure Office in Kraków, and is unavailable for unauthorised persons.

The quarry is characterised by an ecological landscape, where biological elements can function naturally as a result of natural succession. The pit is a model example of leaving a post-industrial site to spontaneous succession, resulting in the emergence of uncommon plant communities. The authors would like to point out that this type of landscape is not very cost-intensive, with its management not involving high spending, and human activity being of secondary importance to its formation. In addition to its attractive cultural landscape, the quarry features valuable historical objects (including the "Szczęść Boże" mine foreman room, vertical furnaces (Figure 7), as well as silos, a field hospital, and a forge, which are deteriorating due to the lack of appropriate maintenance. The pit has also been observed to serve as a place for dumping waste (for instance the toys) (Figure 8).



Fig. 6. The view of the interior of the Liban Quarry (Source: Z. Łacny)

Fig. 7. Vertical lime furnaces in the pit (Source: Z. Łacny)

Fig. 8. The quarry as an illegal waste dump (Source: N. Kowalska)

The Strategy for Tourism Development in Kraków 2014-2020 recognises the resources of Podgórze as having untapped potential for the development of new tourism products and creating opportunities for action for the spatial deglomeration of tourist traffic. Despite its historical and natural value, the quarry (March 2019) has yet to be managed properly. The authorities of Kraków are aware of the problem of excessive tourist traffic in the city. On 5 April 2019, at the UNWTO Mayors Forum for Sustainable Urban Tourism - "Cities for all: building cities for citizens and visitors," Kraków signed the Lisbon Declaration. By doing so, it agreed to adjust its tourist development in a sustainable way, which can help distribute tourist traffic through appropriate planning. This declaration is consistent with the work on a strategic document "The Sustainable Tourism Policy of Kraków" which will be implemented starting from 2021 [25].

4 The history of Ha Long and the current situation at the mining site

Ha Long Bay has unique geomorphological features, ecosystems and biological diversity. As the site has been included two times on the UNESCO list, the Bay also made it to the list of new wonders of the world. Ha Long is an important economic and cultural centre in Vietnam and a key destination for foreign tourists. Despite its many benefits, tourism in Ha Long is associated with excessive property prices, high costs of goods and services, congestion, waste generation, pollution of water, air, and soil, increased noise and reduced availability of natural landscapes. Ha Long is undergoing extensive development as part of the northern development triangle in Vietnam, driven by the mining industry, tourism, and shipping. The literature highlights the necessity for people holding positions of authority to minimise the negative impact of tourism on the natural environment [26, 27].

The Quang Ninh Province is characterised by the largest number of coal mines in Vietnam (Figure 9). Hard coal has been continuously mined there for 160 years [28]. It is estimated that this province holds mineral resources amounting to 3.5 trillion tonnes. One of the largest mines, the Nui Beo mine (owned by the Vinacomin concern), borders directly on Ha Long Bay coast. In 2012, the Nui Beo Mine started the transition from open-pit to underground mining due to geological conditions, environmental standards, and increased tourist traffic in its immediate vicinity. The project cost VND 5.3 billion (approximately PLN 0.9 million), facilitating an output of 2 million tonnes of coal and extending the viability of the plant by 34 years.

Fig. 9. The locations of mining plants near Ha Long Bay (Source: Own work based on Google maps)

In the Hon Gai mining region in Quang Ninh Province, the situation is typical of Vietnamese hard coal mining industry, with mining sites being located in the immediate vicinity of residential areas (Figure 10) [28]. Therefore, the appropriate development of this land, after discontinuing the mining activity, is of crucial importance given the quality of life of its residents.

Ha Long Bay started to gain popularity in the early 20th century. This was, among other things, due to the mining activities carried out by French colonisers. After being included on the UNESCO list in 1994, the number of tourists in Ha Long saw a significant increase (from 236,000 in 1996 to 2.64 million in 2008), and the city became a destination enjoying the fastest growing tourist interest in Vietnam. Despite the apparently clashing tourist and mining activities in Ha Long, actions are being taken to unite these two seemingly contradictory development trends. In 2006, the Quang Ninh Department of Tourism organised pilot tours of mining plants intended to familiarise the visitors with the part and parcel of miners' work and mining technology [29].

5 The possibilities of revitalising the post-mining areas in Kraków and Ha Long

In Kraków, except to Krzemionki, there are also other mine pits, developed to serve recreational functions, which are, therefore, intended for other audiences than, for example, the Old Town. The Liban Quarry, on the other hand, with its historical and natural values, meets the expectations related to cultural tourism. Ostręga [21] in her doctoral dissertation, proposes a concept of quarry development with cultural and educational aims in mind (preserving valuable historical sites, organising thematic exhibitions), supplemented with natural and recreational functions (preserving animate and inanimate nature, creating cycling and walking paths, and a climbing wall). Currently (April 2019), Krakow is applying for a subsidy for the revitalisation of the quarry, which is to include the establishment of a city park with an area of nearly 20 ha, which will feature a cinema, a climbing wall, suspended paths, a museum, and a gallery.

Galla [30] points to the tourism carrying capacity of Ha Long being at its limit. Most visitors stay for a short time (often just for one day), maximising the use of resources while making a minimum economic contribution to the local economy. There is a need for creating tourism products which would attract some tourists to Ha Long Bay and encourage them to stay in the city for longer. This will make it possible to preserve natural heritage while promoting industrial, economic, and tourism development. The author proposes to establish an Ecomuseum at the site of the pits, the activities of which would involve local communities.

The RAME - Mining and Environment in Vietnam programme was implemented from 2007 to 2010. Its objective was to develop an integrated planning concept and methodology

in terms of developing the post-mining area. Under that project, several planning criteria were determined to make decisions about the development of post-mining sites. A concept for development was devised on the basis of the defined criteria. It was proposed to introduce recreational and sports functions and to create a public park in place of the present Chinh Bac Nui Beo waste rock storage facility [28].

Conclusions

Public green areas are desirable elements in the urban fabric of large cities, such as Kraków. These include areas with recreational as well as cultural and educational functions – such as the Liban Quarry. On the other hand, in the case of Ha Long Bay, which struggles with the rapidly growing number of tourists, the appropriate development of the nearby post-mining sites can contribute to minimising the negative impact of excessive tourist traffic on valuable natural areas and to engaging local communities in the development of the city. Taking into account the solutions proposed in the literature and presented in this paper, it appears reasonable to develop urban post-mining sites. This will undoubtedly contribute to:

- putting into use unused, valuable urban areas (location and historical value);
- protecting UNESCO sites against excessive tourist traffic;
- involving local communities in the planning processes;
- improving safety on post-mining sites;
- improving the image of the mining industry (completed revitalisation projects);
- minimising the negative impact of tourism on the natural environment and local resources – sustainable tourism;

Due to varying socio-economic, cultural, and natural conditions, indiscriminate transfer of solutions applied in one country to another is not viable. Nevertheless, some planned or already-implemented solutions in post-mining pits in Vietnam can be taken into consideration and applied in Polish conditions, and vice versa. The authors would like to point out that the mining facilities in the Quang Nihn Province, as in the case of the Kraków quarry, should take into account, already at the planning stage, bits of the history of mining. It forms the basis for the creation of a cultural tourism package based on industrial heritage. Furthermore, it is crucial to intentionally use the potential of nature in reclamation processes by providing natural functions and opportunities for the enclaves of wildlife to develop. Already at the planning and subsequent stages of Liban Quarry development, local communities should become involved in the decision-making processes, as it was proposed in Ha Long. This will have a positive impact on the building of relationships and social identity, which, in turn, will translate into residents' caring about their surroundings, and consequently, help to protect natural and cultural heritage.

The exchange of experience will make it possible to avoid mistakes connected with tourist traffic management and to jointly develop model solutions for the implementation of sustainable tourism in post-industrial sites. As presented in the conclusions, post-mining sites have tremendous potential, not only as new attractive destinations but also as places which allow authorities to reduce tourist traffic in some more popular areas. The presented examples suggest the possibility of achieving attractive development through the use of natural and cultural heritage while taking into account the potential of post-industrial sites. It is also necessary to take into consideration environmental and socio-economic conditions which guarantee the long-term success of such projects. It is estimated that the revitalisation of the Liban Quarry will take place in the near future (probably in 2021). Therefore, it is important to pursue a policy which is aimed at redirecting tourist traffic and utilising mining heritage when planning further tourism development. It is also crucial to monitor traffic and determine

the tourism absorptive and carrying capacity of the newly created attractions (products), to protect their value. These measures will make it possible to continuously learn from experience, and to identify and avoid potential mistakes.

Acknowledgments

The paper was presented during the 5th POL – VIET International Conference Scientific-Research Cooperation between Vietnam and Poland, 08-10.07.2019, AGH UST, Krakow, Poland.

References

1. E. De Kadt, *Tourism: Passport to Development? Perspectives on the social and cultural effects of tourism in developing countries* (Oxford, 1979)
2. T. N. Sequeira, P. Maçãs Nunes, Applied Economics Journal **40,** 18, 2431-2441 (2008)
3. J. Caust, M. Vecco, Journal of Cultural Heritage **27**, 1-9 (2017)
4. V. Schmutz, M. A. Elliott, Sustainability **8**, 3, 261 (2016)
5. Z. Kruczek, Turystyka Kulturowa 3, 29-41 (2018)
6. B. Szmygin, Ochrona Zabytków 1-4, 167-177 (2013)
7. J. Kowalczyk-Anioł, P. Zmyślony, Turystyka Kulturowa 2, 7-36 (2017)
8. Ł. Gaweł, Turystyka Kulturowa 10, 39-52 (2013)
9. R. Seweryn, Turystyka kulturowa w przyjazdach do Krakowa [in:] A. Nowakowska, M. Przydział, *Turystyka w badaniach naukowych. Prace ekonomiczne* (Rzeszów 2006)
10. A. Galla, Culture Heritage, Man and Tourism 135 (2002)
11. Małopolska Organizacja Turystyczna, http://www.mot.krakow.pl, access [04.05.2019].
12. Nhattruongphat.vn, Tiềm năng lớn khi đầu tư dự án Shophouse Europe Hạ Long, https://nhattruongphat.vn, access [25.03.2019]
13. Urząd Miasta Krakowa, Strategia rozwoju turystyki na lata 2014-2020 (2014)
14. Quang Ninh Provincial People's Committee, Final Report. Environmental planning of Quang Ninh Province to 2020 Vision to 2030 (2014)
15. M. Denis, Studia Miejskie, **26**, 25-37 (2017)
16. A. Kaczmarska, A. Przybyłka, Prace Komisji Krajobrazu Kulturowego, **14**, 207-228 (2010)
17. U. Myga-Piątek, Problemy Ekorozwoju, **6**, 1, 145-154 (2011)
18. W. Zgłobicki, J. Warowna, B. Baran-Zgłobicka, G. Gajek, W. Jezierski, Turystyka Kulturowa, **6**, 51-67 (2015)
19. U. Strohmayer, Cultural Geographies, **13**, 4, 557-576 (2006)
20. K. Gasidło, Zeszyty Naukowe. Architektura/Politechnika Śląska, **52**, 65-80 (2013)
21. A. Ostręga, Sposoby zagospodarowania wyrobisk i terenów po eksploatacji złóż surowców węglanowych na przykładzie Krzemionek Podgórskich w Krakowie. Rozprawa doktorska (AGH w Krakowie, Wydział Górnictwa i Geoinżynierii 2004)
22. United Nations, The 2030 Agenda for Sustainable Development (New York, 2015)
23. The European Council of Town Planners (ECTP), The New Charter of Athens 2003: The European Council of Town Planners' Vision for Cities in the 21st century *(*Lizbona 2003)
24. R. Kotewicz, *Z dziejów przemysłu Krakowa w latach 1918 – 1939* (Kraków, 1981)
25. Kraków współtworzy nowy model odpowiedzialnej turystyki, http://krakow.pl, access [4.052019]
26. K. Lloyd, C. Morgan, Journal of Heritage Tourism, **3**, 1, 1-17 (2008)
27. H. L. Pham, Asia Social Science, **8**, 8, 28-39 (2012)

28. K. Broemme, H. Stolpe, C. Jolk, S. Greassidis, A. Borgmann, B. Zindler, T. Mien, Development of methods for post-mining land use planning for coal mines in urban areas in Quang Ninh, Vietnam. Paper presented at the Hu, Zhenqi: Legislation, Technology and Practice of Mine Land Reclamation (Conference Beijing International Symposium LRER. Leiden: CRC Press/Balkema 2014)
29. N. D. Hoa, N. Chesworth, L. Jolliffe, Planning for the future: tourism options for an open pit coal mine at Ha Long Bay, Vietnam. [in:] M. V. Conlin, L. Jolliffe (Eds.), *Mining Heritage and Tourism: A Global Synthesis*, Routledge Advances in Tourism 183-194 (2010)
30. A. Galla, Humanities Research, **9**, 1, 63-76 (2009)

Assessing the current status of underground mine ventilation system in ThanhCong-CaoThang area, HonGai coal company, QuangNinh region, Vietnam

Cao Khai NGUYEN[1,*], Van Thinh NGUYEN[1], Van Quang NGUYEN
[1]Ha noi University of Mining and Geology, Faculty of Mining, Vietnam

[*]Corresponding author: nguyenkhaimdc@gmail.com

Abstract. In underground mine ventilation, there are many causes affecting the efficiency of mine ventilation, even affecting mine safety. In order to have an effective mine ventilation system, the research and evaluation of mine ventilation, in order to get timely solutions to improve the efficiency of mine ventilation, is essential and must be done. regularly.

Thanh Cong - Cao Thang coal mine area of Hon Gai Coal Company, Quang Ninh region, Vietnam is a mine exploited underground. The nature of this mine is the consolidation (connecting) of Thanh Cong areas and CaoThang areas in the period of 2016. After consolidation into Thanh Cong - Cao Thang mine, many factors in the mine ventilation system of The mine site is altered and affects the efficiency of mine ventilation. This article has analyzed and evaluated the current status of Thanh Cong - Cao Thang Area Ventilation System to help research and select appropriate solutions to promptly improve the efficiency of mine ventilation and ensure security, ensure a safe environment and reduce the cost of mine ventilation.

Keywords: Mine ventilation, Working mode of air fan, Main air fan, Thanh Cong-Cao Thang area.

1. Characteristics of current mining and ventilation

Thanh Cong - Cao Thang area is digging from -240 or higher, exploiting from -220 or higher. In general, the mining situation in 2017 with the mine capacity for the fourth quarter is about 405835 tons/quarter, the mine must mobilize 9 long mirror and 11 mirrors. In fact, this construction area consists of 2: Thanh Cong area and Cao Thang area which are merged into one. Cao Thang area is currently exploiting at -160, while Thanh Cong area is exploiting at -220 or more, these two areas are connected by a kiln connecting level -160 from Thanh Cong main well to road through the level -160 Cao Thang area [Ventilation room, 2017].

Currently, the mine area is being ventilated by 03 main fan stations: Thanh Cong area with fan station at the door of +25 (fan of code FBDCZ-8-N0 -24 / 2x315kW) and Cao Thang with 2 stations fans include: fan station at the door tunnel level +20 and fan station at the door tunnel level +29 (with the same fan type FBDCZ-4-N0 -13 / 2x22kW). Wind network diagram is shown as in Figure 1 and Figure 2 ventilation diagram [Tran Xuan Ha, Nguyen Cao Khai, 2017]. In general, Thanh Cong - Cao Thang area shows that the ventilation work is relatively convenient, the fan stations are still working at low capacity as 2 fan stations in Cao Thang area working at the small wing mounting angle. Most (-2.5) while the fan in Thanh Cong area has just worked at the corner of the wing 35^0, also ensure safe ventilation and meet the demand for production for the mine.

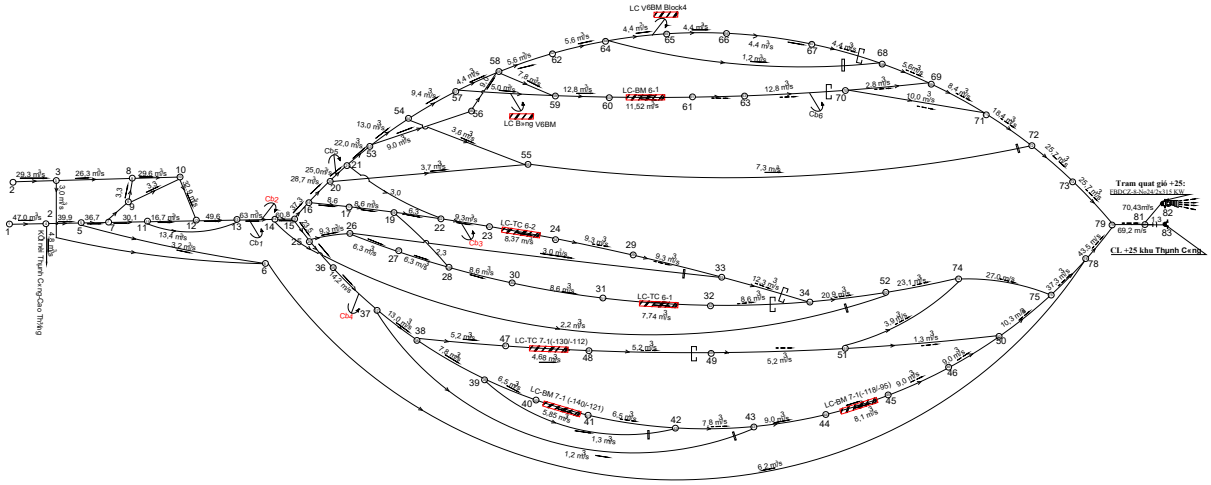

Figure 1. Ventilation diagram of Thanh Cong area mine

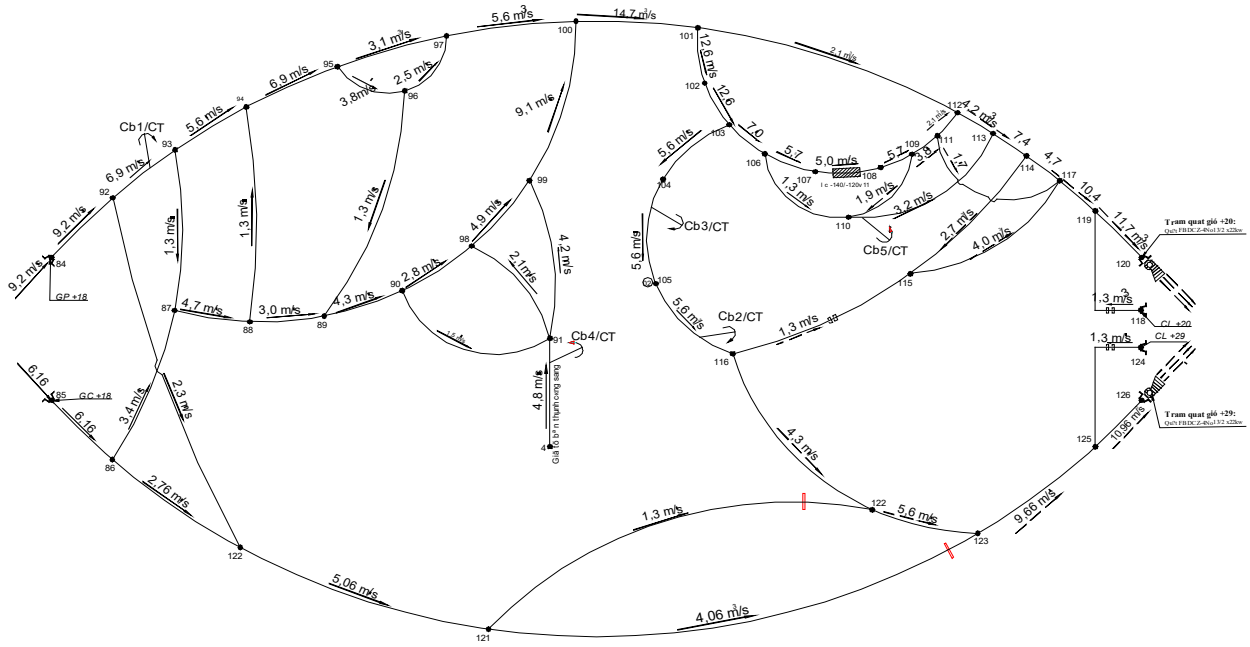

Figure 2. Ventilation diagram of Cao Thang area mine

2. Ventilation calculation for area mine (Thanh Cong - Cao Thang)

2.1. Calculate general air flow for the mine

To calculate ventilation for Thanh Cong-Cao Thang area, we apply the formula [Tran Xuan Ha et al, 2014]:

$$Q_m = 1{,}1(K_{sl}.\Sigma Q_{lc}+\Sigma Q_{cb}+\Sigma Q_{ht} + \Sigma Q_{rg});\ m^3/s \qquad (1)$$

Inside:

1.1 - The coefficient refers to the uneven distribution of wind in wind currents.

K_{sl}- Coefficients to account for the increase in output of the longwall (select kt = 1.1).

ΣQ_{rg} - Total leakage wind flow in mine, m^3/s.

ΣQ_{lc} - Total amount of wind flow required for the furnace oven, m^3/s.

ΣQ_{cb} - Total amount of wind flow needed for the digester mirror, m^3/s.

ΣQ_{ht} - Total amount of wind flow required for station, m^3/s.

Calculating the wind flow for long mirror

With the results of calculating the wind flow for long mirror according to 4 factors: According to the largest number of employees; According to output (methane production); According to dust factor; According to the largest amount of explosives, we choose the air flow for the long mirror according to the biggest factor. Results of total wind flow calculation for 9 long mirror: $\Sigma Q_{lc} = 41,0\ m^3/s$.

Calculating the wind flow for the prepareding mirror

With the results of calculating the air flow, the kiln mirrors prepared according to 4 factors; According to the amount of explosives; According to the escape of methane gas escaping in the oven prepared mirror; According to the largest number of people working and according to the dust factor, we choose the air flow for the oven mirror to prepare according to the biggest factor. Results of calculation of total air flow for 11 prepared furnace mirrors: $\Sigma Q_{cb} = 18,3\ m^3/s$.

Wind flow calculation for pump tunnels and power stations

Based on the capacity and the number of stations we calculate the total wind flow for the stations: $\Sigma Q_{cb} = 7,15\ m^3/s$.

Calculating leakage wind flow in the mine

Based on the number of wind gates and walls in the mine area, we calculate the total leakage of wind flow in the mine: $\Sigma Q_{rg} = 13,1 m^3/s$

Calculate the total wind flow for the mine

The results of calculation of wind flow for the mine are as follows: [Tran Xuan Ha, Nguyen Cao Khai, 2017]

$Q_m = 1,1(1,1 \times 41,0 + 19,3 + 7,15 + 13,1) = 93,13\ m^3/s$

2.2. Calculate the distribution of wind

Thanh Cong - Cao Thang is ventilated by 03 fan stations located at the door of the furnace: Level +25 is fan type FBDCZ-8-No24/2x315kW; The level +20 and +29 is the fan type FBDCZ-6-No13/2x22kW. So we have to calculate the wind flow for 03 fan stations to take charge, to determine the working mode of 03 main fans above. On the basis of wind consumers, the wind-wind network system, we distribute the corresponding wind to the wind branches undertaken by 3 fans. Results of wind flow calculation for branches for fans are as follows: [Tran Xuan Ha, Nguyen Cao Khai, 2017]

- Fan 1 (+25: FBDCZ-8-No24/2x315kW): $Q_{m1} = 70,43\ m^3/s$;
- Fan 2 (+29: FBDCZ-6-No13/2x22kW): $Q_{m2} = 10,96\ m^3/s$;
- Fan 3 (+20: FBDCZ-6-No13/2x22kW): $Q_{m3} = 11,74\ m^3/s$;

The results of wind distribution calculation are shown in figures 1 and 2.

2.3. Calculation of mine lowering

As shown in Figure 1, the mine site has 4 main winds. To determine the lower pressure of the mine, we calculate the low pressure of the wind currents and apply the formula [Tran Xuan Ha et al, 2014]:

$$h_m = \sum h_{ms} + \sum h_{cb}, mmH_2O \quad (2)$$

In which:

$\sum h_{ms}$: The total hypotension is caused by the frictional resistance of the segments that follow each other in a wind flow, calculated from the beginning to the end point. This pressure lowering is calculated according to the formula [Tran Xuan Ha et al, 2014]:

$$h_{ms} = \alpha_i \frac{L_i.P_i}{S_i^3}.Q_i^2 \ ; \text{mm } H_2O \quad (3)$$

In which:

α_i: The aerodynamic resistance coefficient in the ith tunnel on the air flow, kGS^2/m^4;

L_i, P_i, S_i: Length, circumference, cross section of tunnel i;

Q_i: The amount of wind going through the ith tunnel, m^3/s.

$\sum h_{Cb}$: The total hypotension due to local resistance calculated by a wind flow, in fact is often taken from (10 - 25%) H_{ms}.

The results of lowering the flow of the following lines [Nguyen Cao Khai et al, 2017]:

Lowering the flow caused by the fan FBDCZ-8-No24 at +25 is responsible for:

h_1 = 223,01 mmH_2O (through 2 serial tunnel furnace: LCBM7-1 level -140 / 1-121 and LCBM7-1 level -118 / -95);

h_2 = 97,19 mmH_2O (LCTC6-2);

h_3 = 197,29 mmH_2O (LCBM6-1 và LC bằng V6 BM);

h_4 = 213,77 mmH_2O (LCTC6-1);

h_5 = 220,25 mmH_2O (LCTC7-1);

h_6 = 215,94 mmH_2O (LC V6 BM Block4).

Lowering the flow caused by the fan FBDCZ-6-No13 at +29 is responsible for:

h_7 = 90,86 mmH_2O.

Lowering the flow caused by the fan FBDCZ-6-No13 at +20 is responsible for:

h_8 = 110,43 mmH_2O (through long mirror: LC V11 CT -140/-120).

Balance of low pressure mine:

Here, only the +25 fan station section must be equal to the low voltage, because there are up to 6 main stream. There are 2 fan stations at +29 and +20 with only one main stream. In order to balance the pressure lowering of the mine, we apply a balanced method of using wind windows to adjust. The lower pressure of the mine is chosen as h_1 = 223.01 mmH_2O.

2.4. Calculation determines the working mode of the main fans

Determine the wind flow of fans to create

- Calculation of fan wind flow to be created, we apply the formula [Tran Xuan Ha et al, 2014]:

$$Q_q = K_r Q_m, {}^{m^3}\!/_{S}. \quad (4)$$

In which:

K_r - Leakage coefficient at fan station, semi-fixed fan station get K_r = 1.15

Q_m - Airflow required for the whole mine, m^3/s

The results of calculating the airflow for fans are as follows:

- Fan 1 (+25: FBDCZ-8-No24/2x315kW): Q_{q1} = 81,0 m^3/s;
- Fan 2 (+29: FBDCZ-6-No13/2x22kW): Q_{q2} = 12,6 m^3/s;
- Fan 3 (+20: FBDCZ-6-No13/2x22kW): Q_{q3} = 13,58 m^3/s;

Determine lowering the fans to create

Lowering the pressure of the fan is calculated according to the formula [Tran Xuan Ha et al, 2014]:

$$H_q = (k_1.R_m + R_{tbq}).Q_q^2 \text{ , } mmH_2O \quad (5)$$

In wich:

k_1- the coefficient refers to the leakage at the fan station, $k_1 = 1/k_r^2$, k_1 = 0.76

R_m - mine resistance, kμ; For mine site, we have the resistance of kiln branches corresponding to 3 fan stations as follows: R_{m1} = 0.04496 kμ; R_{m2} = 0.75592 kμ and R_{m3} = 0.80118 kμ.

R_{bq}- internal fan fan resistance (Rtbq = a. π/D^4), kμ. For the main fans of the mine site, we have the resistance of the kiln branches corresponding to 3 fan stations as follows: R_{tbq1} = 0.0047; $R_{tbq2} = R_{tbq3}$ = 0.055;

Instead we have the Lowering the pressure of the fans to create:

- Fan 1: +25 (FBDCZ-8-No24/2x315kW): h_{q1} = 255 mmH_2O;
- Fan 2: +29 (FBDCZ-6-No13/2x22kW): h_{q2} = 100 mmH_2O;
- Fan 3: +20 (FBDCZ-6-No13/2x22kW): h_{q3} = 121 mmH_2O.

Determines the working mode of the main fans

The calculation and determination of the working mode of the main fans are as follows: [Nguyen Cao Khai et al, 2017], [Nguyen Cao Khai et al, 2015]

+ Determining equations and building characteristic lines of mines:

The equation of the mine characteristic curve of the branches to 3 fan stations is as follows:

- Fan 1 (FBDCZ-8-No24/2x315kW): $h_1 = 0{,}03887.Q^2$;
- Fan 2 (FBDCZ-6-No13/2x22kW): $h_2 = 0{,}6295.Q^2$;

- Fan 3 (FBDCZ-6-No13/2x22kW): $h_{q3} = 0{,}6639.Q^2$.

+ Working mode of main fans

The results determine the working mode of the main fans as follows:

- Fan 1 (+25: FBDCZ-8-No24/2x315kW), as shown in Figure 3

With fan working parameters: Fan flow generated: Q_{ct1} = 88 m^3/s; Fan-induced pressure drop: h_{ct1} = 305 mmH_2O; Wing mounting angle of impeller: $\theta = 35^0$ and Fan performance: η = 0.73.

- Fan 2 (+29: FBDCZ-6-No13/2x22kW), as shown in Figure 4.

With fan working parameters: Fan flow generated: Q_{ct2} = 15,3 m^3/s; Fan-induced pressure drop: h_{ct2} = 147,4 mmH_2O; Wing mounting angle of impeller: $\theta = -5^0$ and Fan performance: η = 0.72.

- Fan 3 (+20: FBDCZ-6-No13/2x22kW), as shown in Figure 5.

With fan working parameters: Fan flow generated: Q_{ct2} = 15,4 m^3/s; Fan-induced pressure drop: h_{ct2} = 149 mmH_2O; Wing mounting angle of impeller: $\theta = -5^0$ and Fan performance: η = 0,73.

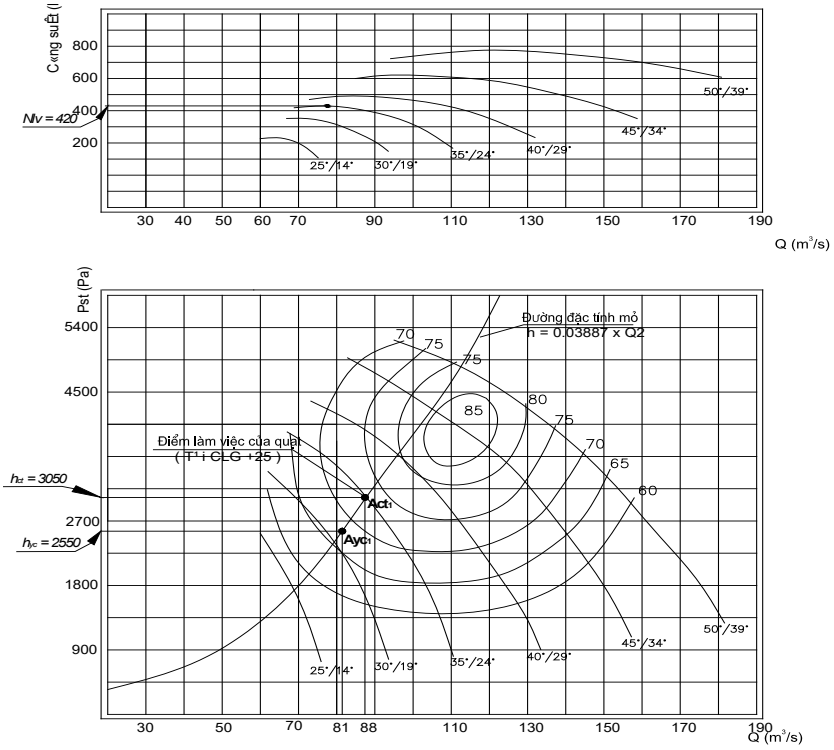

Figure 3. Graph of determining the working mode of the fan FBDCZ-8-No24 at the door of tunnel the level +25 Thanh Cong Area

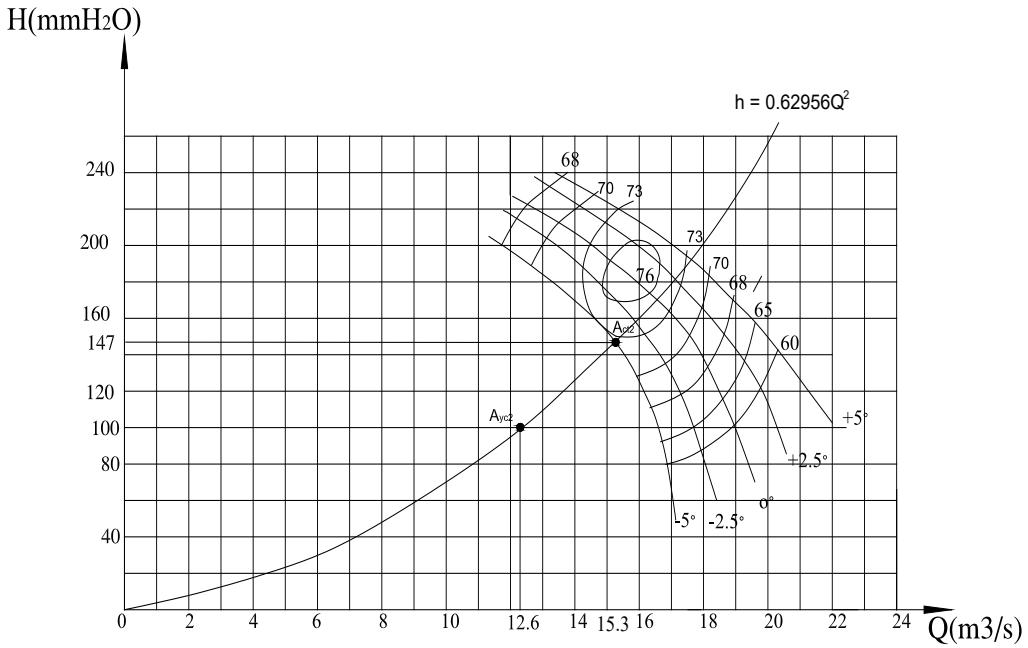

Figure 4. Graph of determining the working mode of the fan FBDCZ-6-No13 at the door of tunnel the level +29 Cao Thang Area

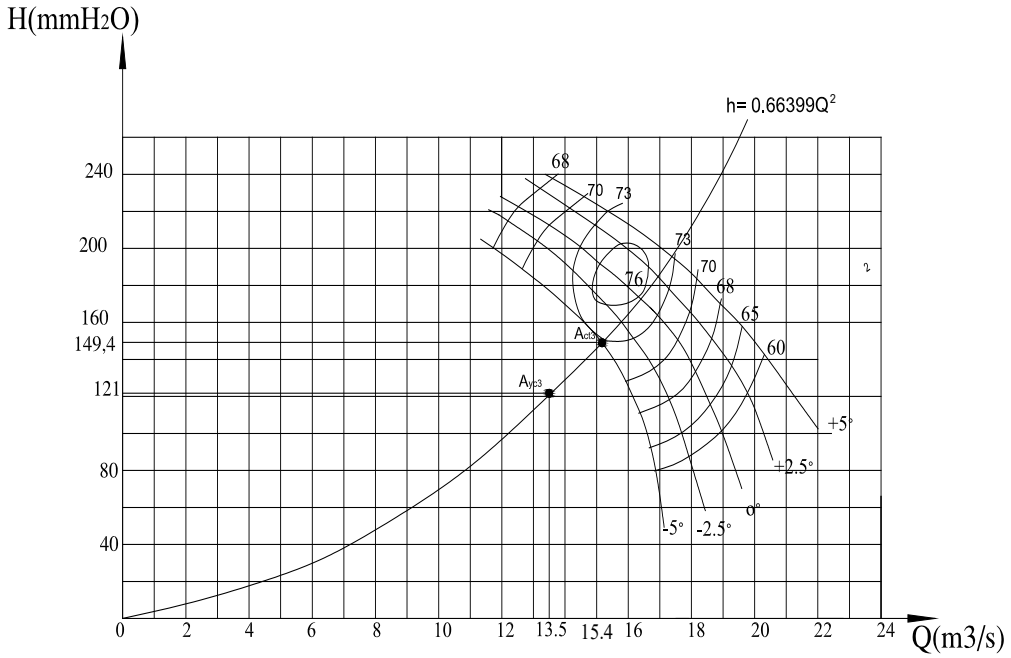

Figure 5. Graph of determining the working mode of the fan FBDCZ-6-No13 at the door of tunnel the level +20 Cao Thang Area

3. Results of assessment of the current status of the mine ventilation system

The results of the survey and assessment of the current ventilation system are as follows:

- General ventilation method for existing mine is the method of use suck ventilation. This is a reasonable ventilation method. The diagram of the wind network is generally quite complicated, with many cross branches.

- The quality of ventilation for longwall kilns is generally not very good about the amount of wind needed to be supplied, because in the 7 kilns operating of mine, there are 3 longwall ovens that still lack wind, although not big, on the other hand the content of toxic gases or harmful (CO_2 and CH_4) are all below the permitted limit.

- In terms of microclimate conditions, the quality of ventilation is guaranteed, however, the humidity is quite high. Therefore, in general, microclimate conditions in the mine are not comfortable.

- For the prepared oven mirrors, it is similar to that in the longwall oven, the quality of ventilation for the new kiln mirrors basically ensures the minimum amount of wind and the ability to dilute toxic gases, explosive gases, but about microclimate conditions are not really good because the humidity is still high.

- The quality of ventilation works is generally not good. At the fan station, there is still a lack of fan window to check the working mode of the fan (flow and low pressure). On the other hand, three main wind gates at the door level of +25, +29 and +20, where 3 main fan stations are located, do not guarantee airtight quality. Therefore, the amount of wind leakage through these three wind gates still exceeds the permitted standard. This makes the three main fan stations work bigger than required.

- All 03 main fan stations have working modes to ensure ventilation requirements. The amount of wind generated is higher than the calculation required for a certain amount of wind: The kiln door is +25 excess 7 m^3/s (about 8.64%), the kiln door is +29 residual 2.7 m^3/s (about 21.4%) and the kiln door is +20 surplus 1.9 m^3/s (about 14.1%).

4. Conclusion

The results of calculation of working regime of the main fans in Thanh Cong - Cao Thang area, Hon Gai Coal companie show that the current ventilation capacity of the fan stations is suitable and ensures to meet the current ventilation. Reserve capacity of the main fans remains, especially the fan station at +25 Thanh Cong area. However, 2 fan stations are at +29 and +20 levels in Cao Thang area although the reserve capacity is still available, but because these two fan stations are used as fan type FBDCZ-6-No13, the ventilation capacity is not large. storage capacity of maximum flow is only about 17m3 / s, although only working at the angle of wing -5 installation, but the wind flow only increases by about 3.5m3 / s. Cao Thang area currently has only 1 kiln longwall, so in the future when Cao Thang area will bring in a new furnace to operate, it is necessary to consider replacing the new fan station. It is considered that the reserve capacity of the +25 fan station in Thanh Cong area is still high, but due to the connection of the two new areas at -160, it is impossible to bring dirty wind from Cao Thang area to turn. Return and exit the +25 level door of Thanh Cong area.

The solution when operating an additional longwall in Cao Thang area to operate to increase the mining output of the area as planned, the company must calculate additionally replace a station fan at the door level +20 or replace Both 2 fan stations in Cao Thang area with a fan station with large ventilation capacity and equivalent capacity of FBDCZ-8-No24 [Babak GA, KP Bocharov, AT Volokhiev. 1982].

References

[1] Tran Xuan Ha et al., 2014. Mine ventilation curriculum. Science and Technology Publishing House, Hanoi, 357tr.

[2] Nguyen Cao Khai et al, 2017. Inspection of wind network in Thanh Cong-Cao Thang area mine, Hon Gai coal company in 2017. Summary report of the project, University of Mining and Geology, pp.27- 40.

[3] Nguyen Cao Khai and others, 2015. Determine the reasonable working regime of the main fan stations to improve the ventilation efficiency for some coal mines in Quang Ninh region. Journal of mining industry, No. 2-2015, Hanoi, Tr.25-29.

[4] Ventilation Room, 2017. Plan for production and ventilation of Thanh Cong-Cao Thang area in 2017. Hon Gai Coal Company-TKV, Tr.1-28.

[5] Babak G.A, K.P. Bocharov, AT Volokhiev. 1982. Main ventilation fans for underground mining. - M .: Nedra, - P 296.

Opiekun : prof. M. Borowski

Recenzenci : M. Borowski,

Mariusz Kapusta : kapustam@agh.edu.pl

Improving the operation of earth fault relays by auto earthing-connection at earth fault situations in 6kV mining grid of Quang Ninh

HoVie tBUN[1,*], Le Xuan THANH[2]

[1,2] HUMG Hanoi University of Mining and Geology, Faculty of Electromechanic, Hanoi, Vietnam

Abstract. Single phase earth-fault in MV grids usually causes overvoltage that harm to human being and electric equipments. In 6kV mining grids of Vietnam, earth fault which is majority incident accounts 55% to 73% of the total faults. When earth fault occurs many grids' eco-technical parameters will be affected. Moreover, the overvoltage and earthing current can lead to serious electric shock accidents caused mainly by stepping-overvoltage or touching-overvoltage. One of earthing relays requirements is to trip in minimum time duration in order to reduce the magnitude of earthing currents and overvoltage. Base on the simulation in Matlab, the paper suggests a prior connection diagram that allows an auto earthing-connection for improving the better performance of relays. The utilization of the diagram will help to decrease the tripping time of relays, reduce the amplitude of internal overvoltage as well as enhance the safety for human being in case of earthing incidents.

1 Introduction

In the Quang Ninh 6 kV electrical network, one-phase earthing is the majority failure, accounting for 61 ÷ 85% of all types of incidents [1]. This incident significantly affects to the normal operation of electrical network as well as apparatus in the mines. In mining 6 kV grids, to ensure the electrical safety, it is impossible for operators to directly contact with parts grounding to earth. It is also impossible to have contacting voltage, step voltage and induction voltage. Therefore, it is necessary to eliminate immediately the earthing point from grid as well as decrease the amplitude of earthing current. One of the most effective solution is to automatically connect the earthing point by a small resistor in order to reduce internal over voltage and decrease the effecting time on human body.

2 Theory and the simulation results

Based on the theory of earthing phenomena in isolating neutral [3,5], the incident earthing current will depend on grid's parameters and short-circuiting the connection diagram describing the method mentioned above is shown in Figure 1.

* Corresponding author: hovietbun@gmail.com

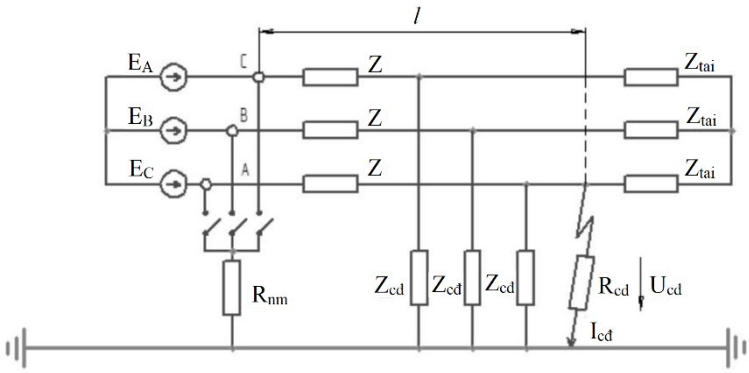

Fig. 1. Connection diagram of earthing circuit with a short-circuiting resistor.

In Figure 1: Z-line impedance from the source to the earthing point;
R_{nm}-Short-circuiting resistor;
R_{cd} – Earthing resistor;
Z_{cd}-Insulation resistance of phase to earth;
l- the length of conductor to earthing point;
I_{cd}-Earthing current;
U_{cd} – Voltage across the earthing resistor;
E_A, E_B, E_C – electromotive force of source;
Z_{tai} – Load impedance.

Earthing current is determined by:

$$I_{cd} = U_f \frac{3Z_{tai}Z_{nm} - ZZ_{cd}}{\left(R_{cd} + \frac{1}{3}Z_{cd}\right)Z^2 + \left(\frac{R_{cd} + Z_{cd}}{Z_{cd}}\left(Z + 3Z_{nm}\right) + 2R_{cd} + Z_{cd}\right)ZZ_t \ \left(3Z_{nm}R_{cd} + Z_{cd}\left(Z_{nm} + R_{cd}\right)\right)\left(Z + Z_{tai}\right)} \quad (1)$$

Because insulation resistance of phase to earth is much bigger than other impedance, therefore the equation (1) could be shorten as equation (2):

$$I_{cd} = \frac{U_f\left(3Z_{tai}Z_{nm} - ZZ_{cd}\right)}{Z_{cd}Z\left(\frac{1}{3}Z + Z_{tai} + \left(R_{nm} + R_{cd}\right)\left(1 + \frac{Z_H}{Z}\right)\right)} \quad (2)$$

From equation (2) some following relations could be obtained:
+ The relation of voltage across the earthing resistor and short-circuiting resistor.
+ The relation of earthing current and short-circuiting resistor and earthing resistor.

As mentioned in [2], the value of earthing current depend significantly on capacitance and insulating admittance of each phase to earth. Two these latter quantities are expressed by (3):

$$C_f = 0{,}00041 + 0{,}00399N_{BA} + 0{,}0079N_{ĐC+MX} + 0{,}01259L_{Tk.qđ} + 0{,}19559L_{C.qđ}, \mu F$$
$$G_f = 1{,}07801 + 0{,}07271N_{BA} + 0{,}10825N_{ĐC+MX} + 0{,}17192L_{Tk.qđ} + 2{,}24998L_{C.qđ}, \mu S \quad (3)$$

Formulate a simulating diagram as figure 2 with the values of components as: C_f =0,021µF/phase, R_f =327,99kΩ/phase, Rd = 2,662Ω, Ld = 0,0047Ω; Stt = 969,1 kVA, Rt = 35,521Ω, Lt = 0,065Ω.

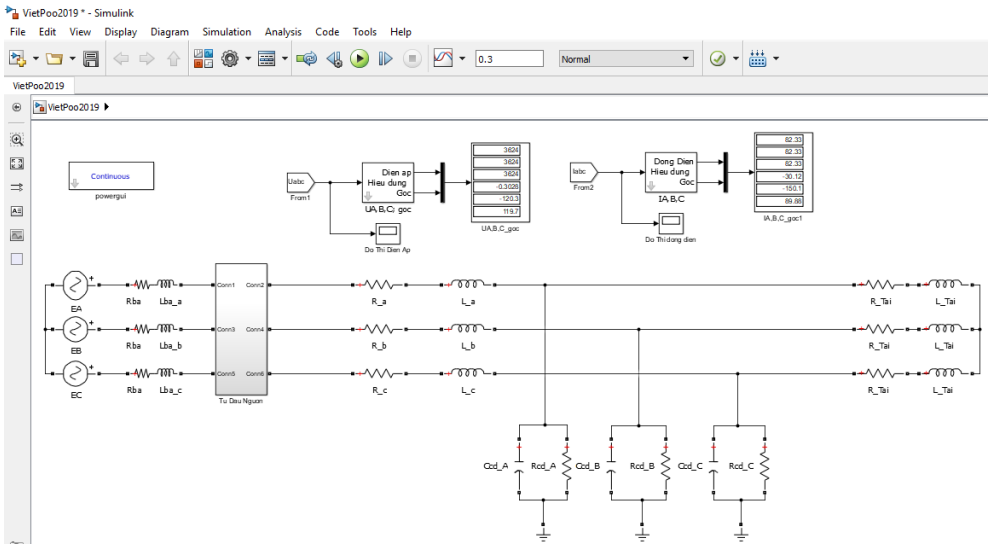

Fig. 2. Simulation diagram of 6kV grid expressing earthing incident.

Figure 3 shows the simulation of 6kV grid with earthing phenomena containing the automatically connection of short-circuiting resistor at t=0,1s.

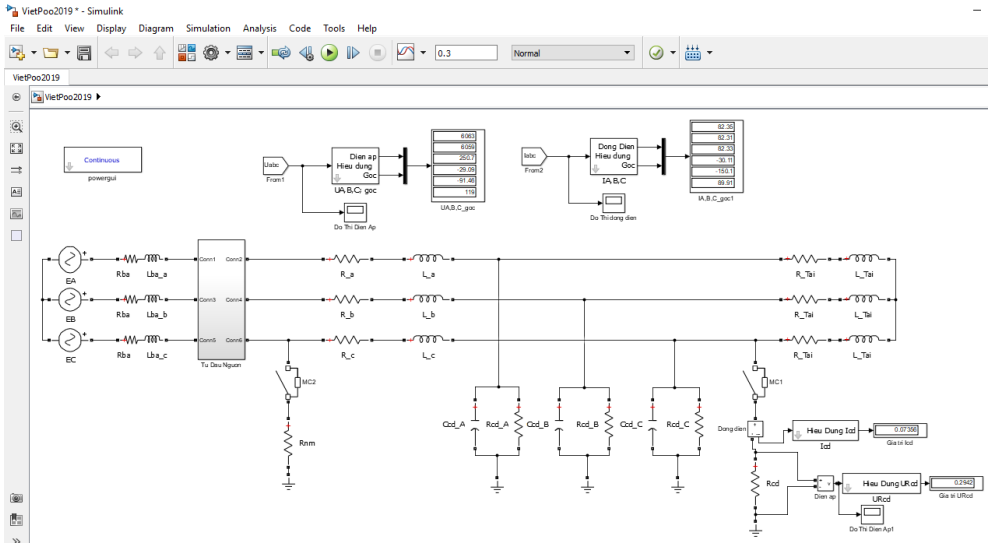

Fig. 3. Simulation diagram of 6kV grid with short-circuiting resistor R_{nm}.

By utilizing a short-circuiting resistor at t=0,1s, the amplitude of over voltage is reduced greatly, the waveform of earthing over voltage (blue curve) is shown in figure 4.

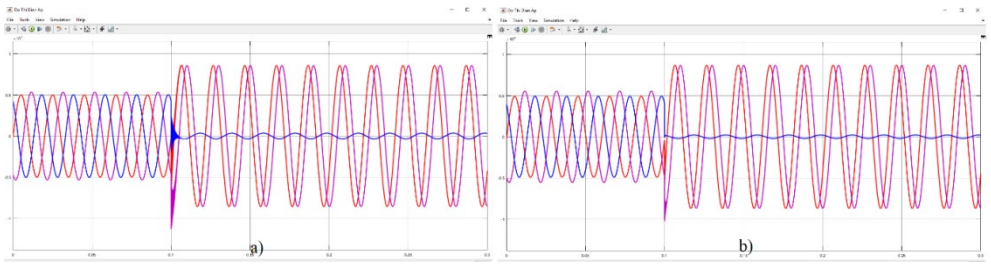

Fig. 4. Earthing voltage wave-forms without a short-circuiting resistor (a) and with a short-circuiting resistor (b). The resistor is short-circuited at t=0,1s.

Implementing some other simulation with different value of R_{nm}, the series value of earthing over voltage depending on value of R_{nm} are form as curve in figure 5. The series value of earthing current depending on value of R_{nm} are form as a curve in figure 6.

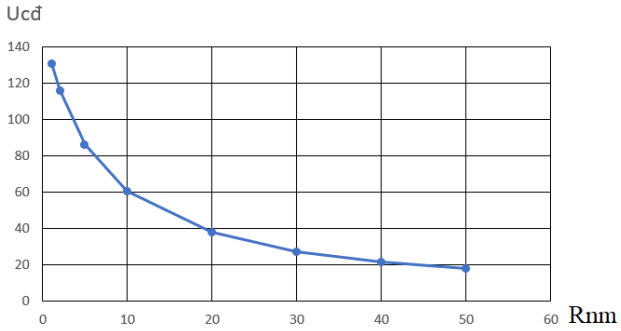

Fig. 5. Diagram showing the relation of earthing over voltage and short-circuiting resistor at R_{cd} = 4Ω.

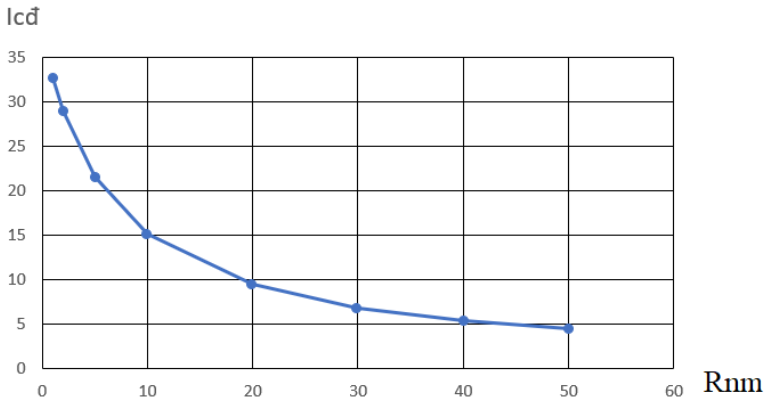

Fig. 6. Diagram showing the relation of earthing current and short-circuiting resistor at R_{cd} = 4Ω.

3 Conclusion

The above simulations show that: By utilizing a short-circuiting resistor at earthing point of 6kV grid, the following advantages could be deducted:

+ The amplitude of earthing over voltage is reduced significantly. In figure 5, the earthing voltage is only one seventh (nearly 20V) if R_{nm} = 50Ω.

+ The earthing incident current is also decreased effectively when the value of short-circuiting resistor is big enough. In figure 6, this current reduced from nearly 35A (without any short-circuiting resistor) to 5A (with short-circuiting resistor R_{nm} = 50Ω.

Obviously, when the over voltage is reduced, its influence on equipment insulation is also decreased. The amplitude of earthing current is reduced, the possibility of appearing arcing current on 2 other phases is also decreased. This advantage is enhanced significantly the reliability of power supply.

References

1. Ho Viet Bun, “Reasearch and evaluate overvoltage transience caused by single phase-ground failures in Cam Pha-Quang Ninh underground mines' 6kV grid”, International

conferrence of Advanced in Mining and Tunelling 21-22 October 2014, Vung Tau, Viet Nam, pp. 409-411

2. Ho Viet Bun (2015), “Research for determining 6kV gird’s insulation indicators in Quang Ninh open pit coal mines”, Second international conference on scientific research cooperation between Vietnam and Poland in earth sciences (VIET-POL 2015), pp. 507-513
3. Сирота, И.М., Кисленко, С.Н., Михайлов, А.М. Режимы нейтрали электрических сетей/– Киев: Наук. думка, 1985. – 264 с.
4. Гуревич, В.И. Некоторые технические аспекты проблемы защиты от замыканий на землю распределительных сетей среднего напряжения/ - журнал «Промышленная энергетика», № 1 – 2001
5. Серов В.И, Щуцкий В.И, Ягудаев Б.М. Методы и средства борьбы с замыканиями на землю в высоковольтных системах горных предприятий, Mockba “Наука” 1985

Developing an Advanced Soft Computational Model for Estimating Blast-Induced Ground Vibration in Nui Beo Open-pit Coal Mine (Vietnam) Using Artificial Neural Network

NGUYEN Hoang[11, 2, *], *BUI* Xuan Nam[1, 2], *TRAN* Quang Hieu[1, 2], *NGUYEN* Quoc Long[1,2], *VU* Dinh Hieu[1, 2], *PHAM* Van Hoa[1, 2], *LE* Qui Thao[1, 2], *NGUYEN* Phu Vu[1,3]

[1] Hanoi University of Mining and Geology, Hanoi, Vietnam
[2] Center for Mining, Electro-Mechanical research, Hanoi, Vietnam
[3]Mining - Geology Design Survey and Construction Consulting JSC, Hanoi, Vietnam

Abstract The principal object of this study is blast-induced ground vibration (PPV), which is one of the dangerous side effects of blasting operations in an open-pit mine. In this study, nine artificial neural networks (ANN) models were developed to predict blast-induced PPV in Nui Beo open-pit coal mine, Vietnam. Multiple linear regression and the United States Bureau of Mines (USBM) empirical techniques are also conducted to compare with nine developed ANN models. 136 blasting operations were recorded in many years used for this study with 85% of the whole datasets (116 blasting events) was used for training and the rest 15% of the datasets (20 blasting events) for testing. Root Mean Square Error (RMSE), Determination Coefficient (R^2), and Mean Absolute Error (MAE) are used to compare and evaluate the performance of the models. The results revealed that ANN technique is more superior to other techniques for estimating blast-induced PPV. Of the nine developed ANN models, the ANN 7-10-8-5-1 model with three hidden layers (ten neurons in the first hidden layer, eight neurons in the second layers, and five neurons in the third hidden layer) provides the most outstanding performance with an RMSE of 1.061, R^2 of 0.980, and MAE of 0.717 on testing datasets. Based on the obtained results, ANN technique should be applied in preliminary engineering for estimating blast-induced PPV in open-pit mine.

1. Introduction

Blasting is one of the most effective methods for rock breakage in open-pit mine. However, its environmental impacts are significant and should be considered, including ground vibration (PPV), air overpressure, and fly rock [14, 17, 32]. Of

[1] *Corresponding author:* nguyenhoang@humg.edu.vn

these side effects, PPV is a significant influence on surrounding structures such as benches, slopes, groundwater, and residential areas [21, 28, 34, 32]. Therefore, the precise prediction of PPV is necessary to minimize adverse impacts on the surrounding environment.

The level of PPV is influenced by different parameters. They can be divided into three main groups: blast design parameters, explosive parameters, and rock mass properties [18, 26, 57]. Of these main groups, the blast design parameters are controllable parameters including blast hole diameter, length of the borehole, explosive capacity, column charge length, length of terming, powder factor, spacing, methods and diagrams of blasting [26, 35]. In the explosive parameters, type of explosive (ANFO, water gel, emulsion, or dynamite), the velocity of detonation (VoD), its density, powder factor (kg ANFO/m^3) are also controllable parameters [24]. Unlike the parameters of the first and second groups, the parameters of the third groups are uncontrollable parameters such as rock hardness, cracking, stratification, burden, and compressive strength of rock [20]. Based on the parameters of these groups, it can be seen that accurate prediction of PPV is not simple. Because of its complexity, many scientists have chosen to approach experimental techniques for estimating PPV based on two major parameters, the explosive capacity (W) and the monitoring distance (R) [7, 22, 37, 43, 51, 59]. However, based on the results of some studies, empirical techniques are often less accurate and do not applied in all sites [23, 29, 36].

Reviewing recent literature shows that the complexity of the parameters that affect PPV can be solved by artificial intelligence (AI). Sheykhi, Bagherpour [55] have developed a hybrid model using Support Vector Regression (SVR) and Fuzzy C-means clustering (FCM) algorithms (FCM-SVR) for predicting blast-induced PPV in Sarcheshmeh copper mine, Iran with 120 blasting events and 7 different parameters. The SVR model and the United States Bureau of Mines (USBM) empirical equation were also used to evaluate the effectiveness of the FCM-SVR model. Their results indicated that the SVR model provided higher performance than the USBM experimental technique. In particular, it achieved optimum performance when combined with the FCM algorithm and the FCM-SVR hybrid model proposed to predict the actual PPV. In another study, Ragam and Nimaje [48] have developed a simple artificial neuron network with a hidden layer consisting of 5 hidden neurons and a feed-forward back propagation algorithm for predicting PPV in ACC mine, Iran. The results showed that the ANN model predicted PPV better than other techniques they have tested. Based on neural network, the group method of data handling (GMDH) model was developed by Mokfi, Shahnazar [39] to predict PPV in a quarry of Malaysia, using 102 blasting operations. They concluded that GMDH forecasting technique could be presented as a powerful technique in predicting PPV with R^2 of 0.911 and RMSE of 0.889. In addition, research on the application of AI hybrid models and experimental techniques was conducted by Hasanipanah, Amnieh [26] with the fuzzy system (FS) and imperialistic competitive algorithm (ICA) to predict PPV in Miduk copper mine, Iran. Their research has shown promising results with an R^2 of 0.942.

Based on the review of the literature, it can be seen that AI techniques have been studied and developed quite firmly in the predicted blast-induced PPV in open-pit mine. Nevertheless, no model can represent all areas of study. Thus, in this study, we develop some ANN models for predicting blast-induced PPV in Nui Beo open-pit coal mine, Vietnam. Another model, namely Multiple Linear Regression (MLR) and the United States Bureau of Mines (USBM) practical techniques were also used in this study to assess the effectiveness of the developed ANN models.

The article is organized into six sections: Section 1 gives an overview of the literatures and the reasons for doing this research; Section 2 summarizes the study area and the data used; Section 3 gives an overview of the methodologies used; Section 4 develops PPV forecasting models; Section 5 presents the results of this work and discussion; Finally, the conclusions and recommendations in this work.

2. Study area and data used

2.1. Study area

The site selected for this study was Nui Beo open-pit coal, Vietnam with a production of 1,125,000 tons/year; the capacity of overburden is 4.815.000 m^3/year. It located between latitudes $20^0$57’50” N and $20^0$58’35” N, and between longitudes $107^0$7’50” E and $107^0$8’50” E (Fig. 1). The most striking feature of this study area is that it is located between Ha Long City, where Ha Long Bay is one of the seven natural wonders of the world recognized by UNESCO [47]. The residential area is adjacent to the mine with a distance of about 100m to the nearest residential unit. Therefore, the mine must be conducted in parallel two methods of rock breaking are drilling-blasting and mechanical equipment. Of these methods, drilling and blasting accounted for 98% of the total capacity of rock breakage.

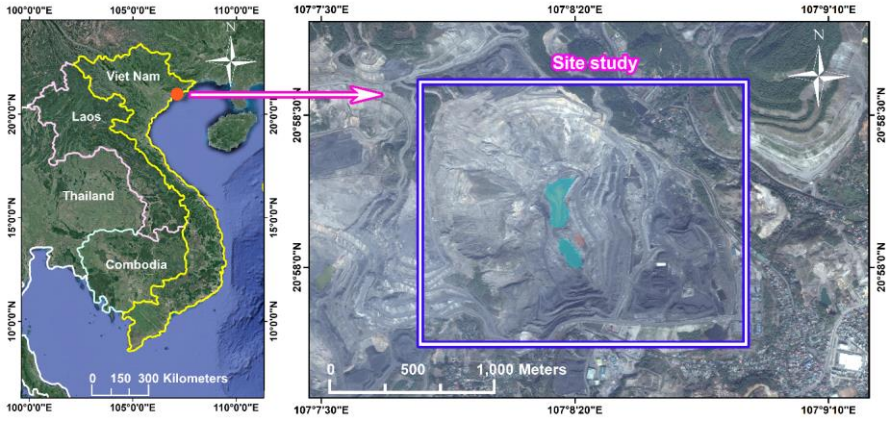

Fig. 1 Location of Nui Beo open-pit coal mine

Explosives used on the mine are ANFO, Z113 and AN13 emulsion with 250mm for blast hole diameter in rock breakage and 42mm diameter for oversize rock breakage. The blasting method was applied in Nui Beo open-pit coal mine is non - electric delay blasting. Explosive capacity in an explosion is up to 20,000 tons. As the mine is near the residential area and the explosive capacity used in each blasting event is large, the impact of PPV is not small. Moreover, the Nui Beo open-pit coal mine has repeatedly faced the lawsuit due to the impact of PPV caused. Therefore, accurate predictions of blast-induced PPV in this area are necessary.

2.2 Describe the data used

As related, the parameters that affect PPV are so many. It is difficult to collect and evaluate all the parameters. Thus, in this study, seven input parameters were used to predict blast-induced PPV in Nui Beo open-pit coal mine, including the elevation between blast sites and monitor (H), explosive charge per delay (W), monitoring distance (R), power factor (P), burden (B), spacing (S), time delay (T). Of these input parameters, R is determined by handheld GPS system; the remaining parameters are taken from 136 blasts design. PPV is measured by Blastmate III (Instatel, Canada) [3] in a range of 0.127-254 mm/s. The data used in this study are summarized in Table 1.

Table 1. Summary of the data used

W	R	H	P
Min. : 1109	Min. :107.0	Min. :-38.00	Min. :0.3500
1st Qu.: 3526	1st Qu.:233.0	1st Qu.: 6.50	1st Qu.:0.3900
Median : 5086	Median :334.0	Median : 24.00	Median :0.4300
Mean : 5455	Mean :357.9	Mean : 23.24	Mean :0.4274
3rd Qu.: 7214	3rd Qu.:471.2	3rd Qu.: 40.00	3rd Qu.:0.4625
Max. :12312	Max. :797.0	Max. : 81.00	Max. :0.5000
B	S	T	PPV
Min. :6.600	Min. :7.400	Min. :6.600	Min. : 0.91
1st Qu.:7.000	1st Qu.:7.700	1st Qu.:6.900	1st Qu.: 5.51
Median :7.400	Median :8.000	Median :7.350	Median :11.10
Mean :7.404	Mean :7.979	Mean :7.303	Mean :11.80
3rd Qu.:7.825	3rd Qu.:8.200	3rd Qu.:7.600	3rd Qu.:17.18
Max. :8.200	Max. :8.500	Max. :8.000	Max. :26.83

3. Background of Empirical, MLR, and ANN

3.1. Empirical

The empirical technique is one of the blast-induced PPV forecasting methods in open-pit mine because they are easy to use and capable of producing results quickly. Of the current experimental techniques, the United States Bureau of Mines (USBM) remained the most commonly used empirical method for predicting PPV and was proposed by Duvall and Petkof [15]. The USBM empirical method is described as follows:

$$PPV = k\left(\frac{R}{\sqrt{W}}\right)^{-b} \quad (1)$$

Where: W is the explosive capacity, Kg; R is the distance between blast face and monitoring point, m; k and b are the site factors and are determined by the multivariate regression analysis.

In this study, USBM empirical method was used to estimate blast-induced PPV in Nui Beo open-pit coal mine. The PPV forecast results using the USBM technique are detailed in the next sections.

3.2. Multiple linear regression

Multiple linear regression (MLR) is a linear equation that fits a dependent variable with multiple independent variables [1]. Numerous studies in rock mechanics and mining have been published based on the MLR method [4, 16, 25, 53, 52, 56, 60]. For example, Ghiasi, Askarnejad [19] successfully used the MLR for predicting rock fragmentation in Gole Gohar iron ore open pit mine, Iran. The results of the MLR method were higher than those of ANN with $R^2 = 0.89$ and RMSE = 0.19. In another study, Shepel, Grafe [54] have also successfully developed the MLR model for evaluating cutting forces in granite treated with high-power (24 kW) microwave radiation. The application of the MLR model allows for a more detailed analysis of the effects of high-power microwave radiation on granite parameters, helping engineers improve their stone cutting productivity. Generally, MLR can be described by the following equation:

$$y = a_0 + a_1 x_1 + a_2 x_2 + ... + a_n x_n \quad (2)$$

Where, x_i (i = 1…n) and y represent independent and dependent variables, respectively. Also, a_i (i = 0, 1, . . . , n) represent regression coefficients.

In this study, MLR was developed to predict blast-induced PPV in Nui Beo open pit coal mine with seven input parameters. The multiple regression formulae for predicting PPV in this site study is illustrated as follows:

$$PPV = a_0 + a_1 W + a_2 R + a_3 H + a_4 P + a_5 B + a_6 S + a_7 T \quad (3)$$

Where $a_0 \div a_7$ are regression coefficients and are determined by the multivariate regression analysis method. The results for determining the multiple regression equations for this problem are presented in the next section.

3.3. Artificial neural networks (ANN)

Artificial neural networks (ANNs) can be considered as an artificial tool based on human brain simulations. These include neurons that are connected to each other in a flexible and fast way [63]. Many scholars have efforted to develop ANN models for various issues in the mining field and achieved the desired results [5, 9, 31, 38, 40, 42, 45]. For example, Muhammad and Ferentinou [44] have developed an ANN model to assess the slope stability based on 141 historical records and 18 input parameters. The results show that ANN produces rapid convergence with high reliability. An ANN model was also developed based on optimized input parameters by the Genetic Algorithm and proposed by Armaghani, Hasanipanah [8] for

predicting air overpressure in Penang, Malaysia. The proposed ANN model yielded results that could not be more excellent.

The basic structure of an ANN model includes an input layer, hidden layer(s) and output layer [50]. In input layer, neurons act as input variables and transmit data to hidden layers (s) via the transfer function. In the first hidden layer, the neurons will receive the result from the input layer and process and calculate the weights and send it to the second hidden layer via the propagation function. The process continues like that until the results are passed to the output layer [64].

The processing of data in the hidden layers is also called training. The outputs depend heavily on the training process. In ANN, supervised learning and unsupervised learning are two types of learning that can be applied to each ANN [46]. In this study, supervised learning was applied to solve the regression problem in predicting blast-induced PPV. Seven parameters are introduced into the input layer and processed according to ANN model as Fig. 2. The ANN models are developed for predicting PPV in this study, and their performance is discussed in greater detail in the next sections.

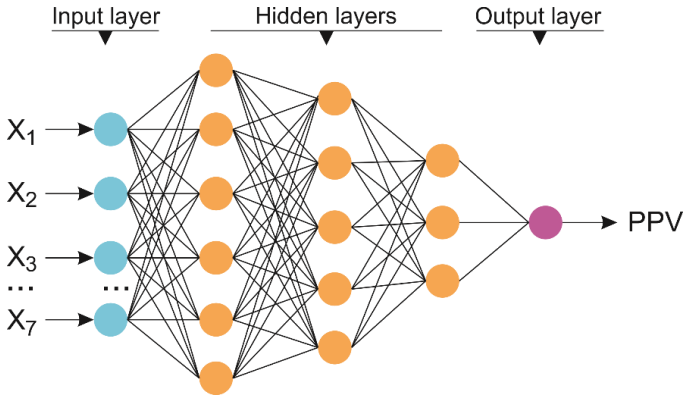

Fig. 2 The general structure of the ANN model for predicting PPV in this study

4. Developing PPV predictive models

For developing PPV predictive models, data needs to be prepared and processed. In this study, 136 blasting events were divided into two sets of data: 85% of the whole datasets (116 observations) for training, and the rest 15% (20 observations) for testing. Based on the training datasets, the predictive models are developed in the next sections.

4.1. Empirical

As related, the USBM experimental technique in Eq. 1 is used to estimate blast-induced PPV. Accordingly, the site factors k and b are defined by multivariate regression analysis method. The SPSS version 18.0 [12] is used to determine the site factors k and b. The results of multivariate regression analysis for the values of k and b are 44.067 and 1.023, respectively. The experimental USBM for predicting PPV in this study is described in Eq. 4:

$$PPV = 44.067\left(\frac{R}{\sqrt{W}}\right)^{-1.023} \quad (4)$$

4.2. MLR

In MLR, multivariate regression analysis techniques are also used to determine regression coefficients according to Eq. 3. SPSS version 18.0 is again used to determine the regression coefficients for MLR in this study. Note that, the training datasets for building MLR model is similar to the for building the empirical model.

Based on that, the regression coefficients for the variables are determined correspondingly in Eq. 3 are -5,044; 0.0015; -0.0047; -0.082; -5.161; 0.046; 1,055; and 0.756. The MLR model for predicting blast-induced PPV in Nui Beo open-pit coal mine is defined by the following equation:

$$\begin{aligned} PPV = {} & 0.0015W-0.0047R-0.082H-5.161P+0.046B \\ & +1.055S+0.756T-5.044 \end{aligned} \quad (5)$$

4.3. ANN

For ANN technique, the most critical problem is neural network design [10]. A neural network is designed that includes training algorithms, hidden layers, and hidden neurons in each hidden layer [30]. The most challenging problem when designing an ANN is determining the number of hidden layers and the number of neurons in each hidden layer [13, 58, 62]. In theory, an ANN with one hidden layer can solve most problems in practice [11]. A neural network with two or more hidden layers can solve problems better depending on the circumstances. However, too many hidden layers in an ANN will increase the processing time of the network [27, 61]. Thus, a "trial and error" procedure with one, two, and three hidden layers is applied for developing ANN models in this study.

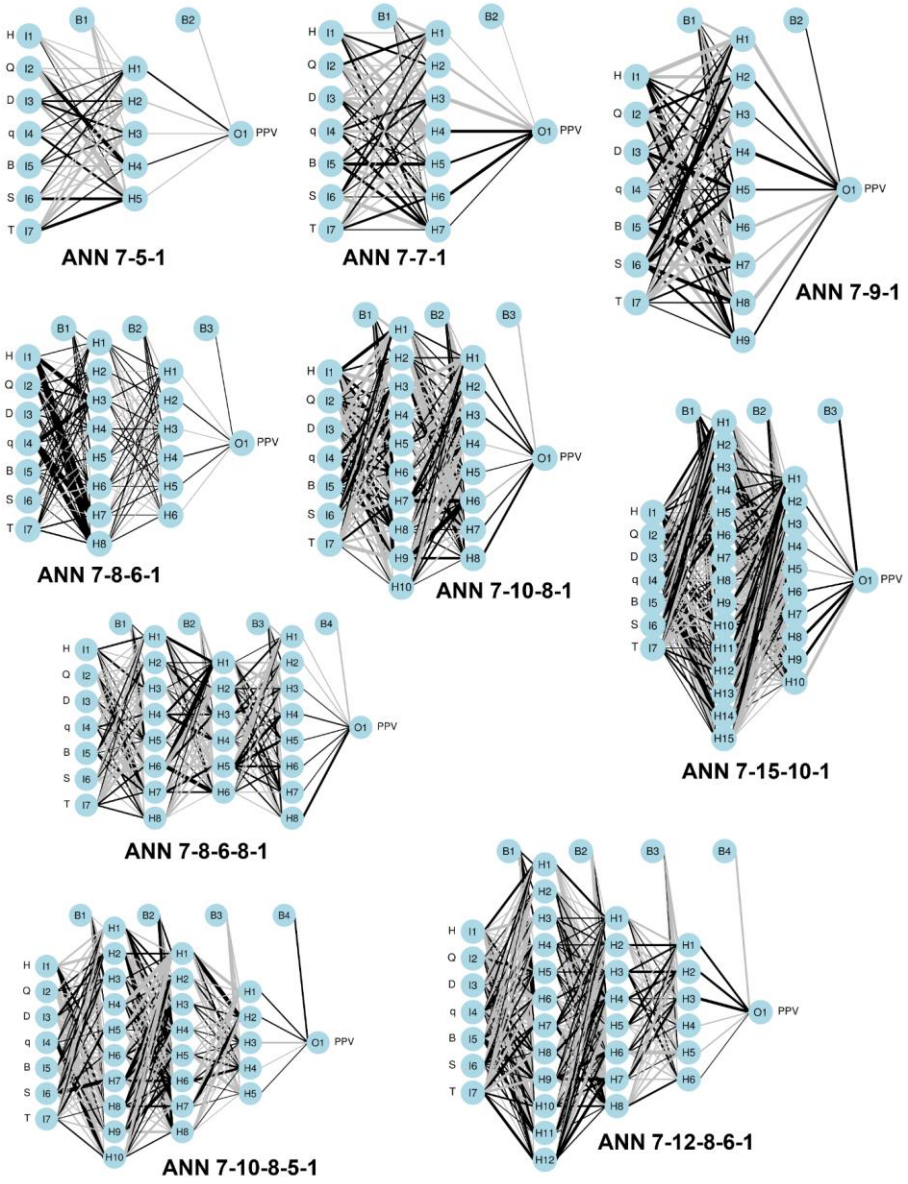

Fig. 3 Structure of the ANN models for predicting PPV

The training datasets in ANN technique is used similarly to empirical and MLR methods. However, the min-max scale method and scale the data in the interval [0,1] was applied to avoid overfitting. Usually scaling in the intervals [0,1] or [-1,1] tends to give better results. As a result, nine ANN models were developed for predicting blast-induced PPV in this site with one, two and three hidden layers in Fig. 3.

In Fig. 3, the black line represents for positive weights and the grey line represents for negative weights. Line thickness is in proportion to magnitude of the weight relative to all others. From I1 to I7 are the input variables, W, R, H, P, B, S, T, respectively. H1 to H15 are the neurons in hidden layers. And O1 is the output

layer, PPV, respectively. B1, B2, B3 and B4 are bias layers that apply constant values to the nodes.

5. Results and discussion

5.1. Performance metrics for evaluating PPV predictive models

To evaluate the performance of the developed predictive models, the performance indicators are used, including Root Mean Squared Error (RMSE), Coefficient of determination (R^2), and Mean Absolute Error (MAE), which are calculated using equation (6-8), respectively.

$$RMSE = \sqrt{\frac{1}{n}\sum_{PPV=1}^{n}(y_{PPV} - \hat{y}_{PPV})^2} \quad (6)$$

$$R^2 = 1 - \frac{\sum_{PPV}(y_{PPV} - \hat{y}_{PPV})^2}{\sum_{PPV}(y_{PPV} - \bar{y})^2} \quad (7)$$

$$MAE = \frac{1}{n}\sum_{PPV=1}^{n} |y_{PPV} - \hat{y}_{PPV}| \quad (8)$$

Where n is the total number of data. y_{PPV} is the measured value, $\hat{y}_{PPV}$ is the predicted value and $\bar{y}$ is mean of measured values. In the most optimal model, R^2 should be equal to 1, RMSE and MAE should be equal to 0, respectively.

5.2. Comparisons of PPV predictive models

Once the forecasting models are available, the performance of the models is evaluated through performance indices in Eq. 6-8 on both the training datasets and the testing datasets. The testing datasets are considered as unseen data for objectively evaluating the quality of developed predictive models. As a result, the performance of predictive models, including empirical, MLR, and ANN is demonstrated in Table 2.

From Table 2, it can be seen that USBM experimental technique provides the lowest performance for estimating blast-induced PPV in this case study with RMSE = 4.446 and R^2 = 0.816 on testing datasets. Examining the literature shows that USBM is also the most widely used experimental technology and many studies have successfully performed with this technique [2, 6, 32, 33, 41, 43]. However, the effectiveness of experimental techniques has not been well appreciated.

Table 2. Performance of predictive models

Model	Training datasets			Testing datasets		
	RMSE	R2	MAE	RMSE	R2	MAE
Empirical (USBM)	5.382	0.63	2.802	4.446	0.816	2.873
MLR	2.809	0.833	1.691	1.647	0.947	1.378
ANN 7-5-1	2.187	0.898	1.374	2.715	0.839	2.253

ANN 7-7-1	0.903	0.983	0.702	1.354	0.960	0.922
ANN 7-9-1	0.917	0.982	0.683	1.949	0.916	1.327
ANN 7-8-6-1	1.164	0.971	0.705	2.273	0.891	1.403
ANN 7-10-8-1	0.727	0.988	0.571	1.621	0.952	1.027
ANN 7-15-10-1	0.928	0.981	0.651	1.915	0.921	1.307
ANN 7-8-6-8-1	0.736	0.988	0.565	1.350	0.960	1.036
ANN 7-10-8-5-1	**0.669**	**0.990**	**0.528**	**1.061**	**0.980**	**0.717**
ANN 7-12-10-6-1	0.840	0.985	0.559	1.594	0.947	1.200

Considering the MLR model on both the training datasets and the testing datasets shows that MLR seems to work quite well in this case with an RMSE of 1.647, R^2 of 0.947, and MAE of 1.378 on testing datasets. The MLR model results showed that the input variables in this study might have a relatively linear relationship. In addition, the number of input variables in the study is quite high. Therefore, the Standardized Rank Regression Coefficients (SRRC) is applied for sensitivity analysis based on linear or monotonic assumptions in the case of independent factors [49]. The results of the sensitivity analysis for the input variables are shown in Table 3.

Table 3. Sensitivity indices of independent factors

	original	bias	std. error	min. c.i.	max. c.i.
W	0.615516	0.000404	0.018758	0.577353	0.645196
R	-0.12097	-0.00018	0.003134	-0.12666	-0.11528
H	-0.33539	0.001342	0.021048	-0.37885	-0.29262
P	-0.03751	-0.00016	0.002435	-0.04177	-0.03159
B	0.003667	7.56E-06	0.000235	0.003091	0.004123
S	0.052638	0.000102	0.004313	0.043578	0.061577
T	0.051717	-6.1E-05	0.003389	0.044385	0.057916

Accordingly, it can be seen that although the performance of the MLR model is rather high, not all input variables have a good linear relationship. Table 3 showed that only the maximum explosive capacity (W), monitoring distance (R), and the elevation between blast sites and monitor (H) are the main factors influencing the performance of the PPV prediction model. In some previous studies, some researchers have concluded that W and R are the two most influential variables in the quality of the PPV prediction model [7, 22, 37, 43, 51, 59]. However, the results of this study suggest that H is a parameter that should be added as one of the three factors that have a significant influence on the performance of the model, including W, R, H.

Regarding the ANN models developed, it can be seen that nine developed ANN models have uneven performance. Some ANN models provide higher performance than the MLR model, but some models perform less efficiently than the MLR model. Therefore, comparing the ANN models with one, two, and three hidden layers is interesting in this study. It can be seen that ANN model with only one hidden layer can handle quite well PPV prediction problem in this case, i.e., ANN 7-7-1 with an RMSE of 1.354, R^2 of 0.960, and MAE of 0.922. The ANN

model with two hidden layers works well for predicting blast-induced PPV in this study. However, the best ANN model with two hidden layers in this study (ANN 7-10-8-1) only achieved an RMSE of 1.621, R^2 of 0.952, and MAE of 1.027, which is lower than that of ANN 7- 7-1 with one hidden layer. On the other hand, take a closer Table 3, it can be seen that not the ANN model with more hidden layers offers lower performance. The evidence is that the ANN 7-10-8-5-1 model with three hidden layers is the best performing model among the nine developed ANN models with RMSE = 1.061, R^2 = 0.980, and MAE = 0.717 on testing datasets. With the difference between RMSE and MAE of the ANN 7-10-8-5-1 model is 0.344, indicating that the model is highly stable. More interesting in this study is the ANN model 7-12-10-6-1 with more hidden neurons provided lower performance than the ANN model 7-10-8-5-1 with an RMSE of 1.594, R^2 of 0.947, and MAE of 1.200 on testing datasets. This shows that too many hidden layers and hidden neurons in each hidden layer not only increases the processing time of the ANN model but also the lack of match between neurons, which reduces the efficiency of the model. Therefore, the proposed ANN 7-10-8-5-1 model is the best model for predicting blast-induced PPV in this study. Fig. 4 illustrates the relationship between predicted and measured values of empirical, MLR, and ANN techniques.

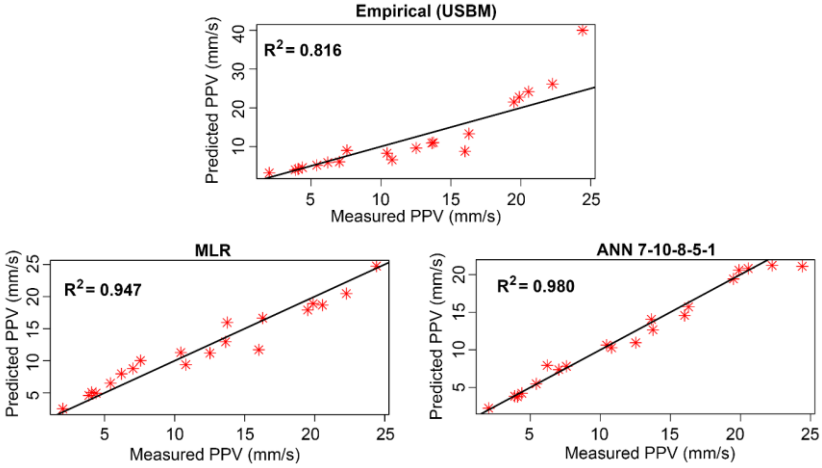

Fig. 4 Measured and predicted PPV values of Empirical, MLR and ANN models

6. Conclusions and recommendations

Blasting is one of the most effective methods for hard-rock fragmentation in mining and civil fields. Besides its advantages, the ground vibration (PPV) caused by blasting operations is one of the disadvantages that need to be estimated accurately. Forecasting blast-induced PPV in open-pit mine can be accomplished using a variety of methods. In this study, we have presented three approaches to solve the problem of PPV forecasting at Nui Beo open-pit coal mine, Vietnam. Based on the results, we draw some conclusions:

- For predicting blast-induced PPV, various approaches should be used to compare and evaluate the specific performance of each approach.
- Empirical techniques should be used as a fundamental approach to forecasting PPV. However, they need to be further researched and developed to improve the accuracy of the model.

- Multiple linear regression (MLR) is a rapid and straightforward method for estimating blast-induced PPV in an open-pit mine. Like the empirical technique, MLR should be used as a second baseline technique to compare and evaluate the performance of the model as well as the relationship between input variables.
- Artificial Neural Network (ANN) is an advanced approach for predicting blast-induced PPV in an open-pit mine. They can solve the complex linear and nonlinear relationships of the input parameters in the PPV prediction. Therefore, they should be researched, developed and applied in innovative engineering to accurately predict blast-induced PPV in an open-pit mine.
- The input parameters for predicting PPV should also be considered in detail. Of the input parameters, we propose the elevation between blast sites and monitor parameter (H) as an essential input parameter that dramatically influences the performance of the PPV prediction model. It should be used with maximum explosive capacity (W) and monitoring distance (R) in all approaches to predict PPV.

7. Acknowledgements

Paper was presented during the 5th POL – VIET International Conference Scientific-Research Cooperation between Vietnam and Poland, 08-10.07.2019, AGH UST, Krakow, Poland. This research was supported by Hanoi University of Mining and Geology (HUMG) and Center for Mining, Electro-Mechanical research of Hanoi University of Mining and Geology.

References

1. Aiken, L.S., S.G. West, and S.C. Pitts, *Multiple linear regression.* Handbook of psychology, 2003: p. 481-507.
2. Ak, H., et al., *Evaluation of ground vibration effect of blasting operations in a magnesite mine.* Soil Dynamics and Earthquake Engineering, 2009. **29**(4): p. 669-676.
3. Alcudia, A.D., et al., *Field comparison of 3-C geophones and microphones to high-precision blasting sensors.* CREWES Res. Rep, 2008. **20**: p. 1-20.
4. AminShokravi, A., et al., *The potential application of particle swarm optimization algorithm for forecasting the air-overpressure induced by mine blasting.* Engineering with Computers, 2018. **34**(2): p. 277-285.
5. Amnieh, H.B., M. Mozdianfard, and A. Siamaki, *Predicting of blasting vibrations in Sarcheshmeh copper mine by neural network.* Safety Science, 2010. **48**(3): p. 319-325.
6. Armaghani, D.J., et al., *Blasting-induced flyrock and ground vibration prediction through an expert artificial neural network based on particle swarm optimization.* Arabian Journal of Geosciences, 2014. **7**(12): p. 5383-5396.
7. Armaghani, D.J., et al., *Feasibility of ICA in approximating ground vibration resulting from mine blasting.* Neural Computing and Applications, 2018. **29**(9): p. 457-465.
8. Armaghani, D.J., et al., *Airblast prediction through a hybrid genetic algorithm-ANN model.* Neural Computing and Applications, 2018. **29**(9): p. 619-629.

9. Bahrami, A., et al., *Prediction of rock fragmentation due to blasting using artificial neural network.* Engineering with Computers, 2011. **27**(2): p. 177-181.
10. Basheer, I.A. and M. Hajmeer, *Artificial neural networks: fundamentals, computing, design, and application.* Journal of microbiological methods, 2000. **43**(1): p. 3-31.
11. Bengio, Y., et al. *Greedy layer-wise training of deep networks*. in *Advances in neural information processing systems*. 2007.
12. Carver, R.H. and J.G. Nash, *Doing data analysis with SPSS: version 18.0*. 2011: Cengage Learning.
13. Caudill, M., *Neural networks primer, Part III.* AI Expert, 1988. **3**(6): p. 53-59.
14. Dindarloo, S.R., *Prediction of blast-induced ground vibrations via genetic programming.* International Journal of Mining Science and Technology, 2015. **25**(6): p. 1011-1015.
15. Duvall, W.I. and B. Petkof, *Spherical propagation of explosion-generated strain pulses in rock*. 1958, Bureau of Mines.
16. Eskandar, H., et al., *Feasibility of particle swarm optimization and multiple regression for the prediction of an environmental issue of mine blasting.* Engineering Computations, 2018(just-accepted): p. 00-00.
17. Faradonbeh, R.S., et al., *Prediction of ground vibration due to quarry blasting based on gene expression programming: a new model for peak particle velocity prediction.* International journal of environmental science and technology, 2016. **13**(6): p. 1453-1464.
18. Ghasemi, E., H. Kalhori, and R. Bagherpour, *A new hybrid ANFIS–PSO model for prediction of peak particle velocity due to bench blasting.* Engineering with Computers, 2016. **32**(4): p. 607-614.
19. Ghiasi, M., et al., *Prediction of blast boulders in open pit mines via multiple regression and artificial neural networks.* International journal of mining science and technology, 2016. **26**(2): p. 183-186.
20. Hajihassani, M., et al., *Blast-induced air and ground vibration prediction: a particle swarm optimization-based artificial neural network approach.* Environmental Earth Sciences, 2015. **74**(4): p. 2799-2817.
21. Hasanipanah, M., et al., *Feasibility of indirect determination of blast induced ground vibration based on support vector machine.* Measurement, 2015. **75**: p. 289-297.
22. Hasanipanah, M., et al., *Forecasting blast-induced ground vibration developing a CART model.* Engineering with Computers, 2017. **33**(2): p. 307-316.
23. Hasanipanah, M., et al., *Estimation of blast-induced ground vibration through a soft computing framework.* Engineering with Computers, 2017. **33**(4): p. 951-959.
24. Hasanipanah, M., et al., *Prediction of blast-produced ground vibration using particle swarm optimization.* Engineering with Computers, 2017. **33**(2): p. 173-179.
25. Hasanipanah, M., et al., *Prediction of air-overpressure caused by mine blasting using a new hybrid PSO–SVR model.* Engineering with Computers, 2017. **33**(1): p. 23-31.
26. Hasanipanah, M., et al., *Prediction of an environmental issue of mine blasting: an imperialistic competitive algorithm-based fuzzy system.*

International Journal of Environmental Science and Technology, 2018. **15**(3): p. 551-560.
27. Hertz, J.A., *Introduction to the theory of neural computation*. 2018: CRC Press.
28. Hustrulid, W.A., *Blasting principles for open pit mining: general design concepts*. 1999: Balkema.
29. Iramina, W.S., et al., *Comparing blast-induced ground vibration models using ANN and empirical geomechanical relationships.* REM-International Engineering Journal, 2018. **71**(1): p. 89-95.
30. Jain, A.K., J. Mao, and K.M. Mohiuddin, *Artificial neural networks: A tutorial.* Computer, 1996. **29**(3): p. 31-44.
31. Khandelwal, M. and T. Singh, *Prediction of blast induced ground vibrations and frequency in opencast mine: a neural network approach.* Journal of sound and vibration, 2006. **289**(4): p. 711-725.
32. Khandelwal, M. and T. Singh, *Evaluation of blast-induced ground vibration predictors.* Soil Dynamics and Earthquake Engineering, 2007. **27**(2): p. 116-125.
33. Khandelwal, M. and T. Singh, *Prediction of blast-induced ground vibration using artificial neural network.* International Journal of Rock Mechanics and Mining Sciences, 2009. **46**(7): p. 1214-1222.
34. Khandelwal, M., D.L. Kumar, and M. Yellishetty, *Application of soft computing to predict blast-induced ground vibration.* Engineering with Computers, 2011. **27**(2): p. 117-125.
35. Khandelwal, M. and M. Saadat, *A dimensional analysis approach to study blast-induced ground vibration.* Rock Mechanics and Rock Engineering, 2015. **48**(2): p. 727-735.
36. Khandelwal, M., et al., *Classification and regression tree technique in estimating peak particle velocity caused by blasting.* Engineering with Computers, 2017. **33**(1): p. 45-53.
37. Kuzu, C., *The importance of site-specific characters in prediction models for blast-induced ground vibrations.* Soil Dynamics and Earthquake Engineering, 2008. **28**(5): p. 405-414.
38. Lal, B. and S.S. Tripathy, *Prediction of dust concentration in open cast coal mine using artificial neural network.* Atmospheric Pollution Research, 2012. **3**(2): p. 211-218.
39. Mokfi, T., et al., *Proposing of a new soft computing-based model to predict peak particle velocity induced by blasting.* Engineering with Computers, 2018: p. 1-8.
40. Monjezi, M., A. Bahrami, and A.Y. Varjani, *Simultaneous prediction of fragmentation and flyrock in blasting operation using artificial neural networks.* International Journal of Rock Mechanics and Mining Sciences, 2010. **47**(3): p. 476-480.
41. Monjezi, M., M. Ghafurikalajahi, and A. Bahrami, *Prediction of blast-induced ground vibration using artificial neural networks.* Tunnelling and Underground Space Technology, 2011. **26**(1): p. 46-50.
42. Monjezi, M., H.A. Khoshalan, and A.Y. Varjani, *Prediction of flyrock and backbreak in open pit blasting operation: a neuro-genetic approach.* Arabian Journal of Geosciences, 2012. **5**(3): p. 441-448.
43. Monjezi, M., M. Hasanipanah, and M. Khandelwal, *Evaluation and prediction of blast-induced ground vibration at Shur River Dam, Iran, by*

artificial neural network. Neural Computing and Applications, 2013. **22**(7-8): p. 1637-1643.
44. Muhammad, F. and M. Ferentinou, *A holistic open-pit mine slope stability index using Artificial Neural Networks.* 2017.
45. Naghadehi, M.Z., et al., *A new open-pit mine slope instability index defined using the improved rock engineering systems approach.* International Journal of Rock Mechanics and Mining Sciences, 2013. **61**: p. 1-14.
46. Perez, L.G., et al., *Training an artificial neural network to discriminate between magnetizing inrush and internal faults.* IEEE Transactions on Power Delivery, 1994. **9**(1): p. 434-441.
47. Pham, L.H., *Tourism impacts and support for tourism development in Ha Long Bay, Vietnam: An examination of residents' perceptions.* Vietnam: An Examination of Residents' Perceptions, 2012.
48. Ragam, P. and D. Nimaje, *Monitoring of blast-induced ground vibration using WSN and prediction with an ANN approach of ACC dungri limestone mine, India.* Journal of Vibroengineering, 2018. **20**(2): p. 1051-1062.
49. Saltelli, A., K. Chan, and E.M. Scott, *Sensitivity analysis*. Vol. 1. 2000: Wiley New York.
50. Schalkoff, R.J., *Artificial neural networks*. Vol. 1. 1997: McGraw-Hill New York.
51. Shahnazar, A., et al., *A new developed approach for the prediction of ground vibration using a hybrid PSO-optimized ANFIS-based model.* Environmental Earth Sciences, 2017. **76**(15): p. 527.
52. Sharma, L., V. Vishal, and T. Singh, *Developing novel models using neural networks and fuzzy systems for the prediction of strength of rocks from key geomechanical properties.* Measurement, 2017. **102**: p. 158-169.
53. Sharma, L. and T. Singh, *Regression-based models for the prediction of unconfined compressive strength of artificially structured soil.* Engineering with Computers, 2018. **34**(1): p. 175-186.
54. Shepel, T., et al., *Evaluation of cutting forces in granite treated with microwaves on the basis of multiple linear regression analysis.* International Journal of Rock Mechanics and Mining Sciences, 2018. **107**: p. 69-74.
55. Sheykhi, H., et al., *Forecasting ground vibration due to rock blasting: a hybrid intelligent approach using support vector regression and fuzzy C-means clustering.* Engineering with Computers, 2018. **34**(2): p. 357-365.
56. Singh, R., et al., *Prediction of geomechanical parameters using soft computing and multiple regression approach.* Measurement, 2017. **99**: p. 108-119.
57. Singh, T., L. Dontha, and V. Bhardwaj, *Study into blast vibration and frequency using ANFIS and MVRA.* Mining Technology, 2008. **117**(3): p. 116-121.
58. Sonmez, H., et al., *Estimation of rock modulus: for intact rocks with an artificial neural network and for rock masses with a new empirical equation.* International Journal of Rock Mechanics and Mining Sciences, 2006. **43**(2): p. 224-235.
59. Taheri, K., et al., *A hybrid artificial bee colony algorithm-artificial neural network for forecasting the blast-produced ground vibration.* Engineering with Computers, 2017. **33**(3): p. 689-700.
60. Triantafyllou, A., et al., *Application of inverse dispersion modelling for the determination of PM emission factors from fugitive dust sources in open-pit*

lignite mines. International Journal of Environment and Pollution, 2017. **62**(2-4): p. 274-290.
61. Vapnik, V. and R. Izmailov, *Knowledge transfer in SVM and neural networks.* Annals of Mathematics and Artificial Intelligence, 2017. **81**(1-2): p. 3-19.
62. Yagiz, S., et al., *Application of two non-linear prediction tools to the estimation of tunnel boring machine performance.* Engineering Applications of Artificial Intelligence, 2009. **22**(4-5): p. 808-814.
63. Yegnanarayana, B., *Artificial neural networks*. 2009: PHI Learning Pvt. Ltd.
64. Zerguine, A., A. Shafi, and M. Bettayeb, *Multilayer perceptron-based DFE with lattice structure.* IEEE transactions on neural networks, 2001. **12**(3): p. 532-545.

Opiekun: prof. dr Tomasz Lipecki
Recenzenci:
Prof. Janusz RUSEK WGGIIŚ
Prof. Slavo LABANT TUKE Koszyce

Green Growth in Mining – the Trends of Southeast Asia and Lessons For Viet Nam

Thi Kim Ngan NGUYEN[1]
1 HUMG Hanoi University of Mining and Geology , Faculty of Economics and Business Administration , Hanoi, Vietnam

Abstract: Against the serious consequences of climate change, a new growth model has been established. The green growth or low carbon growth focuses on the efficient use of natural resources, it also enhances the use of renewable energy and environmentally-friendly technologies. Therefore, the green growth is now a trend with new global rules being shaped. This paper presents the trend of Southeast Asian countries on green growth in mineral mining, one of the economic growth activities which has a negative impact on the environment so that draw lessons for Viet Nam.

1. Setting the scene

In theory, minerals mining contributes to economic growth, job creation and infrastructure improvements. These factors are the driving forces for poverty reduction. However, through a lot of research, scientists have pointed out that: Beside the positive impacts, the mineral mining activities in Southeast Asia countries also have many negative impacts on the socio-economic life, especially the environmental pollution. Up to now there have been no statistic data of all the waste rocks from mines and mines which are being exploited or processed in Southeast Asian countries. Among them there are countries with large scale mining activities such as Indonesia, the Philippines, Myanmar, and Viet Nam. Mining activities destroy the environment because of the accumulation of soil, dust and wastewater in large quantities, causing pollution of air and water. Dust from the ilmenite, rutile and zircon sand extraction which is processed from sand has made many workers in the titanium industry suffer from respiratory diseases, and been under dangers of radioactive. Suspended solids not only contaminate the surface water quality in the mine but also contain heavy metals, mercury and other toxic chemicals which can affect adjacent and downstream rivers. Therefore, the trend of green growth in mining activities of Southeast Asian countries is the goal and the requisites for sustainable development as well.

2. The status of green growth in mineral activities of Southeast Asian countries

The global economic and social fluctuation and natural disasters in recent years have had negative impacts on the economic growth of Southeast Asian countries. Consequently, in order to response to the Green Growth and Green Economy initiative proposed by the United Nations Environment Programme (UNEP) in 2008 and the desire to achieve sustainable development in the long run, the Association of South East Asian Nations (ASEAN) have started to pursue a green growth strategy towards a sustainable growth economy. The essence

of the strategy is the development with low emissions and resource consumption which also ensures sustainability of ecosystems and biodiversity, conserves natural resources and protects the environment, aims to ensure social security, poverty reduction, improve living conditions in all aspects for inhabitants.

Southeast Asia is bordered by three major tectonic plates of Asia-Europe, the Pacific and the Indian Ocean. Geologically, Southeast Asia includes rocks from Precambrian to Quaternary, which develops many different age-related magmatic activities; especially Mesozoic and Cenozoic magma, where there are many subduction zones and volcanic islands. The favorable geological conditions have made Southeast Asian countries become rich and diversified mineral resources. Although each Southeast Asian country has its advantages in some minerals, generally, Indonesia, the Philippines and Myanmar have the greatest potential. [6]

Minerals in Southeast Asia have contributed significantly to the growth of each country's economy, in some countries they are major contributors to the Gross Domestic Product (GDP). However, in recent years, the effects of climate change have partly influenced the growth of mining industry in Southeast Asia. Southeast Asia is considered one of the most serious affected regions from both the global economic crisis and the climate change. Disadvantages of these countries are inadequate economic structure, low actual production value, high input consumption of products that are causing problems for the increase sustainable development. The global economic, social fluctuation and natural disasters in recent years have had negative impacts on the economic growth of Southeast Asian countries. Consequently, the greening of mineral exploitation along with the solutions to adapt climate changes are important policies for mining industry in Southeast Asia in recent years.

2.1. Green growth in the Philippines mineral activities [6][5][7]

The Philippines has a long history of mining and has favorable geological conditions for the creation of a variety of mineral deposits, here is one of the riches minerals in Southeast Asia. Its mineral resources are mainly Cu, Au, Ni, Cr, Fe.

Iron ore mines are closely related to the Tertiary diorite rock, typically the Larap mine. Iron ore reserves are approximately 77 million tons. There are three important copper mineralization zones. The north is associated with the subduction zone to the east of the East Sea of Viet Nam, with the middle Miocene age to late Miocene. The middle zone is associated with the subduction zone of Sulu Sea, with late Paleocene age. The eastern part is associated with the subduction zone of Pacific Ocean, with the Pliocene age. There are 15 Cu and Cu-Au with Porphyry type mines, of which the large mines such as the Atlas Biga mine in Sebu with a reserve of about 5 million tons of Cu. There are four Au-Ag, Au-Cu and Au-Te hydrothermal circuits in Luzon and Mindanao.

Low-temperature gold-silver mineralization is higher than that of porphyrite; gold-silver, telur and copper can coexist as in Baguio. Placer mine in Mindanao contains 54 tons of Au, the remaining mines occupy about 21 to 23 tons of Au. There are 7 mines of laterite weathering on super-mafic rocks, of which Rio Tuba in Palawan has 220 thousand tons of Ni and Nonoc 1 mine in Dinagat has 930 thousand tons of Ni. These mines are large-sized, while the other mines are medium-sized with reserves of about 100 to 200 thousand tons of Ni. The largest source of chromite is from the ophiolite complex in Zabarez province. There are two large-scale chromite mines in Zambarez province, which original came from magma, associated with super-mafic rocks, they are Acoje mine with 640 thousand tons of Cr_2O_3 and Coto/Masinloc mine with about 1,7 million tons of Cr_2O_3.

Currently, the mining industry in the Philippines has shown a trend of green growth, those mine that affect the environment are at risk of being closed. The Philippines is exerting themselves to improve the mining operations in order to limit impacts on the environment

and the local community. President Rodrigo Duterte has expressed a tough stance on the mining industry when claiming that the Philippines will be able to survive without this industry.

Those environmental disasters happened in the past, including the leakage of waste at a copper mine in the central Marinduque province in 1996 has made the rivers contaminated, causing the Philippines mining industry to be strongly opposed.

The Philippines is currently the largest nickel ore supplier in China. By 2016, the Philippines had exported 24 million tons of nickel to China, but the number of nickel ore is exported in the first seven months of 2017 decrease 27%.

On 9th February 2007, the Philippines closed 23 of 41 mines in this country. This was due to their damage to river basins, sedimentation in coastal waters and farmland, suspension of 5 other mines because of environmental concerns, 8 of the closed mines are nickel ore mines – the reason for the sharp rise in nickel prices in the world market. The Philippines Environment Minister – Regina Lopez released the cancellation of 75 mining contracts on 14th February 2007 to promote a campaign to stop the exploitation of resources in sensitive areas. Among the canceled contracts on 14th Feb there was the $5.9 billion Tampakan gold-silver mining project in Nam Cotabato province on Mindanao Island.

2.2. Green growth in Indonesia mineral activity [6]

Indonesia is one of the richest minerals in Southeast Asia. Minerals of Indonesia are mainly Au, Cu, Ni, Sn.

All porphyry in Indonesia are associated with the Miocene-Pilocene volcanic arc. The main mines are Tapada and Sasaki in Sulawesi. There are 6 Cu-Au porphyry mines, of which Batu Hijau mine in Lesser Sunda has about 2.6 million tons of Cu and 233 tons of Au, Grasberg mine has more than 9 million tons Cu and 1262 tons of Au. The Au-Ag, hydrothermal Au-Ag, medium-sized, including the two largest Au-Ag mines: the Kelian mine in Kalimantan with 105 tons of Au and the Gunung Pongkor mine in Java has about 102 tons of Au and 972 tons of Ag. The Au-type thermal mines are Gunung Panti with a capacity of 40 tons of Au and the Awak Masmindo mine in Sulawesi with a capacity of 26 tons Au. Laterite nickel was exploited in Pomalaa and Soroako in eastern Sulawesi. Soroako mine has about 3 million tons of Ni, Pomalaa mine has about 1.9 million tons of Ni and Gagu has 3.9 million tons of Ni. There are about 10 pewter tin and weathering mines with capacity of 750 thousand tons of tin, of which Benlinju and Pemali are large-sized. Apart from these metal minerals, there are also industrial minerals such as limestone, feldspar, clay, sulfur, quartz sand and phosphate.

Among the countries in Southeast Asia, Indonesia is now taking relatively large consequence of environmental pollution. The rising of the sea level and erosion in coastal areas, the increase of the frequency and intensity of severe weather and extreme weather, which causing the extinction of species and the spread of infectious diseases through animals. Facing this situation, the administration of former President Yudhoyono is paying close attention to environmental issues and the significant development of the environmental cooperation between the US and Indonesia, especially the green growth trend in mining activities through the improvement of environmental management in mining activities.

Indonesia's mineral management system is divided into 3 levels (ministerial, provincial, regional – equivalent to district level in Viet Nam). Regardless of the mine's size, the regional level is competent, where the mine is located in the whole region. For mines located between two regions, it is under the jurisdiction of the provincial licensing. The ministerial level licenses those mines located between two provinces to exploit. The ministerial level licenses to exploit and process coal and metal minerals; The provincial level licenses for non-metallic minerals; The regional level licenses for construction stones. This decentralization aims to

clarify the responsibilities, the management and monitoring obligations of each level; especially the interstate mines between two localities.

Green growth in Indonesia is also reflected in restricting the export of raw materials to minerals. The Indonesian government has detailed regulations on deep processing for each mineral group and domestic market regulations, which regulate the rate of domestic sales. The above-mentioned management levels, based on their competence, regulate mineral prices and the price bracket to build reference prices for management. On the other hand, Indonesia finds the resolution of land conflicts between its economic sectors by enaction of the Law on Spatial Planning. Besides, in Indonesia, mining companies are responsible for paying the land use obligations to the central government. Collected taxes on mineral mining are clearly stated in the Mineral Law of 4/2009, especially the division of revenue among the different levels: central levels: 20%; provincial level: 16%; district/regional level: 32%; local people: 32%. The specific taxation of mineral has helped the authorities take the initiative in using these revenues. Lower levels with higher entitlement will help them to have more funds to deal with adverse impacts from mining. *[7]*

Indonesia is a country with rich mineral resources, which is closely controlled by a unified organizational system from central to local. All mineral resources in this country are explored for reserve and zoning, detailed and specific planning. In management, there is a logical and clear, not overlapping; there is a synchronous assignment and coordination between branches and levels. Legal policies are institutionalized for the distribution of benefits in a public and evident way among the state (central, region and local government), businesses and people. Thus, there was no conflict among the parties that leads to mass appeals. Furthermore, there is EITI civil society organization that oversees the law enforcement of the parties, then make recommendations to correct the mistake when a party does not comply with the law. As a result, Indonesia's mineral management has been highly effective towards green growth.

2.3. Green growth in Myanmar mineral activity [6]

Myanmar is rich in mineral resources, the important minerals are copper, gold, lead, zinc, silver, tin, tungsten, antimony, chromite, nickel, gemstone. In terms of potentiality, Myanmar is classified as one of the richest minerals in Southeast Asia.

More than 50 copper occurrences are distributed along three major tectonic units of Myanmar, including three porphyrite copper mines near Chindwin. Letpadaung Taung mine has about 400 million tons of ore, with 0,5% Cu (2 million tons of Cu). These are reserves of world-class size. The iron ore deposits have reserves of about 100 million tons in Pengpet, southern Myanmar. Bawdwin mine is a multi-metal complex consisting of Pb-Zn-Ag, which is a large-scale thermoluminescent vessel with reserves of 9 million tons of Pb and 5.2 million tons of Zn. There are also 13,950 tons of Ag. This mine is considered as the world's richest silver. The gold mines are located in Play Aung Taung and Thayethkhone, Shwekyin and near Myitkyina, along the Ayeyawady River. In addition, the Kyaukpahto and gold potential nearby areas are being explored by domestic and foreign companies. The nickel deposits are found in China town, which is 30km northwest of Mandalay with estimated reserves of 30 million tons of ore, with an average content of 1.1% Ni, about 0.3 million tons of Ni. Potential reserve is 80 million tons, with 1% Ni, equivalent to 0.8 million tons of Ni. Coal deposits are mostly semi-bituminous coal with a reserve of about 200 million tons in the northern region, with Kalewa minerals being the only significant minerals deposit. There are also coal mines in Tanintharyi. Myanmar's main mining company is interested in exploring and exploiting this mineral. Rubi is mined in Mogok, northeastern Mandalay, sapphire and various colored gems including spine, grenadine, peridot, tourmaline, aquamarine, amethyst, citrine, zircon, and lunar rock, etc. which are exploited from Mogok. It can be said that the mining sector

plays an important role in the economy of Myanmar. However, environmental pollution and the consequences from the mining activities have no significant impact on the national economic growth in Myanmar. Aimed at green growth, the Environment Law of Myanmar was promulgated on March 30th, 2012. In the Environment Law, there are some special Provisions that are necessary for foreign investors, including environmental quality standards, the list of projects or activities that require preliminary environmental assessment or full implementation, the list of hazardous wastes in the production process, chemicals and other hazardous substances from industries and agriculture, especially the exploitation of minerals containing noxious substances that may affect strongly the environment at the present or in the long run. Additionally, to control excessive exploitation of jade and gems, the government of Myanmar has tightened the mineral extraction permit. Companies must meet the new environmental regulations to receive this permit.

3. Lessons for Viet Nam

With awareness that green growth is not only a motivation and global economic recovery but also a model and tool for sustainable development, Viet Nam has determined clearly that there is no other way than to promote green growth. Viet Nam has also showed determination to pursue an environmentally friendly development growth model. In 2012, the Vietnamese Government has issued the National Strategy for Green growth and has enacted the Green Growth Strategy Agenda 2014-2020 with 66 actions in 2014. [1]

Viet Nam's green growth strategy sets out three important tasks: 1) Reducing the intensity of greenhouse gas emissions and increasing the use of clean energy and renewable energy. 2) Greening production. 3) Greening the lifestyle and promoting sustainable consumption. In particular, the specific indexes are: Reducing greenhouse gas emissions in energy activities by 10-20% for the period 2011-2020 and 35-45% for the period 2020-2030. On the goal of greening production, the indicators will be approached are: The value of high-tech products in GDP is about 42-45% (2010-2020) and 80% (2020-2030); 100% of newly-established production and business establishments must apply the clean technologies or equipment in order to reduce pollution and waste treatment.

Viet Nam is rich in mineral resources with more than 60 kinds of minerals in more than 500 mines. Mineral mining (including oil and gas) contributes about 10-11% of GDP and contributes 28% to state budget revenues. [2] [3] However, the exploitation of mineral resources in Viet Nam in recent years is still inadequate and unreasonable, due to loss and waste of resources, polluted water in areas with mineral activities, low quality of environmental regarding ambient air and emissions, over limited dust especially in coal and quarries mines, etc. At a result, the mining industry of Viet Nam must also be driven by green growth. From the exploration of green growth in mineral mining in the world and from the reality of mineral exploitation in Viet Nam, there are the lesson learned, as follows:

First, green growth in mineral mining must be linked to the chain: from raw and deep processing to mining and support services. Avoiding the mining of raw minerals and export them. This will reduce the speed of resource extraction, avoid waste of resources and improve the quality of the environment. Also, it is necessary to add more processing conditions and commitments before the mineral extraction permit is issued. In fact, the investment capital for mining is not large, but the processing requires large capital, modern technology, thus, leading to widespread exploitation then cannot achieve the purpose of deep processing.

Secondly, reformation and adaption of green marketing tools (green taxation, green budget) is significant. The tax preference regime should be applied to the mineral exploitation enterprises to support environmental protection activities. In order to avoid the loss of resources and revenues for the state budget, the natural resource tax needs to be shifted from calculated mining output to the approved mineral reserve, depending on types of minerals.

The tax exemption and reduction of the extraction reserve will be decided depending on each case, so that enterprises can enhance the mining and mineral savings. On the other hand, higher tax rates should be applied to raw materials, lower tax rates for refined or processed resources.

Thirdly, the price of mineral products should be implemented in accordance with the market mechanism to achieve these objectives: Forcing business to strictly manage costs, output and product quality to improve efficiency; Overcoming the negative effects of differences in domestic and export prices, especially smuggling; Encouraging the process of mineral exploitation and processing to raise the coefficient of resource recovery; and Forcing consumption of mineral products must be used economically.

Finally, it is necessary to set up specific institutions to implement green growth in mineral exploitation activities, particularly, the public and evident distribution of benefits between the state (central, region and local authorities), enterprises and people.

4. Conclusions and recommendations

The goal is green growth in mining activities, which is based on the process of changing the growth model, restructuring the exploitation through the application of advanced technology, the development of infrastructure system for effective use of mineral resources, reducing greenhouse gas emissions, coping with climate changes, contributing to poverty reduction and driving the economic growth in a sustainable way.

Green growth in general and green growth in mining activities in particular have many opportunities, but also many challenges. This is a long-term process; therefore, all levels, sectors and enterprises need to be fully aware of challenges. Consequently, it will change the method of mining minerals; and consumption of minerals in the direction of efficiency to achieve the goals of the national green growth strategy.

References

1]. Prime Minister, Decision No. 1393 / QD-TTg dated September 25th, 2012; *The National Strategy for Green Growth for 2011 – 2020 and vision to 2050*, (2012)

2]. Le Thanh Van, Nguyen Dinh Hoa, *Green economy development orientation in the mining industry*, (2013).

3]. Nguyen The Chinh and Dang Quoc Thang, *Green Growth Strategy: Trends of the era*, (2014).

4].Central Institute for Economic Management: *Some policy implications for the Implementation of Green Growth in Viet Nam*, (2014).

5]. Nguyen Huy Hoang, *Green Growth in some ASEAN countries in the context of economic restructuring and coping with climate change, Southeast Asian Studies Institute* (ed.), (2015).

6]. Le Van De, *Solid mineral potential of some Southeast Asian countries, Viet Nam Tectonic Association*, (2005).

A case study on the determination of the excavated trench depth in unsaturated soil constructed by trench method without supporting structures

Nguyen Xuan Man[1*], Do Thi Them[2]
[1] HUMG Hanoi Univercity of Mining and Geology, Faculty of Building, Hanoi, Vietnam

[2]House 14, Ngo Thi Sy Street, Langson City, Langson Provincy, Vietnam

[*]Email: mannxdoky@gmail.com; Fon: 0903010864

Abstract: Together with the excavated width, the depth of trench play a vital role in stability as well as economics effectiveness of a trench constructed by open trench method. It is widely recognized that a steeper angle of an open trench, a smaller amount the excavated soil required; however, the trench is unstable. In this case, an external supporting structure system is obliged to prevent the trench from falling into the excavation zone. In addition, an open trench is normally located above the water table, hence under unsaturated condition. One of the most important characteristics of unsaturated soil is negative pore water pressure which brings about the matric suction, higher negative pore water pressure, higher matric suction; consequently, higher shear strength of soil. On the other hand, there is a few theories and research works have been reported on the method of determining a suitable depth of a trench under unsaturated condition. Previous works tend to assume that the distribution of matric suction is either constant or linear with depth; as a result of this, the designed results are often overestimated compared to practical results. In this paper, the effect of distribution of matric suction was taken into account to propose an equation to estimate the depth of a trench that can be applied without supporting structure. Finally, an example of numerical calculation of a depth of the open trench was described.

1 Introduction

One of the most important parameters need to be considered when dealing with the stability of underground construction constructed by open method such as traffic tunnel, cable tunnel (power electricity cable, communication cable), sub-pavement tunnel, even some path of railway tunnel, are that the magnitude of the depth (H), and width (L) of open trench. In other words, the L/H ratio must be met both the stability of underground structure requirement and economic effectiveness. The L/H ratio controls the angle of the open trench, hence amount of excavation work required. The smaller the value of β (as shown in the Fig 1) is, the higher stability of the open trench can be obtained; however, the larger the amount of excavation work need to be done. Economically side speaking, once the value of β equals to 90^0 the amount of excavation work required is lowest, hence the highest of effectiveness

of economic. In spite of this, the stability of the open trench must be taken into account. It is widely observed that under this condition $\beta=90^0$, some external supporting structures (known as the temporary structure) ought to be applied such as earth anchor, retaining wall, struts, sheet pile,. As a result of this requirement, some shortcoming might be seen as follows:

- Due to the existence of the temporary structures, the construction area of underground construction is reduced;
- It is costly since the temporary structures used;
- Progress of construction work is highly affected, even much longer as compared to that in case of without using temporary structures.

Based on these problems, this paper aims to determine the applicable depth of the open trench without supporting structures under the condition that the angle of the open trench,β, equals to 90 degree.

2 Required depth of an open trench

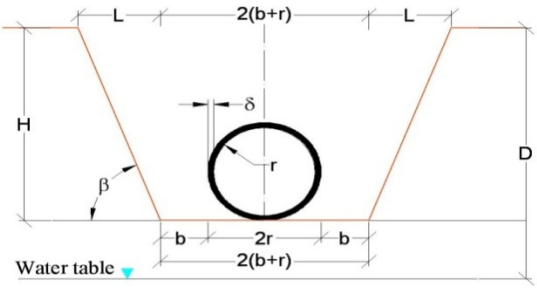

Fig 1. A typical cross section of an open trench

Where: δ is the thickness of structure, (mm); r is the inner radius of circle-structure (or half of width of rectangular shape), (cm); β is the angle of the open trench (degree);

It's widely recognized that the open trench is constructed in somewhere that is normally located above the water table, hence under unsaturated condition. Thus, in order to find out the applicable value of the depth of the open trench,H, without supporting structures with the angle of open trench of 90 degree, the depth of water table is assumed to be D (m) (Fig 1), the type of soil is classified as cohesionless soil and under unsaturated condition.

According to Kartozia B.A.1983, the required depth, H must be fulfilled the following conditions:

$$H \geq (2 \div 5)2r = (4 \div 10)r \tag{1}$$

and, $$D > H + m \tag{2}$$

Where: m is the thickness of backfill soil layer which used to resist the water penetration under high pressure, this parameter can be defined as below Terzaghi K. 1941:

$$m \geq \frac{h}{(\frac{\gamma_s}{\gamma_w} - 1)} \tag{3}$$

Where γ_s, γ_w are the density of soil, and water respectively (kN/m^3);h is the height of pressurized water once groundwater seepage into the open trench.

3 Matric suction in unsaturated soil

One of the most important characteristic of unsaturated soil is the negative pore water pressure. In other words, the pore water pressure due to capillarity is negative (suction), it is defined as a function of the size of the soil pores and the water content. At the groundwater level, the pore water pressure is zero and decreases (becomes negative) once the capillary zone goes up. As the result of the negative pore water pressure, the effective stress increases. To specify, for the capillary zone, z_c, the pore water pressure at the top is $-z_c\gamma_w$, hence the effective stress (Fredlund 2014; Fredlund et al. 2012; Fredlund et al. 1996) stated that profile of matric suction in a horizontally layered unsaturated soil generally depends on several factors; especially the soil properties as given by soil water characteristic curve and the soil permeability, environmental factors including infiltration due to precipitation or evaporation rates and boundary drainage conditions including the location of groundwater level. The matric suction profile will come to equilibrium at a hydrostatic condition when there is zero net flux from the ground surface. If moisture content is extracted from the ground surface such as evaporation, the matric suction profile will be drawn to the left (matric suction increases). If moisture enters at the groundwater surface such as infiltration, the matric suction profile will be drawn to the right (matric suction reduces).

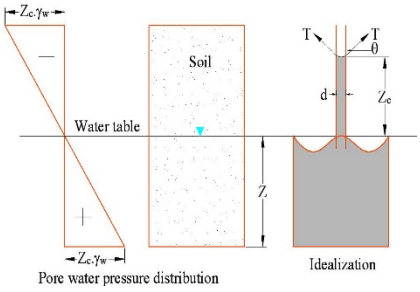

Fig 2. Simulation of capillary in soil (Budhu 2000).

Under steady state, the water flux in and out of the soil reaches the balance. If the magnitude of water flux is the same as the hydraulic conductivity of the saturated soil, the magnitude of the pore-water pressure is constant (Fig 3).

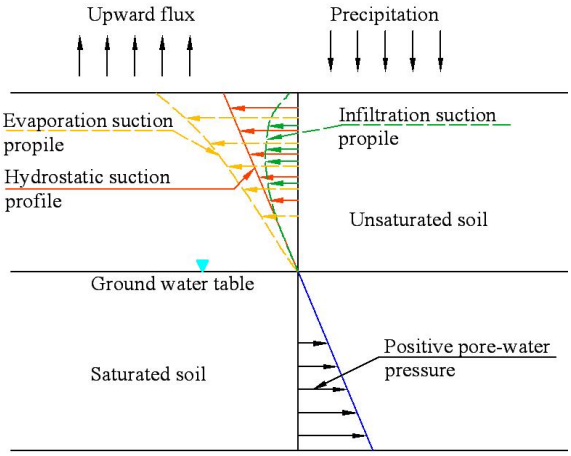

Fig 3. Matric suction profile in horizontally layered unsaturated soil profiles under various surface flux boundary condition ((Fredlund 2014; Fredlund et al. 1996)

From the distribution of matric suction, it's found that the matric suction profile varies with depth and linearly reduced from surface to the water table; however, once the boundary drainage conditions change is due to either upward flux or precipitation, the distribution of matric suction is not linearly. Therefore, in this paper the change in the distribution of matric suction is assumed as a function of the third order polynomial and expressed as below:

$$F_{hd}(y) = a + by + cy^2 + dy^3 \tag{4}$$

Where y is the considered depth of open trench; F_{hd} is the function of matric suction varies with depth. The equation (11) must be met the following conditions:

$$y = 0 \rightarrow F_{hd}(y) = \max = k\gamma_n gD$$

$$y = D \rightarrow F_{hd}(y) = 0$$

By considering and comparing with the practical condition, the Eq (4) can be rewritten as:

$$F_{hd}(y) = \frac{A}{D}\left(D^2 - 2y^2 + y^3 / D\right) \tag{5}$$

$$\text{Or } F_{hd}(y) = AD\left(1 - y^3 / D^3\right) \tag{6}$$

Where $A = k\gamma_n g$, k is the pore water pressure coefficient, which varies with the slope of hydrostatic pressure (or hydrostatic suction profile); g is specific gravity. Taking a look into the Eq (12a, b), the magnitude of matric suction is decrease from a value of AD = $kD\gamma_n g$ (at y=0) to zero (at y=D). The istribution of matric suction is showed in the Fig 4.

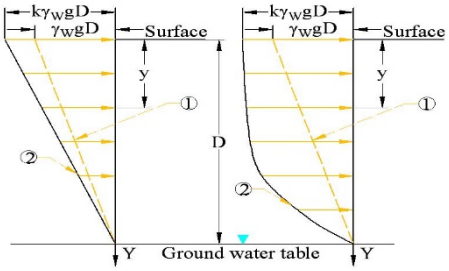

Fig 4. The distribution of matric suction with depth. (1) represent the surface of hydrostatic suction; (2) the distribution line of matric suction.

4 Determination of depth of open trench without supporting structure

4.1 Earth pressure

The horizontal pressures act to the wall of open trench is caused by the active earth pressure, p_a, which can be determined as follow(Bang 1985; Terzaghi 1941; Terzaghi et al. 1996; Wang 2000):

$$p_a = (\sigma_n - u_a) = (\sigma_đ - u_a)\cot g^2(\frac{\pi}{4} - \frac{\varphi'}{2}) - 2C.\cot g(\frac{\pi}{4} - \frac{\varphi'}{2}), \quad (7)$$

$$\text{Where : } \sigma_đ = \gamma_đ.g.y, \quad (8)$$

C is the total cohesion stress which consists of two components, one is the effective cohesion, C'; the other is suction force: $(u_a - u_w)tg\varphi_b$. In other words:

$$C = C' + (u_a - u_w)tg\varphi_b \quad (9)$$

Combination of Eq (9) and (7):

$$p_a = (\sigma_n - u_a) = (\sigma_đ - u_a)\cot g^2(\frac{\pi}{4} - \frac{\varphi'}{2}) - 2(C' + (u_a - u_w)tg\varphi_b)\cot g(\frac{\pi}{4} - \frac{\varphi'}{2})$$
$$= (\sigma_đ - u_a)\cot g^2(\frac{\pi}{4} - \frac{\varphi'}{2}) - 2C'\cot g(\frac{\pi}{4} - \frac{\varphi'}{2})$$
$$- 2(u_a - u_w)tg\varphi_b.\cot g(\frac{\pi}{4} - \frac{\varphi'}{2}) \quad , \quad (10)$$

Substitute Eq (5) into Eq (10):

$$p_a = (\sigma_n - u_a) = (\sigma_đ - u_a)\cot g^2(\frac{\pi}{4} - \frac{\varphi'}{2}) - 2C'\cot g(\frac{\pi}{4} - \frac{\varphi'}{2})$$
$$- 2tg\varphi_b.\cot g(\frac{\pi}{4} - \frac{\varphi'}{2}).\frac{A}{D}[D^2 - 2y^2 + y^3/D] \quad (11)$$

Substitute Eq (8 into Eq (11):

$$p_a = (\sigma_n - u_a) = (\gamma_d gy - u_a)\cot g^2(\frac{\pi}{4} - \frac{\varphi'}{2}) - 2C'\cot g(\frac{\pi}{4} - \frac{\varphi'}{2}) - 2tg\varphi_b.\cot g(\frac{\pi}{4} - \frac{\varphi'}{2}).\frac{A}{D}[D^2 - 2y^2 + y^3/D] \quad (12)$$

,

The total magnitude of active earth pressure acts to the retaining wall with its height of H_t, p_a, can be defined as:

$$P_A = \int_0^{H_t} p_a dy \quad (13)$$

4.2 Determine the magnitude of depth of open trench

The distribution of active earth pressure can be divided into two regions, one is tensile region, the other one is compressive region. Two these regions are separated at a depth of y_k. In the tensile region (from the surface to depth of y_k), the active earth pressure is negative, which causes soil mass behinds retaining wall tends to move away from the retaining wall. The magnitude of y_k may be estimated by combination Eq (10) and Eq (5, 6), together with a condition of $p_a = 0$ and $u_a = 0$:

$$\sigma_d \cot g^2(\frac{\pi}{4} - \frac{\varphi'}{2}) - 2C'\cot g(\frac{\pi}{4} - \frac{\varphi'}{2}) - 2tg\varphi_b.\cot g(\frac{\pi}{4} - \frac{\varphi'}{2}).\frac{A}{D}[D^2 - 2y^2 + y^3/D] = 0 \quad (14)$$

After working out the Eq (14), the value of y_k can be found.

If total active earth pressure Pa acts to the retaining wall is completely dissipated, the corresponding depth under that condition will be the one that can be applied without supporting structure. In other words, the magnitude of depth of the open trench, y_{kc}, can be determined by solving the following equation:

$$P_A = \int_0^{y} p_a dy = 0 \quad , \quad (15)$$

By substituting Eq (11) into Eq (15), and working out the Eq (15) with y is the variable, the y_{kc} can be derived, and its value is a function of

$$y_{kc} = f(\varphi', \varphi_b, u_a, \sigma_d, D, A) \quad (16)$$

5 Numerical caculation

The physico-chemical properties of the studied soil was obtained from a construction site located in the Southeast of Vietnam is described in the Table 1.

Table 1. Soil parameters used in this paper

Description	Symbol	Unit	Value
Unit weight	γ	kN/m3	18
Effective cohesion	c’	kPa	50
Effective friction angle	φ'	Degree	22

Effective friction angle associated with matric suction	φ^b	Degree	14
Pore-water pressure coefficient	k	-	1.5
Other parameters			
Pore air pressure	u_a	kPa	0

5.1 Effect of level of ground water table

By changing the level of groundwater table, D, the relationship between depth of the open trench without supporting structure and D, can be found (Table 2), and (Fig 5).

Table 2. Relationship between k_{kc} and level of groundwatertable

Description	Unit	Values						
Depth of groundwater table, D	m	7	8	9	10	11	13	15
k_{kc}	m	4.38	4.97	5.25	5.83	6.19	7.18	7.34

5.2 Effect of effective friction angle (Fig 6)

Table 3. Relationship between k_{kc} and effective friction angle

Description	Unit	Values						
Effective friction angle,φ'	degree	10	14	18	22	26	30	35
k_{kc}	m	4.85	4.55	4.34	4.21	3.87	3.57	3.32

5.3 Effect of effective cohesion (Fig 7)

Table 4. Relationship between k_{kc} and effective cohesion

Description	Unit	Values						
Effective cohesion, c'	kPa	20	40	50	60	70	75	85
k_{kc}	m	3.71	4.09	4.23	4.31	4.39	4.45	4.63

5.4 Effect of pore water pressure coefficient (Fig 8)

Table 5. Relationship between k_{kc} and pore-water pressure coefficient

Description	Unit	Values				
Pore-water pressure coefficient, k	-	1.0	1.2	1.5	1.7	2.0
k_{kc}	m	3.22	3.69	4.23	4.52	4.98

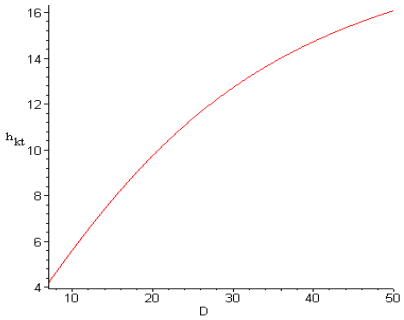

Fig 5. Relationship between k_{kc} and level of groundwater table

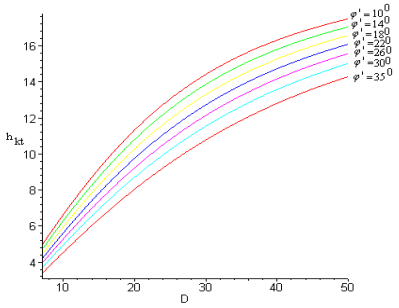

Fig 6. Relationship between k_{kc} and effectivefriction angle

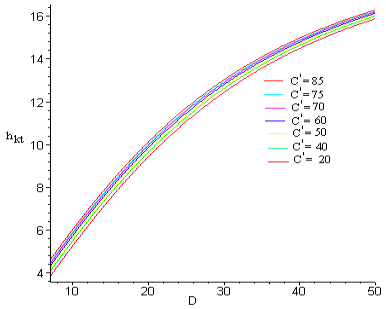

Fig 7. Relationship between k_{kc} and effective cohesion

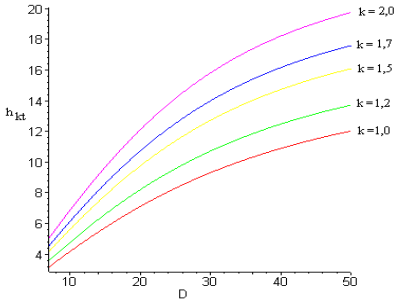

Fig 8. Relationship between k_{kc} and pore-water pressure coefficient

6. Conclusion

♦ Due to the existence of negative pore-water pressure, the total cohesion forces increases. Also, the loss of soil mass which located behind the retaining wall induces the crack. This is a point that can be used to consider whether the open trench needs to be strengthened at a certain depth or not;

♦ Previous works assumed that the distribution of the matric suction is linearly decreased with the depth; consequently, the tolerances are normally higher than those in reality;

♦ In this paper, the distribution of matric suction is assumed to be third order polynomial for determination of the depth of open trench without supporting structure;

♦ As can be seen from numerical calculation:

- The magnitude of k_{kc} is nonlinearly increased with the level of groundwater table; however, once the level of groundwater reaches the certain value, the value of k_{kc} almost constant and tends to reach the critical value;

- Under the same conditions:

+The value of k_{kc} decreases with an increase of effective friction angle;

+The value of k_{kc} does not significantly increase as the effective cohesion goes up;

+The value of k_{kc} is notably increased as the pore-water pressure coefficient, k, increases.

References

1. Bang S. Active earth pressure behind retaining walls. Journal of Geotechnical Engineering 111(3):407-412. (1985)
2. Bishop A, and Donald I. The experimental study of partly saturated soil in the triaxial apparatus. Proceedings of the 5th international conference on soil mechanics and foundation engineering, Paris. p 13-21. (1961)
3. Bishop AW, and Blight G. Some aspects of effective stress in saturated and partly saturated soils. Geotechnique 13(3):177-197. (1963)
4. Budhu M. *Soil Mechanics and Foundations*: Wiley. (2000)
5. Fredlund D, Morgenstern NR, and Widger R. 78. The shear strength of unsaturated soils. Canadian geotechnical journal 15(3):313-321.(2013)
6. Fredlund DG. The emergence of unsaturated soil mechanics. Canadian Geotechnical Journal 51(12):ix-x.(2014)
7. Fredlund DG, and Rahardjo H. Soil mechanics for unsaturated soils: John Wiley & Sons.(1993)
8. Fredlund DG, Rahardjo H, and Fredlund MD. Unsaturated soil mechanics in engineering practice: John Wiley & Sons.(2012)
9. Fredlund DG, Xing A, Fredlund MD, and Barbour S. The relationship of the unsaturated soil shear to the soil-water characteristic curve. Canadian Geotechnical Journal 33(3):440-448.(1996)

Recovery of clean coal from the contaminated waste of Quang Ninh province - Viet Nam

Kim Dung Nhu Thi[1*], Chinh Vu Thi[1]

[1] HUMG Hanoi University of Mining and Geology, Faculty of Mining, Hanoi, Vietnam

[*] Corresponding author: nhuthikimdung@humg.edu.vn

Abstract. The contaminated waste is a by-product generated during coal mining process. This type of products may contain more or less 20% of clean coal, thus their ash content may vary in a wide range of 60 to 80%. This waste normally is stockpiled separately at "temporary disposal dumps" as they would not be regarded as waste in the full meaning, however, it is very sensitive for the miners who attempt to process such a waste. Based on the results of the coal characteristics survey at some surface coal mines of Vietnam, the studying authors have collected a large quantity of representative samples, such as Ha Tu, Nui Beo, Tay Khe Sim, Ha Rang mines and have carried out a number of experiments using low cost and highly efficient separating equipments. These are semi-industrial movable screen jig, fluidization separator, some samples of -0.5 mm size using flotation method. Products of processing include clean coal, which has ash content obtain quality standard of Viet Nam (clean coal is consumed easily) and tailings have ash content over 80%, which can waste. The study results showed that the application of the new machines could allow significant recovery of clean coal from the contaminated waste. This may significantly contributes in reduction of environmental pollution while ensuring the production viability and economic efficiency for the miners.

1 Introduction

The contaminated waste, also known as low-quality coal, is a relative definition of a mixture of waste rocks contaminated with coals at such a ratio that rock volume is much more than coal's. In general cases, it is a special by-product generated in the coal mining process, and in some particular cases, it may be a reject from coal screening plants, which prepare run of mine coals at mines and it is known as "coal screening reject". Characteristics of the contaminated waste include high ash content of 60% to 75% for small sized fractions while it may reach over 80% for coarser sizes. This waste is normally stockpiled separately at "temporary disposal dumps" as this product can not be regarded as

waste, currently however, it is not economical viable and efficient if miners wish to process such contaminated waste by traditional methods.

According to the data of Vietnam National Coal - Mineral Industries Holding Corporation Limited on December, 2012, the amount of low-quality coal of 14 mining companies of the Corporation has reached 8.6 Mt, from which the Coc Sau coal company contributes 2.6 Mt and Cao Son coal company has 1.9 Mt [1]. The contaminated waste quality of each stockpile at mines also varies significantly, however, there is some common characteristic of these coals as they have high ash content exceeding 60%. Selected survey data of temporary disposal dumps in Ha Tu coal mine, as shown in the table 1 [2], clearly indicate this. According to the table 1, the majority of coal size fractions 0-6 mm in the disposal dump have ash content over 40%, only few of this size may have have ash content under 40%.

Table 1. Particle size composition and ash content temporary disposal dumps in the Ha Tu Coal Company [2]

Particle size, mm	Pile 2B		Pile CB3		West Pillar - Mass I	
	Yield, %	Ash content, %	Yield, %	Ash content, %	Yield, %	Ash content, %
+ 35	25.24	81.67	23.72	82.25	26.24	83.6
15- 35	18.71	81.81	21.3	82.65	22.22	81.56
6 - 15	21	60.94	17.87	61.58	20.74	64.91
0 - 6	35.05	49.9	37.11	48.86	30.8	59.8
Sum	100.00	66.21	100.00	66.25	100.00	71.94

Particle size, mm	West Pillar - Mass II		Pile 7A		BT 20 Pillar	
	Yield, %	Ash content, %	Yield, %	Ash content, %	Yield, %	Ash content, %
+ 35	26.99	83.57	24.18	82.07	26.9	83.45
15- 35	22.27	82.26	19.77	81.04	19.45	81.11
6 - 15	22.69	67.62	25.9	60.21	24.9	61.92
0 - 6	28.05	61.40	30.15	48.9	28.75	52.20
Sum	100.00	73.44	100.00	66.20	100.00	68.65

2. Characteristics of some of the contaminated waste samples

The research group have collected contaminated waste samples from the coal mines: Ha Tu, Nui Beo and Khe Sim coal mines. Results of the particle size and ash content analysis of the studied samples are presented in table 2; 3 and 4.

Table 2. Dry sieve analysis result of sample of Ha Tu coal mine [2]

Particle size, mm	Yield, %	Ash content, %
> 35	8.5	87.1
15 - 35	18.84	79.65
6 - 15	17.65	68.08
3 - 6	17.91	59.49
1 - 3	12.79	47.17
0.5 - 1	9.02	44.88
0 - 0.5	15.29	34.12
Sum	100	60.38

Table 3. Dry sieve analysis result of sample of Nui Beo coal mine [3]

Particle size, mm	Yield, %	Ash content, %
> 35	16.40	84.80
15 - 35	12.97	81.74
6 - 15	13.15	66.60
3 - 6	12.90	58.93
1- 3	14.49	51.28
0.5 - 1	9.26	45.00
0 - 0.5	2083	37.81
Sum	100.00	60.34

Table 4: Dry sieve analysis result of sample of Khe Sim coal mine [3]

Particle size, mm	Yield, %	Ash content, %
> 50	22.58	80.19
35 - 50	6.55	78.34
15 - 35	15.15	73.38
6 - 15	16.03	70.78

3 - 6	10.36	65.68
1 - 3	11.34	56.82
0.5 - 1	2.74	41.51
0 - 0.5	15.25	63.59
Sum	100	69.78

Comments:

- The size fraction +15 mm of the Ha Tu coal mine sample, the size fraction +35 mm of the Nui Beo coal mine sample and the fraction +50 mm of the Khe Sim coal mine samples have ash content over 80%, thus these size fractions can be separated and disposed directly otherwise additional clean coal from these sizes can be recovered by using hand sorting method;
- The size fractions 0-3 mm in the coal mines of Nui Beo and Ha Tu have ash content less than 45% that is equivalent to the ash content of the traded fine coal 6B thus they can be commercialized, but the value of the trade is low. Particle size fractions 0-3 mm in the Khe Sim coal mine have ash content over 58%, thus they cannot be used for trading;
- Fine coals of 0-0.5 mm of the two coal mines of Nui Beo and Ha Tu have ash content less than 40%, thus they can be traded, however, their ash content in practice would be significantly increased due to the contamination of the broken fines from the coarse sizes;
- Particle size fractions +3 mm of the mines were sink-and-float analyzed for the assessment of the gravity washability. The assessment of the gravity washability is based on the amount of middlings fraction yields (the yield of S.G. fractions from 1.5 to 1.8). The results indicated that these particles size fractions of the three mines were of easy to average gravity washability.

3. Experimental tests

3.1. Tests on the moving screen jig

Moving screen jig (ROM jig) is a equipment developed at the end of the 20th century for the treatment of run of mine coals. To the present time, this equipment is widely accepted in many countries of the world such as China, the Federal Republic of Germany, South Africa and Australia. The advantages of this machine type are: low energy costs, low cost of the process water, suitability to high-ash content coal. This is why a semi-industrial moving screen jig was chosen to process coal samples of the previously mentioned three mines.

Particle size fractions used for tests include: fraction 3 - 35 mm of Nui Beo and Ha Tu coal mines; size fraction 15-50 mm and 3-15 mm of Khe Sim coal mine.

Table 5. Results of coal processing of particle size of 3-35 mm, Nui Beo coal sample

Products	**Yield, %**	**Ash content, %**	**Combustible matter recovery, %**
Clean coal	18.26	35.63	39.90
Fines - 3 mm	6.04	50.83	10.08
Sum of clean coal	**24.3**	**39.41**	**49.98**

Reject	75.7	80.54	50.02
Primary coal	**100.00**	**70.54**	**100.00**

The procedure for the conditional experiments on the semi-industry moving screen jig is as the follows: adjust the setting of one operating parameter while keeping others fixed, thus optimal operating parameters can be selected. Experiment results of the particle size fractions washing of the three mines in optimal operating conditions are presented in table 5; 6; 7 and 8.

Table 6. Results of coal processing of particle size of 3-35 mm, Ha Tu coal sample

Products	**Yield, %**	**Ash content, %**	**Combustible matter recovery, %**
Clean coal	26.64	36.08	49.12
Fines – 3 mm	18.15	59.29	21.31
Sum of clean coal	**44.79**	**45.49**	**70.43**
Reject	55.21	81.43	29,57
Primary coal	**100.00**	**65.33**	**100.00**

Table 7. Results of coal processing of particle size of 15-50 mm, Khe Sim sample

Products	**Yield, %**	**Ash content, %**	**Combustible matter recovery, %**
Clean coal	7.07	29.04	18.88
Fines - 3 mm	28.20	64.75	37.40
Sum of clean coal	**35.27**	**57.59**	**56.28**
Reject	64.73	82.05	43.72
Primary coal	**100.00**	**73.42**	**100.00**

Table 8: Results of coal processing of particle size of 3-15 mm, Khe Sim coal sample

Products	**Yield, %**	**Ash content, %**	**Combustible matter recovery, %**
Clean coal	21.34	22.94	40.07
Fines - 3 mm	23.17	55.19	25.30
Sum of clean coal	**44.51**	**39.73**	**65.37**
Reject	55.49	74.39	34.63
Primary coal	**100.00**	**58.96**	**100.00**

Comments:

- Treatment of broader size fractions up to 35, 50 mm can produce a reject with the ash content over 80%, but processing the coal particle size fractions of 3-15 mm can give a reject with the ash content only of approximately 75%;
- By jigging, one can recover clean coal with the ash content below 40%, that is equivalent to the traded 6B fines, which is currently traded by the local thermal power plants;
- Including of more fines in jigging would increase the ash content of clean coal (for sample of Ha Tu coal mine and coal particle size 15 -50 mm of Khe Sim coal mine) over 45% that is difficult to be regarded as a clean coal product for trading.

3.2. Tests on the fluidized bed separator

Fluidized bed machine HSBS has a inclined plate structure. The equipment was invented by the late 20th and early 21st century for processing of fine coals. This device has also been already implemented in full industrial scale. Fluidized bed machine is a well suited equipment for processing of coal particle sizes of 0.5-3 mm. Compared to other processing equipment of coal particle size fraction -3 mm, fluidized bed machine has higher capacity and requires little construction area etc.

The research group have tested the coal particle size 0.5-3 mm of Nui Beo coal mine sample on the laboratory scale fluidized bed machine at the optimumal operating parameters as defined by the conditional experiments. The resulted coal recovery are shown in the table 9.

Table 9. Coal processing result of particle size 0.5-3 mm, coal sample of Nui Beo mine

Products	Yield, %	Ash content, %	Combustible matter recovery, %
Clean coal	51.39	10.7	82.61
Reject	48.61	80.13	17.39
Primary coal	**100**	**44.45**	**100.00**

Comment:

- For particle size of 0.5-3 mm, the obtained clean coal has ash content less than 13% (maximum limits of the traded coal fine 3A), combustible matter recovery of clean coal over 82% and this product is suitable for both export and for domestic uses;
- The reject has ash content over 80% that is regarded as suitable for disposal.

3.3. Flotation tests

The research group have performed experiments on floatation machines (on the froth flotation Lab 1 l) for fine coals (particle size of 0-0.5 mm) of Nui Beo sample. The coal slurry was collected from the contaminated waste processing line of the moving screen jig at Ha Tu coal mine. The research has found the optimal froth flotation operating conditions. Froth flotation results of the optimumal conditional experiments of the two coal samples are presented in tables 10 and 11.

Table 10. Coal processing result of particle size 0-0.5 mm, coal sample of Nui Beo mine

Products	Yield, %	Ash content, %	Combustible matter recovery, %
Clean coal	59.93	12.26	92.34
Reject	40.07	80.8	12.76
Primary coal	**100.00**	**39.72**	**100.00**

Comments:

- Froth flotation clean coals of the two samples have ash content of less than 13% that is equivalent to the coal fines 3A and the combustible matter recovery is over 88%;
- The reject has ash content over 80% and can be disposed.

Table 11: Coal processing result of particle size 0-0.5 mm, coal sample of Ha Tu mine [4]

Products	Yield, %	Ash content, %	Combustible matter recovery, %
Clean coal	58,38	11,78	88,89
Reject	41,62	84,54	11,11
Primary coal	**100,00**	**42,06**	**100,00**

4. Conclusions and recommendations

4.1. Conclusions

- Coarse size fractions 35 (50) mm in contaminated wastes have ash content over 80% thus they can be scalped and disposed in permanent waste dumps or can be hand sorted for additional recovery of clean coal;
- Moving screen jigging of particle size 3-35 (50) mm in contaminated waste implemented tests have produced clean coal equivalent to coal fines 5A to 6A with yield from 6 to 26% depending on the quality of the raw coal coal size fractions + 3 mm;
- The amount of fines after jigging could be used in whole or in part depending on the quality of fines and the clean coal quality after jigging;
-When ash content of the raw coal size 0.5-3 mm is higher 40% then it is required to be washed by the fluidized bed machine to produce clean coal with quality equivalent to 3A fine coals. Clean coal of fluidized bed machine can be mixed with coal fines of jigging together with fines coals -0.5 mm of the raw coal to produce fine coal 6A;
- The contaminated waste fines -0.5 mm can be cleaned by froth flotation to recover additional clean fine coals.
- From contaminated waste with ash content of 60-70%, one can recover more 30-50 % clean coals that are of equivalent quality to in 6A fine coals, depending on the quality of the contaminated waste.

4.2. Recommendations

On the data basis of the study of the three samples of contaminated waste, it allows to develop two technological flowsheets as follows:

- Flowsheet of Figure 1, applied when fines particles - 3 mm have ash content under 40%
- Flowsheet of Figure 2, applied when fines particles - 3 mm and ash content over 40%

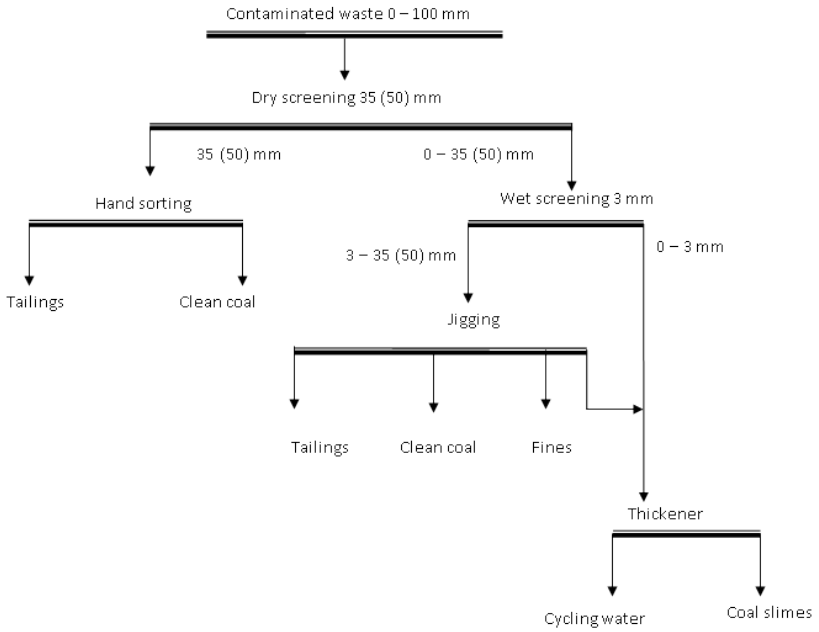

Fig 1. Washing flowsheet for contaminated waste containing size fraction 0 - 3 mm with the ash content below 40 %

Fig 2. Washing flowsheet for contaminated waste containing size fraction 0 - 3 mm with the ash content over 40%.

References

1. Source of the Quacontrol-Vinacomin (2013).
2. Pham Huu Giang, investment-construction project: System of processing by moving screen jig Ha Tu coal company -Vinacomin (2009).
3. Nhu Thi Kim Dung - Research projects funded by the Ministry of Education and Training level: Study on recovery of clean coal from waste rocks contaminated with coal at some coal mines of Quang Ninh Area, (2017).
4. Nguyen Thi Mai - master's thesis: Study of froth flotation of high ash content fines of Ha Tu Coal Mine, (2010).

Geotechnical mechanisms of roof fall ahead of face support in longwall mining

Tien Dung Le[1,*] Duc Hung Pham[1] and Quang Hung Dang[1]

[1] Hanoi University of Mining and Geology, Department of Underground Mining, Hanoi, Vietnam

Abstract. Longwall mining is one of the most productive methods for extracting underground coal seams. Although the understanding of longwall mining-associated geotechnical mechanisms has been significantly improved that contributes to better ground control, roof rock/top coal fall ahead of support (roof fall) has not been fully understood that causes severe damage to equipment and casualty at face. Empirical, theoretical and modelling methods were successfully used in past studies to understand the mechanisms driving roof fall; however, key mechanisms and their interactions during the fall were not satisfactorily investigated due to limitation of each method. This study aims to gain a systematic understanding of roof fall mechanisms in longwall operation. A review of past studies on roof fall is implemented with emphasis on the principles of applied research methods. The study confirms that the interaction between roof strata, coal seam and face support largely controls roof fall while numerical modelling shows great potential in studying roof fall complex mechanisms. The paper's findings provide mining engineers/scientists with a systematic understanding on roof fall from which more effective roof control strategies can be further developed.

1. Introduction

Longwall mining is one of the most productive methods for extracting underground coal seams in many countries such as China, Australia, Poland and Vietnam [1-3]. Although longwall mining technology has been significantly improved from manual by using blasting and hydraulic prop to mechanised by using shearer and self-advanced support, the roof rock or top coal between coal face and support may suddenly fall that causes severe damage to equipment and casualty. This geotechnical problem is ranked to be critical and thus has been studied by mining companies and researchers.

In order to develop sound engineering solutions to roof fall, many scientific works have been implemented to understand the mechanisms and parameters controlling the phenomenon in different geo-mining conditions. Various researching methods such as empirical, theoretical and modelling were successfully applied in past studies; however, due to intrinsic limitation of each method, key mechanisms driving roof fall and their interactions during the fall have not been satisfactorily investigated. This partly results in the fact that there is no single measure to roof fall that is universally applied at present.

* Corresponding author: t.d.le@humg.edu.vn

The paper's content presents a review of past studies on roof fall with emphasis on the principles of applied research methods. The scientific works and reports from coal operation companies in China, Australia, Poland and Vietnam are discussed that cover most types of longwall technology. The paper's findings provide mining engineers/scientists with a systematic understanding on roof fall from which more effective roof control strategies can be further developed.

2. Roof fall mechanism from longwall face in China

According to Bai et at. [4], nearly 50% of the deadly incidents in 2012 resulted from roof falls in longwall faces or roadways that killed 459 workers in China. They reported that more than half of the longwall face roof fall originated from coal wall spall and then proposed a conceptual model of the roof fall and coal wall spall, as illustrated in Fig. 1. Working on the geo-mining conditions of the caving longwall No. 14101 at Mjialiang coal mine, Bai et al. [5] and Bai et al. [4] used continuum modelling as the main tool for analysis of coal wall spall. In particular, a Finite Difference Method-based code was used to successfully find out that coal wall presents a brittle failure mode; failure mode and failure depth are dominated by the shear failure bands that develop from the down and upper corners of coal face; and failure shape is dependent on the geometrical system of discontinuities in coal seam (Fig. 2). In addition, some support characteristics controlling the fall were outlined, which are the setting resistance, advance lag and face guard.

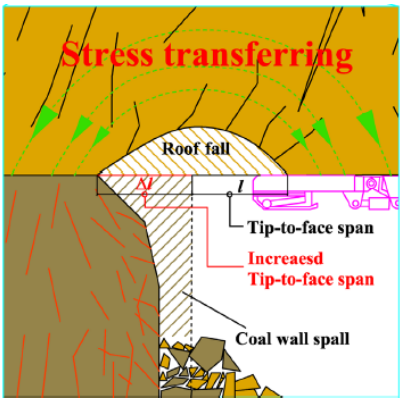

Fig. 1. Conceptual model of roof fall and coal wall spall at longwall face (modified after Bai et al. [4]).

A series of theoretical studies on coal wall spall was reviewed and presented in Bai et al. [6]. Note that these studies are in Chinese and their English translations are not available. The authors stated that in most of the previous studies, coal wall was regarded as an isolated object and the impacts of roof strata, shield support and face guard on coal wall stability were ignored. The authors then based on torque equilibrium to develop a mechanics model incorporating coal wall, roof strata and shield support. Compared to the above numerical studies, this study analysed the role of not only support characteristics but also fractured roof and mining height in coal wall failure, as shown in Fig. 3.

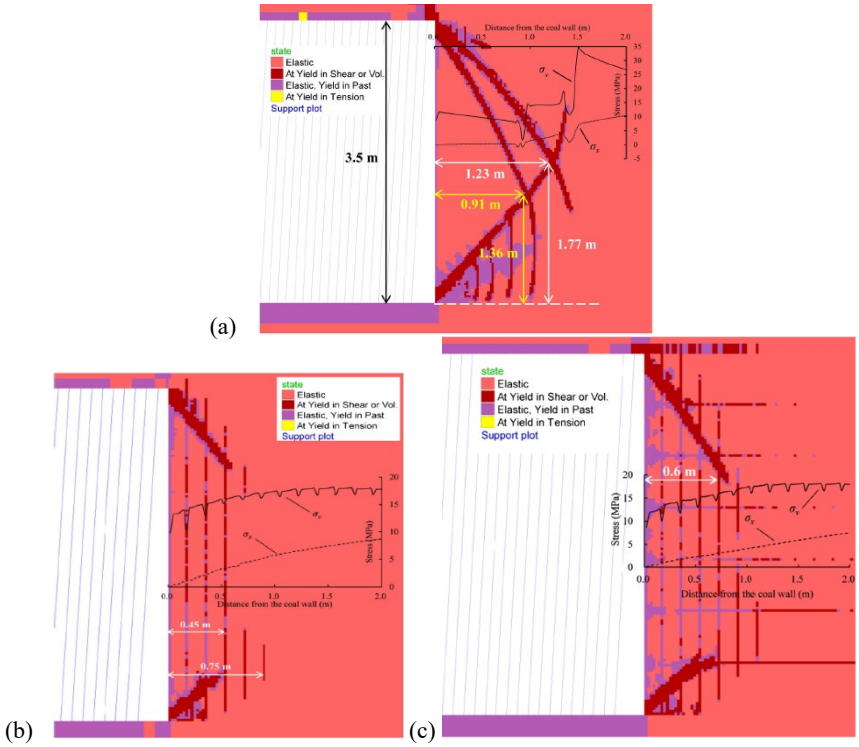

Fig. 2. Coal wall failure with (a) no discontinuities, (b) vertical discontinuities and (c) cross-discontinuities in a continuum-based model (modified after Bai et al. [5]).

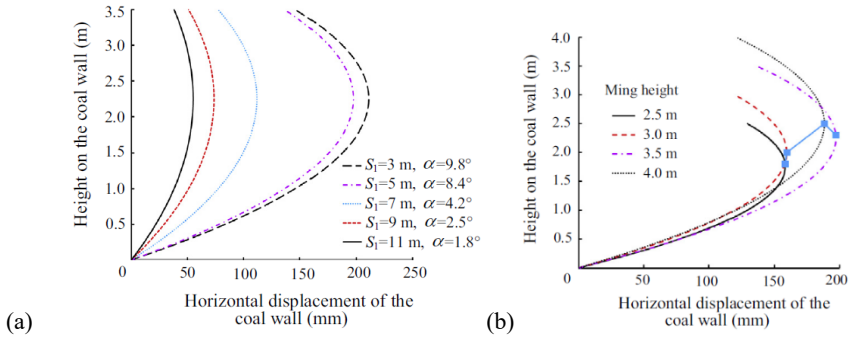

Fig. 3. Relationship between (a) fracture position in main roof and coal face horizontal displacement, and (b) mining height and coal face horizontal displacement [6].

Apart from continuum modelling, discontinuum methods were used in a few coal wall stability studies. By using a discontinuum-based model (Fig. 4), Wang et al. [7] concluded that improving support capacity, cohesion of coal mass and decreasing roof load on coal face are the key to improve coal face stability. Similarly, Yao et al. [8] stated that although tensile fracture dominates the failure in both horizontal and up-dip coal faces, the difference lies in their failure forms: failure is arc-shaped in horizontal faces and V-shaped in up-dip faces. In contrast, the down-dip coal face and its roof are vulnerable to shear failure due to large areas

of shear fractures inside the face. The authors also emphasised that depth of coal face, mining height, panel advance velocity and seam strength are driving factors of the spall.

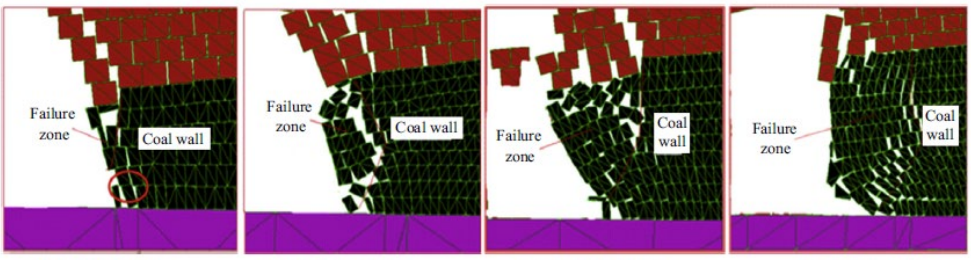

(a)

Fig. 4. Distribution of coal face failure zone at different mining heights in a discontinuum-based model [7].

3. Roof fall mechanism from longwall face in Australia

Based on a program of intensive hydraulic support monitoring in various Australia mining conditions, Frith et al. [9] stated that the roof stability between the face and canopy tip is one longwall face problem that is not only affected by face spall but also more importantly, the amount of roof convergence during mining cycles. The authors found that the likelihood of a roof fall is directly related to the heavily stresses area and the strength and structure of roof strata, as illustrated in Fig. 5. The relationship between roof fall and roof convergence was further validated against the field measurements implemented by Medhurst [10]. This author also outlined key factors driving the fall, which are setting load of support, strength of roof strata, tip-to-face roof span and support capacity.

Using site experience from one mine at Bowen Basin, Queensland over 10 years of longwall production, Payne [11] concluded that weak roof (less than 10 MPa in the bolted horizon) was the main roof control problem at the site. Furthermore, weak and highly cleated coal, water inflow from overlying aquifers, some minor structures, and a diatreme in the main headings have also contributed to the challenges at the mine. In an extreme case, weak roof combined with friable weak coal is particularly prone to roof fall when production slows due to delay or preparation for longwall take-off.

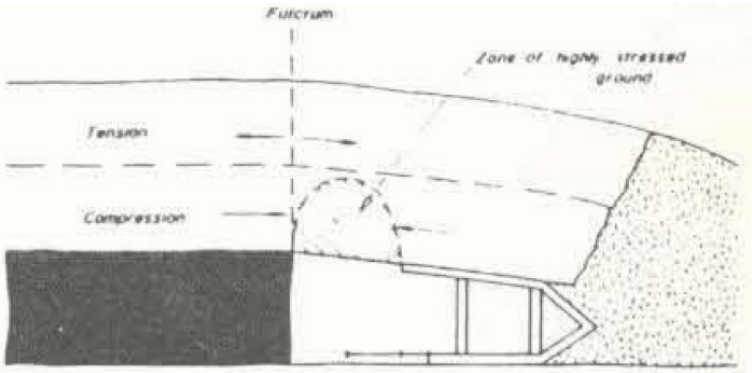

Fig. 5. Cantilevering action of strata resulting in highly stresses immediate roof [9].

4. Roof fall mechanism from longwall face in Poland

In Poland, longwall method is the main mining system used for hard coal mines. Difficult mining conditions such as deep mining, previous mining activities and rock mass tremors result in minor and massive roof falls in longwall faces as stated by Prusek et al. [12]. The author determined seven parameters controlling roof fall (i.e., low self-supporting ability of first roof strata; massive roof layers overhanging behind shield line; distribution of support capacity along canopy length; low bearing capacity of immediate floor strata; face orientation in relation to roof strata joints' direction; face line orientation to faults; longwall inclination) before developing a new method for assessing the risk of roof fall (Fig. 6). It is noted that since the method was mainly based on empirical and expert techniques, the geotechnical mechanisms associated with roof fall were not considered in the assessment.

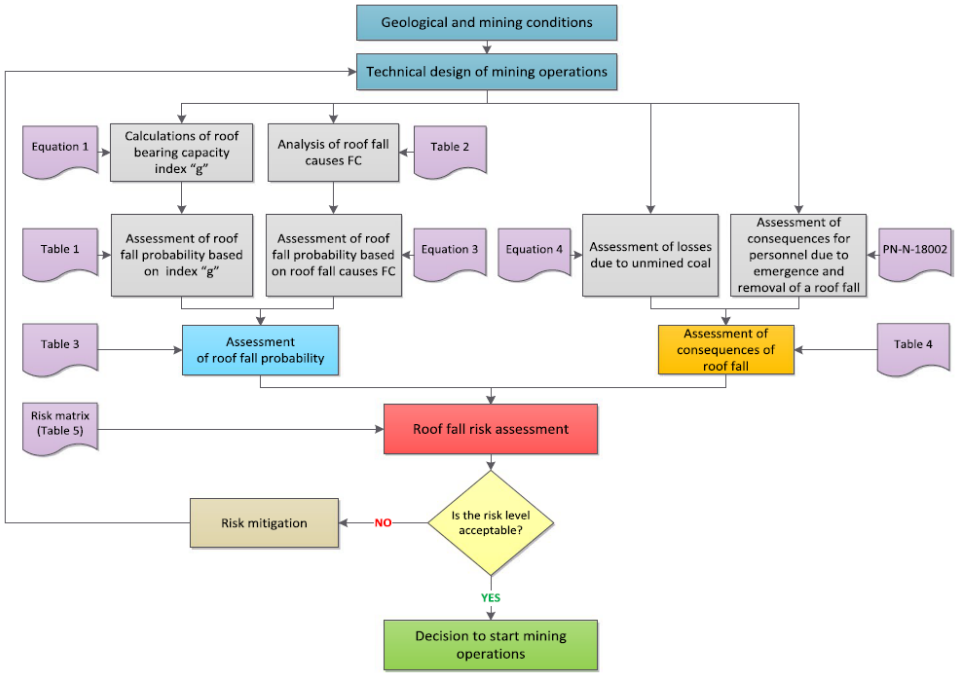

Fig. 6. Support VINAALTA 2.0/3.15 and shearer MB 12-2V2P/R-450E applied at Vang Danh coal mine in period of 2008–2012. Algorithm for assessing roof fall risk in caving longwall [12].

5. Roof fall mechanism from longwall face in Vietnam

Roof fall ahead of support in longwall face has been reported in Vietnam coal industry for a long time but only in recent years the problem has been studied in mechanised longwalls. Vu and Do [13] theoretically analysed the impacts of mine pressure, geological condition, unsupported span of roof, face advance rate, and setting load and unloading of support on coal wall spall and roof fall before proposing some technical measures to the problem. Based on on-site experience when dealing with roof fall in the world, Dao [14] analysed the influence of geological parameters on roof fall and proposed some reinforced solutions to weak coal/rock in accordance with Quang Ninh mining condition. More recent works [15-17] focused on the relationship between coal cohesion and coal moisture based on which a practical solution such as water/chemical injection was developed. A trial application was

conducted at longwall 14-5-11 by using Erkadol-K/Erkadur chemical made in Poland, as shown in Fig. 7.

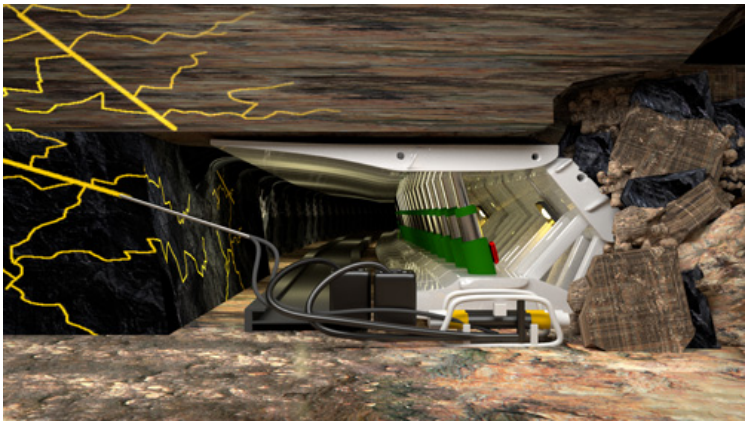

Fig. 7. Chemical injection to prevent coal wall spall and roof fall [18].

6. Discussion and Conclusions

Industrial reports from major coal industries such as China and Australia have outlined that roof fall ahead of face support is basically related to the roof convergence rate and/or coal wall spall. This explains why several investigations (e.g., Chinese and Vietnamese studies) have focused on coal wall spall problem to gain insight into roof fall. Theoretical, empirical and field measurement methods were implemented to successfully determine major causes of the spall/fall in past studies; however, the internal mechanisms during the fall could not be represented nor analysed. Alternatively, numerical methods were successfully used to investigate roof failure and roof fall mechanisms. The continuum methods realistically simulated stress change, material failure mode and coal seam deformation when the fall occurred. Nevertheless, due to the continuum medium of modelling, the investigations could only indirectly study the complete detachment of coal/rock material. Unlike continuum methods, discontinuum methods are capable of modelling the complete detachment in the fall. It is important to note that unrealistic interaction between intact material failure and discontinuity failure is always a challenging issue in plastic-discontinuum model. A solution to this issue has recently proposed in Le et al. [19].

Based on scientific works and reports from China, Australia, Poland and Vietnam coal industries, this paper confirms that roof stability between coal wall and face support is simultaneously controlled by coal seam, roof strata and support characteristics. Numerical modelling is capable of representing material failure and fall mechanisms in different geo-mining conditions; therefore, they show great potential application in studying roof fall. The paper's findings provide mining engineers/scientists with a systematic understanding on roof fall from which more effective roof control strategies can be further developed.

This work was financially supported by Hanoi University of Mining and Geology through Project T18-21. Paper was presented during the 5th POL – VIET International Conference Scientific-Research Cooperation between Vietnam and Poland, 08-10.07.2019, AGH UST, Krakow, Poland.

References

1. K. Kumar, A. K. Singh, A. K. Mishra, R. Singh. Int. J. of Mining Science and Technology, **25(6)**, 885-896, (2015).
2. J. M. Galvin. *Ground engineering - Principles and practices for underground coal mining*. Cham: Springer International Publishing (2016).
3. T. D. Le. *Longwall top coal caving mechanism and cavability assessment*, UNSW Sydney PhD Thesis, (2018).
4. Q.-S. Bai, S.-H. Tu, M. Chen, C. Zhang. Int. J. of Rock Mechanics and Mining Sciences, **88**, 242-253, (2016).
5. Q.-S. Bai, S.-H. Tu, X.-G. Zhang, C. Zhang, Y. Yuan. Arab. J. of Geosciences, **7(12)**, 5067-5080, (2014).
6. Q. Bai, S. Tu, Z. Li, H. Tu. Int. J. of Mining Science and Technology, **25(2)**, 199-204, (2015).
7. J. Wang, S. Yang, D. Kong. Int. J. of Mining Science and Technology, **26(1)**, 111-118, (2016).
8. Q, Yao, X. Li, B. Sun, M. Ju, T. Chen, J. Zhou, Q. Qu. Int. J. of Rock Mechanics and Mining Sciences, **100**, 298-309, (2017).
9. R. C. Frith, A. M. Stewart, D. Price. *11th International Conference on Ground Control in Mining*, The University of Wollongong, (1992).
10. T. Medhurst. *ACARP Project C20032*. Australian Coal Association Research Program ACARP, (2014).
11. D. Payne. *Coal Operators' Conference*, University of Wollongong, (2008).
12. S. Prusek, S. Rajwa, A. Wrana, A. Krzemień. Int. J. of Mining, Reclamation and Environment, **31(8)**, 558-574, (2017).
13. T. T. Vu, A. S. Do. Mining Industry Journal, **6**, 26-29, (2014).
14. H. Q. Dao. *Investigation, proposal and application of rock mass reinforcement solutions to improve efficiency and safety in roadway development and mining at Quang Ninh underground mines*. IMSAT report, (2015).
15. D. N. Le, V. C. Dinh, M. T. Tran, T. C. Luong, Q. T. Tran. Mining Technology Bulletin, **8/2016**, 1-6, (2016).
16. V. C. Dinh, M. T. Tran, T. C. Luong, Q. T. Tran. Mining Technology Bulletin, **12/2016**, 15-21, (2016).
17. T. T. T. Dinh, V. C. Nguyen, M. N. Tran, X. T. Nguyen, V. D. Tran, T. D. Truong, H. H. Nguyen, V. S. Nguyen, T. H. Tran. *Study on underground mining in complex geological conditions (weak roof rock, friable and weak coal) at Khe Cham III coal mine.* VIMCC report, (2017).
18. DSI Underground Group. Erkadur - Erkadol [Online]. Available: https://www.dsi-schaumchemie.pl/en/products/adhesives/erkadur-erkadol, (Accessed 29 Mar 2019).
19. T. D. Le, J. Oh, B. Hebblewhite, C. Zhang, R. Mitra. Int. J. of Rock Mechanics and Mining Sciences, **106**, 84-95, (2018).

Status and prospects of underground coal mining technology in Vietnam

Tien Dung LE[1,*] and Xuan Nam BUI[1]

[1] HUMG Hanoi University of Mining and Geology, Faculty of Mining, Hanoi, Vietnam

Abstract. Underground coal mining in Vietnam plays an important role to not only the sustainable coal industry but also the energy and social security in this country. Although the Vietnam coal industry has produced 35–45 million tonnes of raw coal per annum in past ten years, a great volume of coal resources remains distributed in complex geo-mining conditions and mostly unmined. This paper presents a brief review of the current and potential technologies for cutting coal and controlling roof in Vietnam underground coal mines. From the review, it is concluded that there is an urgent demand on improvement of current technologies as well as on investigation for effective application of more advanced mining methods into the industry, especially for deep mining at Red River Delta—the largest coal basin in Vietnam.

1 Reserves and coal production in Vietnam

Vietnam has been ranked to have a remarkable potential of coal extraction. In this country, there are four major coal types with the corresponding distributions: anthracite coal in North-East basin mainly at Quang Ninh province; bituminous coal in other domestic basins at Thai Nguyen, Lang Son and Hoa Binh provinces; sub-bituminous coal in Red River Delta basin; and peat coal mainly in peat basin at Mekong River Delta. The total coal resources estimated by March 2016 is approximately 48.8 billion tonnes (Table 1) [1].

Coal industry in Vietnam is mostly operated by Vietnam National Coal–Mineral Industries Holding Corporation Limit (VINACOMIN) through surface and underground mining methods. According to [2], VINACOMIN has operated five large surface coal mines with annual production greater than 2 million tonnes (Cao Son, Coc Sau, Deo Nai, Ha Tu and Nui Beo mines), 15 surface coal mines with production from 0.1 to 0.7 million tonnes per year, and some mines with production lower than 0.1 million tonnes per year. Regarding underground mining, VINACOMIN has operated 30 coal mines with nine mines producing greater than 1 million tonnes per year (Mao Khe, Nam Mau, Vang Danh, Ha Lam, Quang Hanh, Khe Cham, Duong Huy, Thong Nhat and Mong Duong mines). Other underground coal mines have small reserves, narrow coal field and are not favourable for mechanised mining technologies. The coal production in the period of 2007–2015 is summarised in Table 2 [3]. In 2017, VINACOMIN produced approximately 33.5 million tonnes and in 2018 the planned production was 36 million tonnes. To 2020, the coal production is forecasted around 42 million tonnes per annum.

* Corresponding author: t.d.le@humg.edu.vn

Table 1. Total estimated coal resources in Vietnam by March 2016, million tonnes [1].

Coal basin	Reserves	Firm resources	Trust resources	Estimated resources	Forecast resources	Total
Total	2,260	161	1,137	2,687	42,632	48,878
North-East basin	2,219	109	395	1,585	1,979	6,287
Red River Delta basin			525	955	40,531	42,011
Domestic basin	41	52	74	32	6	206
Local coal mines			10	8	19	37
Peat coal			133	107	96	336

Table 2. Coal production in period of 2007–2015, million tonnes [3].

	2007	2008	2009	2010	2011	2012	2013	2014	2015 (est.)
Raw coal	45	45	46	47	48	44	43	37	41
Surface	27	25	26	27	26	22	21	17	18
Underground	16	18	18	20	21	21	22	20	22
Others	2.39	1.84	2.02	0.50	0.71	0.51	0.65	0.50	1.00

The technical solutions to the urgently required sustainable mining in Vietnam are to decrease surface mining operation, increase underground mining operation, focus on deep large mines and apply advanced technologies. VINACOMIN has planned to close 19 surface mines by the year 2030 and will operate 19 new coal mines which are mostly underground in the period of 2015–2025 [4]. At the North-East basin, many underground coal mines are operated at 200–250 m below surface and going deeper. At the Red River Delta basin, coal gasification extraction has been investigated for application due to complex geo-mining conditions and social security at the site. It can be seen that these solutions are largely relevant to the mining technology. As a result, the authors hope that an introduction of status and prospect of the underground coal mining technologies in Vietnam in this paper would be an interest to the participants of the 5th Pol-Viet conference.

2 Technologies for underground coal mining in Vietnam

Although Vietnam has more than 100 years of coal extraction, its coal industry officially started in the 1990s in the North-East coal field. Before the 1990s, the mining technology was simple and mostly manual. Coal was broken by blasting and roof was supported by

wooden/steel/hydraulic prop and cage (Fig. 1). This mining technology unsurprisingly resulted in low mine safety and production. Since the 1990s to the early 2000s, coal was still cut and broken by blasting while roof pressure was mainly controlled by hydraulic prop and semi-mechanised support (Fig. 2). The semi-mechanised support has greatly improved the safety at working area, saving the time for roof control and consequently significantly increasing the productivity (up to three times) compared to manual technology. The extraction with semi-mechanised support has been innovated and adapted for unfavourable mining conditions in the North-East coal basin. For example, since 2015 VINACOMIN has applied the soft support namely ZRY (Fig. 2) for medium-thick and steeply inclined seams at Hong Thai coal mine with high production and low coal loss rate.

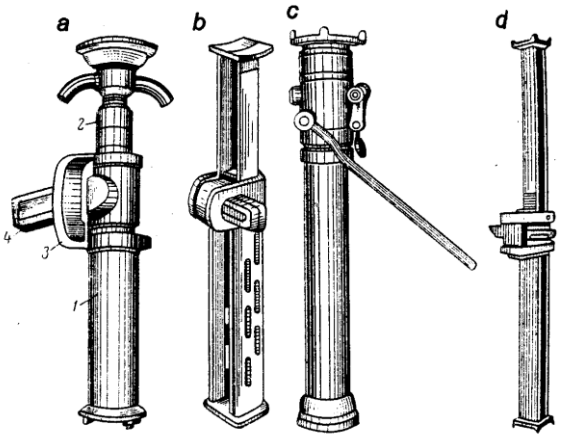

Fig. 1. Steel (a, b, d) and hydraulic (c) props [5].

Fig. 2. (a) Semi-mechanised support ZH-1600 at surface and in underground [5].

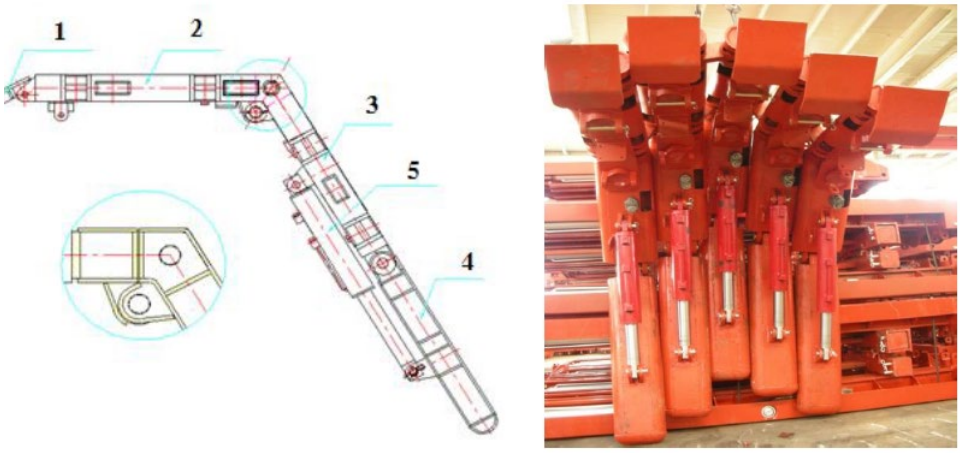

Fig. 2. (b) Soft support ZRY 20/30L at Hong Thai coal mine with 1-oriented bar, 2- roof bar, 3- rear bar, 4- tail bar, 5- piston [6].

In June 2005, the first fully mechanised coal mining technology was trialled at Khe Cham coal mine (now Khe Cham I) [7]. Coal was cut by shearer and roof was controlled by mechanised supports (shield). The production was reported at 1.5–2.5 times as much as that of previous technologies applied at the mine. This technology, however, did not allow to extract the top coal section in the thick seams at Khe Cham I. Since then, the fully mechanised technology has been increasingly applied at VINACOMIN coal mines (Vang Danh, Nam Mau, Ha Lam, Duong Huy and Khe Cham III mines). The technology is now capable of mining thick coal seam and referred to as High Reach Single Pass Longwall and Longwall Top Coal Caving (LTCC) methods. The LTCC face support and shearer operated at some mines are illustrated in Figs. 3–6. It is noted that at Khe Cham III, the equipment was selected to deal with the soft coal and surrounding rock, groundwater issue and inconsistent seam angles at the site.

Fig. 3. Support VINAALTA 2.0/3.15 and shearer MB 12-2V2P/R-450E applied at Vang Danh coal mine in period of 2008–2012.

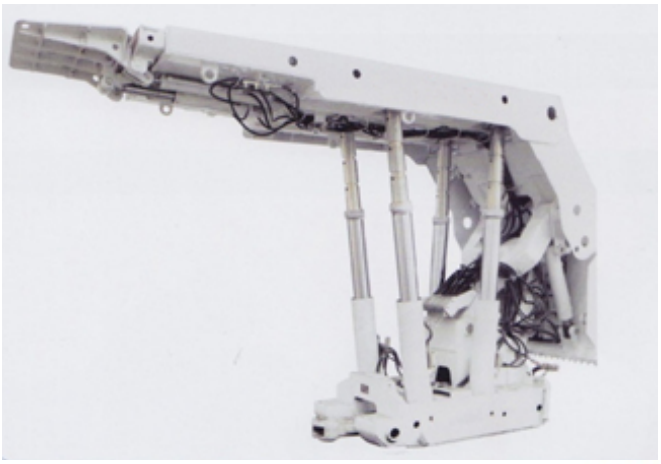

Fig. 4. Support ZF4400/17/28 and shearer MG 170/410-WD applied at Vang Danh since 2017.

Fig. 5. Support ZF4400/16/28 and shearer MG 150/375-W applied at Ha Lam coal mine.

Fig. 6. Supports ZFY5000/16/28, ZFG6200/17/30 and shearer MG150/375-WD applied at Khe Cham III coal mine since 2016.

3 Potential technology for mining Red River Delta coal basin

According to [8], Red River Delta coal basin plays an important role in the energy security of Vietnam because of (1) large reserves of 30–60 billion tonnes and (2) good coal quality for producing electricity, gasification and metallurgy. Unfortunately, the geological conditions here are extremely complex (e.g., weak surrounding strata and closely-located aquifers) while the surface is crowded area with agricultural activities. The governmental coal plan [9] has identified traditional underground mining and Underground Coal Gasification (UCG) (Fig. 7) as applicable technologies for the basin. However, since a reliable geological exploration has not been implemented at the area, the above technologies are considered as potential at present and must be well tested prior to real operation. This also means that there is certainly room for far more technical investigations and development to socially and economically efficient extract Red River Delta coal basin.

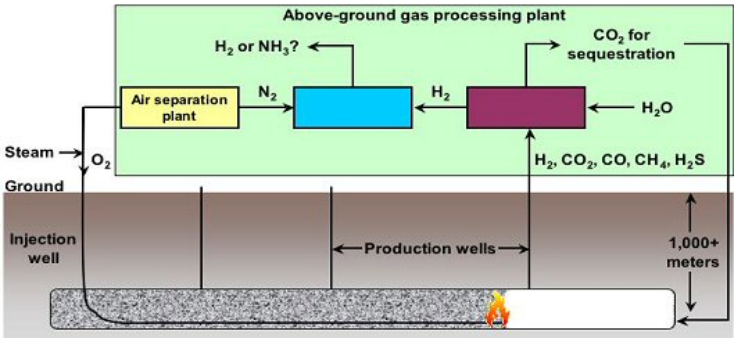

Fig. 7. Principle of Underground Coal Gasification [10].

4 Conclusions

Underground coal mining is becoming more important to the sustainable coal industry in Vietnam. The cutting and roof controlling technologies for underground coal extraction has been significantly improved since the 1990s, contributing to safer mining operation with higher and more efficient coal production. Since a great volume of coal resources is distributed in complex geo-mining conditions in this country (e.g., weak coal and surrounding rocks, thickness and angle of seams varying along strike and dip, hard rock band, deep mining, etc.), there is an urgent demand to improve the mentioned technologies, taking into consideration the advanced techniques in the world for extracting coal in more unfavourable conditions. For the mining at the largest coal basin Red River Delta, the information regarding both geological assessment and potential mining method is insufficient at present that requires more reliable investigations in future.

Paper was presented during the 5th POL – VIET International Conference Scientific-Research Cooperation between Vietnam and Poland, 08-10.07.2019, AGH UST, Krakow, Poland.

References

1. VINACOMIN, *Vietnam-Australia Energy Roundtable* (https://www.austrade.gov.au/local-sites/vietnam/events/energy-mining-mission-may-2017) (2017)
2. X. N. Bui, Q. T. Le, *International Symposium on Earth Science and Technology*, Fukuoka, 155-157 (2011)
3. B. Nguyen, *Vietnam Mining Science and Technology Association* (2015)
4. VINACOMIN, Master plan for development of Vietnam coal mining industry (2009).
5. M. P. Do, D. T. Vu. *Underground Coal Mining Pressure lecture* (2007)
6. H. Q. Dao, T. N. Tran, N. G. Nguyen, T. C. Dao. J. of Mining Industry, **4/2016**, 9-16 (2016)
7. Vietnam Institute of Mining Science and Technology, *Internal Report* (2007)
8. T. S. Nguyen, Thermal Energy Review, **105** (2012)
9. Prime Ministry of Vietnam, *No. 403/QĐ-TTg* (2016)
10. E. Burton, J. Friedmann, R. Upadhye, Lawrence Livermore National Laboratory (2006)

Comparison Of Vietnam And Poland Industrial Wastewater Regulation: A Study Of Trang Bach Coal Mine Wastewater Treatment

HA Doan Manh [1], MIJAŁ Waldemar [2] and POLEK Daria [2]

[1] AGH University of Science and Technology, Faculty of Geology Geophysics and Environment, Krakow, Poland

[2] AGH University of Science and Technology, Faculty of Mining and Geoengineering, Krakow, Poland

Abstract: The research about wastewater treatment in laboratory scale of Trang Bach coal mine in Vietnam was carried out in the year of 2016. We concluded the content of chemical compound that needed to treat the pH, Fe, Mn component and Turbidity & Suspended Solids (TSS) in the wastewater to meet the requirement of the Technical Regulation for Industrial Water of Vietnam. In this article, we suppose to compare the Vietnam and Poland regulations for industrial wastewater based on the result of our research about Trang Bach coal mine wastewater treatment before and then assess the potential to exchange the scientific works about wastewater treatment between Vietnam and Poland.

1. Introduction:

The coal mining industry in Vietnam has played an important role in economic growth [1]. It is estimated that the coal consumption of Vietnam in 2018 is 40 million tons, with 29 million tons for the coal electric plants [4] The current direction of coal industry development plan in Vietnam is not to develop at any cost but to find a way for sustainable socio-economic development, satisfying human's both physical and spiritual needs, enhance the international cooperation to apply the advantage technology into the exploitation and management tasks [2]. In parallel with it, Vietnamese and Polish people have started since the last decade of the 20th century their efforts in promoting human resource capacities and to enhancing international understanding and friendship between the two countries, especially in the mining field [3]. This article is also a result of the research cooperation between Vietnam and Poland. The first author, a Vietnamese student, continues the Master degree in AGH University of Science and Technology, Krakow, Poland (AGH UST) after his graduation in Hanoi University of Mining and Geology, Vietnam (HUMG). Meanwhile, the second author, a Polish Ph.D. student in AGH UST, takes part in the "Erasnus+ exchange program" in HUMG.

The authorities in Vietnam are putting a huge effort to minimize the environmental risk in mining, especially in the wastewater treatment [2].In this article, we suppose to compare the technical regulation for the wastewater of Vietnam and Poland, not only in theory but also in practice, base on our previous research about the wastewater treatment research in laboratory scale for the Trang Bach coal mine in Vietnam. We hope that this will be a contribution for the sustainable development of the coal mining industry in Vietnam as well

as a suggestion for a new direction for student scientific exchange between the two countries in the future.

2. Methodology:

In this article, we will use national technical regulations for the industrial wastewater from both countries, Vietnam and Poland, Vietnam to compare these regulations and point out the differences and similarity between them. After that, we will base on our previous research about the wastewater treatment in laboratory scale for the Trang Bach coal mine, Vietnam as a case study to bring the theory to practice.

3. The technical regulations on the industrial wastewater in Vietnam and Poland:

The current national technical regulation on industrial wastewater in Vietnam is QCVN 40:2011/BTNMT, issued by the Ministry of Natural Resources and Environmental, Vietnam in 2011 [[5]. It controls the maximum allowance value of 33 pollution parameters in industrial wastewater before discharging into the natural channel. These parameters are separated into 2 ranks, rank A is for discharging directly into the sources that be used for water supply, serving human demand (drinking, daily needs,…), otherwise, the rank B is the requirement discharging the wastewater into the other sources [[5]. The Department of Water Resource Management, Ministry of Natural Resources and Environmental, Vietnam is responsible for the supervision of the implementation of this regulation [6]. This regulation is the innovation of QCVN 24:2009/BTNMT - National Technical Regulation on Industrial Wastewater, which was issued in 2009 [[5]. The first regulation about the quality of industrial wastewater quality in Vietnam was promulgated in 1995, named TCVN 5945 – 1995 [7]. Ten years later, it was replaced by the "TCVN 5945 - 2005: Industrial wastewater - Discharge standards" [8]. In 2009, the industrial wastewater regulation of Vietnam was upgraded to " QCVN 24: 2009/BTNMT, National Technical Regulation on Industrial Wastewater" before being represented by the QCN 40:2011 since 2011.

Regulations for wastewater in Poland before discharging to natural channels are represented by Regulation of the Minister of Environment from 18 of November 2014 when pumping sewage into waters or to land and on substances particularly harmful to the aquatic environment and by the Regulation of the Minister of Environment from 27 November 2002 when pumping seawage into the surface waters that used for supply. The regulation first specifies:

- substances particularly harmful to the aquatic environment, causing water pollution that should be eliminated, and substances in particular harmful to the aquatic environment, causing pollution of water, which should be restricted;
- conditions to be met when introducing sewage into waters or into the ground, incl maximum permissible contamination values, and conditions to be met in the purpose of agricultural use of sewage;
- location and minimum frequency of sampling of wastewater, reference methodologies
- analysis and assessment of whether sewages meet the required conditions;

- maximum permissible pollution values for wastewater from sewage treatment plants for household and municipal purposes as well as for wastewater from sewage treatment plants in the agglomeration.

Meanwhile, the second specifies:

- the requirements for surface water used to supply the population in water intended for consumption called hereinafter "waters";
- the frequency of sampling water, methodology reference analyzes and assessment of whether the water meets the required conditions.

The important parameters of wastewater in coal underground mining are pH value, the content of Iron (Fe), Manganese (Mn) and Turbidity & Suspended Solids (TSS) [9]. They are clarified in both regulations from Vietnam and Poland (Tab.1 and Tab.2)

Table 1. The requirement parameters on pH, Iron, Manganese, and TSS in industrial wastewater in Vietnam [5]

	pH	**Fe (mg/l)**	**Mn (mg/l)**	**TSS (mg/l)**
A level - QCVN 40:2011/BTNMT	6 – 9	1	0.5	50
B level - QCVN 40:2011/BTNMT	5.5 - 9	5	1	100

Table 2. The requirement on pH, Iron, Manganese, and TSS in industrial wastewater in Poland [14-15]

	pH	**Fe (mg/l)**	**Mn (mg/l)**	**TSS (mg/l)**
Regulation of the Minister of Environment from 18 of November 2014 (entering sewage into waters or into the soil)	6.5 – 9.0	10	-	50
Regulation of the Minister of Environment from 27 November 2002 (water intended for consumption) – Category A1 will be considered only	6.5 – 8.5	0.1 – 0.3	0.05	25

4. Identification Of The Optimal Dosage Of Chemical Compounds In The Wastewater Treatment Of Trang Bach Coal Mine On Laboratory Scale:

The Trang Bach coal mine is 80km far from Hanoi, the capital city of Vietnam, this is an underground coal mine which has a large amount of contamination in the wastewater due to the accumulation of the material within the wastewater during the exploitation activities [11]. The wastewater in the Trang Bach coal mine is highly acidic and contains a great amount of iron, manganese and suspended solid content [12-13]. The quality of wastewater after treatment in the Trang Bach coal mine sometimes did not meet the requirement of the technical regulation on the industrial wastewater in Vietnam and Poland (Tab.3)

Table 3. The quality of wastewater of Trang Bach coal mine after treatment in 2014, 2015 [12-13]

No.	Value	**2014**			**2015**			QCVN 40:2011 /BMT	Regulation of the Minister of Environment from 18 of November 2014 (entering sewage into waters or into the soil)	Regulation of the Minister of Environment from 27 November 2002 (water intended for consumption) – Category A1 will be considered only
		5-2014	8-2014	11-2014	5-2015	9-2015	10-2015	B level		
1	pH	6.8	4.8	5.2	3	5.6	5.9	5.5-9	6.5-9	6.5-8.5
2	TSS (x10 mg/l)	1.1	6	5.3	3.4	2.7	1.8	10	50	25
3	Fe	0.8	5.9	3.91	5.7	5.0	5.52	5	10	0.1-0.3

	(mg/l)	1	5		1	5				
4	Mn (mg/l)	0.56	0.71	0.64	0.96	1.25	1.46	1	-	0.05

The wastewater samples in Trang bach coal mine were collected in the dry season of 2016, they are highly acidic and contaminated by iron, manganese, and TSS [10]. Table 4 shows the average quality of Trang Bach coal mine's wastewater samples:

Table 4. The quality of wastewater samples in comparison with the regulations [10]

	pH	Fe (mg/l)	Mn (mg/l)	TSS (mg/l)
Result	3.31	5.9	24.4	148
B level - QCVN 40:2011/BTNMT standard	5.5 - 9	5	1	100
Regulation of the Minister of Environment from 18 of November 2014 (entering sewage into waters or into the soil)	6.5 – 9	10	-	50
Regulation of the Minister of Environment from 27 November 2002 (water intended for consumption) – Category A1 will be considered only	6.5 – 8.5	0.1 – 0.3	0.05	25

Firstly, the calcium oxide was used to increase the pH value to meet the requirement of the B level - QCVN 40:2011/BTNMT standard, which also brings a positive effect in decreasing the iron content. Secondly, the authors used the PAC - Poly Aluminium Chloride (Alm(OH)nCl3m-nxH2O, with $m \leq 10$, $2 \leq n \leq 5$) to deal with the manganese and TSS content, the performance of the chemical reaction was supported by the Jar-test stirring standard [10]. The study concluded that on the laboratory scale, the optimal dosage of chemical compounds for the wastewater treatment process in Trang Bach coal mine is 280 mg/l CaO 70 % and 125 mg/l PAC to meet the requirement of national technical regulation on industrial wastewater of Vietnam (Table 5).

Table 5. The quality of wastewater sample after the treatment with 280 mg/l CaO 70 % and 125 mg/l PAC [10]

pH	Fe (mg/l)	Mn (mg/l)	TSS (mg/l)
5.53	0.11	1	0

Final results after wastewater treatment are not accepted by Polish regulations for water conditions to be met when introducing sewage into waters or to land, and on substances, particularly harmful to the aquatic environment and also did not meet an agreement with regulations about water for supply population in water intended for consumption.

5. Discussion and Conclusion

The wastewater quality of Trang Bach coal mine is not good enough to be discharged immediately into the surface water. After treatment process by using 125 mg/l PAC quality is still too low to pass all regulations from Regulation of the Minister of Environment from 27 November 2002 on the requirements to be met by surface waters used for supply population in water intended for consumption. In comparison with both Polish regulations, the content of Fe and TSS meet the requirement but the pH and Mn does not. This result shows that there is a possibility to apply a similar study into the wastewater treatment for the coal mines in Poland.

In term of the corporation enhancement between Vietnam and Poland, based on the education background of the first and the second authors and the positive which was obtained after the time we were working together, we recommend the authorities from both countries to think about a new approach for student scientific exchange between the two countries. The student from Poland could come to Vietnam and do the research with Vietnamese student in laboratory scale, in contrast, the Vietnamese student could improve their skills through exchange programs in Poland under the support of Polish student.

References

1. N. C. Nam, Orientation for sustainable development of Vietnam coal Industry with the energy security (2019)
2. Prime Minister of Vietnam, 403/QĐ-TTg: Adjustment of the development plan of the coal industry in Vietnam to 2020 with the consideration to 2030 (2016)
3. M. Forys, Polish Vietnamese Cooperation: Beginnings, Prospects, Facts, and Figures (2016)
4. Vinacomin, Information about the coal consumption of TKV in 2018 (2018)
5. Ministry of Natural Resources and Environmental of Vietnam, QCVN 40:2011/BTNMT: National technical regulation on industrial wastewater (2011)
6. Ministry of Natural Resources and Environmental of Vietnam, Department of Water Resources Management: Function and Duty (2019)

7. Vietnam Standards and Quality Institute, TCVN 5945 – 1995: Industrial wastewater – Discharge standard (1995)

8. Vietnam Standards and Quality Institute, TCVN 5945 – 2005: Industrial wastewater – Discharge standard (2005)

9. H. B. Dharmappa, M. Sivakumar, Wastewater Recycle, Reuse, And Reclamation, **1**, 1-8 (2009)

10. M. H. Doan, W. Mijal, V4 C. R. M.: I. C. O. E. & M. P., Determination of the optimal dosage of chemical compounds in the wastewater treatment process in Trang Bach coal mine: the laboratory scale, 21-22 (2018)

11. Institute of Mining Science and Technology - Vinacomin, The Introduction of Trang Bach coal mine (2011)

12. Institute of Mining Science and Technology - Vinacomin, Report of the wastewater quality of Trang Bach coal mine in 2014 (2014)

13. Institute of Mining Science and Technology - Vinacomin, Report of the wastewater quality of Trang Bach coal mine in 2015. (2015)

14. Ministry of Environment in Poland - Regulation of the Minister of Environment from 18 of November 2014 on the conditions to be met when introducing sewage into waters or to land, and on substances particularly harmful to the aquatic environment. (2014)

15. Ministry of Environment in Poland - Regulation of the Minister of Environment from 27 November 2002 on the requirements to be met by surface waters used for supply population in water intended for consumption. (2002)

The use of computer programs to solve ventilation issues in Vietnamese coal mines

Hoa BUI[1,*], Piotr ŻYCZKOWSKI[1] and Rafał ŁUCZAK[1]

[1] AGH University of Science and Technology, Faculty of Mining and Geoengineering, Krakow, Poland

Abstract. Having enjoyed an economic upsurge in recent years, Vietnam is now recording increased demand for electrical energy. Its production, for the most part, relies on the coal mining industry, thus resulting in a strong upward trend in mining volumes. Being geologically complex, Vietnamese mines are characterised by a complicated structure of their headings. The local ventilation systems are also affected by there being very few automatic dams and an by increases in airflows delivered to the mine. For this reason, in order to analyse airflows and maintain the proper control of ventilation systems, computer software is required. The article offers a comparison of computer programs – Kazemaru, VentGraph and VentSim – as employed for use in Vietnamese mines. The assessment covered the manner in which these programs are used and how their output data are presented, as well as their range of applications in the conditions of Vietnamese coal mines.

1. Introduction

In recent years, the economy of Vietnam has been growing at a rate of 6-7% (with 6.8% recorded in 2017) [1]. The primary source of energy security is coal mining. Up to 2011, open-pit mines had served as the primary source of coal production [2]. At present, open-pit mining accounts for approx. 40% of the entire coal production and continues to drop. This results from the maximum depth being reached up to which mining is profitable. The hard coal production in the years 2017-2018 and the volume to be mined by 2030 are presented in Table 1.

Table 1. Hard coal production volume in Vietnam in 2017-2018 and the volume to be mined by 2030

Year	2017	2018	2020	2025	2030
Volume (million Mg)	35.6	40.0	47-50	51-54	55-57

The main coal producer in Vietnam is Vinacomin, which expects coal production to reach 40 million Mg in 2019 [3]. Detailed information on Vinacomin's coal production from 2011 to 2017 is presented in Table 2.

* Corresponding author: ironcrossvinacomin@gmail.com

Table 2. Vinacomin's coal production in 2011-2017 [4].

Year	2011	2012	2013	2014	2015	2016	2017
Production (million Mg)	48.232	44.512	42.687	37.430	37.384	34.791	35.037

The planned increase in extraction and the mining of lower coalbeds are connected with problems related to ventilation, transport, operational systems used, occupational safety and natural hazards. Ventilation plays a very important role in underground mining activities, as it is used not only for aerification and air-conditioning, but also for combating fires and underground explosions. The main purpose of ventilation is to provide adequate air parameters, achieve the required air flow velocity and remove gases harmful to humans.

2. Ventilation in Vietnamese mines

The Vinacomin Group, which is responsible for the majority of coal extraction in Vietnam, assumes its continuous growth. Therefore, modernisation and increased mining mechanisation are being introduced, which is connected with the implementation of more efficient machinery and equipment for underground coal mining. This, however, results in higher amounts of combustion engine gases and more heat generated by engines, machinery and heavy-duty equipment. For the above reasons, the issue of ventilation has taken on an increasingly important role.

Due to their specific nature, Vietnamese mines are facing more and more ventilation problems:

- The complex geological structure makes it necessary to build irregular pathway grids, which further complicates the ventilation system and the calculation of ventilation parameters.
- Despite mining depths still being relatively low (up to 300 m), there are problems with high temperatures. This is mainly due to high temperatures outside in the summer and high humidity, but also the continuous development of mechanisation. These factors necessitate increasing the ventilation airflow or, in extreme cases, ceasing coal production.
- Central air conditioning systems have not yet found their place in coal mines. The first on-site air-conditioning units appeared in the Halam mine in Halong.
- The limited number of automatic dams used there contributes to difficulties with airflow and its control.
- Problems also result from dust generated during mining works, transport and processing of coal.
- Coal blasting is often used, which further increases the temperature in the heading and is a source of toxic gases. It was only recently that a long-wall coal cutter was introduced in the Halam mine – Figure 1.

Fig. 1. A long-wall cutter in the Halam mine in Halong.

- The absence of a filling method leads to the occurrence of numerous voids in the excavation areas.
- While increasing their ventilation airflows, many mines have failed to accordingly adapt shafts and ventilation ducts. This has led to problems with airflow, in addition to difficulties in controlling the distribution of air.

With so many changes at hand, the knowledge of airflows and proper control of ventilation systems is necessary. Determining airflow routes, values of resultant resistance, and air distribution requires that calculations for the ventilation system be made. At present, simulations and analyses of such systems in coal mines require the use of computer software.

3. Computer programs used to simulate ventilation systems in underground mines

Computer software has come to be widely used in the simulation and analysis of ventilation systems. A general comparison of such programs can be found in [5], and more detailed descriptions, including analyses of the applied mathematical models, are presented in [6]. Computer software mainly serves as a tool assisting engineers in charge of mine ventilation. Their main duties include:

- developing a digital model of all headings;
- performing ventilation simulations both in normal conditions and during emergency;
- including in simulations disturbances such as fires, sudden methane influxes, gas ejections, and rock bursts;
- ensuring compatibility with sensors of mine monitoring systems;
- forecasting ventilation following changes made to the ventilation system.

Many of these programs provide some additional options:

- simulation of weather conditions;
- simulation of demethanation systems;
- employee records;
- financial calculations.

The most popular programs used by coal mines include: VentSim, VentGraph, Vuma3D, Vnet, ICAMPS MineVent, Kazemaru, 3D-CANVENT^{2000}, AutoWENT and AERO 2010d. The article focuses on Kazemaru, VentGraph and VentSim – three programs which have been most commonly used in the analyses of Vietnam's ventilation systems.

3.1 Kazemaru

"Kazemaru", a program developed by Prof. Masahiro Inoue from the Kyushu University, Japan, is now used in the majority of Japanese coal mines. Its sample modes of usage are described in [7]. The program is characterised by features such as:

- simplicity and user-friendliness;
- data editing using a ventilation diagram;
- maximum number of nodes: 1000, maximum number of ventilation pathways: 1500;
- calculation time of less than one minute for systems consisting of around 100 nodes and 150 pathways;
- inclusion of natural ventilation parameters and ventilator specifications;
- graphic simulation of the distribution of air;
- the possibility of including fires;
- simulation of temperature distribution, gas concentration, and smoke distribution during a fire.

The main program window with a fragment of the ventilation system is shown in Fig. 2; the ventilator specification window is presented in Fig. 3.

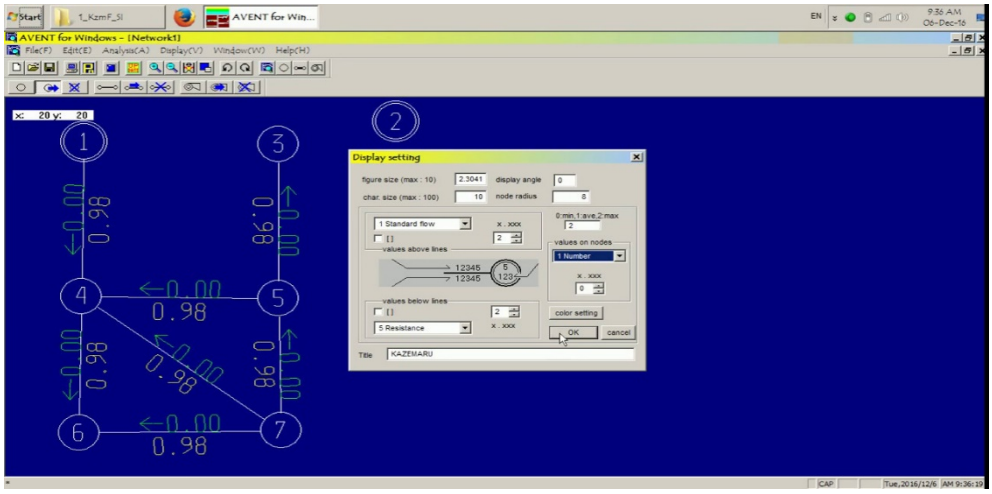

Fig. 2. A fragment of the ventilation system in Kazemaru software.

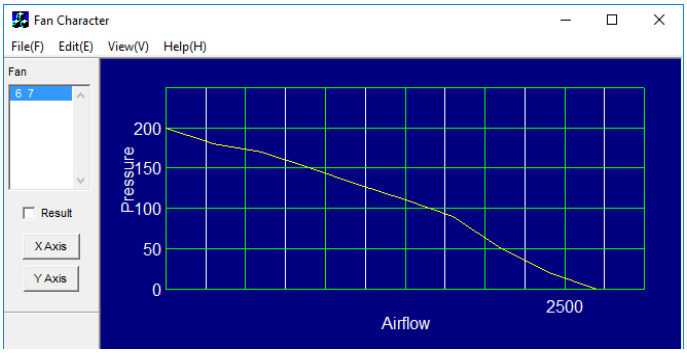

Fig. 3. Ventilator specification window in Kazemaru software.

3.2 VentGraph

VentGraph is a program consisting of combined modules, designed to solve complex problems in mine ventilation systems. It includes the following calculation modules [6, 8, 9]:

- GRAS – determining the set distribution of air in a network of headings in normal conditions and during emergency. The module makes it possible to change the resistance of a selected heading, add a dam with a specific resistance, apply fire depression, change the type of siding, modify ventilator specifications, change the delivery rate of air, methane or carbon dioxide, etc.
- FIRE – calculations to determine the impact of the seat of fire on the level of ventilation. A module which simulates unspecified air and gas distribution in a network of headings following an underground fire. It therefore makes it possible, by simulating various fire variants, to predict how the ventilation system will behave during the fire.
- VentZroby – calculates airflows in the ventilation system and the adjacent goaves, accounting for the impact of fire on ventilation.
- VentWilg – simulates the impact of fire on the distribution of humid air in a network of headings.
- ESCWIN – a module cooperating with the monitoring network to provide support in fire prevention. This module can collect data on the status of an actual ventilation system by leveraging data collected by the sensors of the mine's monitoring system. This provides the mine dispatcher with a quick overview of the available outposts and escape routes and allows them to separate the area subject to fire smoke hazard.

VentGraph has found broad application in Polish and foreign mines. It has been numerously validated [10-12] and used in the analysis of ventilation systems and simulations not related to coal mine ventilation [13-21]. Fig. 4 shows the VentGraph interface with the ventilator specifications and ventilation system structure windows.

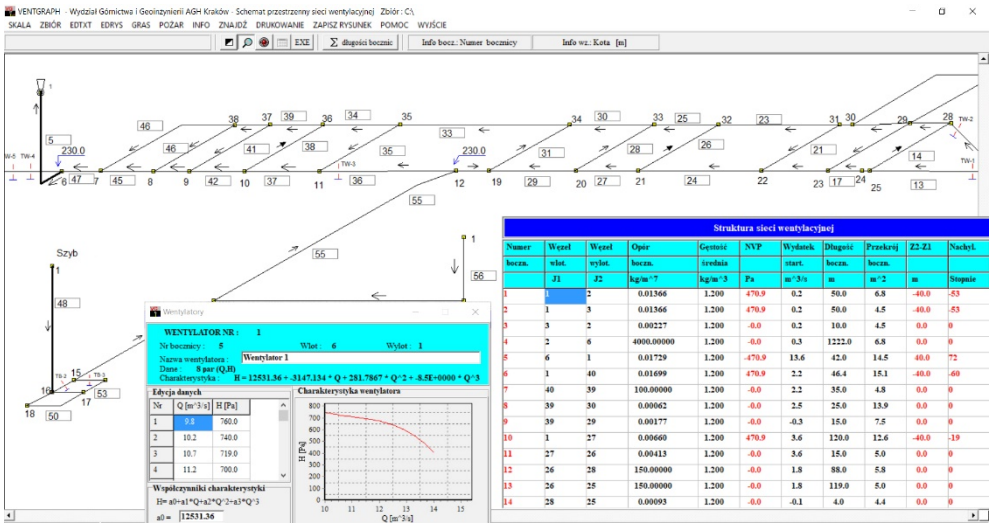

Numer	Węzeł	Węzeł	Opór	Gęstość	NVP	Wydatek	Długość	Przekrój	Z2-Z1	Nachyl.
boczn.	wlot.	wylot.	boczn.	średnia		start.	boczn.	boczn.		
	J1	J2	kg/m^7	kg/m^3	Pa	m^3/s	m	m^2	m	Stopnie
1	1	2	0.01366	1.200	470.9	0.2	50.0	6.8	-40.0	-53
2	1	3	0.01366	1.200	470.9	0.2	50.0	4.5	-40.0	-53
3	3	2	0.00227	1.200	-0.0	0.2	10.0	4.5	0.0	0
4	2	6	4000.00000	1.200	-0.0	0.3	1222.0	6.8	0.0	0
5	6	1	0.01729	1.200	-470.9	13.6	42.0	14.5	40.0	72
6	1	40	0.01699	1.200	470.9	2.2	46.4	15.1	-40.0	-60
7	40	39	100.00000	1.200	-0.0	2.2	35.0	4.8	0.0	0
8	39	30	0.00062	1.200	-0.0	2.5	25.0	13.9	0.0	0
9	39	29	0.00177	1.200	-0.0	-0.3	15.0	7.5	0.0	0
10	1	27	0.00660	1.200	470.9	3.6	120.0	12.6	-40.0	-19
11	27	26	0.00413	1.200	-0.0	3.6	15.0	5.0	0.0	0
12	26	28	150.00000	1.200	-0.0	1.8	88.0	5.8	0.0	0
13	26	25	150.00000	1.200	-0.0	1.8	119.0	5.0	0.0	0
14	28	25	0.00093	1.200	-0.0	-0.1	4.0	4.4	0.0	0

Fig. 4. The ventilation system, the ventilator specifications, and the structure of the ventilation system in VentGraph.

3.3 VentSim

Developed in 1993, in 2009 the program received the 3D simulation functionality. It is now used all over the world, including, since recently, selected mines in Poland. Its enhanced, Premium, version features the following functionalities [22, 23]:

- 3D presentation with accurate object sizes;
- animations of the airflow in the ventilation system;
- maximum number of ventilation pathways: 60000;
- calculations for variable air density;
- inclusion of changes to the ventilators' rotational speeds and ventilator reversions;
- simulations of thermodynamic parameters (cooling and heating, thermal properties of rocks, sources of heat, natural ventilation);
- transport of contaminants (distribution of smoke and contaminants, concentration of contaminants, coal blasting smoke, diesel engines);
- detection of flow recirculation;
- financial calculations.

Similarly to VentGraph, VentSim has many applications, also outside the mining industry. Study [24] describes how the VentSim program is used for the analysis of the ventilation system in the Donghai mine, China. The manner in which VentSim can be applied to analyse the behaviour of a ventilation system after the introduction of mine pit sealing is presented in article [25]. [26] discusses the results of modelling of a ventilation system in the Romanian mines of Lupeni and Uricani. Brake [27] addresses modelling in three fire scenarios: in an underground diesel installation, an underground explosive storage magazine, and on an ore belt conveyor. The simulations of various solutions to increase air flow in the Rosh Pinah mine, Namibia, are described in [28]. The software has also been used to optimise and analyse the ventilation system in the Redeemer [29] and Bronzewing Gold Mines [30] in Australia, the Majiagou mine in China [31], the Western-Razmja mine in Iran [32], and the Konkola Copper Mine in Zambia [33]. [34] presents changes made to the ventilation system to reduce the costs of ventilation in the Zhangcun mine, China.

VentSim was used to perform an analysis of the ventilation system in the Mông Duong mine in Vietnam. Figures 5-7 provide a view of the ventilation system as 2D (Fig. 5) and 3D (Fig. 6) images and as fragments depicting the complex layout of pathways (Fig. 7).

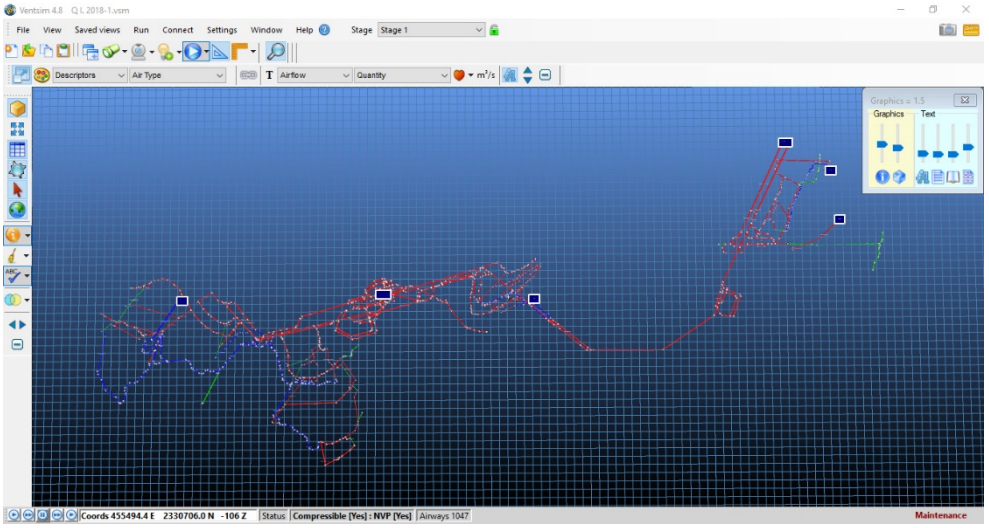

Fig. 5. A 2D diagram of the ventilation system in the Mông Duong mine.

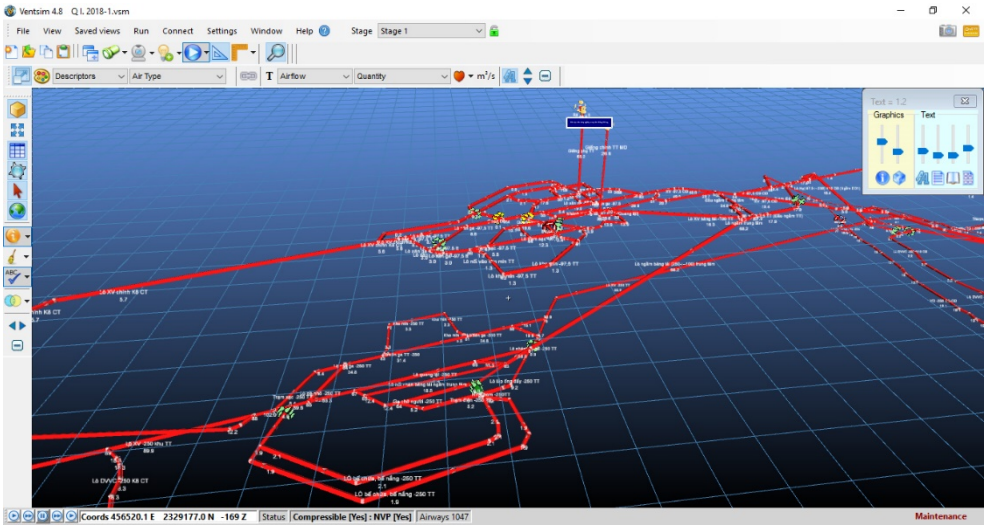

Fig. 6. A 3D diagram of the ventilation system in the Mông Duong mine.

Fig. 7. A fragment of the ventilation system in the Mông Duong mine.

4. Summary

A ventilation system is indispensable in every underground mine, not only contributing to the comfort of work, but also, and primarily, enhancing worker safety. For the purpose of analysis, optimisation or planning of ventilation systems, specifically designed software is used. Vietnamese coal mines use the following three programs: Kazemaru (in the Campha region), VentGraph (selected mines) and VentSim (in the regions of Uongbi and Halong). Having worked with them, the authors could formulate a subjective assessment of these programs (the more stars, the better), as presented in Table 3.

Table 3. Comparison of Kazemaru, VentGraph and VentSim software in Vietnamese mines

Assessment criterion	Kazemaru	VentGraph	VentSim
Computing speed	★★★	★★★	★★★
Data entry speed	★★	★	★
Graphical user interface	★	★★	★★★
Production tracking	-	★★	★★★
Ventilation planning	★★★	★★	★
Calculations for a duct line ventilation system	-	-	★★★
Connectivity with the monitoring network	-	★★	★★

The assessment pertains exclusively to the specific conditions of the Vietnamese mining industry. Currently the computer programs are mostly used to verify the correctness of calculations, not for production tracking or the monitoring of ventilation systems. As coal production and work mechanisation are growing, however, computer software is gaining in popularity and is being deployed on an increasingly broad basis.

References

1. M. Walewski, *Rynki zagraniczne – Wietnam. Raport ekonomiczny, wrzesień 2018*, Bank Gospodarstwa Krajowego (2018) www.bgk.pl/files/public/uploads/graphics/Rynki_zagraniczne_-_Wietnam.pdf (15.04.2019)
2. E. Strzałkowska, P. Strzałkowski, *Górnictwo węgla kamiennego w Wietnamie – wybrane informacje*, Górnictwo i Geologia **6**, 1 (2011)
3. www.vinacomin.vn *Vinacomin sets to produce 40 million tonnes of coal and earn 128 trillion VND in revenue in 2019*. http://www.vinacomin.vn/news-of-vinacomin/vinacomin-sets-to-produce-40-million-tonnes-of-coal-and-earn-128-trillion-vnd-in-revenue-in-2019-20190118160131962 8.htm (15.04.2019)
4. H. Nguyen, *Vietnam Mining Industry Webinar, 20 September 2018*, Australian Government Austrade www.austrade.gov.au/ArticleDocuments/1418/2018_webinar-presentation_Vietnam_mining_industry.pdf.aspx (15.04.2019)
5. M.S. Morar, S.M. Radu, D. Cioclea, I. Gherghe, *Use of IT equipment and specialized programs for solving ventilation networks*, Quality - Access to Success, Supplement 1, Vol. **18**, p121-126. 6p. (2017)
6. W. Dziurzyński, J. Krawczyk, *Możliwości obliczeniowe wybranych programów symulacyjnych stosowanych w górnictwie światowym, opisujących przepływ powietrza, gazów pożarowych i metanu w sieci wyrobisk kopalni*, Przegląd Górniczy **68**, 5 (2012)
7. N. Katsumata, R. Yahagi, H. Kurosaki, S. Kubota, *Feasibility study of ventilation design for underground facilities*, 6th East Asia Forum on Radwaste Management Conference, November 27-29, Osaka, Japan (2017)
8. W. Dziurzyński, T. Pałka, J. Krawczyk, *Ventgraph for Windows User's Guide*, Strata Mechanics Research Institute Polish Academy, Cracow, Poland (2010)
9. W. Dziurzyński, T. Pałka, *Wyznaczenie dróg ucieczkowych w razie pożaru w kopalni podziemnej – nowe możliwości system VentGraph*, Prace Instytutu Mechaniki Górotworu PAN, Vol. **16**, 1-2, p.3-16 (2014)
10. W. Dziurzyński, J. Kruczkowski, *Validation of the mathematical model used in the Ventgraph programme on the example of the introduction of new headings to the ventilation network of mine*, Arch. Min. Sci. Vol. **52**, No 2, p.155-169 (2007)
11. C.J. Pritchard, *Validation of the Ventgraph program for use in metal/non-metal mines,* in Proceedings of the 13th United States/North American Mine Ventilation Symposium, Sudbury, ON, Canada, 13–16 June 2010, pp. 455-462 (2010)
12. W. Dziurzyński, A. Krach, T. Pałka, S. Wasilewski, *Walidacja procedur programu VentZroby z wykorzystaniem systemu monitoringu stanu atmosfery kopalni*, Prace Instytutu Mechaniki Górotworu PAN, Vol. 11, no. 1-4, p.79-112 (2009)
13. W. Dziurzyński, A. Krach, T. Pałka, *A reliable method of completing and compensating the results of measurements of flow parameters in a network of headings*, Arch. Min. Sci., Vol. **60**, No 1, p.3-24 (2015)
14. W. Dziurzyński, A. Krach, T. Pałka, *Airflow sensitivity assessment based on underground mine ventilation systems modeling*, Energies **10**, 1451 (2017)
15. A.D.S. Gillies, H.W. Wu, *Case studies from simulating mine fires in coal mines and their effects on mine ventilation systems*, Proceedings, Fifth Australasian Coal Operators Conference, Ed. N. Aziz and B. Kininmonth, Aus. Inst. Min. Metall., Melbourne, pp 111-125 February (2004)
16. A.D.S. Gillies, H.W. Wu, A.M. Wala, *Australian mine emergency exercises aided by fire simulation*, Arch. Min. Sci., Vol. **50**, No 1, p.17-47 (2005)

17. E. Yaslioglu, E. Simsek, I. Kilic, *Estimation of minimum ventilation requirement of dairy cattle barns for different outdoor temperature and its affects on indoor temperature: Bursa case*, Pak J Biol Sci. **10**(8), p.1264-9 (2007)
18. A.D.S. Gillies, H.W. Wu, *Challenges in undertaking inertisation of fires in underground mines*, in 12th U.S./North American Mine Ventilation Symposium, Reno, Nevada, June 9-12, 2008, pp. 539-546 (2008)
19. R. Hansen, *Smoke spread calculations for fires in underground mines*, research project: Concept for fire and smoke spread prevention in mines, Studies in Sustainable Technology, Mälardalen University (2010)
20. H.W. Wu, S. Gillies, *Analysis of Blakefield South Mine (BSM) Explosion*, Technical Report for Investigation Unit, Mine Safety Performance, Industry & Investment NSW, Australia (2012)
21. P. Zapletal, V. Hudecek, V. Trofimov, *Effect of natural pressure drop in mine main ventilation*, Arch. Min. Sci., Vol. **59**, No 2, p. 501-508 (2014)
22. *Ventsim Visual™ User Guide*, Ventsim Software By Chasm Consulting
23. *Ventsim™ 3D Mine Ventilation Simulation Software, Feature & Pricing Chart*, http://www.ventsim.com/wp-content/uploads/2014/09/features_table_USD.pdf (20.04.2019)
24. F. Weia, Z. Fangpingb, L. Huiqing, *The use of 3D simulation system in mine ventilation management*, Procedia Engineering **26** 1370-1379 (2011)
25. M.O. Bustamante-Rúa, A.J. Daza-Aragón, P. Bustamante-Baena, *Simulation software VENTSIM™ the influence of implementation of work abandoned sealings ventilation of an underground coal mine*, Boletin de Ciencias de la Tierra **37**, pp. 1-2 (2015)
26. M. Şuvar, D. Cioclea, I. Gherghe, V. Păsculescu, *Advanced software for mine ventilation networks solving*, Environmental Engineering and Management Journal Vol. **11**, No. 7, 1235-1239 (2012)
27. D.J. Brake, *Fire Modelling in Underground Mines using Ventsim Visual VentFIRE Software*, The Australian Mine Ventilation Conference, Adelaide, 1-3 July (2013)
28. E. Develo, M. Pillalamarry, E. Garab, *Improving the ventilation system at Rosh Pinah zinc mine*, The Journal of The Southern African Institute of Mining and Metallurgy. Vol. **116**, 301-305 (2016)
29. E. Widzyk-Capehart, B. Watson, *Agnew Gold Mine expansion mine ventilation evaluation using VentSim*, Proceedings of the 7th International Mine Ventilation Congress: June 17-22, 2001, Cracow, Poland (2001)
30. E. Widzyk-Capehart, C. Fawcett, *Life of mine ventilation requirements for Bronzewing mine using VentSim*, Proceedings of the 7th International Mine Ventilation Congress: June 17-22, 2001, Cracow, Poland (2001)
31. J.G. Zhang, C.Y. Suo, *Study of Coal Mine Ventilation System Optimization based on Ventsim*, MATEC Web of Conferences **44**, 02016 (2016)
32. S. Maleki, F. Sotoudeh, F. Sereshki, *Application of VENTSIM 3D and mathematical programming to optimize underground mine ventilation network: A case study*, Journal of Mining & Environment, Vol. **9**, Issue 3, Page 741-752 (2018)
33. K. Dzwiti, V. Mutambo, *Optimization of the Ventilation System Using Ventsim Visual Considering the Full Mine Mechanization Drive at Konkola Copper Mines*, First Zambia National Conference On Geology, Mining, Metallurgy and Groundwater Resources: The Future Mining in Zambia Held at Mulungushi International Conference 22nd – 23rd November 2018, Lusaka, Zambia (2018)
34. X.D. Zhu, Z.L. Lu, H.L. Wang, *Analysis and Application of Energy Saving and Consumption Reduction of Mine Wind Network Based on Ventsim*, Journal of Scientific and Engineering Research, **5**(12):21-26 (2018)

Comparison Of Vietnam And Poland coal resources & coal demand in the past and how it will change in future

MIJAŁWaldemar [1], POLEK Daria [1], Manh HA Doan [2]

[1] AGH University of Science and Technology, Faculty of Mining and Geoengineering, Krakow, Poland

[2] AGH University of Science and Technology, Faculty of Geology Geophysics and Environment, Krakow, Poland

Abstract: The article in individual chapters discuss domestic coal resources in Poland and Vietnam, types of coal occurrence in both countries, the processing status and main domestic mining companies. The last part will be a comparison of mining prospects and plans for the development of coal mining in both countries and a summary of positive practices in both countries.

1. Introduction

Poland is the biggest coal producer in Europe. The coal mining industry plays a key role in energy production. More than 78% of the energy is produced from brown and hard coal. After break down of the global coal market, the coal mining sector changed. Now Poland has 5 main hard coal producers and 4 big producers of brown coal. The most important now in the Polish mining sector is to establish more economic manage system, put more attention on environmentally friendly technologies of exploitation and preparation and be more competitive on the global market but still play the key role in Europe [8].

Vietnam is one of the most important producers of anthracite. After 1995 position of the coal industry and coal in the economy in Vietnam has changed. VINACOMIN is the leading company in Vietnam coal market. Coal industry plays an important role in the fast-growing economy in Vietnam and also in energy production. Vietnam starts putting more responsibility on environmental protection but another thing is increasing production efficiency in processing plants, build new underground mines and close open-pit mines [3].

2. Coal resources and coal basins

The documented balance of coal resources in Poland at the end of 2017 is 60 496 mln tons. Steam coal is 70.67%, coking coal is 28.03% and rest of coal types is 1.30% of all coal resources. Deposits currently in use is 37.19% of balance coal resources (22 497 mln tons). The hard coal deposits in Poland occurred in 3 coal basins:

- Upper Silesian Coal Basin (GZW) - main coal basin on the south area in Poland. In this basin are almost all opened coal mines. Area of GZW is 5 600 km2 and got 80.00% of all documented balance resources of coal.

- Lublin Coal Basin (LZW) - located in the east of Poland. In this basin work 1 coal mine "Bogdanka". The area of perspective deposits got 9 100 km2 and area of documented deposits is 1 200 km2. Only 0.9% of this basin is currently being developed.
- Lover Silesian Coal Basin (DZW) - exploitation was finished in the 2000 year. The main reason for stoped exploitation was hard geological conditions.

Currently, available data shows that coal reserves in Vietnam are about 49.8 billion tons. Coal resources are classified into a few categories: measured & indicated reserves (categories A+B+C1) is 33%, inferred (C2) 39% and prognostic resources (P) is 28%. In Vietnam appeared all types of coal: anthracite (already mined), bituminous coal, sub-bituminous coal, lignite coals, and peat coal. Coal plays a key role in the Vietnam economy and energy sector. Most important coal basins are located in Quang Ninh, Red River Delta, Thai Nguyen, Bac Kan, North Path, Da River, Ca River, Na Duong, Nong Song, Ba River, Mekong River Delta (Fig. 1). Vietnam got one of the biggest resources of anthracite. Quang Ninh coal basin is the most important area for coal mining, where has almost all currently coal mines and coal preparation plants. Quang Ninh basin is located in the northeast part of the country, it occupies the area of about 5900 km2 of which 2800 km2 is forest land and 510 km2 is agricultural. Coalfields in this area is located very close to the coast so it is a very good location to send coal for the international coal market. Exploitation begins in this basin in 1839. Quang Ninh coalfield got 8.7 billion tons of coal resources (anthracite). Most important coal deposits in Quang Ninh basin: Mao Khe, Trang Bach, Nam Mao, Vang Danh, Uong Thuong, Dong Vong, Nga Hai, Khe Tam, Giap Khau, Nui Bao, etc. and are shown in Figure 2. Most important ports are Cam Pha Port and Hon Gai [2, 3, 4, 5, 7, 8, 9].

3. Coal industry policy, companies, and production trends

In 2018 the plan for Polish hard coal mining sector was accepted and signed by the Council of Ministers (published by Ministry of Energy). After break down of coal global market, the most important change was the creation of new mining company Polska Grupa Górnicza S.p. z o.o. in 100% owned by Government. This company consists of coal mines from old companies Kompania Węglowa S.A. and Katowicki Holding Węglowy S.A. New company is an owner of three consolidated mines: KWK Ruda (mines Bielszowice, Halemba-Wirek and Pokój), KWK ROW (mines Chwałowice, Jankowice, Marcel and Rydułtowy), KWK Piast-Ziemowit (mines Piast and Ziemowit) and two individual mines KWK Bolesław Śmiały and KWK Sośnica.

Other coal companies are Jastrzębska Spółka Węglowa S.A. the main coking coal producer (mines KWK Borynia-Zofiówka-Jastrzębie, KWK Budryk, KWK Pniówek, KWK Knurów-Szczygłowice), Tauron Wydobycie S.A. (mines Brzeszcze, Janina, Sobieski), Siltech Sp. z o.o. (private mine), Eco-Plus Sp. z o.o. (private mine), PG Silesia (property of Czech investors) and Spółka Restrukturyzacji Kopalń S.A. (preliminarily aimed for liquidation of unprofitable coal mines). In the last 10 years, coal production is decreasing due to the changing economy and energy sector.

The most important institution is Ministry of Industry and Trade (MOIT) and is responsible for the state management of all energy industries, namely electricity, new and renewable energy, coal and the oil and gas industries. The Ministry is not only determined first-line policy it has also supervisory responsibilities for energy sector such as a state-owned companies VINACOMIN and Electricite de Vietnam (EVN). The Ministry is also responsible for master plans for electricity, coal, oil and natural gas exploitation and supply.

In 2005 was founded VINACOMIN from the merging of Vinacoal and Vietnam Mineral Corp (or Vimico). VINACOMIN Holding Corporation Ltd. with 54 coal mines it is the biggest coal mining company in Vietnam. VINACOMIN hold 5 big opencast mines, 15 open pits, some smaller coal mining sites, and 30 underground coal mines. This is an economic Corporation with 100% owned by the State. 95% of coal production in Vietnam is from VINACOMIN Company. Till 2030 the plan for the coal industry is to gratify coal demand for a fast developing economy. The coal demand in 2030 should reach a level of about 127 mln tons [2, 3, 4, 6, 8, 9].

4. Coal preparation status

Coal preparation in Poland and Vietnam is similar and it can be described by comparing in schedule:

Beneficiation technology	Poland	Vietnam
1. Preparation of coal	Crushers, screens, handpicking belts, metal catchers	Crushers, screens, handpicking belts, metal catchers
2. Initial classification	Vibrating screens	Vibrating screens
3. Coal beneficiation	Jigs, heavy dense medium separators, dense medium cyclones, spirals, flotation	Jigs, heavy dense medium separators, dense medium cyclones, spirals, flotation
4. Dewatering, Thickening & filtration	Screens, centrifugal machines, dewatering sieve, radial thickener Dorra	Screens, centrifugal machines, dewatering sieve, radial thickener Dorra

In both countries are used similar technologies to separate useful coal particles from wastes. The biggest difference is that in Poland to separate medium grain classes are mostly used jigs. This method is very popular. In coal preparation plants in Vietnam, there is a tendency to separate medium grain classes by using dense medium cyclones [1, 3, 6, 9].

5. Development plan and challenges to overcome

In Poland the main target for coal mining industry is to creating conditions conducive to profitable construction, an efficient and modern hard coal mining sector, based on cooperation, knowledge and innovation, which is acting in a friendly way and a predictable software and legal environment, allows for effective use of resource, social and economic capital to ensure high energy independence of Poland and to support competitiveness national economy. Other important points are [8]:

- Recovery and stabilization of liquidity, profitability, and efficiency economic and financial sector of hard coal mining, including through adjustment production capacity to market needs and export opportunities.
- Vertical integration of mining and energy and creating an effective one steam-coke coal group model.

- Satisfying domestic demand for hard coal, including in particular for the production of electricity, heat, and coke.
- Ensuring access to new coal deposits and ensuring an appropriate level of investment where it will ensure the highest efficiency economic.
- Development of employee competencies and knowledge.
- Reducing the impact of the hard coal mining sector on the environment and increasing the use of mining waste and accompanying minerals.
- Innovations in hard coal mining. Creation of the intelligent mine, ensuring a high level of occupational safety.

Most important targets to reach in coal processing [1, 6, 7, 9]:

- Implementation of CMMS (Computerized Maintenance Management System) and PIMS (product information management systems), including the area of production quality forecasting, planning, and integration of the extraction process with the enrichment and sale process.
- Modernization of plants for enrichment technology in the full graining range.
- Full automation of technology sections and complete processing processes.
- Reducing the duration of processes wet to minimize the contact of grains carbon with water.

In Vietnam, between the year 2011 and 2030 will be closed 19 mines with a total capacity of 11 million tons/year. Which 9 opencast coal mines with total capacity 8.2 million tons/year: Nui Beo (3.5 mln tons/year), Ha Tu (1.65 mln tons/year), Southwest Da Mai (1.0 mln tons/year), East Da Mai (0.4 mln tons/year), Bang Nau (0.55 mln tons/year), Northwest Khe Tam (0.03 mln tons/year), Khe Sim (1.05 mln tons/year), West Khe Sim (0.05 mln tons/year) and 10 smaller opencast mines (2.7 mln tons/year). The share of underground coal mines will increase from 45% in 2011 to 75% in 2020 and 80% in 2030 (Government plan for coal industry) [2, 3, 4, 9].

Between 2015 and 2030 coal mining industry will invest to open 19 new mines, 5 mines will be owned by VINACOMIN in North East basin (Quang Ninh), 9 new mines (North East basin) and 5 pilot mines (Hung Yen, Thai Binh in Red River Delta basin). Between years 2016-2030 will be constructed few new preparation plants Khe Than 2, Bao Dai, Dong Trieu-Pha Lai and in 2017 was started the test phase of coal preparation plant Khe Cham IV. The master plan is also presented for the coal mining industry in table [2, 3, 4, 5, 10].

Tab. 5 Master plan for the development of Vietnam coal industry (Mt) [13].

Coal area	*2020*	*2025*	*2030*
Total run-off-mine coal	*92,430*	*119,250*	*120,732*
I. North-East basin	72,330	85,050	83,282
1.1. VINACOMIN	64,530	67,150	59,782
In which: banned area & coal bearer	6200	7400	7300
1.1.1. Uong Bi coal field	19,280	20,550	20,950

1.1.2. Hon Gai coal field	9,350	9,800	8,800
1.1.3. Cam Pha coal field	35,900	36,800	30,032
1.2. New coal mines	7,800	17,900	23,500
II. Other interior basins	3,050	2,650	2,700
III. Out of Vinacomin	3,550	6,550	9,750
IV. Red River Delta basin	13,500	25,000	25,000

Other plans for the coal preparation industry [10]:

- The coal industry will be developed on the basis of efficiently exploiting, processing; making a positive contribution to ensuring national energy security; prioritize domestic demand; ensuring the import and export rationally in the direction of only exporting domestic coal types that do not need to be used
- Promote the investigation, exploration, and evaluation of domestic coal resources and reserves to prepare a reliable resource base for the sustainable development of the coal industry.
- To speed up the business activities and invest abroad to meet coal demand for socio-economic development of the country.
- To ensure that the coal production and consumption meet the requirements for sustainable development, develop coal industry effectively, synchronously and in accordance with the general development of economic sectors; diversify methods of investment and coal trading; to maximize internal resources in combination with expand international cooperation to research and apply advantage technology in exploration, coal mining, processing and use; reduce losses in coal mining and take into account the reasonable investment for environmental protection, labor safety, resource management, risk management
- Implementing coal trading in harmony with the world coal market.
- To develop the coal industry in association with the ecological environment protection and improvement in the coal region, minimizing the impact on cultural conservation areas; actively contributing to the socio-economic and tourist development

References

1. BLASCHKE W., GAWLIK L., BLASCHKE S., Coal preparation technology in Poland, Gospodarka Surowcami Mineralnymi, 2006, Vol. 22(4).
2. TRAN XUAN HOA, Coal export and the future in Vietnam. Clean Coal Day, Tokyo, Japan 2010, available at www.jcoal.org.jp
3. BARUYA PAUL, Prospects for coal and clean coal technologies in Vietnam, Copyright IEA Clean Coal Centre 2010, ISBN 978-92-9029-484-9.

4. NGUYEN BINH, Vietnam coal potential and development orientation. APEC Coal Supply Security Tokyo, Japan 2015, available at www.jcoal.org.jp

5. XUAN NAM BUI, QUI THAO LE, Coal mining industry in Vietnam, Proceedings of International Symposium on Earth Science and Technology 2011, 6-7 December, Fukuoka, Japan 2011, p. 155-158, ISBN 978-4-9902356-1-1

6. BAIC I., BLASCHKE W., Coal Preparation in Poland – Development Trends for Increasing Production Efficiency, Inżynieria Mineralna – Journal of the Polish Mineral Engineering Society, 2017, No 2(40).

7. Bilans zasobów złóż kopalin w Polsce wg stanu na 31.12.2017, available at http://geoportal.pgi.gov.pl

8. Ministerstwo Energii, Program dla sektora górnictwa węgla kamiennego w Polsce, Dokument przyjęty przez Radę Ministrów 23.01.2018.

9. MIJAŁ W., NGUYEN HOANG SON, NGUYEN NGOC PHU, Coal preparation in Poland and Vietnam, Geospatial Technologies and Earth Resources (GTER 2017): proceedings of the international conference on Geospatial Technologies and Earth Resources 2017: Hanoi, Vietnam, 5–6 October 2017, ISBN: 978-604-913-618-4.

10. VINACOMIN website, available at http://www.vinacomin.vn/

Determining for an output capacity of dimension stone exploitation from the computer simulations to generate the fracture network in 3D: case study in some dimensional stone quarries in Vietnam

NGUYEN Anh Tuan[1, *], PHAM Van Hoa[1], PHAM Van Viet[1], LE Van Quyen[1], LE Thi Hai[1] and NGUYEN Tuan Anh[2]

[1] Faculty of Mining, Hanoi University of Mining and Geology, Vietnam.
[2] The mining - Geology design survey and Construction consulting joint stock company, Vietnam

Abstract: In dimension stone quarry exploitations such as the marble quarry, a literature review of the existing numerical modelling techniques has been carried out. According to Distinct Element Method, discontinuities have been treated as boundary conditions between blocks and, consequently, an accurate knowledge of joint distribution and orientation was required. The result of analyzing data and simulating in the fracture rock environment, which is applied to a mining condition of the dimensional stone quarries. The research we introduce in the output capacity of the dimension stone quarry from the computer simulations to generate the fracture network in 3D with an aim of evaluating the size of the blocks. The results of numerical models have been used to optimize some of the technical parameters for dimensional stone extraction and ensuring stable bench in the mining operation.

1. Introduction

In dimension stone quarry exploitations such as the quarry, the stability of the slopes can be considered from the aspect of slope cut or from the aspect of a bench or from gallery width. The research we introduce is the result of analysing data and simulating in the fracture rock environment, which applies to a mining condition of the dimensional stone quarries. Structural geologists usually measure and analyze orientation data in rock masses. The orientation of a discontinuity can be described by its dip and dip direction [1]. The combined orientations of discontinuities determine the shape of the individual blocks comprising the rock mass [2]. The properties of discontinuities relative to stability include orientation, persistence, roughness and infilling [3]. They are often found on the weakest structural plans where diverse displacement can develop. We have used advanced tools for analysing the data of joints and simulating the joint sets. Modelling program RESOBLOK was firstly written by LAEGO and INERIS, basing on the theory of Heliot 1988 [4, 5, 6] which is used to simulate cracking rock. The model result has been used to optimize some of the technical parameters for dimensional stone extraction and ensuring stable bench in the mining operation.

* Corresponding author: nguyenanhtuan@humg.edu.vn

2. Statistical study of the fractures

2.1. Input parameters

Parameters such as discontinuities, the fracture orientation, slope orientation, model dimensions of slope cuts, etc. were considered as inputs to predict number of set, the poles of sets, histogram and statistical of sets, statistical outputs with an aim of evaluating the size of the blocks, then the output capacity of the dimension stone quarry, synthetic indicator of global stability of slope cuts. The complexity of reality does not allow a complete description of the actual field [3,7]. The rock mechanics of rock mass depend mainly on the characteristics of the fracture field. It is therefore necessary to use stochastic models.

Applications are increasingly complex, and some involve a complete description of the fracture field. As fractures are not accessible in their entirety, but only at their intersections with boreholes, outcrops or drifts, one the first steps in the study of a given site is modeling and simulation of the fracture field. Mathematical morphology provides a means of fully characterizing a fracture network. It means stochastic models such as models of fracture systems, we are considering the random set of all the fractures [1, 3]. The knowledge of the functional of models of fracture systems is the random such as the exact equivalence of the spatial law for random functions and any nonrandom set of all the fractures. For any nonrandom set is then unchanged by translation and can be estimated from the sole realization of the fracture network. In practice, it is not possible to consider any nonrandom set of all the fractures. This works, the modeling deals with the scale ranging from tens of centimeters to tens of meters. It means various scales such as metric scale. The method is general and can be transposed to another scale.

2.2. Output parameters

2.2.1. Orientation distribution

The statistical modeling of directional data has been studied for a long time such as Mardia (1972) [1, 8]. The most commonly used models for spherical orientations concerning a fracture set are the truncated Fisher, the Bingham, and the uniform distributions. The expression of these distributions is linked with the reference sphere, is changed is such a way that the “new” North pole coincides with the mean direction of the given fracture set.

2.2.2. Spacing distribution

The intersection of any of the basic models with a line provides a 1D Poisson process [1]. Successive spacing are independent and follow an exponential distribution.

2.2.3. Trace length and fracture size

If fractures cannot be considered as infinite at the scale of the study, the distribution of their size largely determines the frequency of intersection and hence the mechanical behavior of the rock mass. In practice, it is not possible to observe the exact size of a fracture. A 2D survey, however, provides the trace length distribution, which linked with the fracture size distribution. But the experimental histogram of trace length is affected by several biases that have to be corrected.

2.2.4. General network models

All models can be deterministic or stochastic. The first models were deterministic, which is defined by three orthogonal directions of equidistant planes. After this, models with purely random parameters were used, such as the Poisson process. The model presents the advantage of displaying many properties. Stochastic models are considered here, because they are better adapted to usual applications. Their transposition to deterministic models is easy. From a stochastic point view, fracture networks are realization of random sets. The basic models can be found among the random set models, mainly developed by Matérn (1960), Matheron (1967, 1975), Miles (1972) [1], and many others. A comprehensive description from a rock mechanics point of view can be found in Dershowitz (1984), Heliot (1988), Chilès (1989) [1, 4]. All the models described common assumptions: all fractures are planar; all fracture locations are equally probable; all fracture orientations are independent of fracture locations.

3. Methodological

3.1. Design and planning methodology for dimension stone quarry

Methodological approach was pursued, developing and using the following set and sequence of components for modelling of the rock structure mass and discontinuity: interactive geological data base with Mathematica and Dips; visualization tool and interface elements expert with Mathematica, RESOBLOK (and LMGC90/3DEC) (see Fig.1). For the design and planning methodology of dimension stone quarry, 7 following tasks need to be performed:

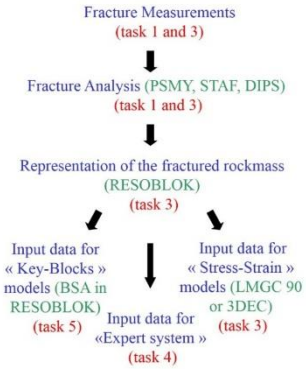

Fig.1. Methodological organization for modelling of the rock mass and discontinuity [7, 8, 9,]: PSMY, STAF and DIPS are the module to analyses the data of joint set; RESOBLOK, BSA in RESOBLOK, LMGC90 and 3DEC are used to simulate cracking rock mass.

Task 1: Site selection, the main objective is to identify the most suitable work sites and experimental layouts considering the geologic conditions.

Task 2: Excavation of the experimental site and installation of the instrumentation system for the collection of the data required in the excavation of experimental quarries.

Task 3: Geomechanical data collection; development of the appropriate 3D rock block models and of the respective geomechanical numerical models.

Task 4: Development and use decision support techniques for predicting cost and quality effective quarry layouts.

Task 5: Numerical analyses of options to predict optimum area openings: determine average block size and shape for each of the quarries; correlation between benches orientations in the fracture network and the recovery and stability of blocks.

The Task 6 and 7 are designing and planning methodology of dimension stone quarry:

Task 6: Field investigation of the exploited block size, quality and value.

Task 7: Design and planning methodology for dimension stone quarry exploitations.

3.2. Analysis of fracture measurements

Fracture measurements had been realised in real sites (Thung Khuoc). The measurements have been done using the scanline method. An analysis has been realised from those measurements with DIPS and PSMY method in order to determine the main sets of orientation and to fit the fracture parameters to statistical laws. The fractures measurements carried out by the operators have been analysed using PSMY method [2, 8]. This data base (orientation, spacing of fractures) was permits to determine which statistical laws adjusted the various fracture sets. The results of this analysis were compared with those established previously from the fracture measurements conducted at large scale in each quarry.

3.3. Realisation of fracture network simulations

The majority of the measured fractures were introduced in the model using the deterministic generator of RESOBLOK. Other fractures were introduced using the statistical generator (the fractures were simulated using the laws established previously) into the zones where no measurement was carried out. As for the other sites, two successive phases are conducted to build the RESOBLOK model: the fracture that have been measured and input the RESOBLOK; then, inside the zones in which the direct observation is not possible (or where no measurements have been done), different sets of discontinuities have been generated using the statistical laws determined previously (PSMY) [2,8].

3.4. Minimum block Size

According to the technical aspect, block size depends mainly on the parameters of mining system, breakability, transport and processing in mine. The minimum size ($V_{min} \geq 0,4$) of each recoverable block is taken to follow the size of dimensional stone on the market and current technologies. The blocks which have the size $V_{min} \geq 0,4\ m^3$ usually contain more faults, cracks which requires further processing to complete products from raw dimensional stone. Blocks with the size $V_{min} \geq 1m^3$ will research to recover.

3.5. Mining optimization to recover maximum blocks

Exploiting dimensional stones based on the technological phases of cutting blocks from fracture rock environment. The mining system of horizontal layers, vertical layers, and direct transport on the bench and selective blocks are mined to follow the minimum block size V_{min}.

3.6. Mining Optimization with stabilizing pit slope

Beside mining optimization to recover maximum blocks, we can to determine some technical parameters, the risky problem is caused by bench and pit slope failure in mining operation, which plays an important role in the mining effect for a long time. This study, we choose an assessment method based on limit equilibrium theory to analyze stability slope of quarry. These stiff blocks are analyzed on the basis of stability algorithm including the vector method proposed by Warburton (1981) [12] and Mohr-Coulomb criterion with safety factor F=1, both of which is set up in RESOBLOK.

The distribution of raw block shapes recovered depends on the fracture of rock mass, mining direction and movement of current benches compared with the direction of the main sets. Improving a mining effect means to increase the recovery rate and decrease the risk of unsafe problems. Optimizing the recovery rate of dimensional stones being available on the market are a target function of the technical parameters: angle between mining direction and joint set, bench height, dip angle of the current bench.

4. Applications

4.1. Some dimensional stone quarries in Vietnam

Vietnam has a high potential in marble, magmatic rocks for producing facing stone and use as facing stone. The marble recovery value is controlled by the sale markets and using industries of construction. We present some dimensional stone quarries in Vietnam such as marble resources in Luc Yen area, Yen Bai province (Luc Yen quarry); marble resources in Quy Hop area, Nghe An province (Thung Khuoc quarry); Granite resources in Thua Thien Hue province (Van Xuan quarry, Fig.2); granite resources in Phu Cat area, Binh Dinh procince (Phu Cat quarry, Fig.3); granite resources in Hoa Quan Bac area, Phu Yen province (Hoa Quang Bac quarry, Fig.4); gabbro diorite of Nui Mot area, Ninh Thuan province (Nui Mot quarry); etc. [13, 14].

Fig. 2. Granite Van Xuan quarry, Thua Thien Hue province [14].

Gabbro diorite resources in Nui Mot area has various colours, such as black-grey and black-green gabbro diorite of Nui Mot area; white marble is in Luc Yen area, Quy Hop area; light- to dark-green of Hoa Quang Bac area; black granite of Van Xuan area. The rocks also have the beauty, high mechanical durability and high degree of block recovery. The economic value of the quarries combined the master plan for investigation, exploitation, quarry, processing and rational use of dimensional stone. The economic efficiency of the quarrying enterprise depends on the recovery ratio of dimension stone. They satisfy standards of production of facing stone and have reputation in both domestic and foreign markets.

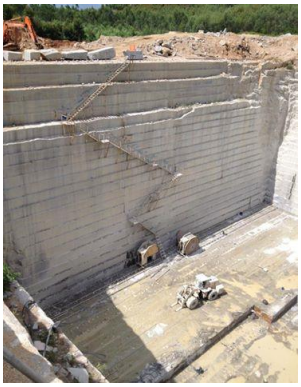
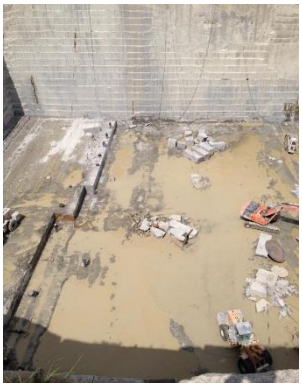

Fig. 3. Granite Phu Cat quarry, Binh Dinh province [14].


Fig. 4. Granite Hoa Quang Bac quarry, Phu Yen province [14].

4.2. Application for marble Thung Khuoc quarry

4.2.1. Analysis of fracture measurements

In this research, the Thung Khuoc quarry, Nghean province, Vietnam [13] exploits the stone which follows the standard of normal construction materials. The marble stone is able to be used for making various tiles. The dimensional stone products chosen and applied in the calculation and model of the discontinuous rock environment.

a) 
b) 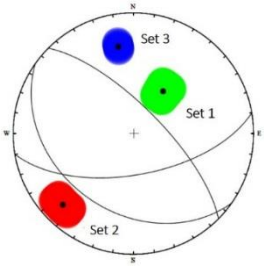

Fig. 6. Experiment pit M.01 (a) and 3 main joint sets of the Thung Khuoc quarry, Schmidt grid in hemisphere.

According to the result of the exploration report, the Thung Khuoc quarry has estimated reserves of about 10 046 128 m^3: in which the normal construction material reserve is about 9.593.189 m^3, the reserves producing tiles and dimension stones are 452.939 m^3. The data of joints in the mine are measured by the stations on the surface (8 stations) and joints in drilling cores (5 drilling holes). 3 sets of joints in the mine are identified in Figure 6 and Table 1.

Table 1. Basic parameters of the key sets in the Thung Khuoc quarry

Parameters	Sets		
	Set 1	Set 2	Set 3
Dip-direction angle (α_d, degree)	210÷220	40÷50	170
Dip angle (β_d, degree)	30÷40	70÷75	60÷65
Distributing degree of set (K)	220	995	1876
Distance between the sets: uniform (a; b) with a and b are respectively the minimum and maximum values	(0,1;1,25)	(0,1;1,25)	(0,1;1,25)

4.2.2. Minimum block size

While an average recovery rate of blocks measured with joints on the surface is 20%, in the drill hole is 27,71% and an average rate of joints approached by exploration on the surface and in drill hole is 23,86%. An experiment pit (M.01) is open with aim of quantifying the recoverable rate of different size blocks, in fact, taking samples to discover its engineering characteristics. The mine M.01 has 7 m long, 4,8 m wide and 3,5m in average height; its volume is 117,6 m^3.

The result of the pit M.01 has collected 9 blocks with the sizes $V_{min} \geq 0,4$ m^3, all of which have 5,48 m^3 accounting for 4,7% of the volume of the pit.

4.2.3. Establishing of joint sets and mining orientation

Beginning from the exploratory data in the pit M.01 and the initial results on raw stone volume which are recovered (size, volume and recovery rate) in a typical area of the Thung Khuoc quarry. The model of fracture rock mass in the pit M.01has been chosen to analysis for optimization purpose of the parameters and the mining direction of the mine such as stabilize bench. The open pit slope ensures mining optimization as well as recovering the maximum size of commercial blocks.

Table 2. Effect of an average number of blocks in the model of the experiment pit to relationship between the direction of main joint sets and the pit.

The direction of main sets, degree			the direction of the trial mine, degree	an average number of blocks, blocks
set 1	set 2	set 3		
210÷220	40÷50	170	35	368
			225	382
			350	404

Figure 7 introduces the models of joint sets in RESOBLOK with 3 different mining directions of the trial mine. The results of examinations in each direction considering several various random models are shown in table 3.

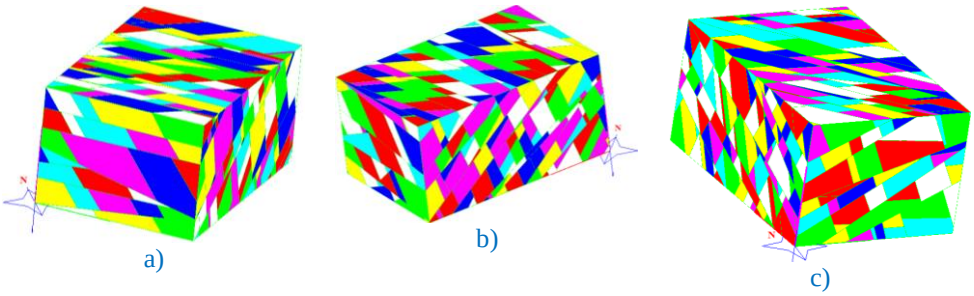

Fig.7. Model of fracture rock mass in the experiment pit M.01: the direction of the model parallels to set 1(a); set 2 (b); set 3 (c).

4.2.4. Determination of mining direction

With a main joint set, the angle of mining bench direction is parallel or perpendicular to the main set, which will allow recovering the maximum volume of commercial blocks (V_{min}). Optimization needs to be tackled when appearing more joint sets in the discontinuous rock mass, the basic parameters in mining bench direction need to be represented properly in order to be able to optimize in the model.

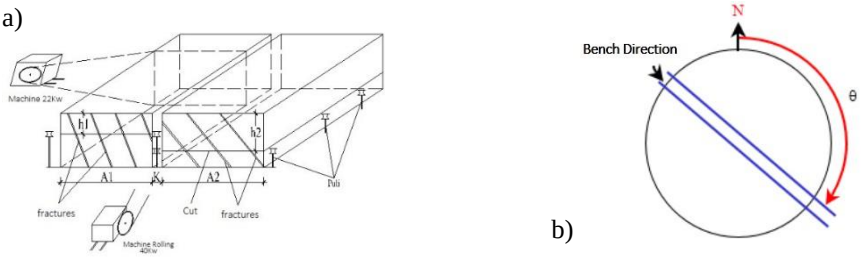

Fig. 8. Plan of mining technology for dimensional stone by wire saw machine and the moving direction of mining benches.

Figure 9 showing the investigating result of 3 typical mining directions is consequently perpendicular to sets 1, 2 and 3. The achievable results are represented on the distributing histogram with a specific order of blocks being equivalent to model volume (in the left column) and the percentage of the volume of the blocks is equivalent to the mining direction of the experiment pit model (in the right column).

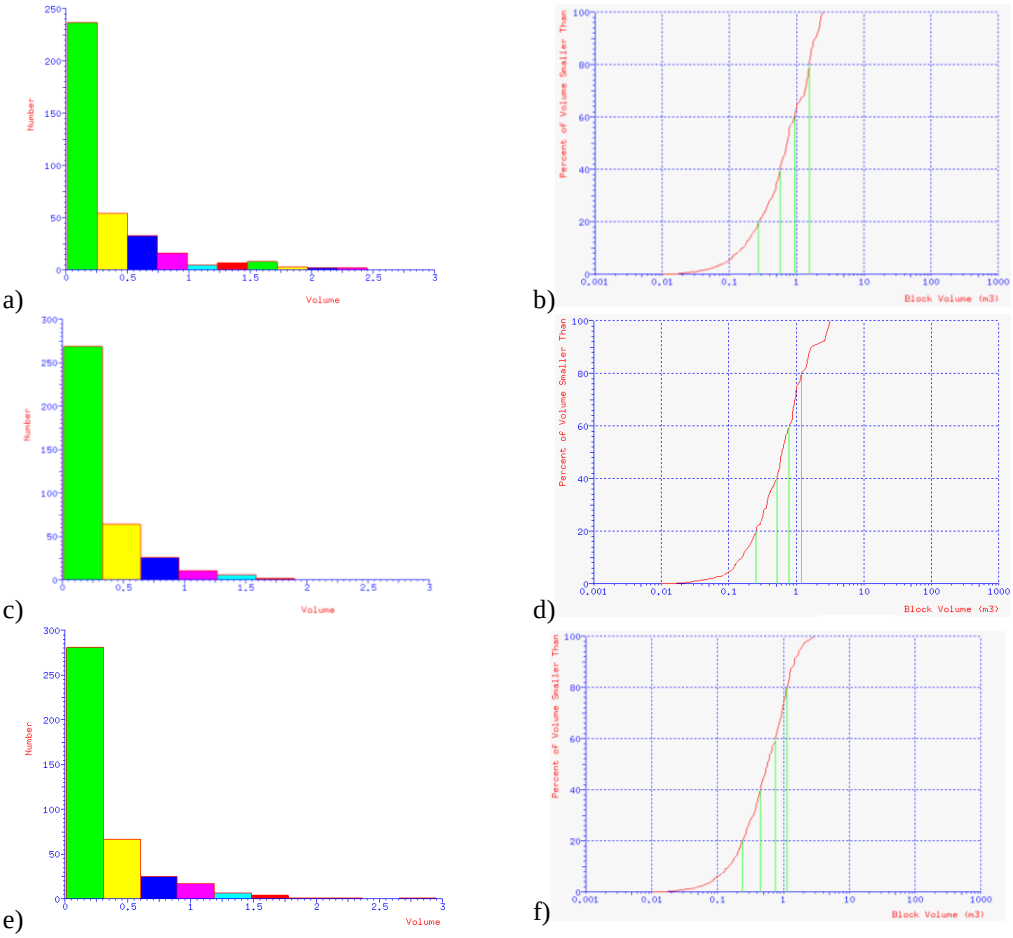

Fig. 9. Histograms distribute a number of blocks with their volumes in the model (in the left columns) and the percentage of blocks with their volumes (in the right column) which are associated with the direction of the pit: (a, b) 35^0 direction; 225^0 direction and (e, f) 355^0 direction.

The direction of the mining benches length where blocks mined relates to the order of new bench opening, the first mining bench position of the mine and the direction of the main joint sets. The data distribution in figure 9 is the distribution of average values collected from a large number of the random statistical model.

- Mining direction of 35^0, the size is with $V_{min} \geq 0{,}4\ m^3$ accounting for 60% and with $V_{min} \geq 1m^3$ accounting for 36%

- Mining direction of 225^0, the size is with $V_{min} \geq 0{,}4\ m^3$ accounting for 60% and with $V_{min} \geq 1m^3$ accounting for 25%

- Mining direction of 350^0, the size is with $V_{min} \geq 0{,}4\ m^3$ accounting for 60% and with $V_{min} \geq 1m^3$ accounting for 28%.

With the result above, the optimum direction involving in the bench direction of 35^0 parallels or is penpercular to primary set direction 1 (set 1), will be able to be recover the most block rate of $V_{min} \geq 1m^3$ accounting for 36%. Difference in the recoverable rate among the blocks with joint measuring methods on the surface (from 18.75% to 21% and an average of 20%), drillcore (from 25% to 28,7% and an average of 21,71%) and mine opening (14,28%) and the numerical model of the discontinuous environment (40%) with a

group of the data from the 3 investigating methods on the surface shows that there are, in fact, a lot of invisible cracks which have not discovered when measuring on the surface. The reason for the difference above is caused by collecting the joint data insufficiently, incomprehensively and accurately. From the results above, the 3 exploratory methods above are not satisfied with the conditions on the numbers, quality of joint data when analyzing and using them for finding out model results.

In this condition, the data collected from the trial mine M01 only hold 2%o of the mine area (about 33,6 m^2 out of the whole area of 16 thousand m^2 with an altitude of from 100 to 230 m^2). Therefore, updating and complementing the number and the exactness of the data is necessary for some the phrases of the mine to improve the quality and certainty of estimated model.

4.2.5. Mining optimization with stabilizing pit slope

Parameters are first applied to compute for numerical model: the mining bench height H=5m, the mining room's width A = 5m, the mining room' length L = 10m, where we examine safety condition with the angle of a bench slope $\alpha = 75°$. The basically mechanical characteristics of rock and joint: rock density of 2,7 tons/m^3, the joint' fiction angle of 30^0, the joint's cohesion of 0, the 3 bench directions (35^0, 225^0 and 350^0) compared with the North are analysed with the stabilities. The result of computing stability on 3 dimensions model has the weak structure shown in figure 10.

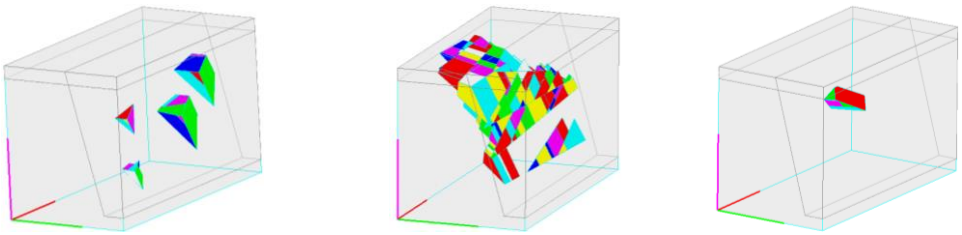

a) b) c)

Fig.10. Distributing model of unstable blocks on the bench is in a bench direction compared with the North, 350 (a) there are 6 unstable blocks with the volume of 1m3; 2250 (b) there are 118 unstable blocks with the volume of 22m3; and 3500 (c) there are an unstable block with the volume of 0,52 m^3.

The analysed results above allow us to select the best mining direction involving recovering and ensuring safe and stability on the bench [9, 11]. When we move the bench with one more mining room, we see that the volume of unstable blocks in the direction of 350^0 being at right angle to joint set 1 is the least, which means that the developing direction of the mine is safe after that it is in the direction of 35^0. The rest direction of 225^0 has the unsafest risk.

4.2.6. Discussion

Beginning with the ability of the dimensional stone's mining and processing technologies with the minimum block V_{min}, we create an order of developing bench in order to recover the rate having size more than V_{min} accounts for the highest. In case, the Thung

Khuoc quarry in the direction of 35^0 compared with the North develops toward 2 sides, which leads to $V_{min} \geq 0.4$ m^3 accounting for 60% of recovery rate and $V_{min} \geq 1$ m^3 accounting for 36% of recovery rate. Moreover, the developing direction of this bench allows the mine to operate relatively safely with $1m^3$ unstable blocks on the 10-length bench.

In the section above, we have already determined the key bench direction of the mine which is perpendicular to the set 1 of 35^0 (set 1) compared with the North. The dip angle of stone layers in set 1 from 30^0 to 40^0. The width and length of mining room are 5m and 10m (some cases depend on particular benches). In some cases of the stable bench, homogeneous rocks are with a dip angle of 90^0. The problem given is to form the target function of specifying reasonable bench height h with certainly geological conditions (including dip angle α and space between two joints L) in order to the most recoverable rate of commercial stones.

5. Conclusions

The article shows the discontinuous model of the rock mass in Thung Khuoc dimensional stone quarry, Nghe An, Vietnam. From the analysing result of the model, we have chosen the developing direction of mining bench optimizing on the recovery rate and safety in the mining operation. This result allows us to calculate the technical parameters being suitable to pit parameters and gallery width as well as the best direction of the bench. Furthermore, we could choose the best mining methods with the aim of increasing mining effect and output, reducing mining expense and needed investment in mining operation, ensuring safety for dimensional stone quarries. Basing on advanced models on the computer, we apply and set up the geometric models of joint sets reliably in the discontinuous environment from the parameters and features of joints. This technology allows predicting the investing expenditure with the most effect and safety in the quarries. Therefore, this could recover the most blocks with the sizes which suit to the market demands.

6. Acknowledgements

The authors wish to thank the 5th International Conference "Scientific-Research Cooperation between Vietnam and Poland" (POL-VIET), and Hanoi University of Mining and Geology, Vietnam to carry out this research is thankfully acknowledged.

7. References

1. S. Priest, *Discontinuity analysis for rock engineering* (Chapman & Hall, 1993).
2. Nguyen Anh Tuan, V. Merrien-Soukatchoff, M. Vinches, Grouping discontinuities of fractured rock mass into main sets : consequences on the stability analysis of open pit benches, (ed. DFNE 2014. Vancouver, Canada, pp.1–8, 2014).
3. E. Hoek, W.Bray, *Rock Slope Engineering civil and mining 4th* (ed. C. D. Wyllie & C. W. Mah, eds., London and New York, 2004).
4. D. Heliot, Generating a blocky rock mass. International Journal of Rock Mechanics and Mining Sciences & Geomechanics Abstracts, **25**, pp.127–138 (1988).
5. Laego-École des Mines de Nancy-INERIS, RESOBLOK, (2008).
6. V. Merrien-Soukatchoff, T. Korini, A. Thoraval, Use of an Integrated Discrete Fracture Network Code for Stochastic Stability Analyses of Fractured Rock Masses. Rock Mechanics and Rock Engineering, **45**, pp.159–181 (2012).
7. A. Thoraval, Analysis of the fracturation from the underground quarries of Levigliani, Lasa, and

Dionyssomarble, Brite/Euram Project BE-5005, (2005).
8. Nguyen Anh Tuan et al., Grouping discontinuities in representative sets: influence on the stability analysis of slope cuts. Bulletin of Engineering Geology and the Environment, **75(4)**, (2016).
9. Nguyen Anh Tuan, Stability conditions of jointed rock slope with contact dynamics method, **56**, pp.11–19, (2016).
10. Nguyen Anh Tuan, Pham Van Viet, Tran Dinh Bao, Optimization of some technical parameters for mining dimesional stone by wire saw machine. The 22nd National Conference on Mining Science and Technique, Pages 171-280 (2011).
11. Nguyen Anh Tuan, Pham Van Viet, Le Van Quyen, Modelling of the rock mass and discontinuity structure aided design and planning methodology for marable Thung Khuoc quarries, Vietnam. Advances in Mining and Tunneling (ICAMT 2016), (2016).
12. P.M.Warburton, Vector stability analysis of an arbitrary polyhedral rock block with any number of free faces. International Journal of Rock Mechanics and Mining Sciences, **18**, (1981).
13. Exploratory report of Thung Khuoc quarry in Quy Hop Town, Thung Nang Commune, Quy Hop District, Nghe An Province, (2012).
14. Exploratory report of Luc Yen quarry; Van Xuan quarry; Phu Cat quarry; Hoa Quang Bac quarry; Nui Mot, (2018).

The status and prospect of mining technology in Vietnam underground coal mines

Hai DUONG DUC[1,*], QUANG Dao Hong[1], Marian TUREK[2] , Aleksandra KOTERAS[2]

[1] Institute of Mining Science And Technology (IMSAT), Hanoi, Vietnam
[2] Central Mining Institute (GIG), Katowice, Poland

Abstract. Vietnam has the 13th largest hard coal reserves globally, with the reserves totaling 2.22 billion tonnes, and estimated resources of 4.07 billion tonnes. Coal use is playing an increasing role in the energy mix and according to current planning, this role is to increase further. In parallel with the development of the Vietnamese coal sector, underground mining also underwent many stages of improvements, especially in the last two decades. This paper analyzes the achievement and the state of the mining technology applied into the underground mining by the Vietnam National Coal - Mineral Industries Holding Corporation Ltd. (VINACOMIN) during 20 year period and proposes the recommendations for the sustainable development of Vietnam underground mining.

1. Introduction

Vietnam has large anthracite resources, with the largest coalfield being located in the Quangninh province. Quangninh coalfield is located in the northeastern part of the country, with 120 km length and 10-30 km width. The most recent update of the master plan for coal development (Master Plan of Coal Industry Development in Viet Nam by 2020, with perspective to 2030) estimates that Vietnam has almost 2.22 billion tonnes of hard coal reserves and almost 4.07 billion tons of resources, in which the measured and indicated resources (categories A+B+C1) occupy 35.3%, the inferred resource (C2) is 8%, and the prognostic resource (P) is 56,7% [1].

Coal extraction is run by the Viet Nam National Coal-Mineral Industries Holding Corporation Ltd. (VINACOMIN), a state-owned enterprise, which plays an important role in national strategies to ensure effective exploitation of mineral resources. VINACOMIN operates 3 main coal regions, i.e: Uongbi, Hongai, and Campha in which mining is carried out in 13 underground coal mines with production than 1.0 million tons per year. For instance, Uongbi region has Mao Khe (1.88 million tons/year), Nam Mau (2.21 million tons/year), Vang Danh (3.15 million tons/year) and Uong Bi (2.6 million tons/year). Hongai region has Nui Beo (2 million tons/year), Ha Lam (3.15 million tons/year) and Hon Gai (2.5 million tons/year). Campha region has Quang Hanh (1.7 million tons/year), Duong Huy (2.15 million tons/year), Thong Nhat (2.1 million tons/year), Khe Cham (1.8 million tons/year), Mong Duong (1.55 million tons/year) and Ha Long (2.15 million tons/year). Average exploitation depth of underground coal mines is 300m below sea level (the equivalent to the depth of 320-700m below the ground surface). Main underground coal mines in Quangninh coal basin is illustrated in Figure 1.

* Corresponding author: duongduchai88@gmail.com

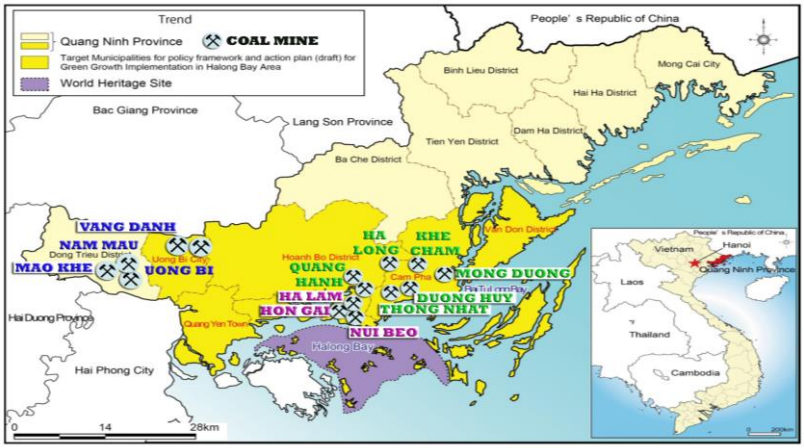

Fig. 1. Main underground coal mines in Quangninh coal basin

In the last twenty years, coal output from the Vietnam underground coal mines increased rapidly from 4.3 million tonnes in 2000 to 22.1 million tonnes in 2018 (grew about 5 times). According to the Master Plan of Coal Industry Development in Viet Nam by 2020, with perspective to 2030, which was adjusted in 2016 [1], and mining plan of VINACOMIN total coal output will reach the level of 41 million tons in 2019, 47.8 million tons in 2020 and 49.3 million tons in 2025. In which, underground mining coal output will increase gradually year by year and will achieve the largest share (to 73%) in the total output of the overall coal industry in 2025. Details of coal production over the period between 2000 and 2018 with forecasts to 2025 are presented in Figure 2.

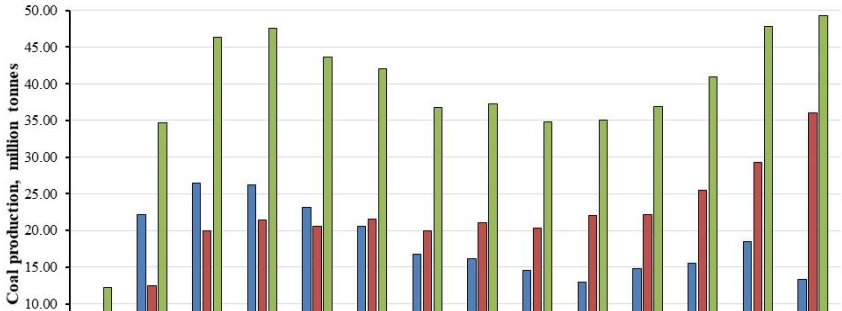

	2000	2005	2010	2011	2012	2013	2014	2015	2016	2017	2018	2019	2020	2025
Open pit	7.89	22.20	26.5	26.2	23.2	20.6	16.8	16.1	14.5	12.96	14.85	15.50	18.48	13.27
Underground	4.31	12.50	19.9	21.4	20.5	21.5	20	21.1	20.3	22.04	22.1	25.5	29.32	36.03
Total	12.20	34.70	46.39	47.58	43.70	42.10	36.80	37.20	34.80	35.00	36.95	41.00	47.80	49.30

Fig. 2. Vietnamese coal production between 2000 and 2018 with forecasts to 2025 [2]

2. Analysis of geological conditions of coal in Quangninh area for underground mining

The application of mining technologies depends greatly on regional geological conditions. Based on data from coal companies [2], information obtained from previous studies [4,5] as well as the Master Plan of Coal Industry Development [1], coal reserves of 13 underground coal mines in Quangninh has been analyzed and evaluated. The results have identified the correlation between geo-mining conditions to the selection of mining technology in Vietnam.

Results from the abovementioned analysis showed that total coal reserves investigated to a depth -600m below the sea level is 1,609,767 thousand tonnes, in which, coal reserves are mainly distributed in the thickness between 3.5 and 10.0 meters with 44.1% and 22.5% of coal reserves have a thickness between 2.2 and 3.5 meters. In addition, 60% of coal reserves have the incline seam dip (from 150 to 350). In addition, a large part of these reserves are located in areas of difficult geological conditions, for example, structural disturbance, dipping seams, complicated surrounding strata, and coal seams are separated by faults that may restrain mining productions. The variation of seam dip and seam thickness is high, causing difficulty in the application of the mechanized mining technologies. So that over the years, underground mining in Vietnam faced many challenges in the extraction of coal seams. The summary of coal reserves at some deposits in Quangninh coalfield is presented in Table 1.

Table 1. Coal reserves by region in 1000 tons

No.	Name of coal mine	Evaluated level (compared to sea level)	Coal reserves, 10^3 tons
1	Vang Danh	to -350m	230,337
2	Mao Khe	to -400m	142,140
3	Uong Bi	to -300m	136,207
4	Nam Mau	to -250m	166,149
5	Nui Beo	to -450m	55,931
6	Ha Lam	to -450m	143,541
7	Hon Gai	to -600m	202,967
8	Quang Hanh	to -300m	48,785
9	Thong Nhat	to -350m	51,984
10	Mong Duong	to -550m	68,854
11	Khe Cham	to -350m	80,083
12	Duong Huy	to -250m	79,914
13	Ha Long	to -400m	202,875
	Total		**1,609,767**

3. Status of underground mining technology in Quangninh coalfield

Underground coal mining has been operating in Vietnam for many years [6]. Coal reserves in the Quangninh area were extracted by French colonialist companies from 1884 to 1955 with total production more than 50 million tons. When the Vietnamese government took control of the country, the state-owned coal companies started renovating the old

mining collieries acquired from the French and also constructed new mines with the aim of increasing the production of coal in Quangninh to 10 million tonnes in 1980. However, due to both the complications of geo-mining conditions and poor mining equipment, coal production remained at 4 to 6 million tonnes per year for many years. The establishment of VINACOMIN in 1994 can be considered a new period in the history of the development of Vietnam's coal industry-the period of innovation in management, production and business activities. This has resulted in a visible increase in coal production in the last twenty years.

In Quangninh coalfield, underground mines have applied various types of mining technologies suited to the geological characteristics. For example: (1) the longwall mining method, exploiting the full seam thickness, applied for the medium thickness seam, dipping up to 350; (2) longwall top coal caving (LTCC) applied for thick coal seam, dipping up to 350; (3) the mining method, retreats along the seam dip, applied to steep seam, medium thickness; (4) the diagonal longwall system using hydraulic support model ZRY for average thick seams up to 4.5m, dip above 450; (5) the sub-level mining method applied for slope seams; (6) the shortwall mining technology using hydraulic support or shield support applied for the steep thick seams. In which, coal seams in the Quangninh area were almost extracted by a single pass longwall method.

It is understood that a proper selection of the equipment synchronization in longwall is one of the key element for a successful operation of the mining technology. Underground mining companies have been struggling to find the most suitable equipment for the extraction of coal seams by longwall methods. Initially, most of the longwall faces were supported by wooden props (Figure 3a), while coal was extracted from the face by the drilling and blasting method. Due to the improvement in coal production, productivity, and the standards of mine safety, VINACOMIN applied hydraulic single props (Figure 3b) since 1997 and semi-mechanized shields model XDY-1T2/LY (Figure 3c and Figure 4a) since 1999. The success of these works has created a "technical revolution" to hydraulically replace the wooden props and improved the overall technical economical parameters. Coal production in the longwall faces supported by hydraulic support has increased rapidly from 100,000 to 150,000 tonnes per year as compared with the production of 50,000-70,000 tonnes per year when the face was supported by wooden props [3]. Coal mining productivity using the hydraulic single props increased to 2.5-5.37 tonnes per man-shift, an average of 3.0-3.5 tonnes per man-shift.

Since 2006, VINACOMIN has continued to apply new hydraulic supports in the underground coal mines, for instance, self-moving hydraulic frame model ZH1600/16/24Z (Figure 4b), model GK/1600/16/24/HTD (Figure 4c) and model ZH1800/16/24ZL. Production increased range from 140,000 to 250,000 tonnes per year, labor productivity from 5.0-7.0 tonnes per man-shift [3]. In addition, working conditions and safety on workplaces has been significantly improved. Mining began more environmentally friendly due to the elimination of wooden support. However, mining operations also required the amount of manual work, and this type of supports are only suitable for extraction by the drilling and blasting. As a result, production is still limited. Therefore, the increase of coal mining production according to the VINACOMIN’s plan, which means an increase in the number of longwalls as well as the number of workers. This is hardly feasible in the current mining situation in Vietnam. This is the opening step for the renovation of underground mining technology, which is a premise for the introduction of mechanized equipment into underground mines in Quangninh coalfield.

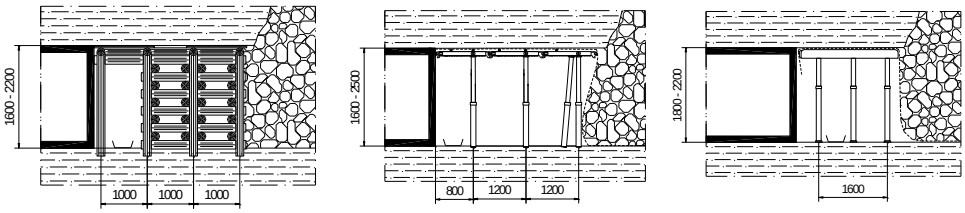

a. Support by wooden props

b. Support by hydraulic single props

c. Support by semi-mechanized shields

Fig. 3. The longwall face supported by wooden props and hydraulic props

a. Self-moving hydraulic beam XDY-1T2/LY

b. Self-moving hydraulic frame ZH1600/16/24Z

c. Self-moving hydraulic frame GK/1600/16/24/HTD

Fig. 4. The longwall face supported by semi-mechanized shields

In 2002, Khe Cham Coal Mine firstly applied the longwall mining method, face supported by self-moving hydraulic beam XDY-JF/LR/T2/120JZ, exploiting the full seam thickness by shearer model MG-200 W1 at the seam No.14.4, level of -10/+32. During the trial period (from April 2002 to September 2005) the longwall exploited 512,918 tons of coal. The highest monthly exploitation output reached 22,300 tons, and the average labor productivity was 5.16 tonnes per man-shift. Based on the results achieved by the first semi-mechanized longwall, in 2005, Khe Cham Coal Mine has continued applying the first mechanized mining technology (Figure 5) in the similar condition, using shield support ZZ-3200/16/26 combined with the shearer MG150/375-W. The mechanized longwall has a hight output of 233-388 thousand tons/year, averaging 289 thousand tons/year; labor productivity from 9.9-11.4 tons/per man shift, an average of 10.3 tons per man shift [3]. The success of the longwall was also a premise for technological innovations in the next exploitation for medium thick seams in Duong Huy and Quang Hanh coal mine since 2015. Compared with the longwall supported by hydraulic support in the same conditions, the average output of the mechanized longwall is 2.3-3.9 times higher, and the average productivity is 2.5-3.0 times higher.

Fig. 5. The mechanized longwall in Khe Cham coal mine [5]

Some mines have investigated the mechanized mining equipment for the extraction of thick and gentle slope seams. For example, in November 2007, Vang Danh coal mine applied the LTCC (Figure 6a), supported by mechanized equipment i.e. shield VINAALTA-2.0/3.15, shearer, Armoured Face Conveyor (AFC) and chain conveyor. As a result, the highest production reported approximately 450,000 tonnes/year. This mining mechanization technology was expanded to Nam Mau coal mine where was applied in 2010 [3]. In the period from 2015 to now, VINACOMIN has applied new LTCC method using double AFC (front conveyor and rear conveyor (Figure 6b), in which, the relocation of the top coal draw process to the rear conveyor) in 3 underground mines. There are longwalls in Ha Lam coal mine (one LTCC capacity of 600,000 tons/year since March 2015, one LTCC having capacity of 1,200,000 tons/year since November 2016), Khe Cham coal mine since April 2016 (capacity of 600,000 tons/year) and in Vang Danh coal mine since November 2018 (with capacity 450,000 tons/year). Labor productivity is relatively high with an average of 33.5-34.0 tons per man-shift, and 4-5 times higher than longwall using semi-mechanized support.

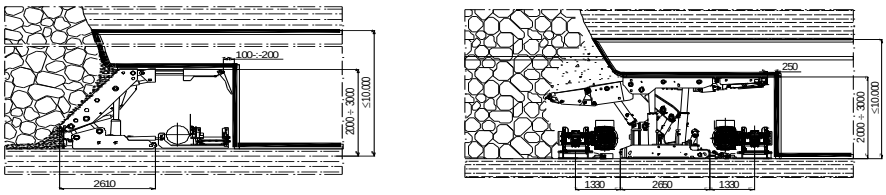

a. LTCC using 1 AFC *b. LTCC using 2 AFC*

Fig. 6. The mechanized longwall method applied for the thick and gentle slope seams [5]

In the steep thick seams, in the period of 2007-2013, Vang Danh and Ha Long coal mines have put into the trial application of shortwall technology, face supported by power shield model KDT-1, KDT-2, and top coal caving by blasting drilling in the long hole. But both of the above works have not reached the set objectives. The main reasons for this are seen in the complex geology conditions (water flowing into the shortwall, fluctuation of seams, large mine pressure).

The mechanization technology retreats along with the seam dip, extracting the high steep thin coal seams by coal plough has been applied since 2008 in Mao Khe and Hong Thai coal mine, supporting by shield support 2ANSHA. Labour capacity and productivity of coal mining mechanized longwall by self-acting shield support 2ANSHA (average

mining capacity is 64.500 tons/year, labour productivity reached 5.6 tonnes per man-shift) was two times higher, the expense for preparation roadway was seven times lower and technology loss (16%) decreased two times than sublevel mining technology, supported by a movable hydraulic beam in the same geological conditions [3]. In addition, since August 2015, Hong Thai coal company (now belong of Uong Bi coal mine) has applied the new diagonal longwall system using hydraulic support model ZRY at seam No.9B, level of +30/+95. By the end of 2015, technology has achieved relatively great results: average coal output of 400 tons/day, labor productivity reached 5.5-6.0 tonnes per man-shift (2-3 times higher compared with sublevel mining method); and coal loss only between 12.6-16.3% [3] [3]. This technology has improved the level of safety and working conditions. More importantly, the application of the diagonal longwall system with the use of support ZRY has reduced the rate of roadway development per tonne of coal production, with only 16,7 metres per 1000 tonnes as compared with average 30-40 metres per 1000 tonnes in the sub-level mining method. Thereby, the experimental project in Hong Thai opened a new way to innovate the mining technology for steep seams. Up to now, VINACOMIN has 6 underground mines applying the mining technology with 7 longwalls.

The results of analyzing the status of underground mining show that, before 1998, underground coal production was only 4,186 thousand tons and coal output mainly from longwalls using wooden props. With the strong innovation of mining technology after 1998, rate of coal production from longwalls using wooden props decreased to 60.1% in 2001, only 9.0% in 2005 and less than 1% in 2018, while coal output from longwalls using hydraulic support increased from 22% in 2001 to 63-64% in the period 2005-2018. In addition, the rate of coal exploited by mechanized technologies has increased rapidly, for example, in 2018 reached 15% of total underground coal output, equal to 5 times compared to 2010 (3%) and equal to 7.5 times compared to 2005 (2%). Underground coal production of VINACOMIN according to mining technology as illustrated in Figure 8.

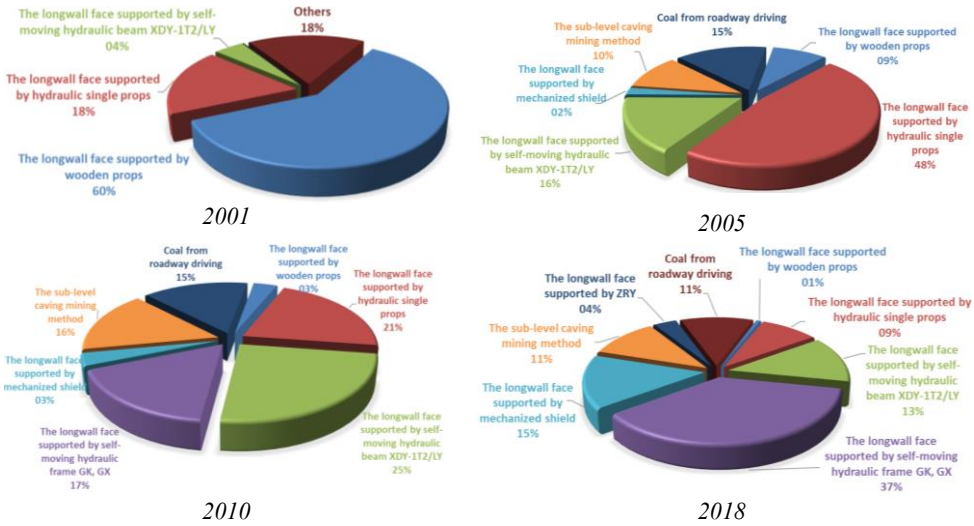

Fig. 8. Underground coal production of VINACOMIN according to mining technologies [2]

4. Prospect of Underground Mining Technology in Vietnam

According to the Master Plan No. 403 [1] and to the 5-year plan of 2019-2023 [3] the total coal output of VINACOMIN will increase for high demand of the national industry, while labor recruitment (especially labor for underground mines) is increasingly difficult. VINACOMIN is actively implementing a number of tasks: (1) Promote application of mechanization, automation, computerization and new advanced technologies into production; (2) Increasing output to reach mine capacity of invested projects; (3) Increase labor productivity, reduce production costs, ensure business efficiency and sustainable development; (4) Improve workplace safety, working conditions, increase income for workers; (5) Reach the objectives for 2020-2023, i.e. reach over 25% of total coal mining capacity by coal production from longwall applying fully mechanized mining technology.

From the actual experience, some main reasons affecting the efficiency of mining technologies application work at underground mines in Quangninh coalfield can be defined as follows:

1. Continue to expand the application of different types of technologies that have successfully implemented in the underground coal mines in Quangninh coalfield for areas with suitable conditions such as:
   - Synchronous mechanization technology to exploit seams with thickness, seam dip up α to 35^0 (most effective when $\alpha \leq 25^0$, similar types of 2 AFC in Ha Lam and Vang Danh) at Nui Beo and Khe Cham II-IV mines (reserves has been planned according to mine construction projects);
   - Mechanized mining technology for medium thick seams, slope up to 35^0;
   - Applying the diagonal longwall system using hydraulic support model ZRY for companies with average thick seams up to 4.5m, dip above 45^0 such as Vang Danh, Quang Hanh, Uong Bi, Ha Long and Hon Gai
2. Develop and apply mechanized mining technologies using lightweight self-support with suitable conditions in Mong Duong, Nam Mau, Ha Lam, Khe Cham II-IV and Uong Bi coal mines;
3. Studying and applying experimental technical and technological solutions to mining in medium thick seam conditions, slope angle to 45^0, seams with "3 soft conditions" (soft coal, roof and floor) at Mao Khe, Uong Bi coal mines.
4. Researching and applying experimental mining technology in thick, steep and suitable reservoir conditions at Vang Danh, Ha Lam, and Nam Mau coal mines.
5. Study and apply the diagonal longwall system using hydraulic support model ZRY replicate mining technology sublevel caving in conditions of steep seams.
6. Viewpoints if high-capacity mechanized complexes cannot be applied such as Ha Lam, Vang Danh, and Khe Cham coal companies. Coal mines must actively coordinate with the consulting company to invite foreign experts to carefully survey geological conditions, suitable application conditions to order and design mechanized complexes suitable to application conditions with capacity from 250,000-350,000 tons per year.

5. Summary

A critical review of the current level of underground coal mining in the Quangninh coalfield showed that over the last 20 years, technology and management have been improved. These improvements resulted in a visible increase in coal production from 9.4 million tonnes in 1994 to nearly 40 million in 2018, in which, coal output from the underground coal mines increased rapidly from 4.3 million tonnes in 2000 to 22.1 million tonnes in 2018 (grew about 5 times). However, this improvement was still limited in

capacity and safety management. The increase in total coal production was mainly based on the increase in the number of longwall faces. In addition, the maximum output of the longwall face is low compared to the longwall faces in developed countries. The main reason for the limits in coal production and safety management is the inappropriate mining equipment used. Mining operations require a number of processes to be undertaken by manual work, resulting in low production and productivity.

In the coming years, the Vietnamese economy's demand for coal product will increase rapidly and this requires an improvement in the mining industry. Unfortunately, open-pit mining will be gradually scaled down and will end in 2030. As a result, there is a need to improve the underground mining sector. In order to ultimately prevent potential problems and realize the potential revenue in the underground coal mines, it is necessary to improve the understanding of the operational issues associated with the application of mechanized mining equipment suitable with conditions of the Quangninh coalfield.

References

1. Vinacomin industry investment consulting joint stock company, *Master Plan of coal industry development in Vietnam by 2020, with perspective to 2030*, Hanoi, Vietnam (2016)

2. VINACOMIN, *Annual output report of mines from 2000 to 2018*

3. VINACOMIN, *Report on evaluation of mining and driving technology application in period of 2016-2018, orientation stage 2019-2023*, Quangninh (2018)

4. Dac P. M. and Tuan N. A, *Investigation of the application of mechanized mining method to thick coal seams in complicated geo-mining conditions in Quangninh*, Technical report, Institute of Mining Science and Technology, Hanoi, Vietnam (2004)

5. Hai D.T, *Developing the application of mining technology and driving roadway in underground mines of Quangninh coalfield*, Technical report, Institute of Mining Science and Technology, Hanoi, Vietnam (2016)

6. VINACOMIN, *History of coal industry development in Vietnam*

Climatic hazard assessment in selected underground hard coal mines in Vietnam

QUAN Truong Tien [1*], Rafał ŁUCZAK[1] and Piotr ŻYCZKOWSKI[1]

[1] AGH University of Science and Technology, Faculty of Mining and Geoengineering, Kraków, Poland

Abstract. The article discusses the possibility of improving the microclimate in underground hard coal mines in Vietnam. Vietnamese underground mines are shallow mines which extract coal deposits accumulated up to 500 m below ground. According to the current Vietnamese laws, coal deposits can be mined if air temperature does not exceed 30°C, although this rule is not always observed, especially during summer. This article analyses the impact of air parameters on the climatic conditions in headings and the use of the air temperature reduction method in selected underground mines in Vietnam.

1. Introduction

Working conditions in underground mines have their specific characteristics differing from opencast mines. Underground mines are primarily characterised by working sites scattered across a large area and human-unfriendly working environment. In addition to technical hazards arising from technological processes, there are also natural threats related to the rock mass surrounding the headings (water, gas, gas and rock ejections, gas and dust explosions, rock bursts, and climatic hazards).

In underground headings there are natural and technological sources of heat reaching the flowing air. This results in high temperatures in the headings, which, in combination with high humidity, leads to a considerable deterioration of climatic conditions. These cause a decline in bodily functions, having a negative impact on perception, concentration, and attention, and causing fatigue. This unfavourable impact of temperature and humidity on the human body is referred to as 'climatic hazard'.

In underground mining, climate is determined by the physical parameters of the air and the environment, such as the chemical composition of air, temperature, humidity, air velocity and the average radiation temperature of the heading's walls. This article analyses and assesses the impact of temperature, humidity and air velocity on the climatic conditions in the headings of selected Vietnamese mines.

* Corresponding author: truongtienquan@gmail.com

2. Microclimate parameters in underground hard coal mines in Vietnam

In Vietnam hard coal is found mainly in the northern part of the country, in the regions Quang Ninh, Thai Nguyen, Bac Kan, North Path, Nong Son, Ba River, Da River, Ca River and Nghe Tinh, marked in Fig. 1.

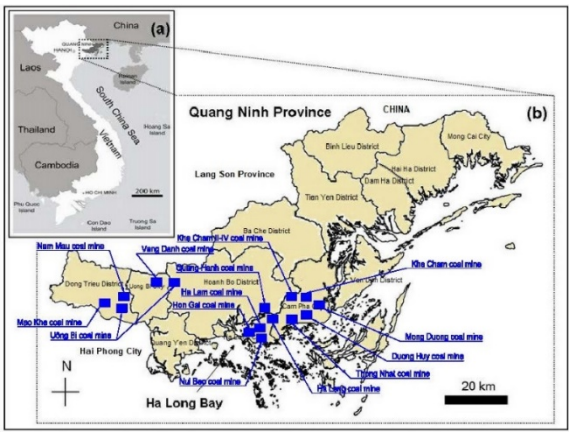

Fig. 1. Vietnamese coal mining districts [1]

Fig. 2. Underground hard coal mines in the Quang Ninh Coal Mining District [1]

The largest hard coal mining district is located in the Quang Ninh province, in the north-eastern part of Vietnam (Fig. 2). Most coal mines in Vietnam belong to the Vietnam National Coal – Mineral Industries Holding Corporation Limited (VINACOMIN).

By the end of 2018 most VINACOMIN's underground mines had completed the mining of deposits over the sea level and began mining deposits found below sea level. The annual average production in these mines is around 1,500,000 Mg. Vietnamese underground mines are shallow mines which extract coal deposits up to 300 m below ground, e.g. Nui Beo, Ha Lam, Mao Khe and Khe Cham III. Deeper mines include Khe Cham II-IV, reaching 500 m below ground.

Now and in the next few years, VINACOMIN will accelerate the mechanisation of coal deposits mining by introducing roadheaders, self-propelled drilling rigs and rockbolt supports with sprayed concrete. Mechanisation will also be applied to longwall headings, where mechanised supports will be used, with wooden supports replaced with hydraulic props. In the Khe Cham, Khe Tam, Ha Lam, Mao Khe, Vang Danh and Nam Mau in which conditions of coal deposit accumulation are favourable, longwall shearers will be used and the system of transporting the excavated material with belt conveyors will be upgraded.

2.1 Air velocity in headings

Vietnamese underground mines use a ventilation system based on main ventilation fans, the so-called central suction system. In addition, in extraction areas supplementary fans are used.

Software used for modelling air flow through mining headings, which are highly scattered, with an irregular network of headings due to their complex geological structure includes such programs as Kazamaru, Ventgraph and Ventsim.

In Vietnam, mining operations are governed by Regulation No. 03/2011/TT-BCT of the Ministry of Industry and Trade, according to which the air velocity in the wall and heading faces cannot be less than 0.25 m/s. In mines with methane hazard categories III and IV air current speed cannot be below 0.5 m/s (in faces with an 15° incline or coal deposits thicker than 2 m as well as face headings with a length up to 100 m). Air velocity cannot exceed: 4 m/s in coal excavations, 8 m/s for tunnel headings, 10 m/s – for air crossings, 12 m/s in shafts and fore-shafts while transporting people and 15 m/s in air ducts. Table 1 presents the volumetric air stream and its velocity in selected underground mines in Vietnam.

Table 1. Examples of air velocity and volumetric air delivery in selected mines in Vietnam

No.	Heading name	Volumetric air stream [m^3/s]	Cross-sectional area of the heading [m^2]	Air velocity [m/s]
A	**Ha Lam mine**			
1	Wall -150 / -160, zone III, coalbed 11	6.9	5.2	1.33
2	Wall 10-2, zone III, coalbed 10	6.0	5.1	1.18
3	Wall CGH 7-2.1	27.0	8.5	3.18
B	**Vang Danh mine**			
1	Bottom gate of wall CII-8-3, coalbed 8, Canh Ga zone	4.6	4.5	1.02
2	Air-heading of wall CII-8A-2, coalbed 8A, Canh Ga zone	5.4	4.8	1.13
3	Air-heading level +106, coalbed 6, Gieng Vang Danh zone	13.2	5.5	2.40
C	**Thong Nhat mine**			
1	Bottom gate of wall KT7	6.7	4.8	1.40
2	Air-heading of wall KT8	11.0	8.5	1.29
3	Bottom gate of wall KT9	2.3	5.7	0.40

Ventilation in underground mines in Vietnam must meet the requirements of the above mentioned regulation regarding air flow and velocity in headings.

2.2 Air temperature and humidity

Air temperature in mine headings depends on the temperature of fresh air supplied from the surface, rock mass temperature, ventilation intensity, mining depth, chemical reactions taking place in the rock mass and other factors caused by people or machines working, and blasting works. In line with Vietnamese regulations (03/2011/TT-BCT), air temperature at the working site cannot exceed 30°C. In underground mines in Vietnam in most cases air temperature is maintained at the level meeting the above standards. However, during summer, when the external air temperature exceeds 35°C, hot air is supplied to the working site through the ventilation system, resulting in air temperature higher than 30°C. In addition, increases in air temperature in headings are caused by technological sources of heat and the operation of mining machines. Another factor contributing to the decline of climatic

conditions is air humidity, which often exceeds 85%. Table 2 presents air temperature and relative humidity values in selected Vietnamese mines.

Table 2. Air temperature and humidity in selected headings of underground mines in Vietnam

No.	Heading name	Air parameters	
		Temperature [ºC]	Relative humidity [%]
A	**Mao Khe mine**		
1	Air-heading, level -80, coalbed 8	29.0	83
2	Carrying gangway, level -80 of wall I, coalbed 8, east	30.6	87
B	**Vang Danh mine**		
1	Carrying cross-heading, level -50 F11-F12, zone II - Gieng Canh Ga	28.9	88
2	Carrying gangway, level +60 of wall CIII-8A-2 - Gieng Vang Danh	28.0	88
C	**Nam Mau mine**		
1	Air-heading of wall I-9-5	29.5	94
D	**Ha Lam mine**		
1	Carrying inclined drift of wall CGH 7-2-2	31.0	93
E	**Thong Nhat mine**		
1	Cross-heading, level +18	29.9	94
2	Carrying gangway, level +8, PV4C	29.2	93
F	**Ha Long mine**		
1	Roadway -50 - V11B -CB Cam Thanh	28.6	88
2	Wall -20/+40 V11B -Cam Thanh	28.8	88
G	**Khe Cham mine**		
1	Carrying gangway of wall 14.5.2.A, coalbed 14.5	28.5	75
2	Air-heading, level -152 of wall 14.5.3.1, coalbed 14.5	29.0	82

As demonstrated in Table 2, air temperature above 30ºC is found in several headings of the Ha Lam and Mao Khe mines, in which a mechanised complex was used for extracting coal from walls. This equipment has high electric power and emits a lot of heat to the ambient air. In order to lower the air temperature in the heading of Vietnamese mines ventilation tools are used, which often are not able to sufficiently lower the temperature at working sites.

3. Air temperature lowering options in underground hard coal mines

In order to improve climatic conditions in underground headings, mining companies mainly use traditional methods of headings ventilation, with artificial air cooling methods being used in selected mines and operating areas. The traditional methods of improving climatic conditions in mines are such that do not require cooling equipment. Effective ventilation of headings may improve climatic conditions, taking the following into account [2, 3, 4]:

- limiting fresh air humidification in downcast shafts and at the upper levels,
- simplification of the ventilation network and, consequently, directing a broader stream of fresh air to walls and driven headings,

- proper exposure and cutting of the deposit, shortening the air supply paths and spoil haulage,
- whenever possible, using dip or descending ventilation in extraction areas,
- performing preparatory works on the side where fresh air transported to longwall headings is available,
- selecting an optimum longwall heading ventilation system,
- tight insulation of cave-in goaves (limiting air flow through goaves),
- avoiding serial ventilation of longwall headings,
- locating the spoil haulage from the longwall in the used air current,
- proper design of heading length, especially of longwalls, to account for the ventilation system's efficiency.

With the rising extraction depth and production concentration, traditional methods of improving climatic conditions may prove insufficient. Thus, there is a necessity to use other methods involving the application of cooling devices. There are three tendencies in the mine air conditioning technology used to artificially lower air temperature at working sites through the use of local, group-based or central air conditioning [5].

Local air conditioning, the diagram of which is presented in Fig. 3, is used to cool air in one heading, in which several air coolers can operate arranged, e.g. in a series.

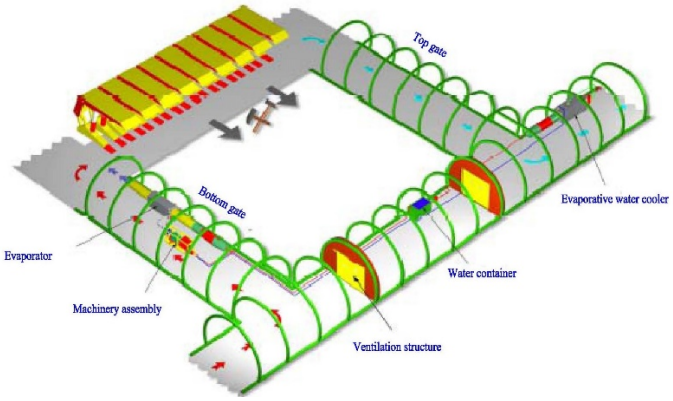

Fig. 3. Local air conditioning diagram [5]

Air conditioning equipment can operate in the indirect or direct system. These devices include an evaporator, which is an air cooler, combined with a machinery assembly consisting of an air-cooled condenser, an expansion valve and an air compressor. The evaporator and the condenser are connected with elastic wires to the coolant circulation. Direct action chillers cool the air stream with an evaporator located directly in the cooled air stream, while heat is collected from the condenser in an open or closed system with the use of technological water. Underground hard coal mines use local direct action chillers with a cooling capacity of 150-450 kW for the air conditioning of face works, driven roadways, cuts and longwalls [2, 5]. In the direct action air conditioning (cooling capacity of 300-900 kW), the evaporator cools the water pumped to the hydraulic air cooler placed in a given heading. The condenser is cooled in a similar way as in direct action systems.

If it is necessary to locate several air coolers in a heading or there is a need to cool the air on a large extraction area, stationary cooling aggregates are used instead of individual

devices. Cooling aggregates supply cold water to air coolers, which is called group air conditioning [5].

Group air conditioning systems (Fig. 4) make use of one or two cooling aggregates combined in a series. The total cooling capacity of the aggregates is from 1000 to 3000 kW. The aggregates are usually located near extraction areas, and the condensation heat is released through evaporative water coolers.

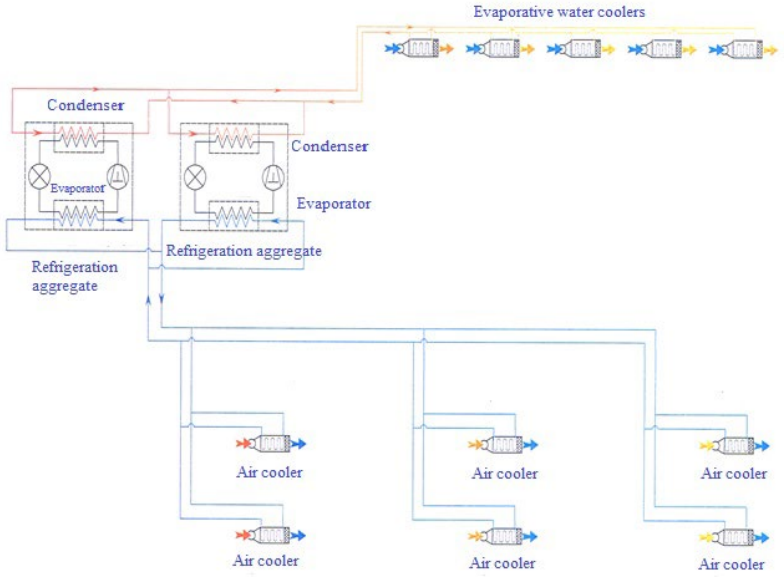

Fig. 4. Group air conditioning diagram [5]

Cooling aggregates, depending on the conditions in a given mine, are usually located near downcast shafts, from which cooled water is transported through isolated pipelines to regional air coolers [4]. In Polish mining, very often group air conditioning systems are used in combination with local air coolers.

In central air conditioning systems (Fig. 5) cooling aggregates with their cooling system can be located on the surface or under ground, or both. Central air conditioning systems use water cooling aggregates, with water pumped to local hydraulic air coolers. In Poland central air conditioning systems are used, for instance, in the Pniówek, Rudna, Budryk and KGHM mines.

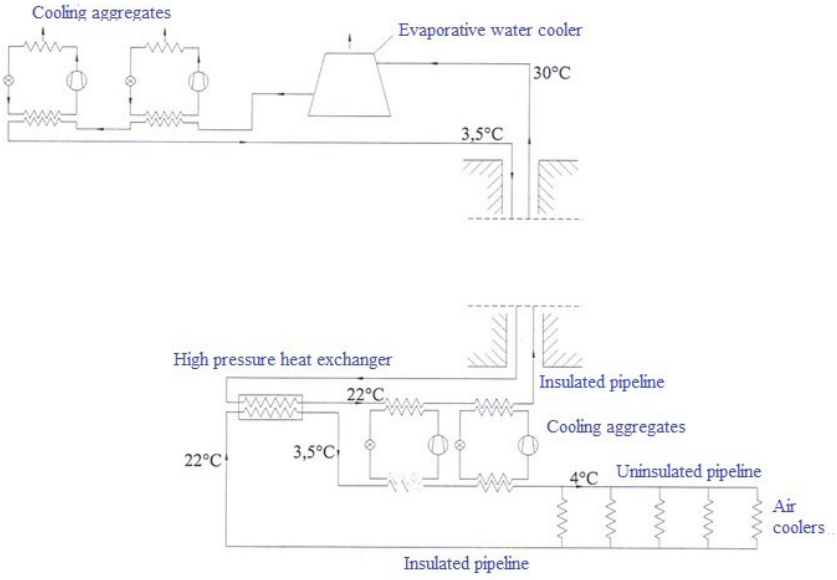

Fig. 5. Central air conditioning diagram [5]

4. Possibilities of applying local air conditioning in the Ha Lam mine in Vietnam

In longwall heading CGH 11-1.14, coalbed 11 in the Ha Lam mine temperature in the summer often exceeds 30°C (Table 3).

Table 3. The air temperature measures in wall 11-1.14 of the Ha Lam mine before installing a local air conditioning system.

Heading name		Months										
		February	March	April	May	June	July	August	September	October	November	December
Bottom gate CGH 11-1-14	°C	28.2	28.7	29	29.5	30.5	31.5	31.5	32	32	29.6	29.1
Wall CGH 11-1-14	°C	29.7	30	30.5	31	31.5	32.5	32.5	32.5	32.5	30.6	30.2
Top gate CGH 11-1-14	°C	30.3	30.7	31	32.5	32.2	33.8	33.5	33.5	33	31.9	30.6
Air stream	m^3/s	22.8	22.3	22.6	24.2	20.5	19.8	21.1	22.7	22.1	22.8	22.3
Surface air temperature	°C	24.2	28.8	32.9	35	36.2	34.8	35.2	32.6	28.6	26.5	24.6

In order to provide appropriate working conditions, in June 2016 a local air conditioning system was installed based on direct action coolers MK300 made in Poland. The air cooler made it possible to reduce air temperature in the heading to 29.4°C. Table 4 contains basic working parameters of the MK-300 cooling device.

Fig. 6 presents air temperature distribution at the surface and in wall CGH 11-1.14 before installing local air conditioning. As can be observed, wall air temperature is below 30°C only at the turn of February.

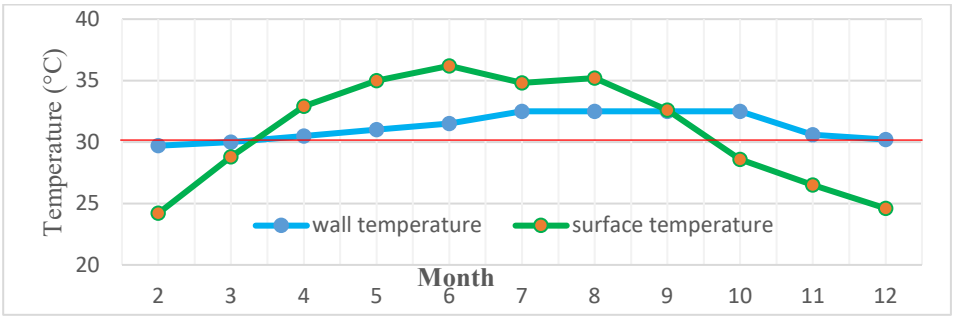

Fig. 6. Air temperature change diagram for wall CGH 11-1.14.

Table 4 contains catalogue data for MK-300 direct action cooler presented in Fig. 7 installed on wall CGH 11-1.14.

Table 4. Basic technical parameters of cooler MK-300 [6]

No.	Item	Parameter
1	Nominal cooling capacity	300 kW
2	Evaporation temperature	(0 ÷ 7°C) T_p = 3.3°C
3	Condensation temperature	(40 ÷ 48°C) T_k = 42°C
4	Volumetric air stream	V_l = 400 ÷ 6700 m^3/min
5	Air temperature at the evaporator inlet	T_{pi} = 31.0°C
6	Air temperature at the evaporator outlet	T_{Ao} = 19.0°C
7	Water temperature at the condenser inlet	T_{wi} = 27°C
8	Water temperature at the condenser outlet	T_{Wo} = 40°C
9	Volume of water cooling the condenser	V_w = 20.0 m^3/h
10	Roadway cooling area (from the evaporator outlet)	150 ÷ 200 m
11	Nominal cooling capacity of the condenser	450 kW

Fig. 6. The MK-300 air cooler used in the Ha Lam mine

5. Conclusions

Ventilation in underground mines in Vietnam meets the requirements regarding air flow and velocity in headings in line with the regulations of the Ministry of Industry and Trade. In line with the regulation, temperature at the working site in an underground mine should not exceed 30°C. In the summer however, in Vietnam external air temperature is high, exceeding 35°C. Also the operation of underground mining equipment and the progressing

automation of coal excavation (the use of mechanised complexes on walls) lead to unfavourable air temperature increases in underground headings.

In order to minimise the negative impact of climatic conditions on production in underground hard coal mines, ventilation methods are used, which do not always prove sufficient. For the purpose of lowering air temperature at working sites, Vietnamese mines have begun to use artificial air cooling in the form of direct action local air coolers.

In the Ha Lam mine, to reduce air temperature on wall 11-1.14, MK300 air coolers made in Poland were used with a nominal capacity of 300 kW. The application of an air compressor system made it possible to reduce the temperature to 29.4°C and thus improve climatic conditions in the heading.

References

1. B. Nguyen, Vietnam coal potential and development orientation, APEC Coal Supply Security Tokyo, Japan (2015).
2. R. Łuczak, Zwalczanie zagrożenia temperaturowego w wyrobiskach górniczych chłodziarkami powietrza bezpośredniego działania typoszeregu TS, Górnictwo i Geoinżynieria, Rok 34, Zeszyt 3/1, Kraków (2010).
3. J. Pawiński, J. Roszkowski, J. Strzemiński. Przewietrzanie kopalń, Śląskie Wydawnictwo Techniczne, Katowice (1995).
4. J. Wacławik, Wentylacja kopalń. Tom I i II, Wydawnictwo Uczelniane AGH, Kraków (2010).
5. P. Łuska, S. Nawrat, Klimatyzacja kopalń podziemnych. Systemy chłodnicze, AGH Uczelniane Wydawnictwa Naukowo-Dydaktyczne, Kraków (2008).
6. Proposing for the installation of the MK-300 experiment cooling device in the longwall 11-1.14 block III in the coal seam 11 in the Ha Lam mine, Quang Ninh, (2016). (Công ty than Hà Lầm, Phương án lắp đặt thiết bị làm mát MK-300 thử nghiệm tại lò chợ CGH 11-1.14 khu III- vỉa 11, 2016.)

Rational grinding circuit for siliceous apatite ore type III of Lao Cai Vietnam

Luan Pham VAN [1*], Phu Nguyen NGOC[1], Ha Le VIET[1]

[1] HUMG Hanoi University of Mining and Geology, Faculty of Mining, Hanoi, Vietnam

Abstract. Apatite ores type III of Lao Cai area, Vietnam is a class of weathered sileceous apatite ores, which may have most variable composition and primary slime content according to the weathering level and location. The three operating flotation plants use similar single-stage grinding circuits to process the highly weathered sileceous apatite ores and to achieve the concentrate grade requirement of 31% P2O5 with the aimed average recovery of about 70%. Single stage grinding circuits have worked well in the past as the designed criteria were achieved, however, mine production has increased sharply and deeper ores are being mined recently, so that the material composition of the run of mine ores have become more complicated and are the ores become more difficult to be floated. As a result, processing criteria of these plants become critically unstable and low. The study is to investigate the suitabity of two-stage grinding circuits for Lao Cai apatite ore type III. The report presents the results of the study on middlings regrinding of hard floatable apatite samples of Bac Nhac Son flotation plant, where high loss of valuable apatite has occured due to low grinding performance. Research results show that regrinding of all middlings to the fineness of 75% -0.04mm not only improves recovery but also help to stabilize technological operations and their processing criteria. The final concentrate grade of more than 31% P2O5, tailings content of less than 5% P2O5 and recovery of over 70% were achieved.

1. Introduction

Apatite is the main phosphate-baring mineral of the calcium phosphate group consisting of chlorapatite ($Ca_{10}(PO_4)_6(Cl)_2$), hydroxyapatite ($Ca_{10}(PO_4)_6(OH)_2$) and fluorapatite ($Ca_{10}(PO4)_6F$) [5]. It is used as the main raw material for the production of phosphorus and its compounds, which are widely used in the national economy. About 90% of the phosphorus demand goes to fertilizer industry while 10% remaining phosphorus demand goes to others such as metallurgy, chemical and paper industries, and animal feedstock [1; 2].

Vietnam apatite ore is a metamorphic sedimentary ore and it is classed into 4 basic types: Type I is the richest apatite ore of the weathered zones with P_2O_5 content of 28-37%; Type II is carbonaceous apatite ore of non-weathered zones with P_2O_5 content of 7-28%;

* Corresponding author: phamvanluan@humg.edu.vn

Class III is siliceous apatite ore of weathered zones with P_2O_5 content of 9-25%; Type IV is a mixed carbonaceous – siliceous ore type of non-weathered zones with a P_2O_5 content of 4-15%.

All existing apatite ore flotation plants of Vietnam were designed to process weathered apatite ores type III containing quartz as the main gangue minerals and to some extend minor dolomite. The flowsheets of existing apatite flotation plants necessarily include two-stage crushing with primary crushed ore washing in rotary washing drums for slime removal; single stage grinding of finely crushed ores down to 70-80% of -0,074 mm size fraction in ball mills; desliming by a combination of hydrocyclones and thickeners; conditioning agitation and direct flotation in conventional mechanical flotation machines. For flotation of apatite, fatty acids are commonly used as collectors, Sodium silicate as depressant of quartz and caustic or ash soda for modifying of pH to 8-9 [4; 5; 6].

Flotation circuits of the existing apatite flotation plants of Vietnam necessarily include a rougher operation, 2-3 cleaning and 1-2 scavenger operations, which allow to achieve concentrate grade of approximately 31% P_2O_5, recovery of about 70%, and tailings P_2O_5 content of 5%. The plants have been operated smoothly until recent years, however, current ROM ore supply to the processing plants has become more and more volatile in terms of both grade, ore characteristics and mineral composition. The general technology, including comminution-separation flowsheets and operating regimes, gradually becomes more unsuitable due to these changes. As a result, unstable processing criteria and huge loss of valuable apatite have occurred. The P_2O_5 contents in tailings of the processing plants sometimes reached 8-9% [3]. In order to overcome this situation, it is necessary to have researches on technology improvement for comminution-separation flowsheets, grinding regimes, flotation operating regimes and even processing equipment etc.

2. Samples and methods of the study

2.1 Samples

The study sample Q3 KT22, MC: 35 - 41, of 160-180 level, was collected from Bac Nhac Son (Lao Cai province) area of the most hardly floatable apatite ores type III. The amount of each sample taken to the laboratory was about 50kg, P_2O_5 content of samples MS1; MS4; MS5 and MS6 are about 8.5%; 18.5%; 13.5% and 17.5% respectively. The mineral composition of the samples is shown in Figure 1 and Table 1.

Table 1. The mineral composition of the samples

No	Mineral	Content, %			
		MS1	**MS4**	**MS5**	**MS6**
1	Clay, sericite, muscovite	27-30	20 - 22	63 - 64	35-37
2	Quartz	61-63	58 - 59	20 - 22	42- 45
3	Apatite	8-10	18 - 20	13 - 15	18-20
4	Iron hydroxide	1	1 - 2	1 - 2	1-2

The study samples consist mainly of apatite, quartz and clay minerals. Apatite mineral is in the form of microparticles and fine-grains. Fine grains of less than 0.01-0.05mm are either scattered or concentrated in group, in spots or thin strips stretched in a direction. Apatite is

colorless, high floating with stainy surfaces and gray interference. The lowest grade MS1 sample contains over 60% quartz minerals, MS5 sample contains over 60% clay minerals.

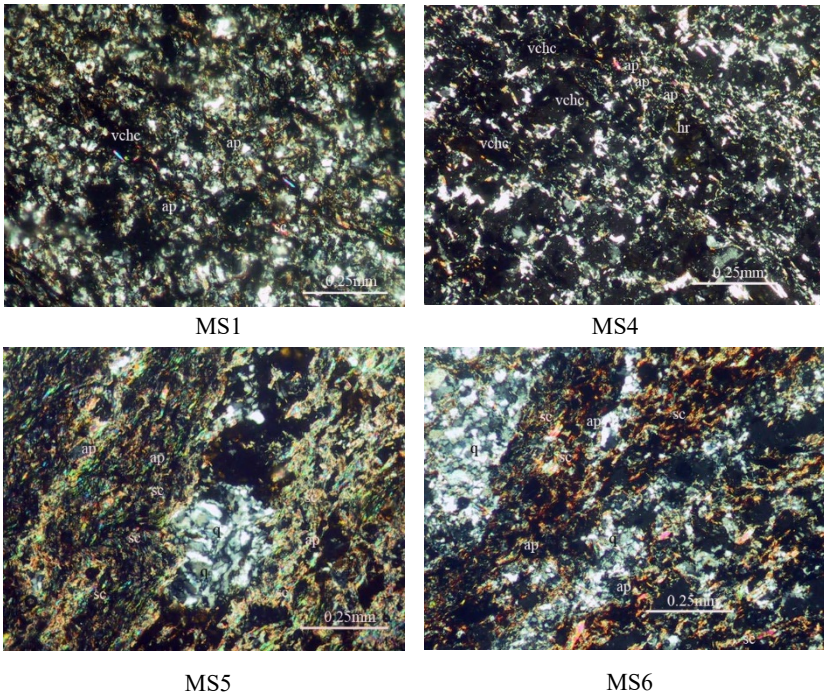

Fig1. Study sample images under microsope

2.2 Methods of the study

The experiments were conducted by the traditional methods i.e serial experiments starting with the exploration of the most important parameters. In each serial test, all conditions were kept unchanged except the explored parameter. The best explored parameter's values of the previous experiment were used for the following series of experiments.

Most tests were conducted at the Laboratory of the HUMG Department of Mineral Processing using mechanical laboratory flotation machines with chamber capacities of 1-3l. The ore samples were crushed down to -3 mm size and then ground in a ball mill of 8l chamber capacity to the required mesh of grind before feeding to the flotation test.

The flotation products were filtered, dried, weighed and prepaired for the final analysis. The efficiencies of each experiment were assessed through a number of technological criteria including actual recovery in concentrate and P_2O_5 contents in both concentrate and tailings.

3. Results and discussions

3.1Conditional experiments

Series of conditional experiments of each ore sample were conducted according to the Figure 2 and the optimal operating regimes were determined as shown in Table 2 and the flotation results at optimal regimes are shown in Tables 3.

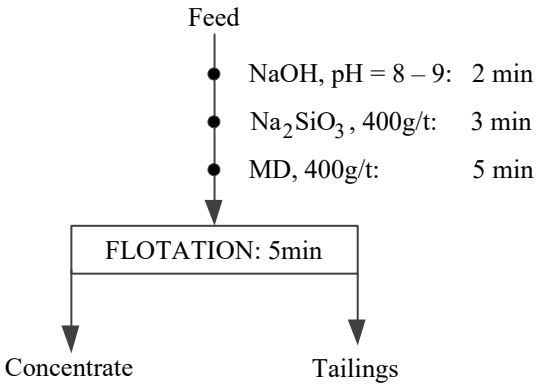

Fig 2. Conditional flotation test

Table 2. Optimal operating regimes of the samples

Operating variables/Sample	MS1	MS4	MS5	MS6
Mesh of grind, % of -0,074 mm	95.7	91.1	91.88	92.72
Solid concentration, g/l	300	300	300	300
NaOH dosage (pH = 8 - 9), g/t	800	800	800	800
Sodium silicate dosage, g/t	400	400	400	400
Collector MD, g/t	400	400	400	400

Table 3. Flotation results of the samples at optimal regimes

Sample	Product	Yield, %	P_2O_5 Content, %	P_2O_5 Recovery, %
MS1	Concentrate	50.24	15.72	93.13
	Tailings	49.76	1.17	6.87
	Feed	100	8.48	100
MS4	Concentrate	65.93	24.85	88.56
	Tailings	34.07	6.21	11.44
	Feed	100	18.5	100
MS5	Concentrate	58.99	20.03	87.78
	Tailings	41.01	4.01	12.22

	Feed	100	13.46	100
MS6	Concentrate	62.82	22.62	81.25
	Tailings	37.18	8.82	18.75
	Feed	100	17.49	100

From the experimental results, it can be seen that most of samples although of different mineral composition and P_2O_5 content, can be processed at similar flotation regimes; All samples require a grind fineness of over 90% of -0,074mm size fraction; Low grade ores (sample MS1) do not require scavenging operations as rougher tailings with P_2O_5 content of 1.17% are suitable for disposal.

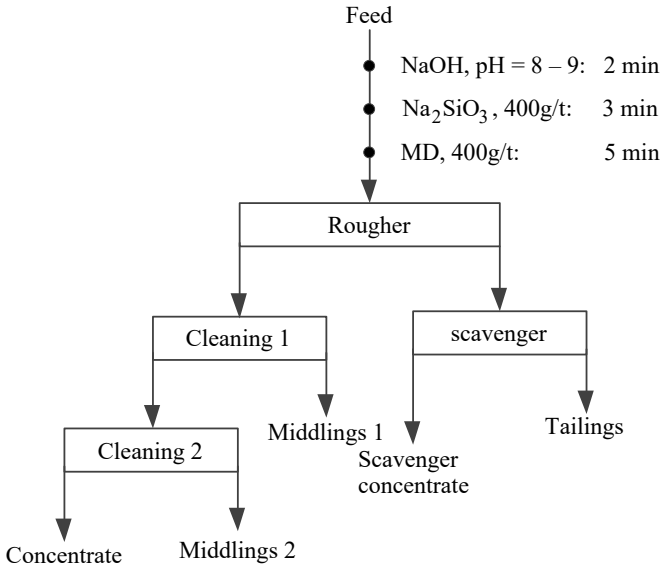

a

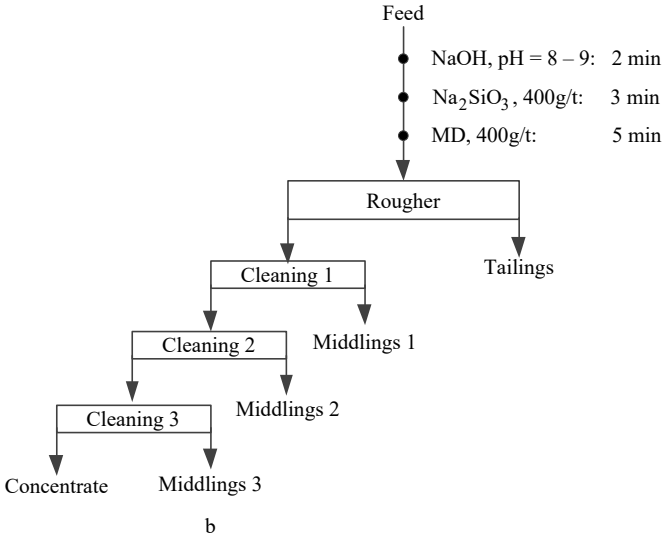

b

Fig 3. Single stage flotation circuit tests

3.2 Single stage flotaion circuit selection

Purpose of the study is to determine suitable number of cleaning and scavenging operations for achivement of the desired concentrate grade and recovery. The study has determined optimal flotation open circuits for the ore samples MS4; MS5 and MS6 as shown in Figure 3a, while for MS1 sample as shown in Figure 3b. Flotation results according to the selected open circuits are shown in Table 4.

From the results of open circuit flotation test results, it is found that low grade ores (MS1) require 3 cleaning operations to achieve the desired concentrate grade but no scavenging operation due to very low P2O5 content in rougher tailings; Flotation middlings of higher grade ore samples, as shown on the Figure 3a, require further treatment due to their very high P2O5 content and low recovery into concentrate.

Table 4. Results of single stage flotation open circuits

Sample	Product	Yield, %	P_2O_5 Content, %	P_2O_5 Recovery, %
MS1	Concentrate	18.5	31.78	69.66
	Tailings	47.92	1.87	10.62
	Middlings 1	18.35	2.11	4.59
	Middlings 2	10.6	7.02	8.82
	Middlings 3	4.63	11.5	6.31
	Feed	**100**	**8.44**	**100**
MS4	Concentrate	35.59	33.28	63.78
	Tailings	26.08	4.37	6.14
	Scavenger concentrate	3.55	13.58	2.6
	Middlings 1	23.06	11.57	14.37
	Middlings 2	11.72	20.77	13.11
	Feed	**100**	**18.57**	**100**
MS5	Concentrate	33.16	29.15	71.87
	Tailings	35.13	2.42	6.32
	Scavenger concentrate	4.85	7.43	2.68
	Middlings 1	16.32	7.19	8.72
	Middlings 2	10.54	13.28	10.41
	Feed	**100**	**13.45**	**100**
MS6	Concentrate	38.12	31.21	68.21
	Tailings	31.28	5.48	9.83
	Scavenger concentrate	5.69	9.31	3.04

	Middlings 1	17.26	11.56	11.44
	Middlings 2	7.65	17.05	7.48
	Feed	**100**	**17.44**	**100**

3.3 Middling treatment selection experiments

Purpose of this study is to determine suitable middlings treatment flowsheets in order to maintain the desired concentrate grade and recovery with minimal loss of value to tailings. At the existing flotation plants, all middlings are returned to rougher operations for further recovery of values to concentrates. Returns of middlings to rougher operations not only increase circulating loads or pulp volumes but also cause rougher flotation disturbances leading to lower processing criteria such as lower concentrate grade and recovery. According to some previous studies, with hard-floatable apatite ore type 3, most middlings particles often are floated well at the rougher stage but badly floated at the cleaning stages due to the locking effect of values with gangue minerals [3]. Therefore, in this study, regrinding of middlings and different flotation circuits were subjects of considerations for improvement of the processing criteria.

Flotation circuit for both case with and without middlings grinding is shown in Figure 4 and results are given in Table 5. From experiments, it was determined that -0.04mm size fraction content in middlings before regrinding and after regrinding of middlings were of about 50% and 75% respectively.

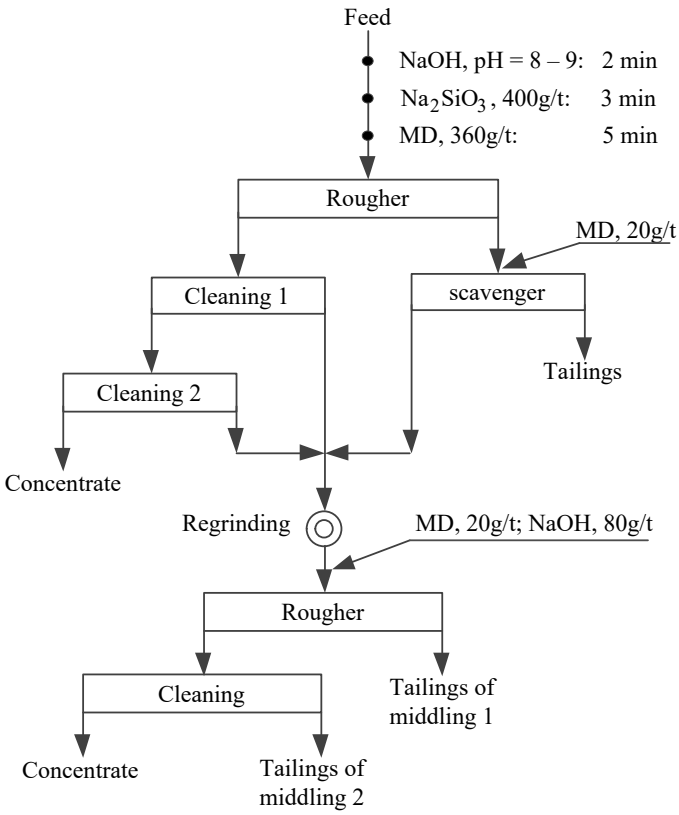

Fig 4. Two stage flotation circuit test

Experimental results in Table 5 show that regrinding of middlings improved the separation efficiency because of better apatite liberation: overall recovery of the samples MS4 and MS5 increased by 6%; and MS6 by 4% while concentrate grades were almost equivalent to conventional single stage flotation. However as per Table 5, high P_2O_5 contents in tailings of middlings flotation (tailings of middlings 1 and 2 in Figure 4), especially high in tailings of the rich samples MS4 and MS6, were due to absence of scavenging flotation of these tailings. This indicates that actual middlings flotation circuits should include a scavenging operation and a return of cleaning tailings to the rougher operation.

Table 5. Flotation results with and without middlings regrinding

Sample	**Product**	**Without regrinding of middlings**			**With regrinding of middlings**		
		Yield, %	**% P_2O_5**	**Recovery, %**	**Yield, %**	**% P_2O_5**	**Recovery, %**
MS4	Concentrate	35.58	33.27	64.19	35.05	33.42	63.35
	Middlings concentrate	1.65	26.77	2.4	6.17	27.73	9.25
	Total of concentrate	**37.23**	**32.98**	**66.59**	**41.22**	**32.57**	**72.6**

	Tailings	26.82	4.74	6.89	26.52	4.66	6.68
	Tailings of middling 1	8.2	10.58	4.7	20.94	11.17	12.65
	Tailings of middlings 2	27.75	14.5	21.82	11.32	13.18	8.07
	Feed	**100**	**18.44**	**100**	**100**	**18.49**	**100**
MS5	Concentrate	27.97	32.57	68.49	28.04	32.61	67.29
	Middlings concentrate	3.11	27.45	6.42	7.3	26.55	14.26
	Total of concentrate	**31.08**	**32.06**	**74.91**	**35.34**	**31.36**	**81.55**
	Tailings	36.77	2.49	6.88	36.13	2.47	6.57
	Tailings of middling 1	27.66	7.63	15.87	22.73	5.28	8.83
	Tailings of middlings 2	4.49	6.92	2.34	5.8	7.15	3.05
	Feed	**100**	**13.3**	**100**	**100**	**13.59**	**100**
MS6	Concentrate	34.61	32.05	62.78	34.73	32.05	62.71
	Middlings concentrate	0.52	25.86	0.76	3.49	25.12	4.94
	Total of concentrate	**35.13**	**31.96**	**63.54**	**38.22**	**31.42**	**67.65**
	Tailings	32.02	5.27	9.55	31.9	5.26	9.45
	Tailings of middling 1	23.89	14.18	19.17	22.3	13.1	16.46
	Tailings of middlings 2	8.96	15.26	7.74	7.58	15.07	6.44
	Feed	**100**	**17.67**	**100**	**100**	**17.75**	**100**

Conclusions

From the study results of some hard-floatable apatite ore type III from Bac Nhac Son area, Lao Cai, some conclusions can be made as the followings:

1. Mineral composition of apatite ore type III samples of Bac Nhac Son area includes apatite, quartz, clays, sericite. However, apatite is finely disseminated in quartz that is the main cause of low efficiency;
2. Lowgrade ores such as MS1, it should be floated in open-circuits in order to obtain concentrate of the required quality, middlings and tailings can be disposed without retreatment;
3. Recovery of flotation circuits with middlings regrinding generally increase recovery of P_2O_5 to above 72% while overall concentrate grade . So it is obvious that middlings regrinding of finely disseminated and high grade ores is more rational. Middlings regrinding and its floation may give more stable processing criteria due to absense of rougher operation disturbances, lower circulating loads and assured

flotation time. Besides, two stage grinding remarkedly reduces slime generation and reduce energy consumption compare to the existing single stage grinding;

4. It is necessary to continue studying on optimizing mesh of grind of grinding stages and middlings flotation circuits in order to reduce energy consumption, to improve the processing criteria. Further studies should develops most suitable flowsheets and floation regimes for hardly floatable apatite ores type III for coping with recent changes in the ROM ore supply to processing plants.

References

1. FAO, *Use of phosphate rocks for sustainable agriculture* (2004)
2. Jessica Elzea Kogel, *Industrial minerals & rocks : commodities, markets, and uses* (Society for Mining Metallurgy and Exploration, 2006)
3. Pham Van Luan, Mining Industry Journal, **5**,13-16, 2017
4. R. C. Santana , C. R. Duarte , C. H. Ataíde & M. A. S. Barrozo, Separation Science and Technology, **46**,1511–1518, 2011
5. S. Komar Kawatra and J.T. Carlson, *Beneficiation of phosphate ore* (Society for Mining Metallurgy and Exploration, 2014)
6. Srdjan M. Bulatovic, *Handbook of flotation reagents. Volume 3 _ chemistry, theory and practice _ flotation of industrial minerals* (Elsevier, 2015)

Choice of powered roof support FAZOS-15/31-POz for Vang Danh hard coal mine

Krzysztof SKRZYPKOWSKI[1] Waldemar KORZENIOWSKI[1] and Trung Nguyen DUC[2]

[1]AGH University of Science and Technology, Faculty of Geology Geophysics and Environment, Krakow, Poland
[2] Institute of Mining Science and Technology, Hanoi, Vietnam, (PhD student at AGH)

[1] Corresponding author: skrzypko@agh.edu.pl

Abstract. The article presents the choice of a Polish powered roof support from FAMUR Group for the conditions of one of the hard coal mines in Vietnam. In the analytical calculations, the strength and structural parameters of the rock mass from the Vang Danh mine region were adopted. The longwall face is 93 m long and the thickness of the coal layer is equal 3 m. For the needs of the choice of support, the load of the longwall face determined and the capacity of the powered roof support were determined. On the basis of the permissible roof deflection method, the condition of excavation maintenance was characterized. In the calculations, it was assumed that the condition of using a powered roof support type FAZOS-15/31-POz, except in addition to complying of the working range and permissible value of longwall face inclination, is to ensure proper roof maintenance conditions, which are determined by the index of load capacity of the roof „g".

1 Introduction

The main task of the support is to protect the working space in the operating front. By supporting the working space it is understood to prevent the fall of roof rocks into the excavation face and take over a dynamic loads. In order to fulfilled the tasks of support , it is necessary to check the possibility of using a given type of support in specific geological and mining conditions [5]. Due to the possibility of using the knowledge of support loads to better understand the phenomena occurring around it, programs recording the work parameters of complete longwall mining systems were created [3, 7]. In an underground hard coal mines mining complex consists of shearer loader, armoured face conveyor and powered rood support that determines the safety and efficiency level of the mining process [17]. One of the decisive factors affecting on the correct choice of powered support is the cooperation between the base of the support and the floor of longwall face [6]. For longwall panel with caving, the roof rocks fall by gravity causing the filling of post-mining area. In underground excavations the compressibility of filling materials play a special role preventing, e.g. decreasing the surface and allow to manage the waste [13,14]. Very often mining supports cooperate with different types of reinforcement. In terms of rock mass prones to tremors, mining support should be adopted to energy – absorbing [11,12]. Correct selection of the load-bearing capacity of the supporting section to the size of the loads from the rock mass is not a guarantee of ensuring the stability of the longwall face. This is due to the fact that the possibility of creating in the longwall face with the maintenance of the roof, very often decides other reasons, for example, irregularities in the construction of the powered roof support or to use them [8]. The main factors affecting the choice of mechanized support were presented in the table 1. The general criterion on the basis of which the most often selected is the powered roof support in the mine is the compliance of the scope of its operation with the planned exploitation height [18]. Lack of detailed calculations of the load of the support and its capacity, as well as resistance to dynamic loads, may lead to a series of undesired events, for example the fall of roof rocks, clamping the support or its damage [15]. The phenomenon of loading a mining support with the weight of rocks may occur in the case of roofs with very low strength or in which there are completely damaged rocks. The behavior of the excavation support at such a load depends on the weight value of rock masses. The static load value lower than the load capacity (load capacity) does not cause dynamic phenomena. Only exceeding the operating values leads to clamping the support, which results from the operation of the protections. In a mechanized support, this is to open the outflow from the under-piston space of the stands through a working or pressure valve and to clamp the sections. If the load remains above the working load, the support is completely closed with all overloading consequences. In order not to allow such

a situation, it should be paid special attention to the selection of support and methods of protection. The mentioned two cases of behavior of a longwall face support can be presented by the relation [16]:

$$Q_i \cdot b < F_{zr} \rightarrow V = 0 \quad (1)$$
$$Q_i \cdot b > F_{zr} \rightarrow V > 0 \quad (2)$$

where:
Q_i – static load of a longwall face, $[N \cdot m^{-1}]$,
b – Centre sparing of powered roof support, [m],
F_{zr} – roof support capacity, [N],
V – velocity camping of powered roof support, $[m \cdot s^{-1}]$.

Table 1. Factors affecting on the choice of powered roof support

Geological	Production	Equipment
Coal seam thickness (thinning and thickening) and inclination	Length of face	Minimum and maximum working height of powered roof support
Faults (throw and inclination angle)	Length along the strike	Canopy load distribution
Depth of exploitation	Reserve of coal	Support yield ratio over the lift of the panel and set to yield ratio
In situ stress	Extraction height	Harmony between powered roof support and armoured face conveyor
Natural hazards (mainly: water, tremors)	Upper and lower mineable seams	Overall dimensions of support in transport position
Caving behaviour	Rate of face advance and production capacity	Mass of powered roof support
Strengh, deformation and structural properties of coal seam and surrounding rocks	Ratio of face to top coal	Possibility of remote control and monitoring

2 Stages of rock mass behavior loading in the longwall face

The relaxed rock mass can be divided into two parts (Fig. 1). The lower part is the immediate roof, which forms the most cracked layers and creates a chaotic rubble rocks in the goaf. The upper part is formed by the main roof, consisting of strongly fractured rocks, they retain the form of geometrical continuity in the goaf [16]. In the overlying rock layers above the relaxed rock mass, which can be described as a disturbed rock mass, as a result of the deflection of the layers during coal seam mining, cracks are also formed. The frequency of these cracks is less frequent than in a relaxed rock mass and they do not lose their geometrical continuity during settlement. This process takes much longer and is delayed compared to the layers of the relaxed roof. The phases of behavior of the rock mass follow one another and are connected with the increasing run along the strike of longwall face. In these phases there are differences related to the course of phenomena occurring in the roof of the longwall. A longwall face start-up phase can be distinguished. In the roof, blocks of rock are formed, which can fall freely. The impact of the support on the support in this period is negligible in relation to natural factors occurring in the longwall face. The next phase is the phase of incomplete caving, in which the goafs are already filled. The rubble rock is not yet tight and does not give proper support in relation to the rock layers that load the longwall face. Roof support capacity should cause mutual disintegration of the rock blocks between them in the roof of the longwall face. In the case of insufficient capacity of the support in the excavation, there may be signs of strong rock mass pressure. The last phase of a full caving occurs as the longwall runs progress, in the case of roofs that are prone to collapse. During the full creation of the caving, his zone achieves the largest possible range. Layers composed of rock blocks, over a longwall face and in the above-lying rock mass, obtain carrying capacity when the close contact of blocks is created. It results from the resistance of layers on one side to rubble rock caving and on the other hand to the boundary surface of the relaxed rock mass. The mechanized support is designed to help keep rock blocks contact by supporting them [1].

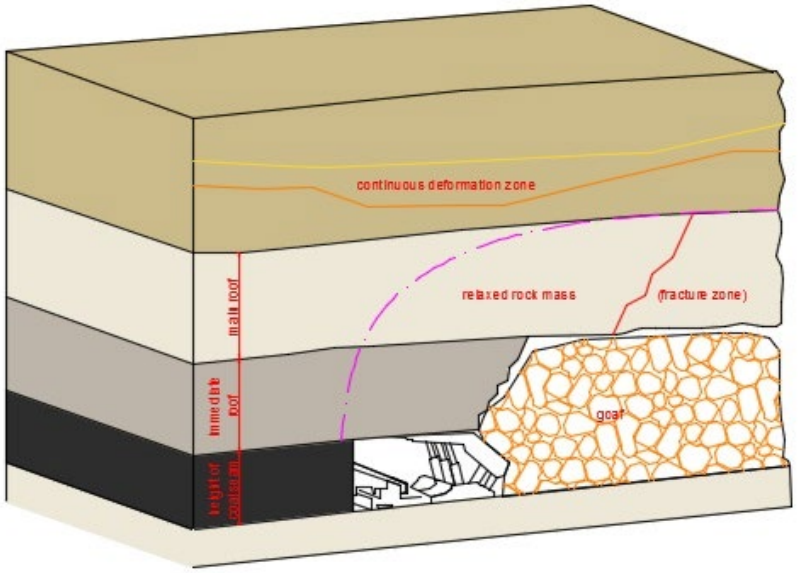

Fig. 1. Scheme of relaxed rock mass around longwall face with caving

3 Geological and mining within the mining area

Strength and structural parameters of coal and surrounding rocks were determined on the basis of boreholes no. LK.64 and LK.401 (Fig. 2). The average value of compressive strength for coal seam is equal 25 MPa. The depth of designed exploitation is equal 320 m. Immediate roof is built from siltstone, with varying thickness from 18.5m to 25m. Sometimes immediate roof is argillit glass format, with thickness from 0.2m to 0.6m. Compressive strength varies from 8 MPa to 163 MPa, (the average value is equal 45 MPa). Main roof is built from gritstone, with varying thickness from 9.3m to 14.3m. Compressive strength varies from 15 ÷ 272 MPa, (the average value is equal 70 MPa). Immediate floor is built from siltstone evenly distributed, sometimes is built from argillite. Compressive strength varies from 5 to 70 MPa, (the average value is equal 30 MPa).

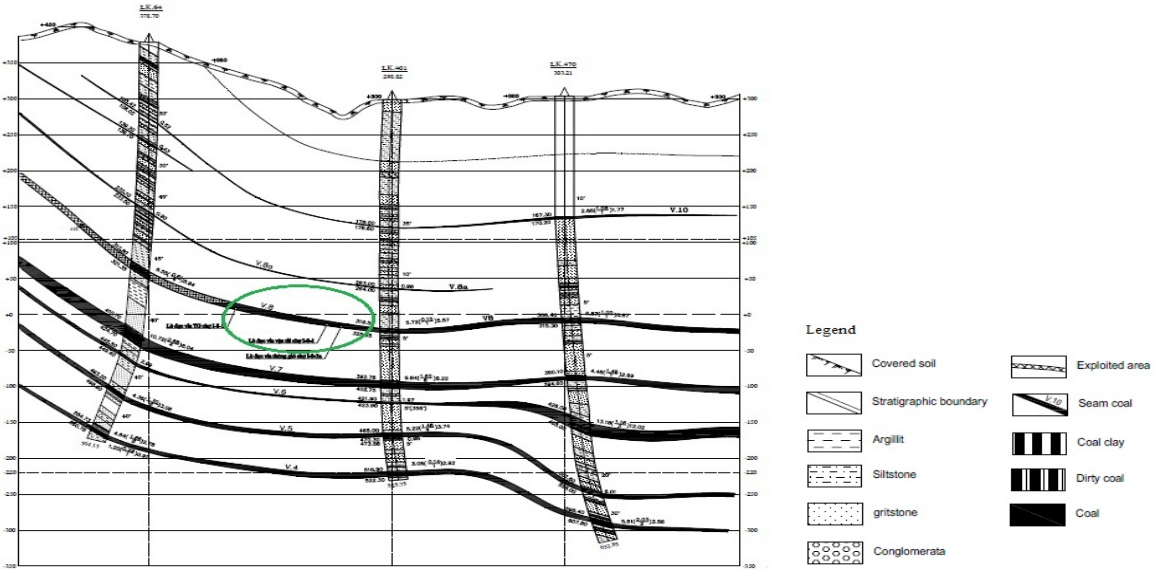

Fig. 2. Geological cross section through the boreholes

4 Geological and mining within the mining area Choice of powered roof support

The length of longwall face will have 93m and the length along the strike will have 355m. Designed longwall faces belong to coal seam no 8 and applies to the level from -20 to 0. The thickness of coal seams varies from 5.19m to 5.91m, (the average value is equal 5.54m). The height of first layer will be equal 3m. The inclination of coal seam varies from 5° to 15° (the average value is equal 11°). Coal seam has up to 2 clamping stones layers with a total thickness up to 0.5m (the clamping stones component is mainly clay). Coal seam will be divided into two layers. Within geological and mining conditions, powered roof support, type: FAZOS-15/31-POz (Fig. 3) was chosen [2]. The basic technical specifications of this support for the working conditions in the Vang Danh hard coal mine are shown in Table 2.

Table 2. Technical specifications of powered roof support FAZOS-15/31-POz

Feature	Value
Support height [m]	1.5 – 3.17
Operational height range (no burst of coal seam) [m]	1.7 – 3.0
Operational height range (coal seam prones to burst) [m]	1.8 – 3.0
Centre spacing [m]	1.5
Longitudinal inclination [°]	up to 35
Transverse inclination [°]	± 15°
Roof support advance [m]	up to 0.8
Number of hydrualic legs [-]	2
Diameter of leg [m]	0.2
Leg support capacity: setting load [MN]	0.785
Leg support capacity: yield load [MN]	1.508
Supply pressure [MPa]	25.0
Roof support capacity [MPa]	48.0

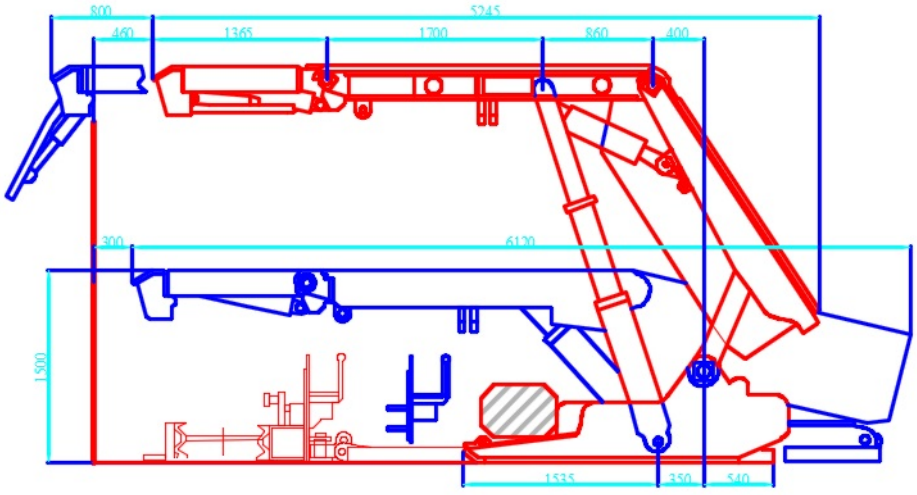

Fig. 3. Powered roof support FAZOS-15/31-POz

4.1 Load of the longwall face for the purpose of selecting the powered roof support [based on 4, 9-10]

The load of a longwall face, when the mechanized support is selected, is expressed by the value of the load moment of the M_Q which is the product of the load value of the excavation and its operating arm. For caving longwall faces with high compressive strength, it is calculated from the dependence:

$$M_Q = \frac{n_Q \cdot n_u \cdot a_p \cdot h_s}{\left(\frac{47,1}{R_c}+0,184\right)^2 \cdot (0,0025R_c+0,5)^{1,5}}, \text{ [MNm]} \quad (3)$$

where:

n_Q – coefficient of load intensities, [-],

$$n_Q = 1 \text{ for } 0.3 \leq \frac{q}{R_{cz}} \leq 0.5 \quad (4)$$

$$n_Q = \frac{q}{R_{cz}} = \frac{8}{25} = 0.32 \quad (5)$$

q – rock mass pressure, [MPa],
R_{cz} – compressive strength of coal in the seam, (R_{cz} = 25)[MPa],
n_u - coefficient of inclination, (n_u = 1, for inclination less than 20°), [°],
a_p - coefficient of periodic pressure, [-],

$$a_p = a_{p1} \cdot a_{p2} \quad (6)$$

$$a_p = 0.508 \cdot 1.44 = 0.73 \quad (7)$$

a_{p1} – coefficient taking into account the influence of suspended over goaf by rigid layers forming the solid roof rock mass for Rc ≥ 40 MPa,

$$a_{p1} = \frac{1}{\frac{25}{R_c - 40} + 0.3} + 1 \quad (8)$$

$$a_{p1} = 0.508$$

a_{p2} – coefficient taking into account the influence of suspended over goaf by rigid layers with a thickness greater than $3h_s$, lying above the solid roof rock mass up to a distance of $10h_s$ from the roof of the longwall face,

$$a_{p2} = -0.04 \cdot \left(\frac{h_b}{h_s}\right)^2 + 0.4 \cdot \frac{h_b}{h_s} + 1 \quad (9)$$

$$a_{p2} = 1.44$$

where:
h_s – reduced height of longwall face, [m],

$$h_s = 0.8 \cdot H, [m] \quad (10)$$

H – height of longwall face, [m]
R_c – a real roof compressive strength, determined of the basis of in situ tests in a given field of exploitation, (Rc = 55), [MPa],
h_b – in the calculations it was assumed that h_b = 3, [m],

$$M_Q = \frac{1 \cdot 1 \cdot 0{,}73 \cdot 2{,}4}{\left(\frac{47{,}1}{55} + 0{,}184\right)^2 \cdot (0{,}0025 \cdot 55 + 0{,}5)^{1{,}5}} = 3.181 \text{ [MNm]} \quad (11)$$

4.2 Determination of roof support capacity [based on 4, 9-10]

The average roof support capacity (Pz) in the longwall face should be calculated for the least favorable case, i.e. for the length of face in which the support is moved. In the ongoing course of reasoning, application to the moment of load of the face, the supportive moment of the mechanized support in the excavation is used, this value is determined by the dependence:

$$M_P = P_Z \cdot l_z, [MNm/m], \quad (12)$$

where:
l_z - the operating arm of the support force of the powered roof support, (l_z = 4), [m],
P_z – average roof support capacity in a given longwall face, dteremined in MN per 1m section of face, perpendicular to the longwall front, calculated from the dependence:

$$P_Z = \frac{i \cdot n_k \cdot n_w \cdot P_r}{3 \cdot b} \left[\frac{(1 - n_o) \cdot (d_{02} - d_{01})}{\frac{100 \cdot e^{-3{,}5 \cdot e^{-8 \cdot n_{cz}}}}{Z_{śr}} + \left(1 + e^{-1{,}8 \cdot e^{-2 \cdot n_{cz}}}\right)} + 2 \cdot n_m \cdot n_o \right], [MN] \quad (13)$$

where:
i – number of hydraulic legs, [-],
n_k - the reduction factor of the leg's capacity, taking into account its deviationin relation to the perpendicular to the base, (n_k = 1),
n_w - the transfer coefficient of the capacity of support to the roof of the face, dependent from the support span, for caving faces:

$$n_w = 1 - 0{,}4 \cdot e^{-7 \cdot e^{-0.5 \cdot L_w}} \quad (14)$$

$$n_w = 1 - 0{,}4 \cdot 2.71^{-7 \cdot 2.71^{-0{,}5 \cdot 4.70}} = 0.79 \quad (15)$$

where:
L_w - the sum of the roof length of support, the width of the "path" at the face of the longwall and the cut depth of shearer loader, ($L_w = 4.70$), [m],
P_r - leg support capacity: yield load [MN],
b - centre spacing, counted along the longwall face, [m],
n_o - value of the setting to yielding load ratio in the hydraulic legs, [-],,
n_m – coefficient of impact of floor strength ($n_m = 1$),
n_{cz} – coefficient of work of powered roof support ($n_{cz} = 1$),
d_{01} - the distance of the support leg from the face of the longwall, counted on the roof, before the start of mining, ($d_{01} = 3.3$) [m],
d_{02} - the distance of the support leg from the face of the longwall, counted on the roof, after completion of mining, ($d_{02} = 4.1$) [m],
$Z_{śr}$ - the average clamping value of the excavation over its span, equal to $d_{02} - d_{01}$, ($Z_{śr} = 9.44$), [mm].

$$P_Z = \frac{2 \cdot 1 \cdot 0.79 \cdot 1.508}{3 \cdot 1.5}\left[\frac{(1-0.52)\cdot(4.1-3.3)}{\frac{100 \cdot 2.71^{-3.5 \cdot 2.71^{-8 \cdot 1}}}{9.44} + \left(1+2.71^{-1{,}8 \cdot 2.71^{-2 \cdot 1}}\right)} + 2 \cdot 1 \cdot 0{,}52\right] = 0.57 \text{ [MN]} \quad (16)$$

$$M_P = P_Z \cdot l_z = 0.57 \cdot 4 = 2.28 \text{ [MNm/m]} \quad (17)$$

4.3 Determination the state of maintenance of the roof in the longwall face with caving

The method of determination the maintenance of the excavation depending on the load-bearing capacity of the longwall face support in the system with caving is based on the permissible deflection of the excavation roof and allows also determine the correct range of support [4]. In the method of this calculation, the size of the load index of "g" roof layers is subject to the ability to maintain their geometrical continuity over the excavation. The value of the load index of the roof layers depends on the average size of convergence calculated along the length of the excavation and depends on the relation of the support's capacity to the excavation load. Capacity of the support and the load of the excavation depends on natural factors, ie on the construction and properties of the rock mass, but also on technical factors resulting from human activity. The roof capacity index is calculated from the formula:

$$g = \frac{1}{\frac{Z_{L1}}{Z_g} + 0{,}3} \quad (18)$$

where:
Z_{L1} - inclination of the roof occurring on the first meter of the excavation span measured in mm subsidence, per 1m of the roof span,

$$Z_{L1} = \frac{1}{0{,}012 \cdot \frac{M_P}{M_Q} + 0{,}02}, \text{ [mm]} \quad (19)$$

$$Z_{L1} = \frac{1}{0{,}012 \cdot \frac{2.28}{3{,}181} + 0{,}02} \quad (20)$$

$$Z_{L1} = 34.96 \text{ [mm]}$$

Z_g - the limit value of the roof inclination formed from a given type of rock, above which it becomes a set of loose rock blocks, also counted in mm subsidence, per 1m of the roof span,

$$Z_g = \frac{k_e}{\frac{0{,}05}{R_c} + 0{,}006}, \text{ [mm]} \quad (21)$$

where:
k_e – coefficient dependent on the mining system (for caving, $k_e = 1$),
R_c – real roof compressive strength, determined on the basis of tests in a given field of exploitation, ($Rc = 55$), [MPa],

$$Z_g = \frac{1}{\frac{0{,}05}{55} + 0{,}006} = 144.736 \text{ [mm]} \quad (22)$$

considering the dependence of Z_{l1} and Z_g, the load capacity index of the roof "g" was calculated:

$$g = \frac{1}{\frac{Z_{L1}}{Z_g} + 0{,}3} = \frac{1}{\frac{34.96}{144.736} + 0.3} = 1.84 \tag{23}$$

The value of the load index of the roof below 0.7 indicates very poor conditions for roof maintenance, which may mean a risk of a roof fall. Values in the range from 0.7 to 0.8 indicate that the condition of maintaining the roof is difficult. A value equal to 0.8 or more indicates correct roof maintenance.

5 Summary

The selection of a powered roof support for the geological conditions of the Vang Danh hard coal mine in Vietnam at a depth of around 300m is important for safe and efficient exploitation. Based on the calculated load capacity of the roof "g", it can be stated that the FAZOS-15/31-POz support has been well chosen and can provide workplace safety and can be a decisive factor in the effectiveness of exploitation conducted in geological and mining conditions of individual longwalls. Due to the complexity of the problem of cooperation of mechanized support with the roof rock mass, mathematical models obtained as a result of theoretical research and experimental research conducted in mining conditions should be used. In the case of a longwall face, fall of roof rocks may occur, which contribute to the loss of fluidity of the coal production process in the longwall, and also contribute to the increase of accident hazards for the working crew. Contemporary, modern underground hard coal mining is characterized by monitoring systems of mechanized support by roof loads, thanks to which it is possible to inform the crew in a very quickly and safety way and precisely identify potential danger zones. In order to apply the prediction of the load, tests and calculations in real conditions first must be performed, which will then be applied in numerical algorithms. The use of solutions of Polish Universities, Research Institutes as well as mining companies can be successfully implemented for the underground conditions of mines in Vietnam.

The acknowledgements

Paper was presented during the 5th POL – VIET International Conference Scientific-Research Cooperation between Vietnam and Poland, 08-10.07.2019, AGH UST, Krakow, Poland.

This study was developed as part of the statutory work No. **11.11.100.005**

References

1. A. Biliński, T. Kostyk, Prace naukowe Głównego Instytutu Górnictwa, **773**, (1992)
2. FAMUR website: https://famur.com, (2019)
3. Ł. Herezy, D. Janik, K. Skrzypkowski, Stud. Geotech. Mech., **40** 1, (2018) doi.org/10.2478/sgem-2018-0007
4. M. Jaszczuk, *Ścianowe systemy mechanizacyjne*. Wydawnictwo Śląsk, Katowice, (2007).
5. W. Korzeniowski, Ł. Herezy, K. Krazue, Z. Rak, K. Skrzypkowski, *Monitoring Górotworu na podstawie analizy pracy sekcji obudowy zmechanizowanej*. Wydawnictwo Akademia Górniczo - Hutnicza, Kraków, (2013)
6. J. Markowicz, S. Rajwa, S. Szweda, Arch. Min. Sci., **62**, 1, (2017) doi.org/10.1515/amsc-2017-0013
7. M. Płonka, S. Rajwa, MINING – INFORMATICS, AUTOMATION AND ELECTRICAL ENGINEERING, **4**, 536, (2018) doi.org/10.7494/miag.2018.4.536.45
8. S. Prusek, M. Płonka, A. Walentek, Arab. J. Geosci, **9**, (2016) doi.org/10.1007/s12517-015-2171-2
9. S. Rajwa, Prace Głównego Instytutu Górnictwa, Katowice, (2014).
10. S. Rajwa, M. Płonka, Z. Lubosik, A. Walentek, W. Masny, *Principles of safe use of powered supports*. School of Underground Mining, Ukraina, (2008).
11. K. Skrzypkowski, E3S Web of Conferences, **71**, 00006, (2018) doi.org/10.1051/e3sconf/20187100006
12. K. Skrzypkowski, E3S Web of Conferences, **35**, 01006, (2018) doi.org/10.1051/e3sconf/20183501006
13. K. Skrzypkowski, E3S Web of Conferences, **71**, 0007, (2018) doi.org/10.1051/e3sconf/20187100007
14. K. Skrzypkowski, W. Korzeniowski, K. Poborska – Młynarska, Arch. Min. Sci., **63**, 4, (2018) doi.org/10.24425/ams.2018.124983

15. K. Stoiński, *Obudowy górnicze w warunkach zagrożenia wstrząsami górotworu*. Praca zbiorowa. Wydawnictwo Główny Instytut Górnictwa, Katowice, (2018)
16. K. Stoiński, *Zmechanizowane obudowy ścianowe dla warunków zagrożenia wstrząsami górotworu*. Praca zbiorowa. Wydawnictwo Główny Instytut Górnictwa, Katowice, (2000)
17. D. Szurgacz, Journal of Sustainable Mining, **14**, 4, (2015) doi.org/10.1016/j.jsm.2015.12.001
18. M.E. Yetkin, F. Simsir, M.K. Ozfirat, P.M. Ozfirat, H. Yenice, S. AFR. J. IND. ENG., **27,** 1, (2016) doi.org/10.7166/27-1-1366

Study on some solutions for enlarging the application scope of the fully mechanized longwall coal mining technology according to seam dip angle at underground coal mines in Quang Ninh coalfield

Trung NGUYEN DUC[1*], Waldemar KORZENIOWSKI[1], Krzysztof SKRZYPKOWSKI[1] and Nguyen PHAM TRUNG[2]

[1] AGH University of Science and Technology, Krakow, Poland, Faculty of Mining and Geoengineering

[2] Institute of Mining Science And Technology, Hanoi, Vietnam

Abstract: The paper summarizes the applied experience, the technical solutions to limit the adverse effects of slope angle in the mechanized longwall mining at underground mines in the world. The paper proposes some solutions for enlarging the application field of the fully mechanized longwall mining technology according to seam dip angle at underground coal mines belonging to Vinacomin.

The current, Vietnam National Coal – Mineral Industries Holding Corporation Limited (Vinacomin) is promoting the application of the mechanized coal mining technology, in order to improve capacity and labor productivity, meet the demand for the economy. In which, the process of applying mechanized technology to mining coal seams with dip angle $\alpha \leq 35^0$, solved the requirements of capacity, productivity and labor safety. However, in condition ofsome inclined seams with a dip angle $\alpha > 20^0$, the level of efficiency of the technology decreased sharply (equal to 25 to 30-percent compared to the stable period). Although the device is designed with the ability to work when the angle is up to 25^0, even to 35^0.

The results of assessment mechanization application process in coal mines in Quang Ninh in the past ten years show that: Stable working time of longwall accounts for 38% to 45% of total operating time [2]. The remaining time, the longwall often encountered trouble, in which the slope factor plays an important role (accounting for 17% of the total unstable operation time and accounting for 38.6% of the geological problems). If the dip angle is greater than 20^0, the equipment in the mechanized longwall will work with low reliability, usually occurs sliding, must stop troubleshooting, affects the durability of the device and reduce exploitation efficiency.

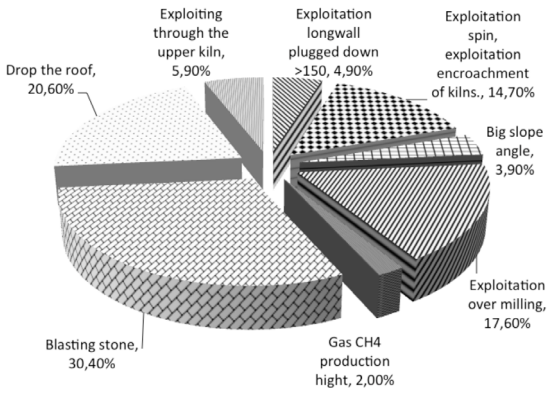

Figure 1. Proportion of factors affecting the reduction of longwall production

Therefore, study on some solutions for enlarging the application field of the fully mechanized longwall mining technology is necessary for underground coal mines in the Quang Ninh coalfield.

I. Study on some solutions for enlarging the application scope of the fully mechanized longwall mining technology at underground coal mines

In the world, to exploit coal seams of medium to thick thickness, dip angle above 20º by mechanized longwall, there are some following solution:

1. Improving the structure of the support.

This method link individual support units into clusters by the anti-topple jacks and face conveyor with power support by anti-slip device. The addition of large hydraulic jacks with thrust (or pull) along the direction of the dip angle of the longwall, linking the canapy and base of the single power support as above is quite effective in keeping the supports and face conveyor not fall over by the impact of the dip seam, thereby increasing the scope of application according to the working angle of the power supports and conveyor.


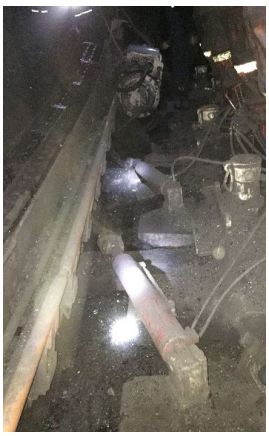
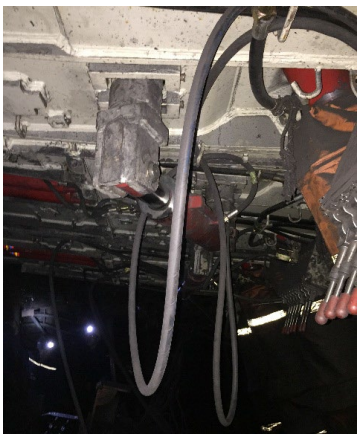

a. Anti-drift system of power support | b. Anti-drift system of face-conveyor | c. Anti-topple system of power support

Figure 2. Hydraulic jacks against drifting, anti-topple of face conveyor at mechanized longwall, Quang Hanh Coal Company

This solution has been practically applied and highly effective in some mechanized longwall mining at the medium thick seams in Chinese underground mines such as Doanh Coc Son and Xuong Hung of Ban district - Guizhou; Dai Hung mine - Tao Trang; mine No. 10 - Binh Dinh Son - Ha Nam Province; Tuan Duc Mine - Hac Cuong Mine - Hac Long Giang Province .... The mechanized longwall have a length of 100 ÷ 150m, have coal output of 350,000 ÷ 600,000 tons/year, some favorable cases, the longwall capacity reaches 1.5 million tons/year, labor productivity reaches 20 ÷ 50 tons/work, the exploitation coefficient reaches 90 ÷ 95% [2]. In Quang Ninh region, the longwall CGH TT-6-1 located in the coal seams 6 of the Trung Tam area, Quang Hanh coal mine has been equipped with anti-drift hydraulic jacking system, the longwall relatively stable operation in sloping conditions of about 25º.

2. Solution of longwall mining in the direction of selling oblique to reduce slope angle.

This solution set the coal face of longwall in the semi-oblique direction to reduce the dip angle of the longwall. The degree of dip angle of the longwall α_{lw} (compared to the true dip angle of coal seams α_{cs}) depends on the semi-oblique angle between coal faceand the strike of the coal seams (or the line of dip) γ.

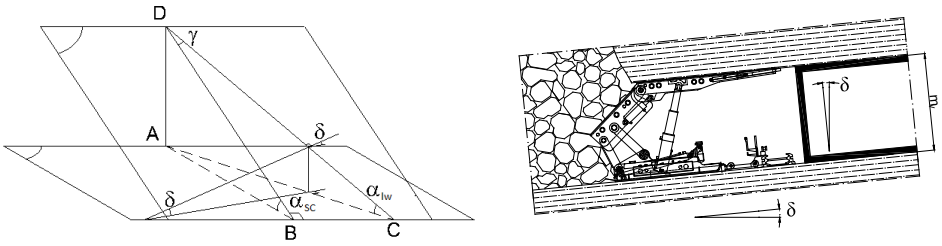

Figure 3. Diagram to calculate the dependence of the dip angle of longwall α_{lw} and the angle of the coalface into the semi-oblique angle γ

The relationship between the dip angle of the longwall α_{lw}, the true dip dip angle of the coal seam αv, inclined angle of the coal face δ with the semi-oblique angle of the coal face compared to the the line of dip -γ, is represented by the formulas:

$$\sin \alpha_{lw} = \sin \alpha v \times \cos \gamma; \sin \delta = \sin \alpha_{cs} \times \sin \gamma \quad (1)$$

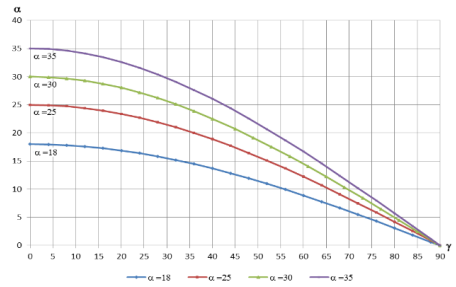

Figure 4. Chart of the dependence of the dip angle α_{lw} in the semi-oblique angle of longwall γ

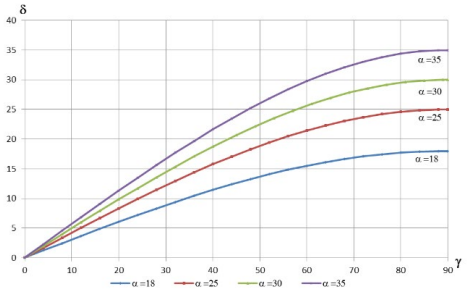

Figure 5. Chart of the dependence of the inclined angle of the coalface δ to the semi-oblique angle γ

Based on the chart in Figure 4, Figure 5 can be seen in the case of the longwall kiln perpendicular to line direction of coal seam (semi-oblique angle $\gamma = 0^o$), the slope angle of the longwall will be equal to the slope of coal seam. For example, if coal seams have dip angle $\alpha_{cs} = 25^o$ and thesemi-oblique angle $\gamma = 35^o$, the dip angle of the longwall will be 20^o, corresponding to a decrease of 5^o compared with the seam dip angle.

However, if set the conveyor gateway area of the longwall go ahead the air-return gateway area, we will create a semi-oblique angle as above, the coalface of longwall will tilt accordingly at an angle of about $\delta = 13 \div 14^o$, easy to happen risk, for example, failed roof, coal falling. Thus mining operations may stop and major reinforcement begin immediately.

To avoid this phenomenon, we can set the coal face in the opposite direction, The head area of longwallt is over the foot are of the longwall (Figure 6b) or the foot areas are still advanced ahead of the longwall but the coal face is straight (Figure 6a).

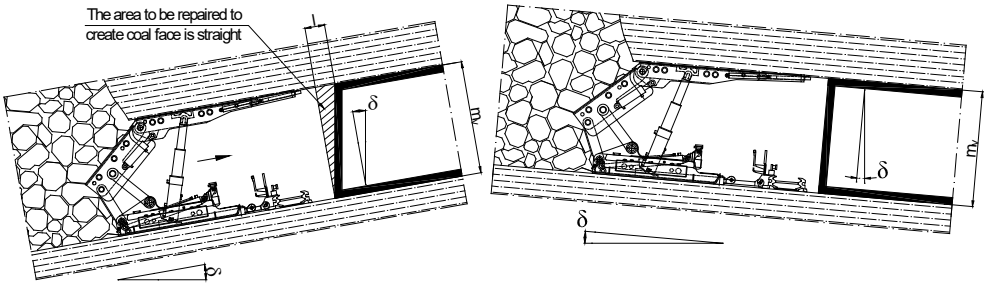

a, support case of longwall legs first *b, support case of longwall head first*

Figure 6. The type of coal face in a semi-obliqued longwall

Along with the layout of semi-obliqued longwall, the arrangement: supports - face conveyor (Figure 7a) is often preferred over the oblique form (Figure 7b) because the structure of the link between the face conveyor and the hydraulic anti-topple jacks (or hydraulic anti-slip device) is simpler, easier to fabricate and more durable, as well as the supports structure of the supports can be reduced significantly less.

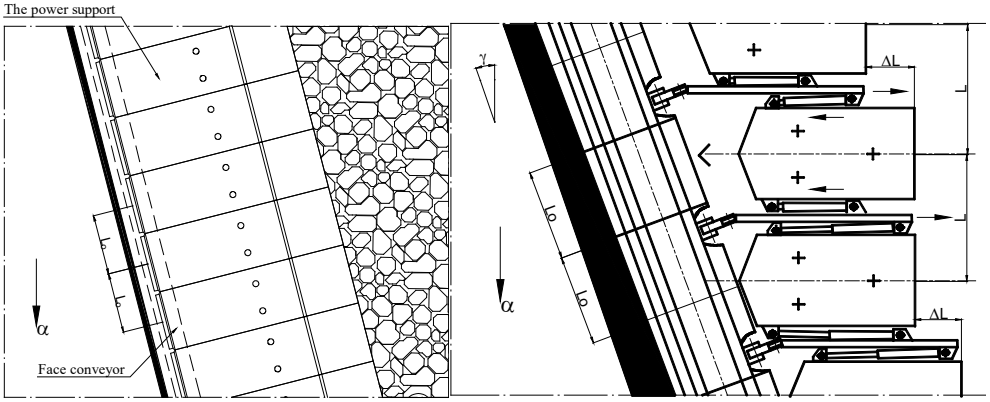

a, The power support - face conveyor are perpendicular in a semi-obliqued longwall

b, The power support - face conveyor are oblique in a semi-obliqued longwall

Figure 7. The arrangement of the power support – face conveyor in a semi-obliqued longwall

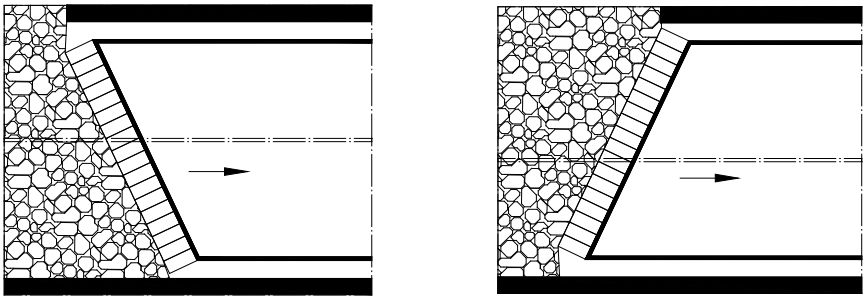

a, Longwall legs first

b, Longwall head first

Figure 8. The arrangement of longwall on strike

However, the arrangement of mining in the form of the first part of the longwall goes ahead, the major disadvantage is that according to the mining schedule, the support system and the face conveyor will automatically move down, although it is not affected (or subjected to little) impact by the dip angle. Meanwhile, the coal face of the longwall has legs ahead, often with the opposite direction of movement, the support and the face conveyor move themselves upwards according to the progress of mining and effectively overcome the drift downwards [3, 4] ..

With the above arrangement, combined with the solution of using hydraulic system, anti-topple jacks and anti-drifting, the longwall has made relatively good exploitation, avoiding impacted slippery due to the influence of seam dip angle. Underground coal mine applied simultaneously with the above two solutions bring good results. For example, the Tuan Duc mine, Heilongjiang province, China used support HY-300, the KYBLK-70 scraper with combine machine KWB-3RW exploiting coal seams with average thickness of 2.75m, the 35º dip angle gives mining capacity of 350 thousand tons/year, labor productivity of 10 tons/work or Dong Vinh II mine, Hac Long Giang province using support ZZ4800 / 15/30, SGZ-764/2 × 200 and shearer MG250 / 601QWD in the longwall length of 114m to exploit coal seams with thickness 2.7m, dip angle 34º for a capacity of 1.580,000 tons/year, labor productivity reaches 45 tons/work shift [2].

3. Solution to organize diagrams of mechanized mining coal face in longwall.

This solution use a shearer in one direction from top to bottom. The movement direction of the machine from bottom to top is done in the form of no-load movement. The control of shearer in the direction from top to bottom has create the device thrust upward reduce the slippage effect of the face conveyor indirectly to reduce the slippage effect of the support because the support and the face conveyor are always linked together.

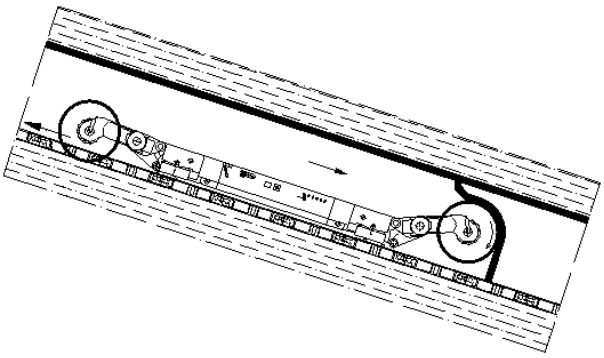

Figure 9. Diagram of shearer mining coal faceshearer

This solution has been applied at the longwall 10121, 12 mines of Lao Oc Co mine, Quy Chau province (China), exploiting seams with thickness 1.5 ÷ 5.5 m, average 3.5 m, dip angle 32 ÷ 45º. Synchronous equipment includes the ZFQ4000/15/26 power support, combine MXG-250/600QWD and the SZ730/400 face conveyor for a 190,000 tons/year capacity.

In order to reduce the influence of the seam dip angle, the coal mine has organized a mining diagram in one direction from top to bottom, the direction of the moving upwards is done in the form of no-load. Accordingly, when the coal face is cut, the previous cutting drum of the shearer cuts off the top coal, the next one cuts the flat coal, each one arranges a driver. Due to the steep angle of the longwall, during the time of coal mining, the machine operator must stand inside the column of anti-rig pillars, use the control to manipulate the control of the machine to avoid falling coal and rock. Due to the longwall dip angle is large, after cutting coal, the moving position of the support is at least 20 m from the combination of the shearer, to prevent rolling rock from causing accidents for workers at the time of moving the support apply the sequence from bottom to top.

4. Solution top coal cavingand reduce the dip angle of the conveyor gateway area of the longwall.

This solution is only applied to mechanized longwall top coal caving. Characteristics of the mechanized longwall top coal caving is that after the recovery, the exposed area of the support on the top coal is significantly reduced and under the influence of the dip angle, the rear base of power support tends to drift downwards in steep direction, making the support less stable.

In order to overcome this phenomenon, it is possible to arrange a conveyor gateway located on the side of the roof to create the scope of the foot of the longwall create a segment with a low slope angle (Figure 10). At the same time, increasing the recovery progress of coal (usually, after about 2 steps of exploiting and executing the recovery of coal down). This solution can improve the stability of the support by indirectly increasing the contact area of

the support with the top coal and a part of the foot of the longwall with a low, almost non-slip slope will create a base for the support will not drift down.

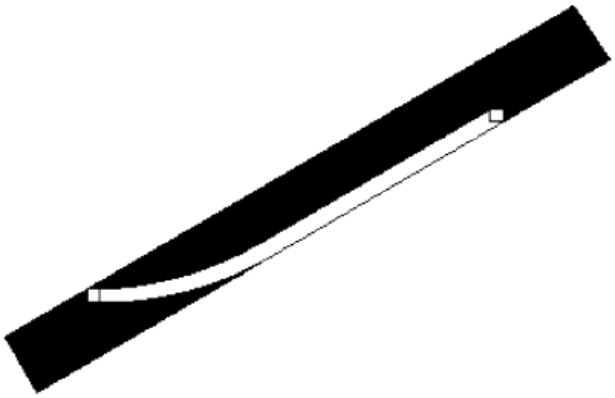

Figure 10. Preparation diagram to reduce slope angle at the foot of the longwall

This solution has been applied in the longwall 44407 at Vuong Gia Son coal mine - Noi Mong area to exploit soft coal seam (f = 1), thickness of 13.5 ÷ 23m, dip angle 38 ÷ 49º. The length of longwall is 145m, located at a depth of 260 ÷ 320m compared to the topographic surface with longwall height is 2.4m (the remaining coal is lowered to the ceiling) with a capacity of 53,000 tons/month. In addition, at the longwall 5335 U Lan mine - Noi Mong area has also applied mining mechanization technology in very soft coal seam conditions (f = 0.6 ÷ 1.2), average coal seam thickness 8.0 m, dip angle from 25 ÷ 35º. The length of the longwall according to the line of dip is 110 m, the depth of exploitation is -350 m compared to the topographic surface, the longwall output reaches 70,000 ÷ 80,000 tons/month.

II. Conclusion

Some solutions for enlarging the application scope of the fully mechanized longwall mining technology at underground coal mines as above, limiting the adverse effects of seam dip angle has been drawn from practical experience in underground mines around the world. The consideration of the application of the above solutions may help mechanized longwalls at Quangninh underground coal mines to improve the exploitation efficiency.

Reference material

1. Dr. Tran Xuan Hoa, “Nghiên cứu nâng cao mức độ cơ giới hóa và hiện đại hóa khai thác than hầm lò và định hướng ứng dụng cho các mỏ than hầm lò vùng Quảng Ninh”, Institute Of Mining Science And Technology- Vinacomin (2011).

2. Msc. Dang Thanh Hai, “Phát triển áp dụng cơ giới hóa đào lò và khai thác tại các mỏ than hầm lò vùng Quảng Ninh giai đoạn 2013 ÷ 2015, lộ trình đến 2020”, Institute Of Mining Science And Technology- Vinacomin (2016).

3. Msc. Tran Tuan Ngan, “Một số vấn đề về lựa chọn dàn chống, tổ chức khai thác và điều khiển đá vách trong khai thác vỉa dốc nghiêng, dốc đứng có chiều dày trung bình và mỏng”,

4. Коровкин Ю.А., Савченко П.Ф., Теория и практика длиннолавных систем, «Техгормаш» Москва (2004).

A study on relationship of duct leakage and parameters of ducts in Quang Ninh mine

*Phuong Thao Dang, Vu Chi Dang

Hanoi University of Mining and Geology, Hanoi, Vietnam

18 Vien Street, Duc Thang Ward, Bac Tu Liem District, Hanoi, Vietnam

* Corresponding author: dangphuongthao@humg.edu.vn

Abstract

Air leakage of auxiliary ventilation ducting systems is the most common reason for the insufficient fresh air in the working face in underground mine. This value is important design parameter for mine auxiliary ventilation system that operates more effectively, with lower cost.

Therefore, determination of air leakage along auxiliary ventilation ducting systems has been examined. Also, factors which affect air leakage in the ducting system have been investigated. Experimental data are made on 0.7 m and 1 m diameter ducts over sections of ducts installing towards the working face in Quang Ninh mine.

Keywords: air leakage, auxiliary ventilation, duct, analytic function, working face.

Introduction

In Quang Ninh, coal underground mines have high methane content and total length of new driven roadways is large for expanding mining areas and growing coal output. Therefore, ventilation is one of the most important considerations in coal underground mines. Ventilation efficiency depends on fan performance parameters and duct aerodynamic characteristics. The most common auxiliary ventilation system is comprised the ductwork and the axial fan. Flexible duct used is lightweight, easy to handle and install. However, ventilation ducting system leakage can, in many cases, supply an insufficient quantity of air to provide a healthy, safe environment in the workplace.

In Viet Nam, in the past, due to flexible ducts were often imported from abroad, parameters of the duct as duct leakage, duct resistance were referenced from abroad handbook to design the auxiliary ventilation system. However, currently, flexible ducts have

often been produced domestically, determination of a relationship of the duct leakage and the duct aerodynamic characteristic must been undertaken.

The result is also the basis for making plan to equip ducts and fans for the auxiliary ventilation system in Quang Ninh coal underground mine.

Theory of duct leakage

Factors affecting on air leakage through the duct

A literature review on air permeability of different duct materials shows that flexible duct usually has a greater air leakage than other types of the duct [1, 2 and 3]. This is due to the fact that duct fabrication was previously unsatisfactory. However, in recent years, flexible duct has been improved quality. It shown that in some mines, amount of duct leakage has small, but in the case of poor installation practices, air leakage is high.

Factors such as duct size and diameter, aerodynamic parameters in duct airflow influencing on duct air leakage have been examined.

Ducts of different sizes and diameters

Air leakage of the ducting system is affected by the length of duct. Obviously, when the duct length is longer, the ducting system requires more joints. For flexible ducting system, air leakage through these joints cannot be avoided. The degree of the air leakage in the ducting system depends on duct diameter; if the duct diameter - D is larger, the degree of the leakage is smaller due to the resistance of the duct that is inversely proportional to D^5 [1].

In practice, in Quang Ninh mines, PVC coated fabric duct is suitable for high power fan in order to reduce level of the air leakage and increase durability of the ducting system, especially at site where a duct connects to the fan.

Duct is available in various lengths, generally in 10-50 m lengths but the ducts of 20 m length are common used in Quang Ninh mines. Typical duct diameters range between 0.6 m and 0.8 m but rarely can use as 100 m.

Table 1. Different diameter types of the double-sided PVC coated duct used in Ha Lam mine (Dec. 2018)

Diameter mm	**Cost 10^3 VND/m**	**Total length of ducting system m**	**Length of the duct m**
500	101	800	20
600	125	1800	20
700	150	2600	20
800	177	2000	20
1000	216	2000	20

Aerodynamic parameters

Aerodynamic parameters which, is factors, determine level of air leakage through ducting system. Many researchers have shown that air leakage is proportional to airflow through the ducting system [2, 3, 4 and 5].

Pressure loss H influences degree of air leakage through ducting system. However, at value of $H \geq 200$ mmH_2O, the air leakage is significantly reduced [2]. In practice, the pressure

is always greatest adjacent to the fan and so air leakage at the location near the fan leaks significantly more than that at location further away. It was shown that at the pressure of 150 daPa – the pressure inside ducting system during mining roadways being driven in mine, air pressure along length of the duct remains stable due to duct material that protects elastic deformation [5]. However, increasing the pressure to 2000-3000 daPa, permeability through ducting system increases the two – three folds. These pressure values are much higher than the pressure value inside the ducting system during working operations (the highest pressure value is 500-700 mmH_2O).

Auxiliary ventilation in mining roadways being driven in Quang Ninh underground mine

Auxiliary ventilation systems used is the force system, in which the fresh air is led to the face through the fabric duct. Fabric ducts and different types of fans are used for the auxiliary ventilation system. The hundreds of auxiliary fans are required for example, over 100 fans in Mao Khe, Vang Danh coal mines.

At present, roadways in Quang Ninh coal mines have a cross-section 10-15 m^2, maximum 30-32 m^2, over ten thousands meters of new driven roadways are driven annually. In order to expand mining areas, two inclined shafts with the length of over 1600 m and 1 km in Khe Cham and Mao Khe Coal mine respectively have been done. Due to coal mining activities extending to the depth, the lengths of the roadway for getting one thousand tons of coal become longer, for example, from 11-12 m increase up to 17-18 m in Mao Khe, Hon Gai and Ha Long coal mine; particularly up to 20-25 m in Giap Khau, Dong Vong mine in certain years.

In underground mining operation, it is necessary to provide sufficient airflow requirement to ensure a healthy, safe environment in the workplace. Improper selection of fans and ducts can degrade the effectiveness of the ventilation system and increase the cost of ventilating the mine.

Model for duct leakage

Duct leakage

When air flow is moved in ducting system, air leakage is always presented. Air leakage is a complicated aerodynamic phenomenon. If there is not air leakage through the duct, the pressure of the fan generated and the air flow throughout the ducting system can be described by a model quite accurately. Air leakage can be described in the following two physical models [6].

- Discrete – air leakage leaks through joints of ductwork
- Continuous – randomly distributed outlets along the ductwork walls.

For estimating level of the air leakage, the researcher [7] proposed the flow of the air leakage leaks in turbulent flow mode; but researcher [8] proposed flow of the air leakage in laminar flow mode. The work [9] shown that the mode of the air leakage is quite complicated and close to exponential function. Therefore, the results of the air leakage coefficient have been shown in the form of tables or graphs for certain types of duct.

Duct leakage in Quang Ninh mine

With fabric duct being used in Quang Ninh coal mines, it shows that air leakage depends on duct fabrication, installation and maintenance of the ductwork as well as the usage time in certain conditions in mine.

Level of air leakage is mainly influenced by the following factors: total length, diameter of the ducting and airflow in the ducting system:

- Currently, in Quang Ninth mines, airflow volume Q_{face} supplying to the face changes from 2 to 8 m^3/s for the duct of D = 0.6 ÷ 0.8 m; sometimes 1.0 m for large cross-section roadway.
- When the length of the duct is extended from 100 m to 700, 800 m, air leakage will increase quite markedly. Leakage sometimes exceeds 15-20% initial flow volume designed over 100 m ducting length.

Relationship between air leakage and parameters of duct

It is shown how to derive the function indicating a relationship between leakage coefficient p and ducting length L (m), airflow in ducting system Q (m^3/s) supplied to the working face for different diameters of the duct:

$$p = f(L, Q) \quad (1)$$

Accordingly, assuming that air leakage coefficient in the ductwork can be described to be in the form of:

$$p = 1 + c * L^a * Q^b \quad (2)$$

Where: p: Leakage coefficient;
L: Duct length, m;
Q: Quantity of airflow in the ducting system, m^3/s;
a, b, c: constants.

The way to linear the equation (2) is to use the natural logarithm equation (2).

$$\ln(p - 1) = lnc + alnL + blnQ \quad (3)$$

With ducting length L_i, the quantity of airflow in the ducting system Q_i is measured; the air leakage coefficient p_i is calculated as $p_i = \frac{Q_0}{Q_i}$;

Where: Q_0 the quantity of airflow beyond the fan, m^3/s;
Q_i the quantity of airflow reaching the end of the ducting length - L_i.

The experimental data are made on 0.7 m and 1 m diameter ducts over sections of ducts installing towards the working face in actual field conditions in Ha Lam coal mine.

Each set of data: ln (p_i), ln (L_i) and ln (Q_i) under given data – duct diameter, with i=1, 2…n.

Linear regression analysis by using Stata software to fit these experimental data can derive the relationship between the air leakage coefficient, the quantity of the air in the ductwork and the ducting length. Therefore, the air leakage coefficient for the ductwork of 0.7 m diameter can be estimated based on the experimental data (Table 2) at Ha Lam Coal mine by the regression method.

As a result obtained from Stata software, the air leakage coefficient for the duct of 0.7m diameter can be found based on data at Ha Lam Coal mine:

$$p = 1 + 2.0042048.10^{-4} * L^{1.051706} * Q^{0.677522}$$

L_{max}: Duct length total (4)

Table 2: Experimental data for the duct of 0.7m diameter measured at Ha Lam Coal mine

The Face	Q_o m^3/s	L_{max} m	Q_{face} m^3/s	p	Values of p_i, Q_i correspond to ductwork length L_i when extending driven roadways					
					L_1		L_2		L_3	
					Q_1	L_1/P_1	Q_2	L_2/P_2	Q_3	L_3/P_3
Haul Road level -185÷ -160 Area III- Seam 11	6.8	290	5,0	1.261	6.4	80 / 1.063	5.8	160 / 1.104	5.0	290 / 1.261
Ven. Roadways level -270÷ -250 Area III - Seam 10	5.2	190	4.8	1.1554	4.9	89 / 1.06	4.9	120 / 1.106	4.8	180 / 1.123
Ven. Roadways level -50 Area VI - Seam 10	5.2	245	4.5	1.1304	5	120 / 1.102	4.9	160 / 1.091	4.5	240 / 1.16
Ven. Roadways level -70÷ -60 Area II- Seam 10	5.2	120	4.7	1.0612	5.0	30 / 1.02	5	60 / 1.04	4.9	80 / 1.0612
Ven. Roadways of the Long wall 7-3.1	6.8	258	5.2	1.3077	6.2	60 / 1.033	5.8	120 / 1.104	5.2	250 / 1.248
Ven. Roadways Level -290 Area I - Seam 7	*6.8*	235	5.5	1.236	6.6	80 / 1.061	5.8	225 / 1.172		

L_{max}: Duct length total

Table 3: Experimental data for the duct of 1m diameter measured at Ha Lam Coal mine.

The Face	Q_o m^3/s	Q_{face} m^3/s	L_{max}	Values of p_i, Q_i correspond to ductwork length L_i when extending driven roadways													
			p	Q_1	L_1/P_1	Q_2	L_2/P_2	Q_3	L_3/P_3	Q_4	L_4/P_4	Q_5	L_5/P_5	Q_6	L_6/P_5	Q_7	L_7/P_7
Vent. Haul Roadways -290 ÷ -210 Area III to IV, Seam 10	9.2	6.9	900 1.334	9.1	50 1.011	9	140 1.023	8.6	320 1.09	7.8	600 1.179	7.6	740 1.211	7.2	760 1.278		
Ven. Roadways 7.2.1 Seam 7	12.2	8.6	1280 1.419	11.1	180 1.099	10.8	370 1.129	10.3	540 1.184	9.8	740 1.244	9.6	860 1.271	9.2	960 1.336	8.8	1180 1.386
Haul Roadways, 2.1 Seam 7	12.2	8.6	1250 1.419	11.6	180 1.051	10.7	380 1.14	10.2	500 1.22	9.8	680 1.245	9.2	780 1.2708	9	920 1.355	8.6	1160 1.418

Use the F-test can evaluate Pro (F) = 0.0000 with significance level is 0.5. This low a value would imply that the regression parameters are nonzero and the regression equation does have some validity in fitting the data.

Data set (Table 3) for the duct of 1m diameter at Ha Lam Coal mine have been analyzed as the same above. So that, it can be found:

$$p = 1 + 2.554.10^{-5} * L^{1.164} * Q^{0.686} \quad (5)$$

Prob > F = 0.0000 with significance level is 0.5. This implies that the regression equation does have some validity in fitting the data.

Conclusion

In Quang Ninh mine, Viet Nam, in the past, fabric ducts were often imported from abroad, so that parameters of duct as duct leakage, duct resistance were referenced from abroad handbook. However at present, there is no data of the leakage coefficient of the duct produced domestically. Accurately estimating the leakage coefficient is thus crucially important to proper duct sizing and fan selection.

The leakage coefficient of the ductwork can be determined based on the general evaluation of the influence of the factors, in which the duct length and diameter, airflow in the ductwork are very important.

A conceptual prediction model has been proposed based on the experimental data at Ha Lam Coal mine. Using linear regression analysis to fit these experimental data can estimated the air leakage coefficient in the ducting systems in Ha Lam coal underground mine.

Also, the research result has been used to optimize the auxiliary ventilation system. Optimization of the auxiliary ventilation system can save cost and energy.

Acknowledgements

Authors would like to thank to Ha Lam coal company Team for the support with site access and field investigation. Paper was presented during the 5th POL – VIET International Conference Scientific-Research Cooperation between Vietnam and Poland, 08-10.07.2019, AGH UST, Krakow, Poland.

References

1. D.A.Telyakovsky, V. Komarov, Mine Ventilation, Mir Publishers, Moscow (1969).

2. И.С. Родькин, Проветривание горных выработок при строительстве шахт, М., изд-во Недра, (1970).

3. K.Z.Ushakov Handbook of mine ventilation, Publishing House Nedra Moscow in Russian (1988).

4. Б.И. Медведев, В.П. Сухоруков, К расчету неплотных вентиляционных воздухопроводов, Уголь Украины, No**7**, (1988).

5. Е.В. Столбченко, Обоснование рациональных параметров вентиляционных систем местного проветривания, NGU.Недра (2013).

6. T.Stefanov, E. Vlasseva, Untight pipeline ventilation systems' calculations, 50 years University of Mining and Geology "St. Ivan Rilski" Annual, Vol. **46**, part II, Mining and Mineral Processing, Sofia, pp.155-162, (2003).

7. V.S.Vutukuri, Air Leakage in Ventilation Ducting and the Design of Auxiliary Ventilation Systems, the Mining Engineer, No. **262**, July (1983).

8. И. А. Швырков, О потерях воздуха при вентиляции рудников, Безопасность тр. в горн. пром-сти..№ 9. С**.5–15**, (1933).

9. А. А.Мясников, И.А.Камышанский, Определение перепада давления в трубопроводах переменным расходом по длине, Физ.- техн. Проблемы разраб. Полезных ископаемых, No **2**, (1973).

Study on the possibility of using artificial pillar to replace the protection coal pillar of the preparation roadways during the mining process at underground coal mines in Quang Ninh region, Vietnam

Cuong Dinh Van[1,*], Thanh Tran Van[2] and Tuan Nguyen Anh[3]

[1] Institute of Mining Science and Technology - Vinacomin (IMSAT), Hanoi, Vietnam
[2] Hanoi University of Mining and Geology (HUMG), Hanoi, Vietnam
[3] Vietnam National Coal-Mineral Industries Holding Corporation Limited (VINACOMIN), Hanoi, Vietnam
[*] Corresponding author: dinhcuongvimsat@gmail.com

Abstract: The coal reserves in protection pillar of roadways are expected to be left in the mining process in underground mines in Quangninh coal basin which is relatively large (about 16% of the total reserves). If it can be exploited, it will help to save non-renewable coal resources, reduce the cost of preparing roadway meters, extend the mine life and increase the efficiency of construction investment. In the world, in order to reduce coal loss in protection pillar of roadways, mining technology to exploit and use artificial protection pillars are quite popular. Accordingly, in order to simultaneously exploit coal in the protection pillar and maintain the transport roadway as a ventilation roadway for the longwall in below level, the post-mining coal pillar will be replaced by artificial pillars formed from the stone backfill cribs, columns, metal cribs, chemical materials or low-grade concrete mortar mixes formed from fly ash, bottom ash of thermal power plants, combined crushed waste rock and a cement additive,... This paper will evaluate the possibility and propose a number of mining technological scheme as well as the type of construction materials suitable for artificial columns.

1. Introduction

In the underground coal mines of Quang Ninh region, longwall mining system is widely applied and always contributes most of the coal output. In this mining system, in order to maintain the transportation roadway in the coal seam of the upper stratified as a ventilation roadway for the lower-level longwall mining, the mining process along the axis of coal will leave a coal cribs bordering the transportation roadway as a protection pillar. Depending on the depth of exploitation, the geological characteristics of the area the roadways have to be protected, the coal pillar is in the direction of slope from 15 ÷ 20m, corresponding to the coal reserve of about 13 ÷ 15% of the total coal reserve. Dynamic in the mining space of the longwall mining (length of longwall in the direction of popular slope from 100 ÷ 150m). This is a ready-to-be-delineated reserve of prepared roadways, if it can be exploited, it will allow significant savings of non-renewable coal resources, reducing the risk of endogenous fire in areas with coal spontaneous combustion. At the same time, the coal mining in the protection pillars will make use of the existing constructions, so they do not have to pay for the cost of mining depreciation, contributing to reducing the cost of meters for preparation roadway, thereby allowing reducing production costs, prolonging mine life and increasing construction investment efficiency. To solve this problem, the mining technology scheme of using artificial pillars to replace coal-protection pillars for preparation roadways has been successfully applied in many countries around the world, effectively meeting the requirements.

2. Experience of applying artificial pillars to replace coal pillars to hold up the preparation adits in the world

Technology to exploit and use artificial pillars to replace coal pillars to hold up the preparation roadway has been widely applied in the world. In particular, the materials used for the construction of the pillars can be clustered columns, wooden/metal cribs, backfilling brick/stone masonry or chemical materials. Recently, the material is a low-grade concrete mixture composed of ash and ash from thermal power plants, crushed waste rock combined with additives, cement is also applied and becoming more and more popular. The overview is as follows:

2.1. Artificial pillars are made of backfill stone

The artificial protection pillars by backfill stone is applied when exploiting coal seams of small thickness (usually below 2.0m) according to the seamless front exploitation system, driving the preparation roadway in accordance with the enlarged front scheme. In order for the working space to meet the prescribed requirements, the cross section of

longwall, the cross section of ventilation roadway and the cross section of transportation roadway have to be dug by carried forward will have to cut off part of the floor or roof. Stone after cutting will be transported to the scope of construction of artificial protection pillars, which will simultaneously allow maximum exploitation of resources, not transporting stones out of the door and limiting the risk of fire endogenous (Figure 1). This method was previously used quite popularly in the former Soviet Union (Centeralnaya-Bokovskaya mine exploited the coal seam No.51 Nadbokovskiy with a thickness of 1.0m; Volodarskiy mine exploited the coal seam H8, Maidannovskiy with thickness of 1.1÷1.15m [2-4]).

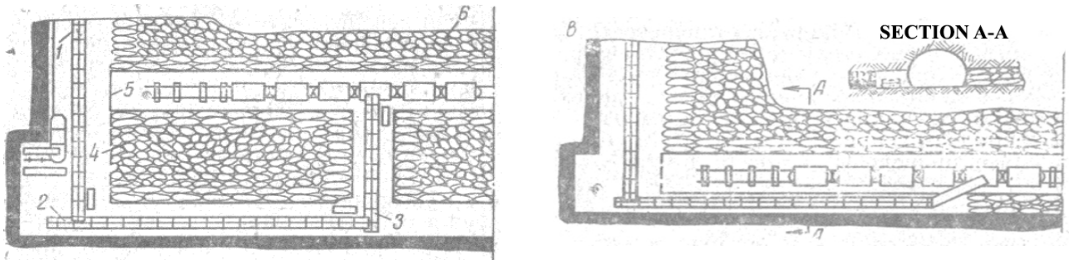

a. In case of large slope angle b. In case of small slope angle (<15^0)

1 - scraper conveyor in longwall ; 2, 3 - scraper conveyor for transporting coal; 4.6 - Stone backfill stone from blasting stones at longwall along seam 5; 5 - transportation roadway along seam

Figure 1. Diagram of construction for artificial pillars by stone backfill according to the exploitation system closely face

Construction diagram as shown in Figure 1 has disadvantages of backfill stone with large shrinkage so the area of using preparation roadway is expected to decline sharply after construction. In addition, the lower-floor longwall mining (if any) in the mining process will have to pass through the insertion stone 4 (Figure 1b) of the expanded stage longwall -face or to dig the new ventilation roadway (Figure 1a), so basically only applicable to the final longwall mining in the floor. This disadvantage will be overcome when organizing concurrent excavation of transport roadway (upper-floor longwall), ventilation (lower-floor longwall) by expanding face of longwall. Then, the coal pillars between the two roadways will be exploited to create storage space for waste rock from the longwall mining along the seam during excavation (Figure 2) without having to be transported out; the ventilation work is done by low pressure. General should be simple and cost-effective.

For example, this scheme has been applied in Russia could include Lugansugol coal mine (construction of roadway along the coal seam in a thickness of 1.5 ÷ 1.8m, excavation area of 14.5 m^2, excavation by blasting drilling) combined with the slitting machine, the excavation speed reaches 501 m/month) and Kaliningol mine in Tula coal region (construction of roadway along the seams in coal seams with a thickness of 1.2 ÷ 1.5 m, excavation area of 8.0 m^2, using ПК-3 Combain, speed reaches 1,635 m/month). In China, the Ba Yi Coal Mine (Shandong province) also applies this scheme to construct pairs of ventilation roadway and transportation roadway when exploiting the coal seam No.16 with a thickness of 0.8 m; the road is in square shape. Height and the width of the roadway is 2.0 m, the length of the extended face section between the two stone-insulated roadway is 8.0m.

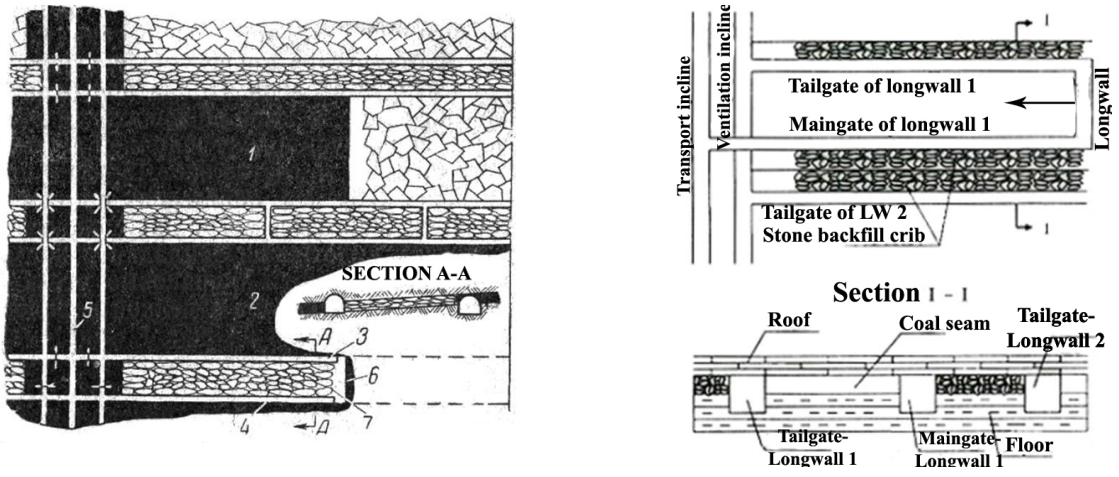

a. Scheme applied in Russia *b. Scheme applied in China*

Figure 2. Construction diagram for artificial pillars by backfill stone according to the long-column exploitation system in the direction

2.2. Artificial pillars of crib form, clustered columns and support pillar

Artificial protection pillar made by clustered columns, wooden cribs, or support pillar are applied in larger coal seams. With protection pillar a crib form, to increase load capacity, it can be reinforced by filling the gap between by waste rock, sandbag, cement or mineralized material (chemical). Research by Polish scientists [7] has shown that the maximum compressive strength of wooden cribs is only 44 kN, but when filled with mineralized materials is increased to 166 kN, by sand bags 116 kN, (sand can be replaced with waste rock) 119 kN, details are shown in Figure 3.

a. Crib filled with chemical materials

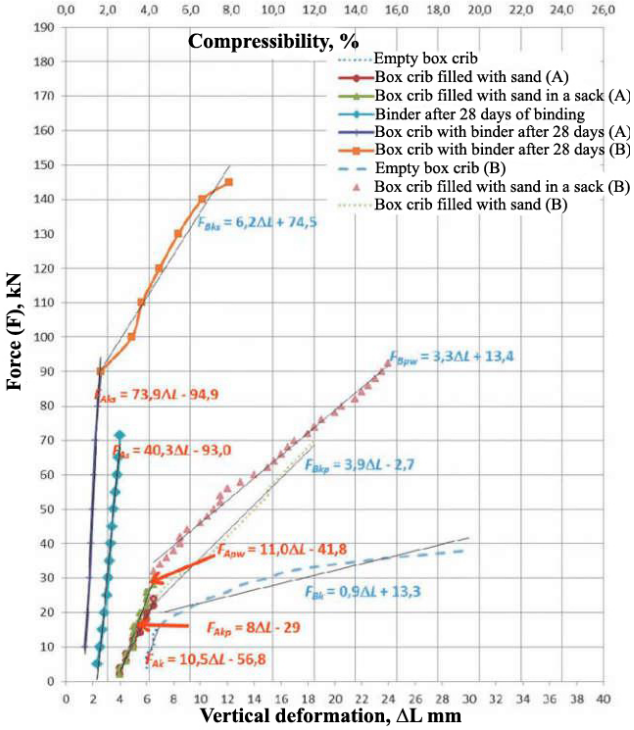

b. The intensity of compressive resistance of the crib according to the fill material

Figure 3. Comparison of compressive resistance strength and deformation level of crib according to fill material [7]

The concrete protection pillar was tested at Ziemowit mine (Poland). The concrete protection pillar with a diameter of 0.6m, is used to protect the roadway along the seam with the height from 4.0÷4.3m, width of 5.0÷5.5m when exploiting the longwall 902 and 904 at the seam No.209 (seam thickness 4.5m, slope angle 4°). The results of successful application, the protected adits ensure the required size as a ventilation adit for the next longwall (903 and 905), reducing 30 ÷ 60% of the cost compared to the new digging (Figure 4). However, this solution will not solve the problem of air leakage and gas, heat, water from the exploited area into the adjacent longwal.

a. concrete protection pillar in adit

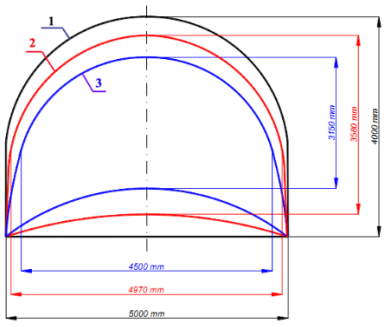

1-Size when digging;

2-The size of the scope of the junction longwall ;

3-Size at the position of 200m behind the face of the longwall

b. Results of protection for adit along the seam 062

Figure 4. Results of applying solutions to replace coal pillars to hold up the roadway prepared by concrete pillars at Ziemowit mine (Poland)

2.3. Artificial pillars are continuous stone strip

To overcome the disadvantages of the structure of artificial protection pillars by columns, crib or concrete pillars (high timber costs, potential fire, air leakage, gas, heat, water from the exploited area), some underground mines in the world have built artificial pillars to form continuous stone strips at the edge of the roadway to be protected, thereby ensuring tightness and good isolation of the area exploited. Artificial pillars have the same height as the coal seams exploited, the width depends on the bearing capacity and construction materials, but usually equal to 0.7÷1.1 times the thickness of seams. In Poland, materials used to build protective pillars are usually formed from a mixture of water, cement, fly ash and other solid aggregates to increase the compression resistance of the pillar. The pillar after construction from 6÷7 hours will freeze under pressure, after 28 days the compressive capacity can reach 24 MPa [6].

In China, the replacement of coal pillars with artificial pillars is also quite popular. It can be mentioned that Xin Yuan Mine (Yang Mei Coal Group, Shandong Province) applied this solution to protect the roadway along the seam and supply clean air for the synchronized mechanization longwall mining 3107 at the seam No.3. (thickness of 2.8m, slope angle of 40°). The roadway is anti-anchor reinforced plastic combined with cable anchors, width of 4.0m, and height of 2.8m, length of roadway of 1592m, depth of topographic terrain surface of 500m. The artificial strip pillar is constructed with a mineralized mixture (chemical) of high water content (chemical-water-additive ratio is 1-5-1), pillar's size: height x width is 2.8x2.0 m, pierced through the pillar's body are arranged with additional steel anchors to increase compression resistance. The results of application are good, the size of the road ensures the requirements, and the stable strip pillar is not destroyed, the maximum mine pressure affecting the pillar is 12.75 MPa, details are shown in Figure 4 [13].

a. Location of construction for artificial strip pillar b. The artificial pillar has been completed

Figure 4. Artificial pillar strip o the preparation roadway at Xin Yuan mine, Yang Mei Coal Group, Shandong Province

Besides the advantages of ease of construction, high bearing capacity, fast execution time, less shrinkage, good isolation of exploited areas, solutions for construction of artificial pillar by chemical materials with disadvantages: The point is high cost. Recently, a number of mines in China such as Duan Tai, Xi Nan, Wo Long Hu, Ping Mei, Da Zhuang, ... have used construction materials for artificial protection pillar of materials including mixed Combine fly ash, bottom ash of thermal power plant; combine a quantity of cement additive. The results of application are as good as chemical materials, while the cost is significantly reduced. At the same time, the use of fly ash and bottom ash also allows the settlement of a large amount of solid waste from thermal power plants in neighboring areas [8-12].

3. Potential of using artificial pillars to replace coal pillars to hold up preparation adits in Vietnamese underground mines

Evaluation results from applied 12 underground coal mines in Quang Ninh area (as Mao Khe, Vang Danh, Nam Mau, etc...) [1] showed that the reserves in the coal protection pillar are expected to be left in the mining process about 150.2 million tonnes, accounting for 16.25% of the total coal reserves (924.2 million tons). These are available reserves, will be zoned by the preparation roadway there its the longwall mining area, the reliability will be certain, if exploited, it will reduce the loss of resources and improve construction investment efficiency for mine, details see figure 6.

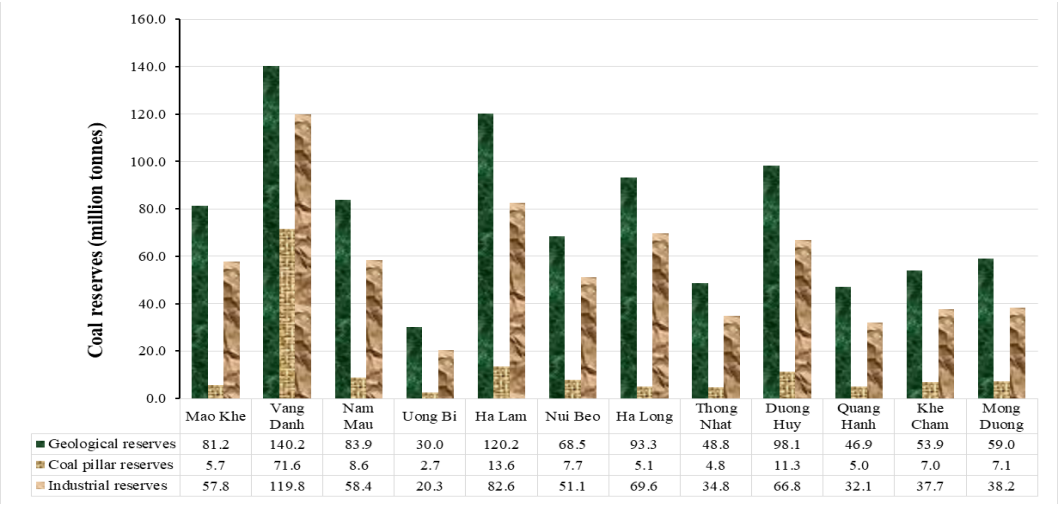

	Mao Khe	Vang Danh	Nam Mau	Uong Bi	Ha Lam	Nui Beo	Ha Long	Thong Nhat	Duong Huy	Quang Hanh	Khe Cham	Mong Duong
Geological reserves	81.2	140.2	83.9	30.0	120.2	68.5	93.3	48.8	98.1	46.9	53.9	59.0
Coal pillar reserves	5.7	71.6	8.6	2.7	13.6	7.7	5.1	4.8	11.3	5.0	7.0	7.1
Industrial reserves	57.8	119.8	58.4	20.3	82.6	51.1	69.6	34.8	66.8	32.1	37.7	38.2

Figure 6. Coal reserves distribution in protection pillars according to mine projects

For the Vietnamese mining industry, the width of the coal pillar protecting the preparation adit is usually determined according to the formulas of Professor Protodiakonov [5] as follows:

$$L_{tr} \geq \frac{\cos\alpha}{5} \times \zeta \times \sqrt{\frac{L_d \times H}{f}}, (m) \quad (1)$$

Where:
L_d - Length of slope direction of the longwall mining, m;
α - Slope angle of coal seam, degree;
H - Average mining depth, m;
f - Solid coefficient of floor rock according to the scale of Protodiakonov;
ζ - Coefficient refers to the strength of coal and roof rock.

From the formula (1) mentioned above, the depth of exploitation factor has a great influence and is proportional to the size of the protection coal pillar. Underground coal mines in Quang Ninh are exploiting the upper floors of the mine's project, the exploitation depth compared to the surface of the terrain is not large; the size of coal pillars protects in the preparation roadways. Has ranged from 15÷20m. According to the plan of the underground coal mines, in the coming time, it will have to dig deeper (550÷750m compared to the terrain surface [1], see Table 1 in detail), then the size of the protection pillar will increase, proportional to with it, coal losses also increase.

Table 1: Plan to go deep in some underground coal mines in Quang Ninh region

No.	Name of coal mine	Mining level		Average depth, m (calculated for the deepest level)
1	Ha Lam	Level I	-50 ÷ -300	550 ÷ 600
		Level II	-300 ÷ -450	
2	Nam Mau	Level I	+125 ÷ -50	645 ÷ 695
		Level II	-50 ÷ -200	
3	Vang Danh	Level I	±0 ÷ -175	700 ÷ 750
		Level II	-175 ÷ -300	
		Level II	-50 ÷ -150	
4	Duong Huy	Level I	+38 ÷ -100	590 ÷ 640
		Level II	-100 ÷ -250	
		Level III	-250 ÷ -350	
5	Thong Nhat	Level I	-35 ÷ -120	615 ÷ 665
		Level II	-120 ÷ -350	
6	Quang Hanh	Level I	-50 ÷ -175	500 ÷ 550

		Level II	-175 ÷ -300	
7	Mong Dương	Level I	-100 ÷ -250	650 ÷ 700
		Level II	-250 ÷ -400	
		Level III	-400 ÷ -550	
8	Khe Cham	Level I	-100 ÷ -300	550 ÷ 600
		Level II	-300 ÷ -450	

From the above analysis, combining experience in the world shows that the application of technology to exploit coal and use artificial pillars to replace coal pillars to protect preparation roadways in Vietnamese underground coal mines is very necessary and feasibility. However, due to the specific tropical climate, the annual rainy season is prolonged, the amount of heavy rainfall, meanwhile, at many mines when exploiting the upper layers, collapsing stone walls appears, and shifting the cracking of interconnects. To the surface of the terrain, the problem of surface water infiltrating / flowing into the exploited area, then exporting to the lower exploitation floor is entirely possible. Therefore, the solution use the artificial materials and structures to replace protective coal pillars applied in Vietnamese underground mines must have some adjustments to suit the actual conditions. On that basis, in the conditions of Vietnam, it is possible to apply some solutions to use artificial pillars to replace coal pillars to protect the preparation adits in the process of exploitation as follows:

- (1) Using artificial protection pillars are stone strips. To overcome the disadvantages of high shrinkage, wind leakage, it is possible to add a concrete mortar of low-grade concrete (cement or fly ash of thermal power plant) to the stone strip inserted after construction. This solution can be applied to reservoir conditions up to 2.0m thick, the area is less affected by surface water and groundwater. For details see Figure 7.

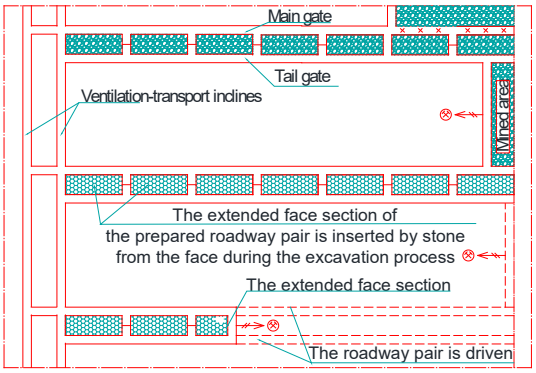

a. Stone strips in mining longwall system along the strike

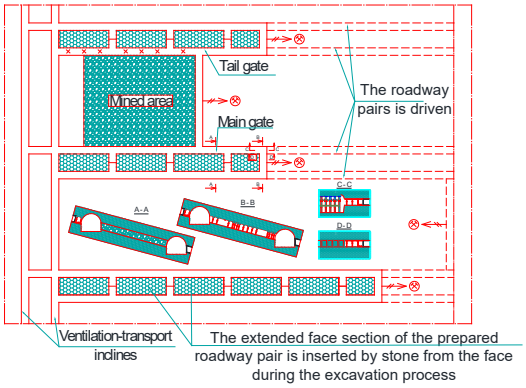

b. Stone strips in longwall system with simultaneous mining and driving roadway

Figure 7. Artificial pillars formed by stone backfill

- (2) Using artificial protection pillars are in the form of wooden crib structured (inside filled with waste rock, sand bags or mineralized materials) or by concrete pillars: This type of artificial pillar can be applied to seam conditions has large thickness (experience at Ziemowit mine is up to 4.5m). Similar to the solution of using stone inserts, the structure of artificial pillars of this type is also not suitable for application in areas affected by surface water and groundwater. In particular, in the coal seam area with self-burning coal characteristics, this solution will not be applied due to the disadvantages of wind leakage into large mining areas, easily leading to the burning of protection coal pillars in the area.

- (3) Using artificial protection pillars in continuous strips: Materials used to build artificial pillars are chemical materials (chemical mineral) or concrete mixes including fly ash, bottom ash of thermal power plants, combined a quantity of cement additives (Figure 8). This solution will be suitable to use for many conditions of different seam thickness, good isolation ability should be applied to areas affected by surface water, groundwater as well as in coal mining conditions. Capable of self-igniting. Besides, in the conditions of Vietnam, Quang Ninh province is currently the province with the most coal-fired power plants in the country with a total generating capacity of about 5,550 MW, equivalent to the amount of ash discharged annually about 7.5 million tons/year, is a huge challenge for thermal power plants in storage and handling issues to ensure the safety of the living environment of local residents and the regional landscape. If it is possible to use ash to build artificial pillars to protect the preparation adits during coal mining in the underground mines of Quang Ninh, at the same time as reducing coal loss, it will also contribute to reducing the pressure load. Above forces for thermal power plants.

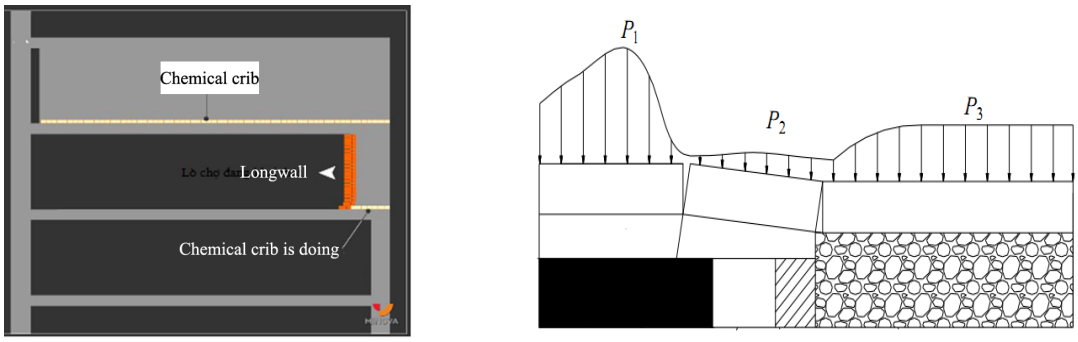

a. Diagram of construction the strip pillars b. Expected changing the pressure of the force on the strip pillar

Figure 8. Technological diagram of exploitation and use of artificial pillars made of chemicals or concrete mixtures

4. Conclusion

Applying technology to use artificial pillar to replace coal pillars to hold up the preparation roadways during coal mining in Vietnamese underground coal mines is necessary to reduce the loss of non-renewable coal resources and the cost for a meter of preparation adits, production costs and improve the efficiency of mine construction investment. However, the Vietnamese mining industry has not had much experience; there is also no in-depth research on this field. The solutions given by the authors in the basic scope of the report only at the proposed level based on foreign experience. Therefore, in order to meet the requirements of Vietnam's coal industry, it is necessary to study and cooperate with experienced foreign partners (eg Poland) to jointly research and apply the technology testing using artificial pillars to replace protective coal pillars in real conditions at Vietnamese underground coal mines, as a basis for evaluating, improving and replicating technology.

References

1. Investment project for construction of underground coal mines in Quang Ninh, Vietnam.

2. Проведение штреков широким забоем на шахте «Центральная-Боковская», бюллетень ЦИТИ (1957).

3. Разработка угольных пластов без выдачи породы на поверхность, Косович В.Л., 125с, Углетехниздат (1958).

4. Краткий справочник горного инженере угольной шахты, Бойко А.А., 642с, Москва (1963).

5. Задачик по подземной разработке угольных месторождений..

6. Piotr Niełacny, *Praca doktorska: Dobór technologii utrzymywania wyrobisk przyścianowych w jednostronnym otoczeniu zrobów na podstawie pomiarów przemieszczeń górotworu,* Akademia Górniczo-Hutnicza w Krakowie (2009).

7. Waldemar Korzeniowski, Krzysztof Skrzypkowski (2012), Badania porównawcze nośności i chrakterystyk obciążeniowo-odkształceniowych kasztów o różnym wypełnieniu, Przegląg Górniczy, **Nr 4**, 36-40, (4/2012).

8.**刘德明**, 赵平谦, **晏立森**. **平煤股份一矿戊**8-22180**工作面沿空留巷膏体充填材料的**应用研究[J]. 华东科技:**学**术版, 372-372, (8/2013).

9. **柳成懋**, **戚洋**. **沿空留巷膏体充填工作面**顶板控制技术[C]. **全国采**矿学术会议 (2015).

10. 张大虎, **范祥峰**. **膏体充填沿空留巷技**术在卧龙湖煤矿的应用[J]. **安徽科技**, 50-51, (8/2010).

11. 张年有. **膏体充填沿空留巷技**术研究[J]. **煤**矿现代化, 4-6, (1/2017).

12. **刘国磊**, **温朋朋**, 贾广辉. 济阳煤矿膏体充填沿空留巷技术[J]. **煤**矿安全, 43(12):94-96 (2012)

13. 张自政, **博士学位**论文: **沿空留巷充填区域直接**顶稳定机理及控制技术研究, **中国**矿业 (2015)


Geology
Geophysics

Pure SiO_2 extraction through aluminosilicates synthesis from incinerated solid wastes

Vu Dinh Hieu[1,*], BUI Xuan Nam[1], BUI Hoang Bac[2], NGO Thi Thanh Nga[3]

[1] Faculty of Mining, Hanoi University of Mining and Geology, Duc Thang, Bac Tu Liem, Hanoi, Vietnam
[2] Faculty of Geology, Hanoi University of Mining and Geology, Duc Thang, Bac Tu Liem, Hanoi, Vietnam
[3] Institute of Hydropower and Renewable Energy, 8/95 Chua Boc, Dong Da, Hanoi, Vietnam

Abstract. In this study, Pure SiO_2 solution extraction from incenerated solid wastes following after aluminosilicate synthesis. The optimum conditions for obtaining both the pure SiO_2 solution and the substantial amounts of unique residue material should be 200°C of reaction temperature, 1:30 of sample:NaOH, 2M NaOH, and enough reaction time over 24 hours. The optimization of the pure SiO_2 extraction proposes an effective way for recycling the abundant incinerated solid waste as well as other waste ashes.

Keywords: Solid wastes, Coal fly ash, Synthesis, SiO2 solution extraction

1. Introduction

In Vietnam, many incinerators have been built for disposing waste and also for generating electric power. Incineration is one of effective ways to reduce the great volume and weight of municipal solid waste (MSW). However, in terms of byproduct, incinerating MSW has produced a big amount of solid residual materials daily. The solid residual material is also a waste, called the incinerated solid waste, which is generally hazardous in nature. Due to the limited landfill space and environmental problems, the recycling of this solid waste is a necessary and burning issue.

Recently, several approaches have been made to minimize the environmental impacts from coal fly ash as well as to recycle them effectively. As the main components of the coal fly ash are similar to these of natural zeolites with high amount of SiO_2, Al_2O_3, one of the most common approaches for recycling this ash is converting to different types of zeolite such as phillipsite, zeolite Na-P1, zeolite X and faujasite [1] [2] [3]. Zeolites are useful materials with high ion exchange property and are usually applied to environmental treatment such as uptake of heavy metals from polluted waste water [4] [5] [6].

Similar to coal fly ash, chemical composition of the incinerated solid waste mainly consists of SiO_2 and Al_2O_3. Some reports of conversion this type of waste to zeolite have been published. Yang *et al*. successfully synthesized zeolite from the municipal incinerator fly ash [7]. Fan *et al*. synthesized zeolite X and hydroxy-sodalite from waste ash from MSW and coal co-combustion power plant and applied them to Zn^{2+} contaminated wastewater treatment [8]. In practice, during processing of zeolite synthesis, Si and Al are the major components extracted from the raw waste ash with other cations such as Na, K, Ca, and Mg to form zeolites. The previous studies were only focused on synthesizing zeolites using some waste raw materials, but not concerned about residual solution after synthesizing zeolites. In general, if some aluminosilicate, such as zeolites, are synthesized from the waste raw material with high Si content, a substantial amount of dissolved Si

* Corresponding author: vudinhhieu@gmail.com

would be fixed into the structure of synthesized phases with Al and other cations, but the excess of Si would still remain in the residual solution as the only dominant cation. That is, the synthesized aluminosilicates would be a great role filtering the dissolved cations from the solution. The purity and quantity of dissolved Si in the solution should be determined by the type, quantity, and quality of synthesized aluminosilicate, which is depending on the factors, such as the reaction temperature, the ratio of solid/solution, the concentration of NaOH solution, and the reaction time. In this study, the authors considered how to extract the pure SiO_2 solution effectively from the incinerated solid waste following after aluminosilicate synthesis. Several researchers have tried to extract pure SiO_2 from coal fly ash in the previous step for zeolite synthesis [9] [10] [11], but not to get pure SiO_2 as a final product. The pure SiO_2 can be used for industrial applications as fumed silica, raw material for semiconductor, and a source for synthesis of zeolite and other silicates, etc.

In this study, we considered how to extract the pure SiO_2 solution effectively from the incinerated solid waste following after aluminosilicate synthesis. Several researchers have tried to extract pure SiO_2 from coal fly ash in the previous step for zeolite synthesis, but not to get pure SiO_2 as a final product. Therefore, the objective of this study is to establish the optimal condition for the pure SiO_2 extraction and to define the factors, controlling the purity and quantity of the extracted SiO_2. The results may be applied to effectively recycling a huge amount of the incinerated solid waste from municipal incineration plants as well as other sources of waste ashes.

2. Experimental

2.1. Materials

The incinerated solid waste samples used in this study were collected from a municipal incineration plant of the Uong Bi Thermal Power Plant at Uong Bi City, Quang Ninh Province. These were considered to be representative of the production of that plant. Depending on the cooling methods after incineration, the solid wastes were divided into two types. One was cooled quickly using water (WCS, water cooling sample) and the other was cooled by air condition (ACS, air cooling sample). For each type of sample, it was ground into small particles by using ball-mill grinder for 15 minutes and then mixed thoroughly. The powder with under 75μm (200-mesh sieve) in particle size was used to synthesize zeolite and to extract SiO_2 in next steps. Coal fly ash sample was also obtained from the Cam Pha thermal power plant for comparison.

2.2. Pure SiO_2 extraction

The mixture of ground sample (3.3 ~ 30 g) and NaOH solution in determined ratios (1:10, 1:20, and 1:30 g ml^{-1}) was reacted at different temperatures (100, 150 and 200 ºC) for different reaction time (1 ~ 9 days) in autoclave system. The concentration of NaOH solution is also tested with different cases of 1, 2, and 5 M. 25 experimental cases with different conditions were examined. The reacted solution was then filtered through a membrane of 0.45 μm. The obtained products include the solid residue and the residual Si-rich solution. The solid residues containing the synthesized zeolite-type materials were washed with distilled water several times and dried at 100 ºC for 1 day. The concentrations of Si and Al in the extracted solution were determined by using ultraviolet-visible spectroscopy (UV) for checking the purity and quantity of Si in the solution.. The experimental scheme for the SiO_2 extraction process is shown in Figure 1.

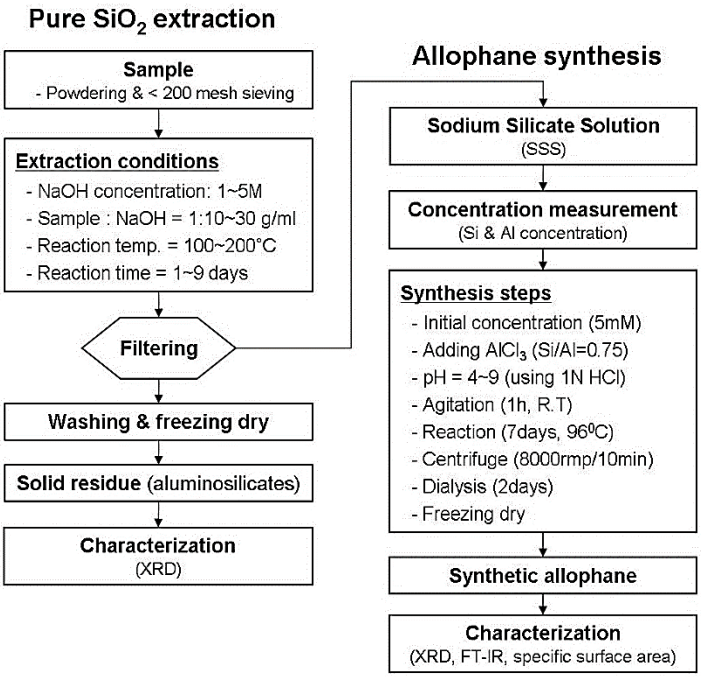

Figure 1. Schematic diagram showing the procedure for the pure SiO2 extraction from the incinerated solid wastes through zeolite synthesis.

2.3. Characterization

The characteristics of the incinerated solid wastes and synthesized minerals were determined by using various techniques such as X-ray diffraction (XRD) analysis, scanning electron microscope (SEM) with energy dispersive X-ray spectroscopy (EDX), Fourier Transform Infrared (FT-IR) spectroscopy, and specific surface area measurements (BET).

X-ray powder diffraction patterns of the incinerated solid wastes and synthesized minerals were measured using a Mac Science MXP-3 model powder diffractometer with Cu-Kα radiation at 40 kV and 30 mA. All samples were scanned from 2 to 70° at a goniometer rate of $2\theta = 2°min^{-1}$. Crystalline phases of materials presenting in the sample were identified by using the software named Joint Committee of Powder Diffraction Standards (JCPDS). The relative percentages of the synthesized minerals were calculated by using FULLPAT method for XRD patterns (Chipera et al., 2002). The morphological properties and major elements of the incinerated solid wastes and synthesized minerals were examined by using the scanning electron microscope (SEM) with energy dispersive X-ray spectroscopy (EDX) [JEOL, JMS 5800]. The FT-IR spectra for the synthesized minerals were obtained in transmission mode on pellets containing a pressed mixture of approximately 1.5 mg of the sample and 100 mg of KBr. The IR spectra were recorded in the range between 4000 and 400 cm^{-1} (PerkinElmer) with 200 scans. The specific surface area of the products containing zeolites was measured from N_2 gas adsorption at 77 K by using NOVA 3200 BET instrument, Quantachrome Corporation, USA.

3. Results and discussion

3.1. The incinerated solid waste properties

The chemical compositions of the raw samples and coal fly ash are shown in Table 1. The incinerated solid wastes (ACS and WCS) contained mainly SiO_2 (45.68~47.07 wt.%), Al_2O_3 (10.25~12.40 wt.%), CaO (10.80~16.14 wt.%), and a little amount of oxides of Fe, Mg, Na, Mg, K, P, Ti etc. The high content of CaO may be due to the addition of lime into the incinerator. Some difference in bulk composition between ACS and WCS is probably due to the inhomogeneity of incinerated solid wastes. Coal fly ash was characterized by the relatively high SiO_2 (49.97 wt.%) and the low CaO (3.59 wt.%) contents. The powder of incinerated solid waste with sizes under 75 μm includes solid particles (SEM images are not shown here), which are different from coal fly ash particles with hollow sphere structure [12].

Table 1. Objectives of management in mineral operation.

Component	Incinerated solid wastes (wt. %)				Coal fly ash (wt. %)	
	Air cooling		Water cooling			
SiO_2	45.68		47.07		49.97	
TiO_2	0.66		0.33		1.38	
Al_2O_3	10.25		12.40		21.64	
FeO*	6.20		3.13		8.35	
MgO	2.80		3.66		1.42	
MnO	0.28		0.78		0.23	
CaO	16.14		10.80		3.59	
Na_2O	7.56		9.07		0.56	
K_2O	0.99		0.75		2.83	
P_2O_5	4.65		5.01		3.64	
V_2O_5	0.34		0.64		0.49	
Cr_2O_3	1.24		0.85		2.01	
NiO	0.52		1.34		0.74	
ZnO	1.87		1.55		2.39	
PbO	0.80		1.33		0.77	

* Total Fe treated as FeO.

The XRD pattern of the incinerated solid shows a big hump of between 20 to 35º of 2θ, indicating the presence of a large amount of amorphous phases in the sample (Figure 2a and 2b), while that of coal fly ash indicates that quartz (SiO_2) and mullite ($3Al_2O_3 \cdot 2SiO_2$) are main crystalline phases in the sample (Figure 2c) The BET specific surface area of the incinerated solid wastes powder passed through 200-mesh sieve is around 0.5 $m^2 g^{-1}$.

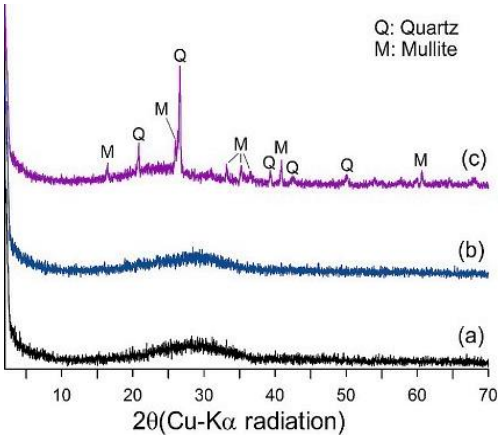

Figure 2. XRD patterns of air cooling sample (ACS) (a), water cooling sample (WCS) (b), and coal fly ash (c)

The high content of SiO_2 in chemical composition and the presence of a substantial amount of amorphous aluminosilicates in the samples strongly support that the incinerated solid wastes should have a great potential as raw materials for effective recycling through aluminosilicate synthesis and pure SiO_2 extraction.

3.2. Characterization of residues

Some crystalline materials were synthesized as by-product residues during the extraction experiments. The type of crystalline phases and the percentage of each type, and the total percentage of the crystalline phases were determined using XRD analysis and considered as the potential factors controlling the purity and quantity of extracted SiO_2 solution.

These residues were identified by XRD measurements and the patterns were shown in Figure 3 and 4. Hydroxysodalite ($4Na_2O{\cdot}3Al_2O_3{\cdot}6SiO_2{\cdot}H_2O$), tobermorite ($Ca_5(OH)_2Si_6O_{16}{\cdot}4H_2O$), Na-P1 zeolite ($Na_6Al_6Si_{10}O_{32}{\cdot}12H_2O$), hydroxycancrinite ($Na_{14}Al_{12}Si_{13}O_{51}{\cdot}6H_2O$), and pectolite-1A ($NaCa_2HSi_3O_9$) were identified as the main materials and the relative percentages of the minerals for each experimental condition were listed in Table 2.

Tobermorite, the Ca-rich silicate, was observed as a major component in most conditions for both ACS and WCS (7.8~38.5 %), except the conditions at 200°C for 72 hours for WCSs (No.22 and 24 in Table 2), where pectolite-1A, another Ca-rich silicate was identified as a dominant phase (20.6~31.7 %), instead of tobermorite. It is likely that tobermorite was transformed to pectolite-1A by increasing the reaction time at 200°C. The dominant occurrence of the Ca-rich phases should be due to high Ca content in bulk composition. Hydroxysodalite (8.6~22.2 %) and Na-P1 zeolite (3.9~12.4 %) were found in most conditions at 100°C reaction temperature, while hydroxycancrinite was identified as a dominant component only in the condition at 200°C for both ACSs (24.4~41.9 %) and WCSs (12.4~31.2 %) (Figure 3~4 and Table 2). The material in experimental condition of No.14 (200°C, 1:10 ratio, 5M NaOH, 36 hours) was matched well with typical hydroxycancrinite (PDF 46-1457) as a dominant phase (41.9 %), but the others in the conditions at 200°C were matched more with hydroxycancrinite-type unnamed phase (PDF 31-1270) as one of major phases (24.4~39.1 % for ACSs and 12.4~31.2 % for WCSs, Table 2).

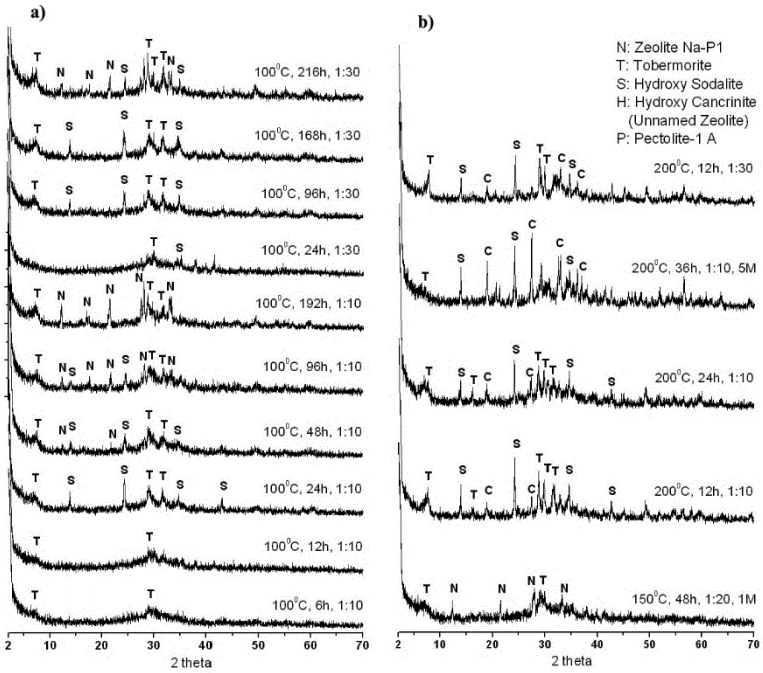

Figure 3. XRD patterns of the synthetic products of air cooling samples (ACSs) at 100°C (a) and 150~200°C (b) with the different experimental conditions.

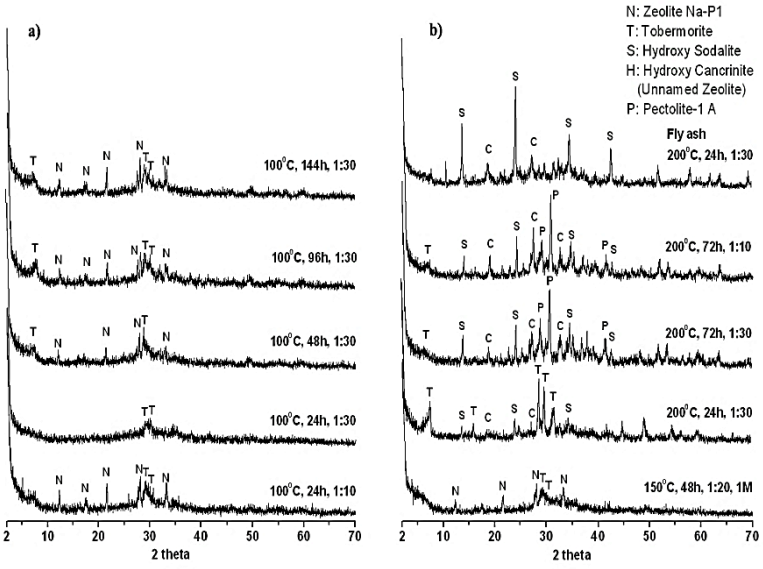

Figure 4. XRD patterns of the synthetic products of water cooling samples (WCSs) at 100°C (a) and 150~200°C (b) with the different experimental conditions.

The sums of the percentage of synthesized residues at 200°C (No.12~15 for ACSs and No.22~24 for WCSs in Table 2) were much higher than those at 100~150°C, indicating that the dissolution and crystallization reactions were much more active at 200°C. There was no distinct difference in the sums of the percentage of synthesized minerals between 1:10 and 1:30 of sample:NaOH ratio at 200°C. For the coal fly ash raw material, hydroxycancrinite-type phase (unnamed, PDF No. 31-1270) appeared as a dominant phase (71.6 %) with a little amount of tobermorite (7.8 %) at 200°C, 24 hours, 1:30 of sample:NaOH ratio, and 2M NaOH experimental condition (No.25 in Table 2), probably due to the difference in bulk composition. Most of XRD patterns show a little hump between 20 to 35º of 2θ, indicating that a significant amount of amorphous phases still remained in the sample.

The existence of the synthesized materials in the reacted residues was also confirmed by SEM analysis. Figure 5 shows the scanning electron microscope (SEM) and EDX chemical data of some synthesized materials at the representative conditions. Ca-rich aluminosilicate, tobermorite, was observed in the condition at 200°C, 24 hours, 1:30 ratio, and 2M NaOH for WCS (Figure 5a, No. 23 in Table 2), hydroxysodalite was in the condition at 100°C, 24hours, 1:10 ratio, and 2M NaOH for ACS (Figure 5b, No. 3 in Table 2), and hydroxycancrinite was in the condition at 200°C, 36hours, 1:10 ratio, and 5M NaOH for ACS (Figure 5c, No. 14 in Table 2). In general, most of the obtained synthetic materials showed crystalline forms with various size, but not typical, and the substantial amounts of incinerated solid wastes still remained in the reacted residues, indicating the dissolution and crystallization reactions were not undergone completely under the given alkaline conditions.

The specific surface area of the representative synthetic product containing zeolites is 41 m^2g^{-1} for ACS at 200°C of reaction temperature, 1:30 of sample/NaOH ratio, 12 hours of reaction time, 2M of NaOH concentration, and 54 $m^2 g^{-1}$ is for WCS at 200°C of reaction temperature, 1:30 of sample/NaOH ratio, 24 hours of reaction time, 2M of NaOH concentration.

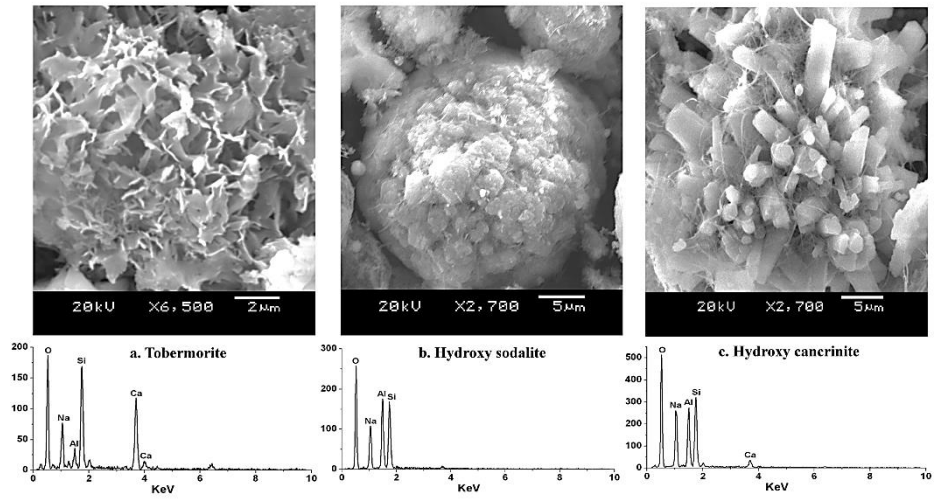

Figure 5. SEM images of the synthesized minerals with the EDX chemical data. {(a) tobermorite at 200°C of reaction temperature, 1:30 of sample/NaOH ratio, 24 hours of reaction time, and 2M of NaOH concentration for WCS (No.23 in Table 2); (b) hydroxysodalite at 100○C of reaction temperature, 1:10 of sample/NaOH ratio, 24 hours of reaction time, and 2M of NaOH concentration for ACS (No. 3 in Table 2); (c) hydroxycancrinite at 200°C of reaction temperature, 1:10 of sample/NaOH ratio, 36 hours of reaction time, and 5M of NaOH concentration for ACS (No.14 in Table 2)}.

3.3. Pure SiO_2 extraction

The results for all experimental conditions of SiO_2 extraction were summarized in Table 2. The reaction temperature, sample/NaOH solution ratio, reaction time, and the concentration of NaOH solution were considered as the factors controlling the purity and quantity of extracted SiO_2. The concentrations of Si and Al in the extracted solution and the yields of extracted SiO_2 for each condition were also suggested in Table 2. The weight and the yield of extracted SiO_2 from the solid waste were calculated using the equations as follows.

$$SiO_2\,(g) = \frac{Si\ conc.\ in\ solution\ (mg/l)}{1000} \times \frac{60.085\,(SiO_2\ molecular\ weight)}{28.086\,(Si\ atomic\ weight)} \times \frac{Solution\ volume\ (ml)}{1000}$$

$$Yield\ of\ SiO_2\ extraction\ (\%) = \frac{Extracted\ SiO_2\ (g)}{Weight\ percentage\ of\ SiO_2\ in\ sample \times Sample\ weight\ (g)} \times 100$$

The results revealed that the yields (%) of WCS (6.81 ~ 24.40) were generally higher than those of ACS (3.07 ~ 15.67). For the ACSs, the concentrations of Al were still high (19.4 ~ 59.5 mg/l) until 48 hours reaction time with the low values (about 4%) of SiO_2 yields at 100°C and 1:10 of sample/NaOH ratio (No.1~4 in Table 2), indicating that the conditions were not enough for dissolving the raw sample and for synthesizing aluminosilicates. As mentioned above, the dissolved Al and cations can be removed from the solution by being fixed into the structure of synthesized aluminosilicates during the reaction. The concentrations of Al decreased steeply (<10 mg l^{-1}) after reacting for 96 hours, due to relatively enough time for zeolite synthesis (No.5~6 in Table 2). At 100°C and 1:30 of sample/NaOH ratio, the extracted solutions were also pure (low Al concentrations) after reacting for 96 hours, with the steep increase of SiO_2 yields (7.24~14.23 %) (No.7~10 in Table 2). At 200°C and 1:10 of sample/NaOH ratio, Al concentrations were less than 5mg/l in spite of the relatively short reaction time (<36 hours), but the SiO_2 yields were very low (3.1~5.6%) (No.12~14 in Table 2). However, the SiO_2 yield dramatically increased to 15.7% at 1:30 ratio with keeping Al concentration low (5.3 mg l^{-1}) (No.15 in Table 2). There is no distinct change in the yield of SiO_2 extraction at 5 M NaOH and 1:10 ratio (3.09 %) (No.14 in Table 2). At 150°C, 1:20, 1M NaOH, and 48 hours conditions, the SiO_2 yield was relatively good (12.7 %) (No.11 in Table 2).

For the WCSs, the concentrations of Al were less than 10 mg l^{-1} for most of experimental conditions, except No. 18 (11.6 mg l^{-1}, Table 2) at 100°C, 1:30, 48 hours, and 2M NaOH. The SiO_2 yield was 6.81 % at 1:10 and 100°C (No.16 in Table 2), while those were 13.1~16.6 % at 1:30, 100°C, and 24 ~ 144 hours reaction time (No.17~20 in Table 2). There is no distinct change in the yield of SiO_2 extraction at 150 °C, 1:20, 1 M NaOH, and 48 hours conditions (14.0 %) (No.21 in Table 2). The SiO_2 yield was maximum (24.4 %) at 200 °C, 1:30, and 24 hours reaction time (No.23 in Table 2), but that is minimum (8.33 %)

at 200 °C, 1:10, and 72 hours reaction time (No.22 in Table 2). For the coal fly ash, the SiO_2 yield was 13.9 % at 200 °C, 1:30, and 24 hours reaction time (No.25 in Table 2).

3.4. Controlling factors pure SiO2 extraction

The experimental results of this study can be summarized as follows; (1) tobermorite, the Ca-rich silicate, was synthesized as a major component in most conditions for both ACS and WCS, except the conditions at 200 °C for 72 hours for WCSs, where pectolite-1A, another Ca-rich silicate, was identified as a dominant phase, instead of tobermorite, (2) hydroxycancrinite formed as a major phase at 200 °C of reaction temperature, not depending on the sample/NaOH ratio, (3) the SiO_2 yield dramatically increased at 1:30 of sample/NaOH ratio and 200 °C rather than at 1:10 and 100°C with keeping Al concentration low, even at the short reaction time, (4) the SiO_2 yields for WCSs were much higher than for ACSs (Table 2).

Table 2. Summary of the experimental conditions, the percentage of synthesized minerals, and the yield of SiO_2 extraction. {[1] Hydroxysodalite (PDF 41-0009), [2] Tobermorite (PDF 19-0050, 19-1364), [3] Zeolite Na-P1 (PDF 39-0219), [4] Hydroxycancrinite (PDF 46-1457), or Unnamed zeolite (PDF 31-1270), and [5] Pectolite-1A (PDF 33-1223). "-" indicates to negligible values, or not detected in XRD patterns}

No.	Reaction conditions	Percentage of synthesized minerals					Solution conc.		SiO_2 solid
	Temp.-Solid-Ratio-Time-NaOH	HS[1]	T[2]	N[3]	H[4]	P[5]	Si	Al	Yield
	[(°C)-(g)-(g/ml)-(h)-(M)]	(%)	(%)	(%)	(%)	(%)	(mg/l)	(mg/l)	(%)
	I. Air Cooling Samples (ACSs)								
1	100-10-1:10-6-2	-	8.99	-	-	-	745.0	59.5	3.94
2	100-10-1:10-12-2	-	11.35	-	-	-	728.3	48.0	3.85
3	100-10-1:10-24-2	22.16	14.54	-	-	-	774.9	20.2	4.09
4	100-10-1:10-48-2	12.31	13.11	3.86	-	-	716.7	19.4	3.79
5	100-10-1:10-96-2	8.59	9.5	5.9	-	-	770.3	8.3	4.07
6	100-10-1:10-192-2	-	14.77	12.37	-	-	581.5	3.1	3.07
7	100-20-1:30-24-2	-	8.45	-	-	-	491.6	56.9	7.79
8	100-3.3-1:30-96-2	15.36	15.17	-	-	-	888.9	4.3	14.23
9	100-3.3-1:30-168-2	20.01	15.17	-	-	-	456.0	8.4	7.30
10	100-3.3-1:30-216-2	8.58	22.15	8.72	-	-	452.6	4.3	7.24
11	150-25-1:20-48-1	-	13.64	8.86	-	-	1203.0	9.7	12.70
12	200-30-1:10-12-2	-	27.93	-	39.12	-	1056.0	2.4	5.58
13	200-30-1:10-24-2	-	17.55	-	24.37	-	845.7	3.4	4.47
14	200-30-1:10-36-5	-	7.8	-	41.87	-	584.3	-	3.09
15	200-10-1:30-12-2	-	28.81	-	28.44	-	988.7	5.3	15.67
	II. Water Cooling Samples (WCSs)								
16	100-10-1:10-24-2	-	14.99	8.84	-	-	1433.5	3.5	6.81
17	100-20-1:30-24-2	-	10.11	-	-	-	1166.4	5.3	16.60
18	100-3.3-1:30-48-2	-	15.71	7.93	-	-	1056.1	11.6	15.20
19	100-3.3-1:30-96-2	-	14.76	8.96	-	-	1043.2	7.2	15.00
20	100-3.3-1:30-144-2	-	14.48	10.11	-	-	910.5	2.0	13.10
21	150-25-1:20-48-1	-	11.64	8.84	-	-	1467.1	3.8	14.00
22	200-30-1:10-72-2	-	-	-	31.16	31.69	1751.3	4.8	8.33
23	200-10-1:30-24-2	-	38.5	-	12.43	-	1709.2	6.2	24.40
24	200-10-1:30-72-2	-	-	-	22.00	20.62	1612.4	3.9	23.00
	III. Coal Fly Ash								
25	200-10-1:30-24-2	-	7.82	-	71.66	-	1174.1	4.7	13.90

These results strongly suggest that only for the maximum yield of pure SiO_2 extraction, the conditions with 1:30 of sample/NaOH ratio and 200 °C of reaction temperature should be required. The reaction time was not an essential factor for increasing the yield of pure SiO_2 extraction, but it was an important factor determining the quantity of synthesized zeolite. For example, the percentage of hydroxycancrinite showed a little increase at 72 hours reaction times with no significant change in the yield of SiO_2 extraction (No. 25 in Table 2). The reaction t [1]emperature is a critical factor controlling not only the yield of SiO_2 extraction, but the zeolite type (hydroxysodalite and/or Na-P1 zeolite at 100°C, and hydroxycancrinite at 200 °C) and the quantity (sum of zeolite percentage; 7.9 ~ 22.2% at

100°C, 12.4 ~ 41.9% at 200°C, Table 2). The increase of NaOH concentration should be a factor to improve zeolite synthesis, but to reduce significantly the yield of SiO_2 extraction (No.14 in Table 2). The higher SiO_2 yields for WCSs rather than those for ACSs indicate that the fast cooling of the melted wastes in incinerator is better for the SiO_2 extraction, owing to the increase of amorphous form. The existence of Ca-rich silicates, tobermorite and pectolite-1A, is a critical factor reducing the pure SiO_2 yield by fixing a substantial amounts of Si into the structure, depending on the molar ratio of Ca:Si in the chemical formula. If the lime addition was minimized, the yield of SiO_2 extraction should be increased distinctly, and a single type of zeolite can be synthesized.

On considering all experimental results, the optimum conditions for obtaining both pure SiO_2 and the substantial amounts of unique zeolite should be 200 °C of reaction temperature, 1:30 of sample/NaOH, 2 M NaOH, and enough reaction time over 24 hours.

4. Conclusions

In this study, we have successfully extracted the pure SiO_2 solution from the hazardous incinerated solid wastes using alkaline dissolution method. The experimental results can be summarized by the dramatic increase of pure SiO_2 yield at 1:30 of sample:NaOH ratio and 200°C, even at the short reaction time, and the relatively high SiO_2 yields for WCSs rather than ACSs. The high ratio of sample:NaOH was inevitable for keeping high purity, high concentration, and high yield of SiO_2 solution, though it was not proper for economical extraction. The types of the solid residues precipitated during the reaction had an important role to control purity and yield of the extracted pure SiO_2 solution. While the formation of Ca-rich silicates, tobermorite and pectolite-1A, was a critical factor reducing the yield of the pure SiO_2 solution by fixing a substantial amounts of Si into the structure. Therefore the yield of SiO_2 extraction and the quality of residue materials can be improved distinctly by minimizing the addition of Ca-lime into the incinerator.

In conclusion, the optimum conditions for obtaining both the pure SiO_2 solution and the substantial amounts of unique residue material should be 200°C of reaction temperature, 1:30 of sample:NaOH, 2M NaOH, and enough reaction time over 24 hours. The optimization of the pure SiO_2 extraction proposes an effective way for recycling the abundant incinerated solid waste as well as other waste ashes.

Acknowledgements

This work was financially supported by National Foundation for Science and Technology Development (NAFOSTED) under grant number 105.08-2014.10.

References

1. C. J. Park M, "Synthesis of philipsite from fly ash," *Clay Science*, vol. 9, pp. 219-229, 1995.
2. J. Y. K. U. N. I. Tanaka N, "First observation of SiO2/Si(100) intergaces by spherical aberration-corrected high-resolution transmission electron microscopy," *Journal of Electron Microscopy*, vol. 52, pp. 69-73, 2003.
3. M. S. P. C. J. P. I. S. Gross M, "Synthesis of fauiasite from coal fly ashes under smooth temperature and pressure conditions: A cost saving process," *Microporous and Mesoporous Materials*,, vol. 104, pp. 67-76, 2007.
4. L. S. L. H. L. Y. Lin C.F, "Stabilization of cadmium contaminated soils using synthesized zeolite," *Journal of Hazardous material*, vol. 60, pp. 217-226, 1998.

5. Q. X. A. C. Moreno N, "Utilisation of zeolites synthesized from coal fly ash for the purification of acid mine water," *Environmental Science & Technology*, vol. 35, pp. 3526-3534.
6. Z. A. A. E. G. M. El-Kamasha A.A, "Modeling batch kinetics and thermodynamics of zinc and cadmium ions removal from waste solutions using synthetics zeolite," *Journal of Hazardous Materials*, pp. 211-220, 2005.
7. Y. T. Y. Yang G C C, "Synthesis of Zeolite from municipal incinerator fly ash," *Journal of Hazardous Materials*, vol. 62, pp. 75-89, 1998.
8. Z. F. Z. J. L. Z. Fan Y, "Effective utilization of waste ash from MSW and coal co-combustion power plant - Zeolite synthesis," *Journal of Hazardous Material*, vol. 153, pp. 382-388, 2008.
9. S. G. J.-J. M. Hollman G.G, "A two-step process for the synthesis of zeolites from coal fly ash," *Fuel*, vol. 78, pp. 1225-1230.
10. E.-K. A. E.-D. M. El-Naggar M.R, "Two-step method for preparation of NaA-X zeolite blend from fly ash for removal of cesium ión," *Journal of Hazardous Materials*, vol. 154, pp. 963-972, 2008.
11. Q. X. L.-S. A. A. J. J. M. N. H. T. M. S. K. Moreno N, "Determining suitability of fly ash for silica extraction and zeoloite synthesis," *Journal of Chemical Technology and Biotechnology*, vol. 79, pp. 1009-1018, 2004.
12. K. A. G. Kutchko B.G, "Fly ash characterization by SEM-EDM," *Fuel*, vol. 85, pp. 2537-2544.

Opiekun: prof. dr Jadwiga Jarzyna

Recenzent: Taki GÜLER, takiguler@mu.edu.tr

lub Ercan POLAT, epolat@mu.edu.tr (zaczerpnęłam z Inżynieria Mineralna, 2017)

Recenzent: Paulina Nowak paulina-nowak@gkpge.pl

Methods of adjusting geophysical parameters in the calculation of numerical simulation of an oil and gas reservoir to obtain reliable simulation results

TOAN Phan Trong*

PVEP PetroVietnam Exploration Production Corporation, Branch in Ho Chi Minh city, Vietnam

Abstract. The method of numerical simulation is widely used today to manage the flow obtained from an oil/gas reservoir. However, the geophysical data provided for the simulation program is unreliable, so the numerical simulation results in large errors compared to reality. The paper presents some methods for correcting geophysical data in numerical simulation to obtain reliable simulation results.

Introduction

Natural gas and oil are gathered from reservoir by production wells. The assessment of oil and gas reserves in reservoirs, the forecast of production flow and management of reservoir resources and others often uses the Digital Simulation Technology (DST) widely. However, the results of DST are difficult to match the actual reservoir conditions.

The change in pressure in the reservoir gives us a picture of the moving of oil and gas in the reservoir, so that most of the digital simulation problem will calculate the pressure distribution in the reservoir in a time period of any. Pressure at any position in the reservoir can be calculated from the digital simulation, while the pressure measurement at that position is not possible. Therefore, numerical simulation results always need more measurement data to standardize. In fact, it is only possible to measure pressure in the reservoir at some locations with wells. Therefore, the measurement data is not sufficient to standardize digital simulation results.

This article presents some experience to accurately determine of geophysical parameters while solving the digital simulation problem to increase conformity actual of digital simulation results.

Reservoir pressure field determination by numerical simulation

The structure of petroleum reservoir consists of several layers overlapping dimensional oz. The thickness of each layer is very small comparing to the length and width of the layer.

---

*Author email: toanpt@pvep.com.vn

On the other hand, vertical permeability in the reservoir is very small comparing to the other directions. Therefore, studying a petroleum reservoir can only study any layer representing the reservoir. A three-dimensional problem of multi-layer research can be transferred to a two-dimensional problem of studying a class. In order to present the experience of adjusting the geophysical parameters of the oil and gas reservoir, without losing the generality of the digital simulation method, this article investigates the digital solution to solve a two-dimensional boundary problem of finding pressure distribution in a natural gas reservoir, one-layer structure, thickness h. The reservoir is divided into block grid. Each element of the grid (cell) is a rectangular box with dimensions like in figure 1. Block grid elements (called grid cells) are numbered and have a defined position according to the row index i (along the ox direction) and column index j (along the oy direction) as Figure 2.

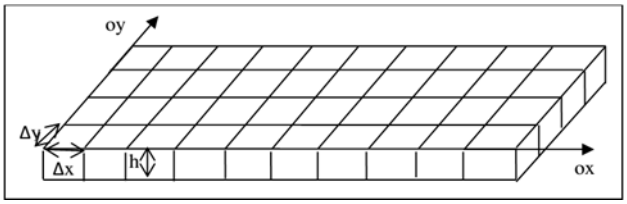

Figure 1. Image of a block grid. Each block of the grid has dimensions Δx , Δy and h

	j =1	*2*	*3*	*4*	*5*	*6*	*7*	
i=1	1	2	3	4	5	6	7	
2	8	9	10	11	12	13	14	
3	1	16	17	18	19	20	21	
4	2	23	24	**25**	26	27	28	
5	2	30	31	32	33	34	35	
6	3	37	38	39	40	41	42	
7	4	44	45	46	47	48	49	

Figure 2. 2-dimensional reservoir presented by ox and oy directions. Dark cells form the outer boundary of the reservoir. Cells are numbered for their position in the reservoir. Location of cell 25 is arranged with production well, which is inter boundary of the reservoir

For example, a two-dimensional boundary problem applies to the gas reservoir as follows:

two-dimensional partial differential equation with pressure unknown *p* (pressure equation) describes pressure changes in the reservoir:

$$\frac{\partial^2 p}{\partial x^2} + \frac{\partial^2 p}{\partial y^2} = \frac{\emptyset \mu c}{0.006328k} \frac{\partial p}{\partial t} \tag{1}$$

conditions of outer boundary:

$$\left.\frac{\partial p}{\partial x}\right|_{\Gamma x} = \left.\frac{\partial p}{\partial y}\right|_{\Gamma y} = 0; \quad p|_{\Gamma} = p_{init} \tag{2}$$

conditions of inner boundary (at well position):

$$p_w = const < p_{init} \tag{3}$$

initial conditions: t=0 at the time of the original reservoir, there were no production wells; t = t_0 at any time, the reservoir is in production.

$$p|_{t=0} = p_{init} \tag{4}$$

or,

$$p|_{t=t_0} = p_{(x,y)} \tag{5}$$

Geophysical parameters in the porous environment of the reservoir related to pressure are as follow:

$$\phi = \phi(p) \tag{6}$$

$$\mu = \mu(p) \tag{7}$$

$$\kappa = \kappa(p) \tag{8}$$

$$c = c(p) \tag{9}$$

Here: p_{init}, $p_{(x, y)}$, p_w, k, h are respectively the initial pressure, pressure in any position, well pressure (internal boundary pressure), permeability and height of gas reservoir; c is the compression coefficient of the gas, μ - viscosity of the liquid and ϕ - porosity, respectively.

At the initial state of reservoir at t = 0, geophysical parameters in each grid cell are determined by upscalling technology [1,2]. With DST, these data are combined with the finite difference method [3,4] to find the solution of the boundary problem. The solution (P) of the boundary problem is a set of pressure values p defined at the center of each grid cell at any time t.

Partial differential equation (1) is converted into corresponding finite difference system of equations and apply to all positions of grid-cell. The solution (P) is obtained from solving the following system of algebraic equations:

$$|A|\vec{x} = |B| \tag{10}$$

$$\vec{x} = \frac{|B|}{|A|} \tag{11}$$

Here $|A|$ and $|B|$ are coefficient matrices. $|A|$ is square matrix in diagonal form. $|B|$ is the column matrix. The components of the vector $\vec{x}$ is the unknown pressure at the center of each grid-cell.

In the next step we divide time t into small enough time intervals Δt and $t = n\Delta t; n = 1,2,3...N.$ To determine the pressure field (P) at time t, we must calculate N set of pressure field $(P)_n$ with n = 1,2,3 ... N. The steps to calculate are as follows:

The first step in n = 1:

In the initial state t = 0, reservoir pressure everywhere has the same value, equal to the initial pressure of the reservoir.

Using geophysical parameters in the initial pressure state of each grid cell we calculate components of $|A|$ and $|B|$ corresponding to p_{init} pressure state.

We solve equation (11) to find $(P)_1$ at the time of time $t_1 = n\Delta t = \Delta t$

Step to calculate pressure in time t_2, n = 2:

We calculate geophysical parameters in the pressure state $(P)_1$ for each grid-cell according to the expressions (6-9).

Next, we calculate the components of $|A|$ and $|B|$ according to known data at the pressure state $(P)_1$.

We solve equation (11) to find $(P)_2$ at the time $t_2 = n\Delta t = 2\Delta t$

Continue to the last calculation step in n = N:

We calculate geophysical parameters in the pressure state $(P)_{N-1}$ for each grid-cell according to the expressions (6-9).

We calculate the components of $|A|$ and $|B|$ according to known data at the pressure state $(P)_{N-1}$.

We solve (11) to find $(P)_N$ at the time $t = t_N = n\Delta t = N\Delta t$.

Methods to adjust geophysical parameters

The geophysical parameters of each grid-cell in the initial state t = 0 are generated from the upscaling technology. In these data set there is lack of measuring results to standardize, so they are not accurate data. Therefore, the results of the digital simutation problem are difficult to match the actual conditions of the reservoir. To overcome this, geophysical parameters at each grid cell should be standardized according to the actual conditions of the reservoir. Here, there are some experiences.

On the basis of set of actual measurement data of geophysical parameters at different locations of the reservoir, we can find expressions (6-9). From these expressions, we determine the value of geophysical parameters when knowing the pressure p in any position (i, j) of the reservoir. If p is correct, it will be calculated the exact geophysical values, and vice versa. Correct adjustment of geophysical parameters is equivalent to adjustment of pressure p at different locations in the reservoir. Expressions (6-9) are always re-standardized whenever new measurements are added.

DST allows determining the pressure field $(P)_n$ at each step of calculation n. The set of pressure values of $(P)_n$ is determined exactly with reservoir conditions, which will be used to adjust the geophysical parameters in grid cell locations at the next calculation steps.

In the step of calculating n any corresponding time period Δt , the solution $(P)_n$ is determined by solving the system of equations (11). Repeat s times for solving the equation (11) in step n, then the results obtained $(P)_{ns}$ are not the same. When s is large enough, $(P)_{ns}$ changes little. It is necessary to select a sufficiently small change of $(P)_{ns}$ for step n. Therefore, it is important to note that when determining a solution $(P)_{ns}$, a sufficient level of accuracy is required at each time step Δt .

When solving the system of equations (11) at the time step n = 1 with the initial condition (4). At time t = 0, assume that the pressure at the center of the grid-cells is equal and equal to the pressure p_{init} of the reservoir. However, boundary conditions (5) can be applied instead of (4). It means using any pressure value instead of p_{init} or choosing any set of pressure values (P) for the initial pressure state of the reservoir. Mathematically, after doing s times the system of equations iteration (11) we always determine an exact solution at the necessary level for this system of equations. However, pressure values according to boundary conditions (5) are usually assumed pressure. They are not measured values in the initial state corresponding to the position of each grid cell. Therefore, geophysical parameters calculated by expressions (6-9) will not be accurate for each grid-cell in that initial state. Thus, the determination of the coefficient matrices $|A|$ and $|B|$ in the system of equations (11) will be different from the case of determining them when using the condition (4). So, it should be noted that when solving the system of equations (11), it is not only mathematically accurate but also accurate in terms of physical meaning and timing.

Solving the system of equations (11), using the initial condition (4) will be favorable because the reservoir pressure is the same everywhere. The value of geophysical parameters is changed over time from the same initial time point t = 0. However, simulation for reservoir status with long time will take a long time to calculate. If using the initial condition (5), there will be two difficulties in practice. One is that it is impossible to measure simultaneous pressure at all grid locations. The second is the very small number of grid positions that can measure pressure. However, the simulation program uses initial conditions (5) for much less computational time. Below, there is the Hypothetical Simulation Method which presents the experience to transform the initial condition (4) to (5) and vice versa. This helps the simulation program to be applied in practice even when using the initial conditions (4) or (5).

Description of Hypothetical Simulation Method

Solve the system of equations (11) using the initial condition (5) with pressure $p_{(x, y)}$ in different positions but it is unclear at what time, called hypothetical simulations. Pressure difference $dp = p_{init}-p_{(x, y)}$ or $p_{(x, y)} = p_{init}-dp$ at each position of grid-cell with coordinates (x, y) is determined. Hypothetical simulations also determine the period of time $n\Delta t$ at which the pressure $p_{(x, y)}$ at any position (i, j) changes a dp value. So, we can convert the initial condition (4) to (5) using the expression $p_{init} = p_{(x, y)} + dp$ and vice versa, convert (5) to (4) using the expression $p_{(x, y)} = p_{init}-dp$.

In fact there are very few pressure values measured from the reservoir due to the limited number of wells. Therefore, it is always necessary to add new pressure measurement values to the digital simulation program to standardize geophysical parameters. However, these parameters can be standardized by the digital simulation program by the method below.

Description of the method

p_{init} is the measured pressure. Suppose the initial condition (4a) is generated from the initial condition (4) by setting the p_{test} pressure in any grid position (i, j). If $(P)_n$ is the solution of the boundary problem using the initial condition (4) at time step n and $(Pa)_n$ is the solution of the boundary problem using the initial condition (4a) at time step n, then the solution $(P)_n$ and $(Pa)_n$ differ only in adjacent positions (i, j). Thus through DST, these adjacent positions have been adjusted pressure to suit the p_{test} pressure. In general, the solution of the boundary problem at the area near reservoir positions where reliable pressure, will be adjusted in the direction of actual fit of the reservoir. Therefore, it is

possible to use the pressure of the cells near the well as the initial condition to adjust the pressure of the cells far from the production well for suitable actual conditions of reservoir.

Conclusion

Digital simulation technology is now widely used in oil and gas industry. Finding out the methods to make digital simulation results well suited to the actual conditions of reservoir is always difficult problem. There are many different methods to solve this problem. The paper presented some methods as good experiences to adjust geophysical parameters to suit actual conditions of reservoir.

References

1. Lei Zhang, *Metric Based Upscaling for Partial Differential Equations with a Continuum of Scales*. California Institute of Technology, Pasadena, California. (2007)
2. Weibing Deng, Ji Gu, Jianmin Huang, *Upscaling methods for a class of convection-diffusion equations with highly oscillating coefficients*. Nanjing University, People's Republic of China. (2008)
3. I.J. Taggart, W.V. Pinczewski, *The use of higher-order differencing techniques in reservoir simulation.* SPE Reservoir Engineering, P. 360-372. (1987)
4. M. D. Stevenson, M. kagan And W. V. Pinczewski, *Computational Methods In Petroleum Reservoir simulation.* Computers & Fluids **Vol. 19**. No 1. P. 1-19. (1991)

Opiekun : Jadwiga Jarzyna
Recenzent : Jadwiga Jarzyna
Drugi recenzent z Wietnamu

Improvement of Seismic Researches for Petroleum and Gas Hydrate Exploration in Vietnam

MAI Thanh Tan[1], MAI Thanh Ha[2], NGUYEN Dinh Chuc[2], PHAN Thien Huong[1], DUONG Van Hao[1], KIEU Duy Thong[1]

[1] Hanoi University of Mining and Geology, 18 Vien Str., Tu Liem Dist., Hanoi,

[2] PetroVietnam Exploration Production Corporation (PVEP), 117 Tran Duy Hung St., Hanoi

Abstract. Vietnam is located in Southeast Asia, with diverse and complex geological conditions. Over the years, seismic methods have been effectively applied to solve many different geological tasks such as interpreting geological structure, petroleum and mineral exploration, research gas hydrate, etc.

In this report, we present some achievements using seismic methods for petroleum exploration to find not only structural traps but also stratigraphic traps in sedimentary basins, in non-traditional fractured granite basement reservoirs, and in the initial stage of gas - hydrate exploration. The development of seismic acquisition methods such as 3D / 4C seismic, HRS has been applied. Advanced seismic processing and interpretation methods has been used, such as seismic filters (T-P, Radon, SRMA…), seismic imaging (Pre-stack Migration/PSTM, Control Beam Migration/CBM), seismic inversion (SI), Amplitude Versus Offset Analysis (AVO), Seismic Sequence Stratigraphy Analysis, Seismic Attribute Analysis, Artificial Neural Network (ANN), etc. The results allow improving seismic interpretation, hence helping oil and gas exploration efficiency.

Introduction

The continental shelf of Vietnam as a structural unit of continental crust Kontum - Borneo plate consolidated from the end of Mesozoic, the beginning of Pre-Tertiary together with spreading of marginal "East Sea" having transitional oceanic crust forms a common tectonic frame of South - East Asia. Geological development history allows formation of sedimentary basins with petroleum, gas hydrate potential on continental shelf and East Sea region (Gwang, et al, 2001). The distribution of sedimentary basins in the continental shelf of Vietnam is shown in figure 1.

On the continental shelf of Vietnam, oil and gas has been produced from Eocene, Oligocene, Miocene complexes and from Pre-Cenozoic fractured basement rocks. New technology has been applied to improve the efficiency of seismic processing and interpretation for oil and gas exploration focusing on complex objects such as stratigraphic traps, fractured granite basement reservoirs, or gas hydrate in deep water area (Al-sadi, 2016; Nanda, 2016).

Enhancement of seismic data analysis for stratigraphic traps

Different from structural traps related to tectonic activities with dome-shaped trap types, in sedimentary basins of the Vietnamese continental shelf, especially in the flank pinch-out and/or onlap area, many types of stratigraphic traps exist with complex distribution and formation. Stratigraphic traps are related to sediment depositional, environmental changes, or related to erosion, which covered by low permeability layers. They are usually not large in size, and the geological data are normally limited to analyze stratigraphic traps. In order to solve this problem, it is important to enhance seismic data interpretation, such as applying seismic sequence stratigraphy and using seismic attributes (Tan et al, 2018).

Seismic sequence stratigraphy is based on analysis of patterns of seismic reflectors and analysis of sequences and system tracts using a depositional sequence model as the main interpretation tool (Catuneanu, 2006). Analyzing

reflection patterns, seismic reflection terminations, seismic facies, etc., applying seismic sequence stratigraphy allow determining stratigraphic units, identifying stratigraphic traps types such as pinch-outs, alluvial fans and predicting lithology distribution. The research results obtained from analyzing seismic data in flank of Southeast Cuu Long Basin clarify the presence, distribution and sedimentary facies of stratigraphic traps (Chuc et al, 2018). Image of stratigraphic pinch-out trap in Southern margin of Cuu Long basin is shown in figure 2 and seismic section interpreted by seismic stratigraphy with sedimentary sequence, system tracts and stratigraphic traps is shown in figure 3. This facies pattern and its external form derived on figure 4 reveals that the sediments were deposited during regression of water level with high depositional energy. The pinch-out traps were formed due to the tapering off sand layers landward or toward the horst, then these sand layers were overlaid by finer-grained sediment deposited in the high stand stage of water level that played as top seal for the traps.

Seismic attribute analysis is based on the application of different attributes to enable the interpretation of depositional environment as well as the identification of internal patterns in stratigraphic units. There are many seismic attributes studies (RMS amplitude, spectral-decomposition, seismic inversion, average instantaneous phase, etc.) applied in this area (Chopra and Marfurt, 2008; Tan et al, 2018). RMS amplitude in the study area showing facies changing from delta plain to delta front, delta slope and the area delta sand bodies traps developed, the stratigraphic trap has fan-shaped deposited in deltaic environments during low stand stage of water level and distribution on a large area (Fig. 5a). The average instantaneous phase attribute (Fig. 5b) reveals that the boundary at which seismic phases change approximately coincides with the boundary upper part of Oligocene fan. The fan-shaped amplitude anomalies are interpreted to be the sand distribution that approximately coincides with the highest thickness area observed on the isochore map. The Spectral Decomposition map in 25 Hz of Lowstand System Tract/LST of upper part of Upper Oligocene is shown in figure 6. Note the changes in seismic phases at the boundary which approximately coincides with upper part of Oligocene fan.

Study of reservoir in fractured zones of granite basement

In Vietnam, oil and gas are not only found in sedimentary environments, but also in fractured zones of granite basement rocks. Oil and gas migrated from the source rock in sedimentary environment through faults and accumulated in the fractured zones of the uplifted zone of granite basement (Fig.7).

The unique characteristics of basement reservoir require a careful evaluation and unique processing and interpretation methods. Identifying of fracture zones distribution is important for extrapolation of favorable target for exploration. However, because of the absence of stratified, coherent reflectors, illumination of basement faults is more problematic than illumination of faults within the sedimentary sections. With the complex interference pattern, non-layered and steeply dipping nature of faults and fractures, it is important to enhance seismic data processing, reducing noise and multiple reflections (Ha et al, 2009; Tan et al, 2016). To solve the above problems, some effective data processing methods were implemented:

- Applied seismic filters for removing multiple reflections from strong reflection surfaces in sediments and revealing the weaker seismic signals inside basement.

Seismic signals from fractured granitic basement are very low quality, containing a lot of noise and multiples. Multiples are related to strong reflection surfaces of the Miocene, Oligocene sediments, and top-basement. Multiple suppression methods can be used based on either prediction criteria or normal move-out differential to improve the weak primary reflections. Using seismic filters enhances the signal-to-noise ratio and improves seismic signals significantly. Thus, using filters such as f-k, Tau-p and Radon transform for multiple attenuation is not only successful in improvement of seismic signals for sedimentary units but also works well in fractured, non-layered and structural complex basement in the Cuu Long Basin. Comparison of seismic section before and after reprocessing with applying seismic filters shows images of fault and fractured in the basement more clearly (Fig.8),

- Enhance efficiency seismic migration for imaging steeply dipping fault and fracture plane events and using of seismic attributes for further delineate and map out fractures.

Migration of seismic data corrects reflection from dipping surface to their true positions, collapses diffractions, increases spatial resolution and resolves areas of complex geology. Kirchhoff Migration is one of seismic migration methods that are extensively used in both layered environment and non-layered fractured basement by summing the energy along diffraction curves. The advantage of this type of migration is that it can enhance signals of steeply dipping objects and moderate lateral velocity variations. In a single-arrival migration algorithm, only one arrival is imaged, depending on certain predefined criteria. In order to reduce the disadvantage, Controlled Beam Migration (CBM) can handle multi-arrival ray paths, and preserve steeply dipping reflections, resulting in a cleaner image.

Figure 9 shows that improved imaging by CBM is allowing a better understanding of the orientation, spacing and potential connectivity of the fracture zones within basement.

For further identification of fault signature, beside dynamic attributes (amplitude, frequency, spectrum…), Geometrical attributes has been applied to well-established vector attributes including structural dip and azimuth and amplitude energy gradients to provide greater interpreter interaction we could mathematically generate simple axis rotations and project the two orthogonal dip or energy gradient components along the surface against the direction of illumination. Figure 10 shows that using Geometrical Attributes allows to show clearly two main fault directions inside the basement and images of fracturing zones between the faults.

Study of Gas Hydrate for the first step in Vietnam

Gas hydrates are the accumulations of methane (natural gas) trapped in ice-like structures with water. They represent an immense energy resource underlying large portions of the world's marine continental shelves and Arctic continental areas (Collet, 2002; Yuri, 2010). Figure 11 shows the area with favorable conditions for formation and existence of gas hydrate in East Sea of Vietnam.

Gas hydrate has very different characteristics compared to traditional exploration objects. They are formed under high pressure and low temperature conditions, so they exist only in shallow layers of the seabed in deep waters, with complicated geological conditions. In recent years, many researches have been conducted to identify the premise signs of gas hydrate potential within Vietnam economic water area, with surveys using a combination of methods (Westbrook et al, 2008) such as High Resolution Seismic (HRS), Multibeam Echo Sounding, Hydro Acoustic, Gravity Corer, Water Sampling, etc. Seismic data is processed based on petroleum seismic data processing algorithms with the use of SRMA, Tau-P, Radon, FX filters, Pre-stack migration, seismic attribute analyses (Ojha and Sain, 2009), but note on the GH located in the shallow layers of the seabed in deep waters may be revealed using seismics of high frequency range. The achieved results detected the signs of existence of Bottom Simulated Reflected (BSR), Gas Hydrate Stability Zone (GHSZ), blank zones (BZ), channels, pockmark, study upper sedimentary cover structure, mark out fracture zones and faults, serving pathways for gas-saturated fluids, migrating upwards.

Figure 12 shows an example of velocity analysis related to the Bottom Simulating Reflector (BSR). The correlation of Echo-sounder and seismic data documents have shown the signal of the pockmark at a depth of 1347.54 m (Fig. 13). The blank zone in the seismic section in eastern slope of the continental shelf of Vietnam is shown in figure 14. The result of seismic attribute analyses (Amplitude Envelop, Instantaneous Frequency, Instantaneous phase, First derivative of amplitude, second derivative of amplitude and Frequency gathered at 75Hz) shows high potential of location of BSR at the time of 1.8 s. This result need to be more integrated with geochemistry, geothermal and sea-bottom temperature data (Fig. 15)

Conclusions

Vietnam East Sea has many sedimentary basins with petroleum and gas hydrate potential. In addition to common targets such as structural traps, there are also non-traditional targets such as stratigraphic traps, fractured basement traps, gas hydrate in the deep sea. With the application of seismic sequence stratigraphic and seismic attributes analysis, we can identify the existence, distribution and characteristics of stratigraphic traps in the flank zones of sedimentary basins, contributing to increase accuracy of oil and gas potential assessment. Efficiency improvement of 3D seismic data processing using Radon, Tau-P filters, PSTM, CBM, and applying seismic attributes ... allows identifying zones of faults and fracture inside basement related to oil and gas traps. The initial survey results in Vietnam's deep sea waters show signs of existence of Gas Hydrate resources (BSR, GHSZ, pockmark …) and further research is needed.

Acknowledgements

The authors gratefully acknowledge HUMG, PVN and MONRE for granting permission to publish this paper, and our colleagues for helpful suggestions.

References

Al-sadi, H.N., 2016. Seismic Hydrocarbon Exploration. 2D and 3D Techniques. Advances in Oil and Gas Exploration & Production, 325 pp., DOI 10.1007/978-3-319-40436-3

Catuneanu, O., 2006, Principles of Sequence Stratigraphy, Alberta: Elsever B.V., pp. 178-197.

Collett, S.T., 2002, Energy resource potential of natural gas hydrates, AAPG Bulletin, V.86, No.11, pp. 1971-1992

Chopra, S., Marfurt, K., 2008, Merging and future trends in seismic attributes, The Leading EDGE, pp. 298-316,.

Chuc, N.D., Huy, T.N., Ha, M.T., Bach, H.V., Tan, M.T., 2018, "Assess Late syn-rift plays in Cuu Long basin," offshore Vietnam, Offshore Technology Conference Asia, Kuala Lumpur, Malaysia, OTC-28537-MS, ISBN: 978-1-61399-552-5.

Gwang, H. L. et al, 2001, Geologic Evolution of the Cuu Long and Nam Con Son Basins, Offshore Southern Vietnam, South China Sea, AAPG Bulletin, V85, No. 6, pp. 1051-1082

Ha, M.T., Marfurt, K. J., and Olebiju O, 2009, Attribute illumination of basement fault, examples from Cuu Long basin basement, Vietnam and the Midcontinental, USA, Petrovietnam Journal. V.6 -2009, pp.10-20

Nanda, N. C., 2016, Seismic Data Interpretation and Evaluation for Hydrocarbon Exploration and Production, 224 pp., DOI 10.1007/978-3-319-26491-2

Ojha, M., Sain, K., 2009, Seismic attributes for identifying gas-hydrates and free-gas zones: application to the Makran accretionary prism, Episodes, vol. 32, no. 4, pp. 264–270.

Tan M.T., Ha M.T., Marfurt K.J., Hieu N.T., Hanh N. T. M., 2016, Enhancement of Seismic Data Processing and Interpretation of Fracture Zones on the Upper Part of Granitic Basement in Cuu Long Basin, Vietnam, Acta Geophysica, 64 (6), pp.2214-2231, DOI: 10.1515/acgeo-2016-0082

Tan, M.T. et al, 2018, Enhancement of seismic data analysis for stratigraphic traps in the flank of Southeast the Cuu Long Basin, Offshore Vietnam, The fifth Regional Congress on Geology, Minerals and Energy of Southeast Asia (GEOSEA XV)

Yuri, F.M., 2010, Natural gas hydrates - A promising source of energy, Journal of Natural gas Science and Engineering, Vol.2, Issue 1, pp. 49-59

Westbrook, G. K., Chand, S., Rossi, G., Bünz S., Camerlenghi A., Carcione J.M., Dean S., Foucher J.-P., Flueh E., Gei D., Haacke R.R., Madrussani G., Mienert J., Minshull T.A., Nouzé H., Peacock S., Reston T.J., Vanneste M. and Zillmer M., 2008, Estimation of gas hydrate concentration from multi-component seismic data at sites on the continental margins of NW Svalbard and the Storegga region of Norway, Marine and Petroleum Geology, vol. 25, no. 8, pp. 744–758.

Figure Captions

Figure 1. The sedimentary basins in the continental shelf of Vietnam

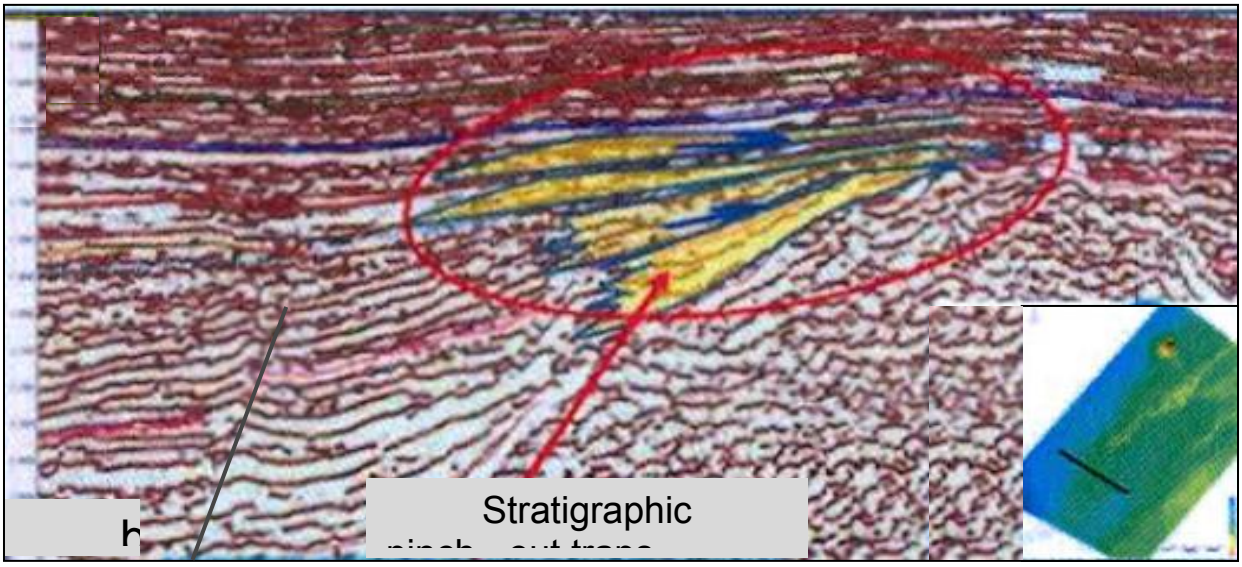

Figure 2. Image of stratigraphic pinch-out trap in Southern margin of Cuu Long basin

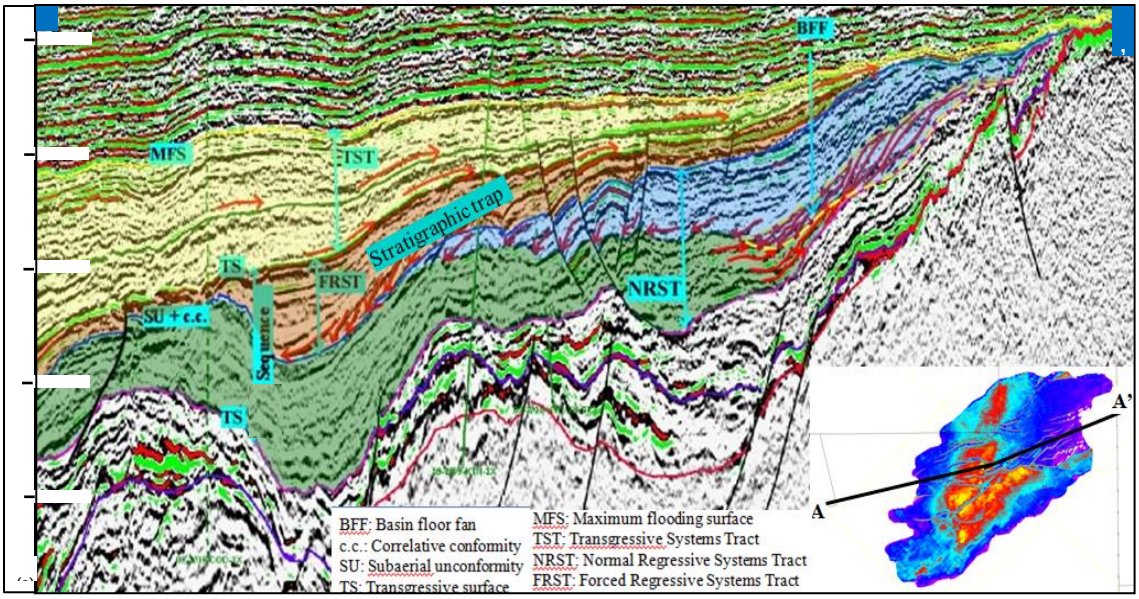

Figure 3. Seismic section interpreted by seismic stratigraphy shown sedimentary sequence, system tracts and stratigraphic traps in NE Cuu Long basin

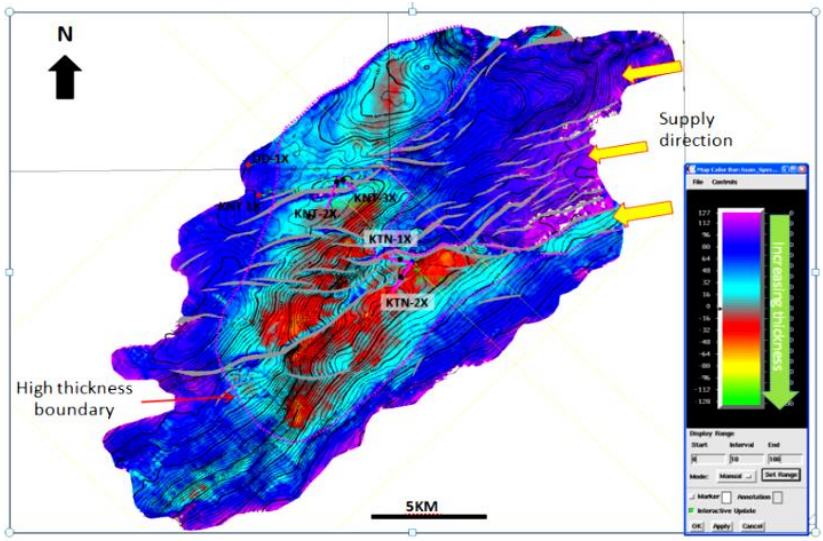

Figure 4. Isochore map showing thickness changing of fan-shaped distribution

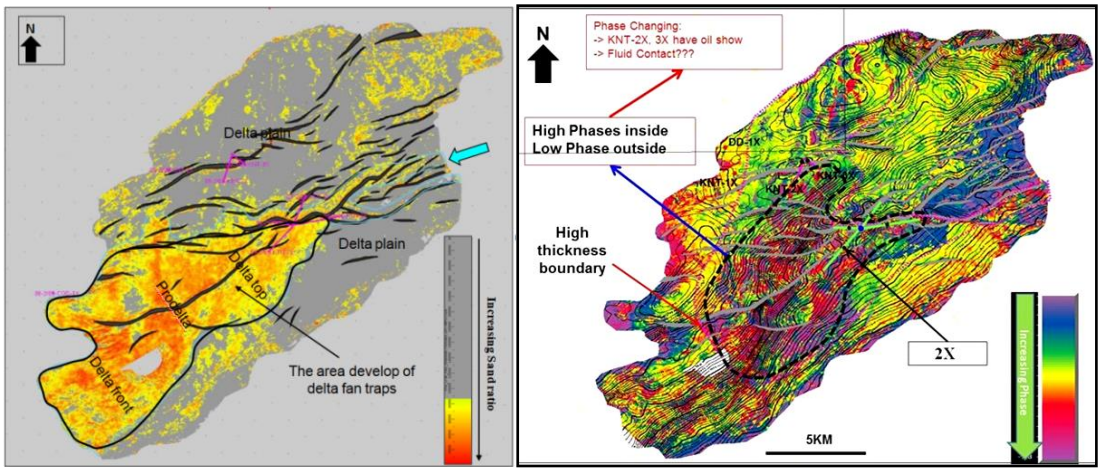

Figure 5. RMS amplitude map (a) and Average instantaneous phase map of Upper part of Oligocene in the study area

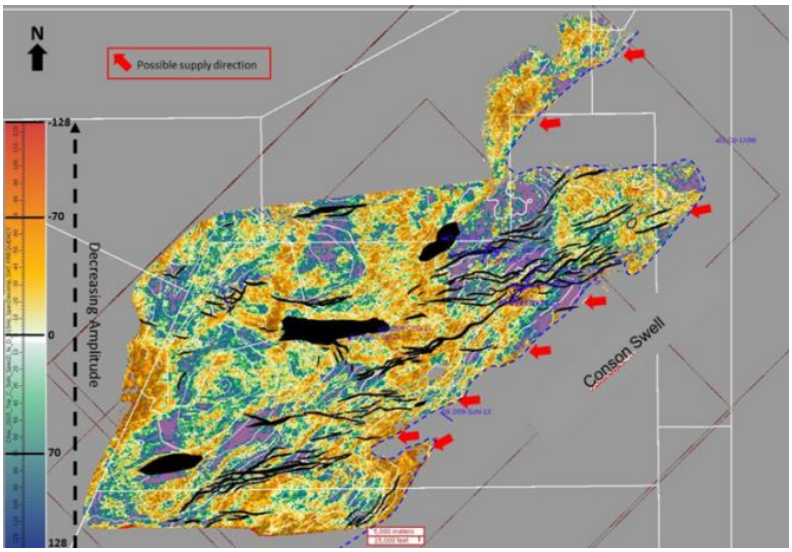

Figure 6. Spectral Decomposition map in LST (Sequence C) of Upper Oligocene

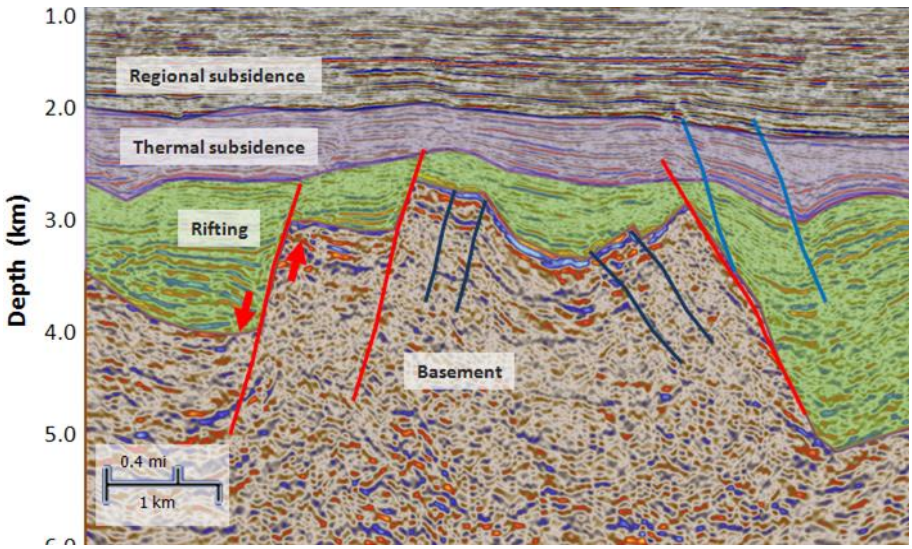

Figure 7. The fractured granite basement traps in Cuu Long basin

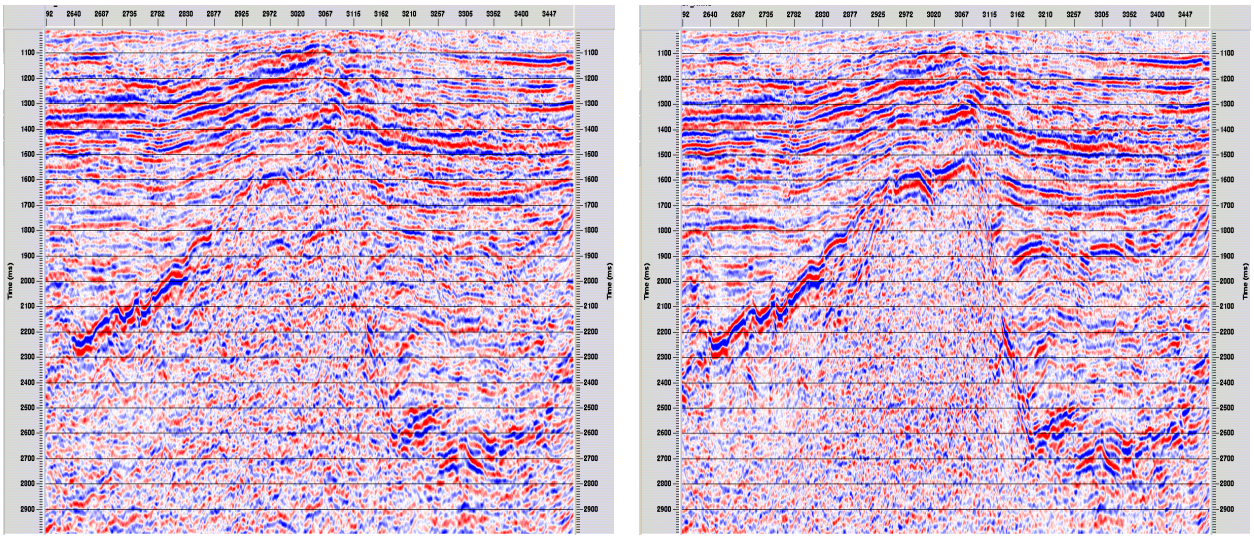

Figure 8. Seismic section before (a) and after (b) reprocessing with applying seismic filters

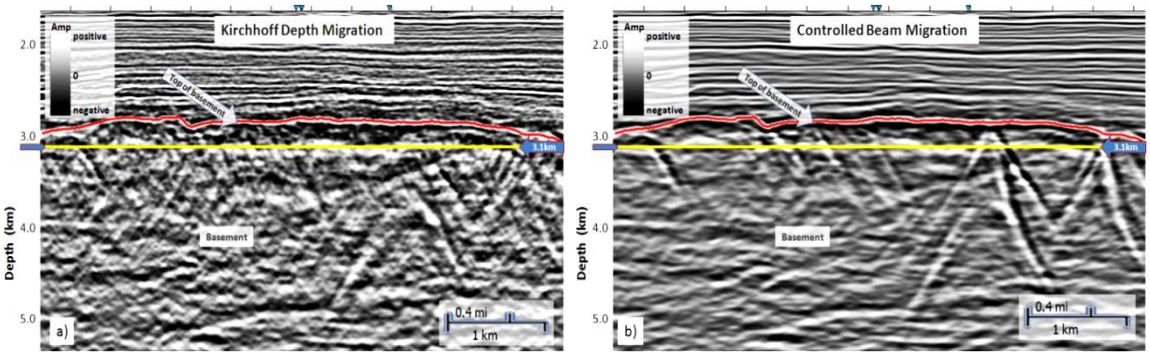

Figure 9. Seismic section with Kirchhoff Migration (a) and CBM (b)

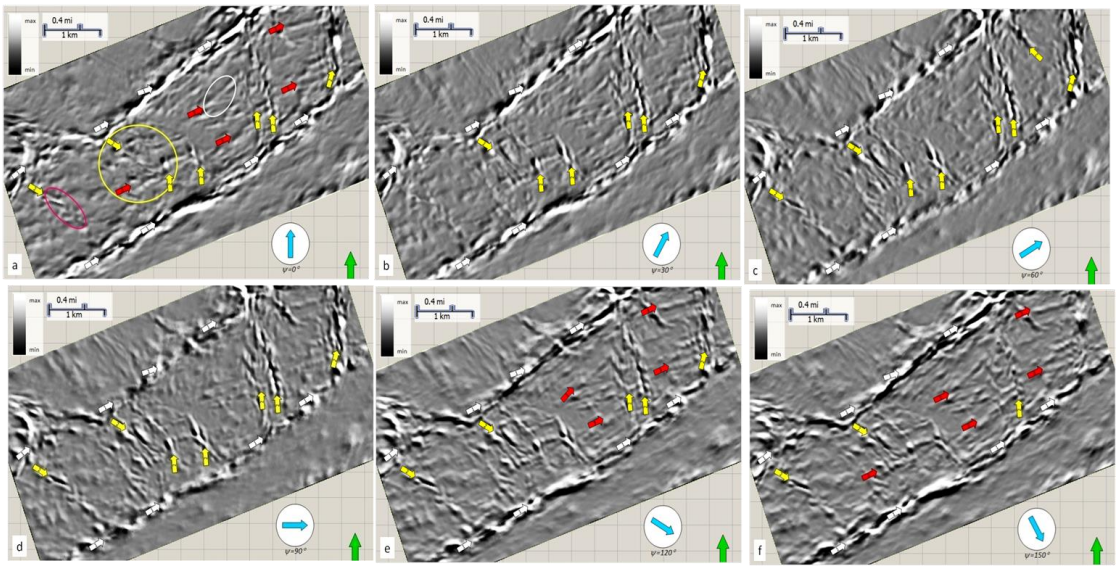

Figure 10. Improving image fault and fractured basement by using Geometrical Attributes

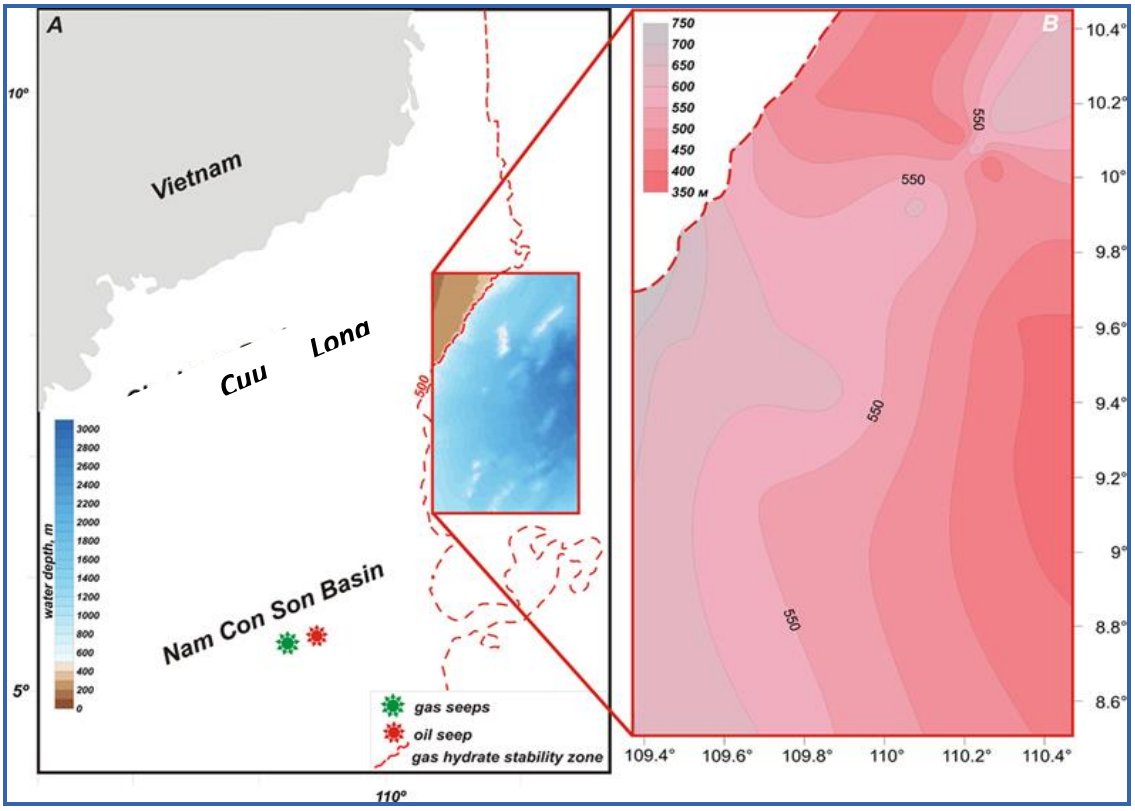

Figure 11. Methane Hydrate Stability Zone in Vietnam

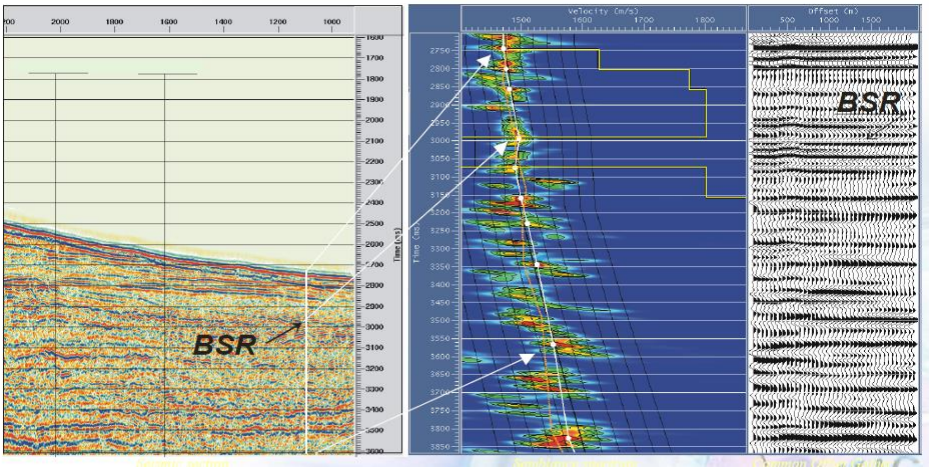

Figure 12. Velocity analysis is related to the Bottom Simulating Reflector (BSR)

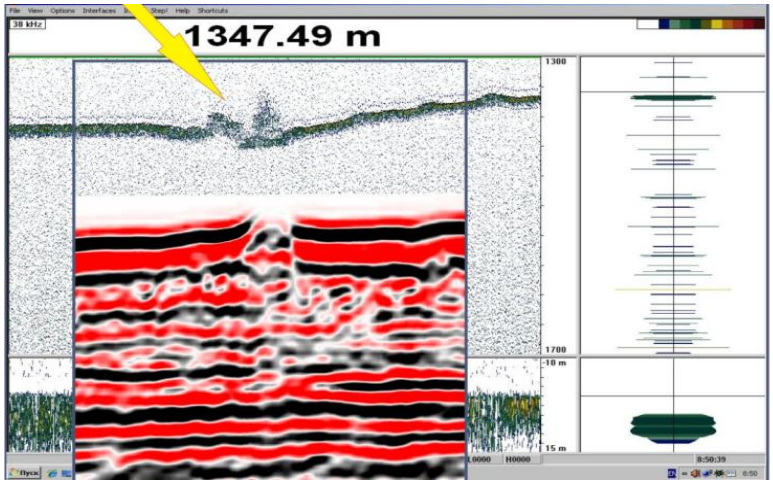

Figure 13. Echo-sounder and seismic data correlations

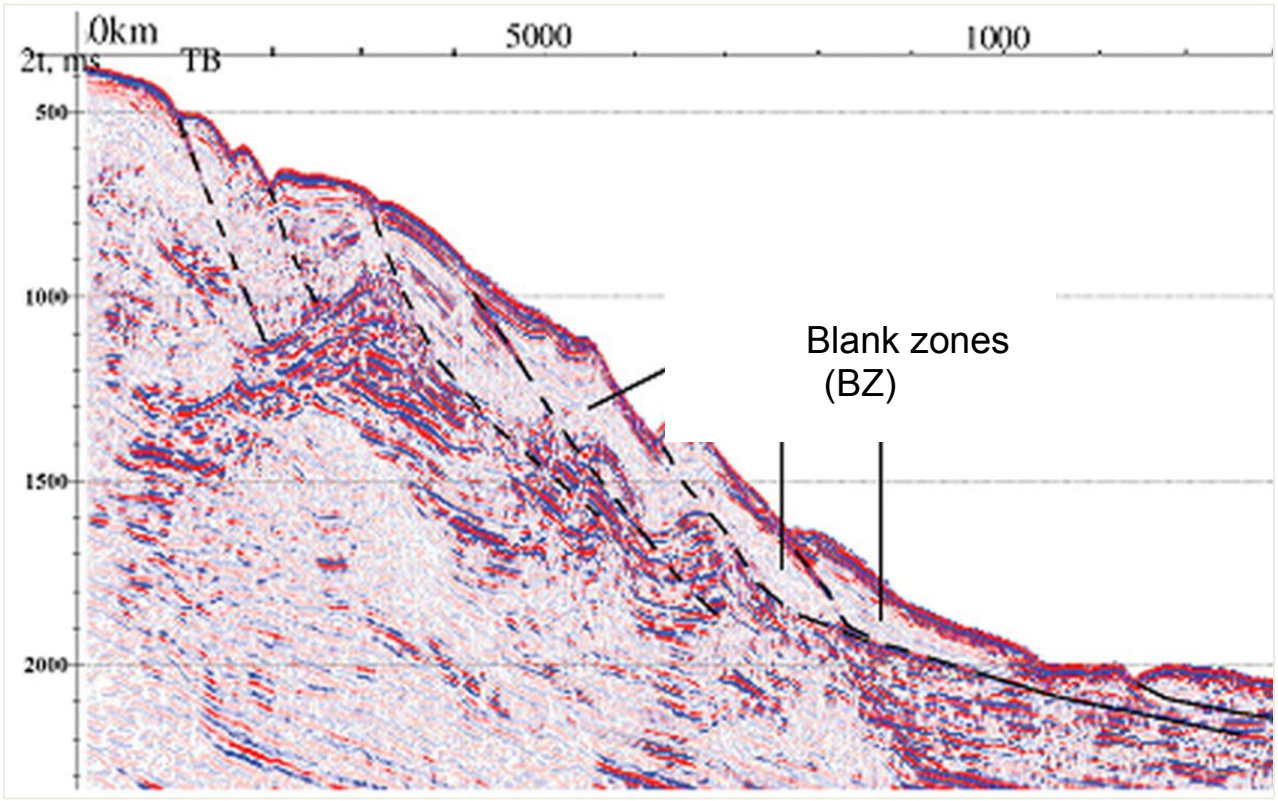

Figure 14: The blank zone in the seismic section in the continental shelf of Vietnam

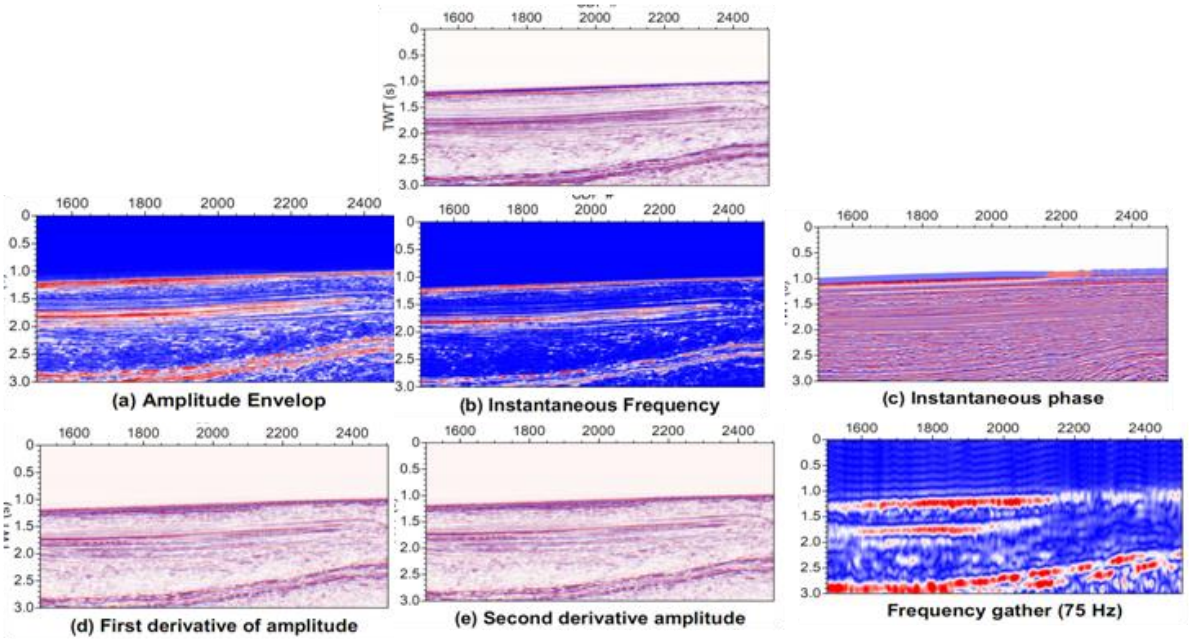

Figure 15: Seismic attributes for high potential of location of BSR

Opiekun: JJ

Recenzent: JJ

Recenzent: Dr Ha Quang Man - Ha Quang Man <manhq@pvep.com.vn


Geodesy and Mining
Surveying

Application of information technology to improve the management of mineral resources in Quang Ninh province - Vietnam

DAO Van Chi[1,*)], NGUYEN Cao Khai[1)], LE Tien Dung[1)], ZHANG Leilin[2)]

[1)] Hanoi University of Mining and Geology, Hanoi, Vietnam
[2)] Anhui University of Science and Technology, Huainan, China
* Corresponding author: daovanchi.mdc@gmail.com

Abstract. The current mining operation of mineral resources in Quang Ninh province-Vietnam is increasingly complicated. Correspondingly, the management of the mine sites becomes more difficult. Records and documents of minerals and mine sites are archived in different forms. Database systems are stored dispersedly and insufficiently; in many cases lack accuracy, topicality and have not been linked to each other systematically. These lead to many difficulties in accessing and extracting information for the implementation of management as well as for investors and people with related interest. In this paper an advanced software has been developed for the management of mineral resources and has been applied for Quang Ninh province. The software has improved the supervision and administration of the mining operation in the province.

1. Introduction

The development of Information Technology (IT) has profoundly changed the economy, culture and society of many countries including Vietnam. IT has been applied in various fields, promoting the economic development, transferring the economic structure and altering the social structure. It contributes to creating more professions, deeply changing the modern industries, improving the competition of traditional industries through assistant systems such as telecommunications, electronic commerce and multimedia services. Many developing countries in the past successfully improved and utilized IT and achieved great developments such as India, China and Korea. It is noted that the application of IT in the world are mostly limited to education, secure and military sectors. Applications in the management of mineral resources are modest and highly manual. The management files and documents are largely stored in hard copies, map files in AutoCAD, MapInfo, MicroStation, and soft files such as PDF, Word and Excel documents. Database systems are archived dispersedly and insufficiently; in many cases lack accuracy, topicality and have not been linked to each other systematically. These cause many difficulties in accessing and extracting information for execution of management and for investors and people with related interest.

In Vietnam, the operations of mineral resources in large scale and under strict administration from the government are mainly located in Quang Ninh province which owns abundant and diversified mineral resources. How to manage, protect, extract and

utilize these resources more properly, economically and efficiency is an urgent demand for the sustainable development of socioeconomic issues in this province.

Statistics from Quang Ninh Environment and Natural Resources Department indicate that in total there are 243 mines extracting 33 minerals of 6 different categories in this province. The raw productions per year are more than 1.4 million cube meters of limestone building materials, 474.000 cube meters of clay products, 79.000 tons of sand-soil building materials, 6.5 million tons of limestone cement, 1.3 million tons of clay cement, 76.000 cube meters of mineral water, 40 million tons of coal and 2000 tons of other minerals [1]. The mining and processing operations are being expanded that contribute to creating thousands of jobs for residents and promoting the socioeconomic development of Quang Ninh. However, the booming development of mineral operation has considerably impacted living environment such as air and water pollutions. Many mine sites do not strictly conform with the approved design that consequently causes waste of resources. The illegal mining operations sometimes remain uncontrolled that may trigger security problems. Some operators do not apply the management appropriately, obey rules and they lack administrative ability.

When the forth industrial revolution commences, it will be the revolution of connecting things, internet of services, etc. It greatly impacts the domestic economy, official government and especially mining companies with many unskilled labors [2]. IT can be a highly feasible solution for these above problems in Quang Ninh and for the management of mineral operation in general. The application of IT is expected to improve ability of governmental administration; reduce tasks processing time; better support for archive, search and processing applications in the mineral sectors. This paper presents the development of an advanced software for these requirements.

2. Fundamentals and database

2.1 Fundamentals for development of database and software

The development of database and management software has been implemented in compliance with the designated procedure attached in Circular 26/2014/TT-BTNMT promulgated by Vietnam Ministry of Natural Resources and Environment (MONRE).

Checking, editing and presenting specialized maps of Quang Ninh minerals has been implemented in compliance with the designated procedure attached in Circular 37/2011/TT-BTNMT promulgated by MONRE.

Geographic Information System (GIS) is an advanced technology that is being applied widely in developing database of natural resources and environment. Once completed, the system easily shares and connects to other systems of natural resources and environment. The applied modules in the software are as follows:

- GIS (ArcGIS Desktop) for editing and presenting specialized maps; building and updating database,
- WebGIS (GIS system distributed through network) for online distributing and broadcasting geographic information through internet.

Program applications are developed on web-based technology with client-server protocol. The management, storage, sharing and security are performed quickly and efficiently. The working environment is multiform, and the interface is friendly in both Vietnamese and English. The programming language is common (Java, VBA, SQL) which eases the maintenance, exploitation and development of the software.

2.2 Development of mineral resources database for Quang Ninh

The following information is included:

- General data of mineral resources in Quang Ninh,
- Data of areal distribution of mineral resources in Quang Ninh,
- Data of operating mines,
- Data of administrative offices and person or companies working in the industry,
- Other data (e.g., annual reports from companies and governmental offices).

The development of mineral database for Quang Ninh is implemented in compliance with Circular 26/2014/TT-BTNMT. The procedures are as follows [3]:

- Check and analyze the data collected,
- Design a database model,
- Create data of category and super data,
- Create data of database,
- Edit database,
- Test final project.

Objectives of management are shown in Table 1.

Table 1. Objectives of management in mineral operation.

Order	Name of objective	Description
1	Administrative division	District, Province/City, Ministry
2	Unit running mineral operation	Organization, company and individual participated
3	Information of mineral	Information on governmental planning, authorization, state of mining, photos
4	Areal distribution of mineral	1. Zone in operation plus sparsely distributed area 2. Zone of prohibited mineral operations 3. Zone of provisionally prohibited mineral operation 4. Zone of nationally reserved minerals
5	Mine site	Mines are being operated and not yet operated
6	Specialized map of mineral	Specialized maps of minerals in Quang Ninh
7	Report of mineral operation	Sample reports of annual mining operation
8	Legal document	Legal documents of mineral and mining operation

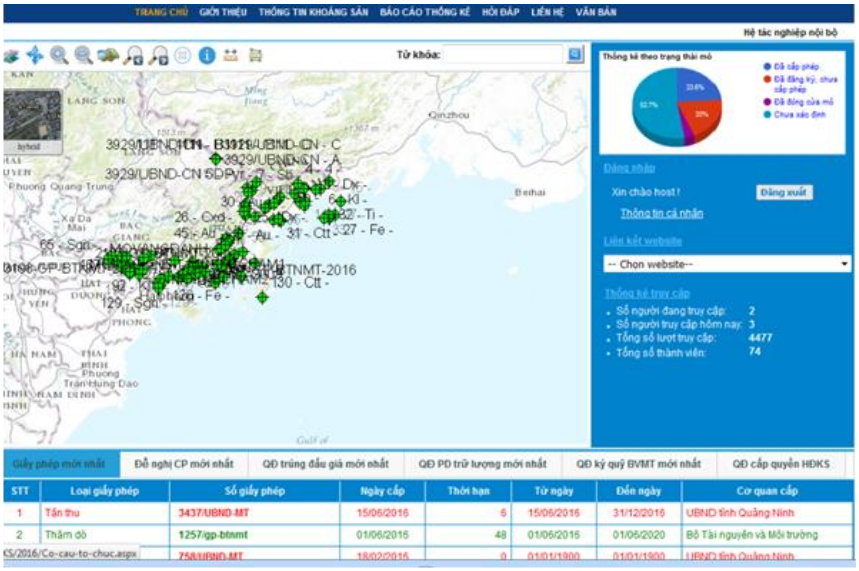

Fig. 1. Software interface: objectives of management.

3. Software for management of mineral operation

3.1 Computerization of management skills and process

The skills and processes are computerized as follows:

- Management of prohibited and provisionally prohibited mining operations; to determine zones not for auction of mining right authorized by the provincial people's committee; to consult and propose measures protecting unmined minerals; to schedule and run auction of mining right authorized by the provincial people's committee after approval,
- Management of scheduling exploration, extraction and utilization of mineral in the province; to timely detect and report new minerals to the provincial people's committee and to MONRE; to appraise file of recognized norms estimating mineral reserves; to appraise file of reserves approval; to audit and inventory the reserves which can be licensed by the provincial authority,
- Management of appraising files for the authorization, extension, withdrawal and return of exploration license; files for transference of exploration right and mining right; files for return of a part of exploration and mining areas; projects of mine closure; files for auction of mining right licensed by the province; to appraise pre-authorization of mining right,
- Management of appraisal of reports on mineral exploration for common building material, peat and sparsely distributed minerals authorized by the provincial people's committee,
- To audit and inventory the approved mineral reserves and periodically report to MONRE; to periodically report on mineral operation in the province or irregularly report by request from the provincial people's committee or MONRE.

3.2 Administrative functions of software

The administrative function of the software is a tool extracting and searching information for the enforcement of governmental mineral management in Quang Ninh. The software provides functions to manage mineral area; to manage planning, exploration and extraction of mineral; to manage files of mining licenses; to make a statistical report on exploration and to inventory mineral reserves; to notify current status of mining operation [1]. The detailed functions are given in Table 2.

Table 2. Administrative functions of software

Order	Case of application
1	Functions: management of mineral areas Management of information of (1) prohibited mineral operation; (2) provisionally prohibited mineral operation; (3) non-auction zones for mining right
2	Functions: management of schedule, exploration, extraction and utilization Management of file of (1) mineral schedule, exploration, extraction & utilization; (2) recognized norms estimating mineral reserves; (3) approved mineral reserves; (4) administrative division & administrative levels; (5) objectives in operation.
3	Functions: management of records/files on mineral operation Management of file of (1) mineral exploration license; (2) mineral extraction license; (3) transferring mineral exploration right; (4) transferring mineral mining right; (5) mine closure project; (6) auctioning mineral mining right
4	Functions: management of reports on mineral exploration Management of report on (1) mineral exploration for common building materials; (2) peat exploration; (3) sparsely distributed mineral exploration
5	Functions: statistic and inventory of mineral reserves (1) Management of report on statistic and inventory of approved mineral reserves; (2) Management of report on periodic statistic and inventory of mineral reserves; (3) Management of periodic report on mineral operation; (4) Notification/warning of mineral reserves as time goes by; (5) Warning of mining capacity of mine sites; (6) Warning of mineral exhaustion of mine sites
6	Functions: management of system catalogue Management of (1) legal documents on geology & mineral; (2) catalogue of source; (3) catalogue of mineral groups; (4) catalogue of mineral types; (5) catalogue of companies; (6) catalogue of administrative divisions

4. Conclusions

The application of the software provides a channel for exchanging information between administrative levels; improves the coordination between governmental offices; and facilitates the governmental administration. The software timely updates current mining operation with high reliability. This acts as a fundamental source for domestic and international investor to evaluate their potential investment in Quang Ninh. The environment of investment is accordingly improved. The program plays a role in propagating and improving the community awareness on mineral legal policies, rights and duties of the people's committee and residents.

The software facilitates management of natural resources; timely updates information for authorities; reduces time and manpower in manual searching and summarizing information in periodical management; accesses and decreases cost.

Organizations and individuals easily and quickly access the authorized information on geology and minerals. They are supported with favorable conditions to catch up with general and detailed planning projects of Quang Ninh. Thus, they can reduce the risk of

making inappropriate decisions due to untrue or insufficient information. Finally, time and effort will be largely saved due to the exchange and reuse of data.

Paper was presented during the 5th POL – VIET International Conference Scientific-Research Cooperation between Vietnam and Poland, 08-10.07.2019, AGH UST, Krakow, Poland.

5. Acknowledgements

Paper was presented during the 5th POL – VIET International Conference Scientific-Research Cooperation between Vietnam and Poland, 08-10.07.2019, AGH UST, Krakow, Poland.

6. References

1. Ministry of Natural Resources and Environment. *Application of IT in development of database and software managing mineral operation in Quang Ninh*, Hanoi (2016).
2. C. Dao, H. Tran. *Conference on Demand of Coal Production for Economy – Status and Solution*. Hanoi (2017).
3. Ministry of Natural Resources and Environment. *Process and economic-technical norms for development of natural resources and environment database*, Hanoi (2014).
4. H. Pham. *25th National Conference on Scientific and Technical Mining. Science and Technology*, Hanoi (2016)
5. P. Le. *Software Technique*. Information and Communications Publisher. Hanoi (2014)
6. D. Le. *Software Technology*. Science and Technics Publishing House. Hanoi (2015)
7. Quang Ninh Environment and Natural Resources Department. *Development of land database for Uong Bi, Cam Pha*, Quang Ninh (2013)
8. Project Management Unit of National Resources and Environment Database. *Development of national resources and environment database in 2010-2014*, Hanoi (2014)
9. Ministry of Natural Resources and Environment. *Development of general architect of informative system for natural resources and environment branch*, Hanoi (2010)
10. Project Management Unit of Sharing Software System for Informative System in Natural Resources and Environment Branch. *Development of sharing software system for informative system in natural resources and environment Branch*, Hanoi (2009)
11. Bac Giang Environment and Natural Resources Department. *Development of natural resources and environment database of Bac Giang province*, Bac Giang (2011)

Opiekun: prof. dr Jadwiga Jarzyna

Recenzenci: dr inż. Janusz Magiera - magiera@geol.agh.edu.pl

dr inż. Andrzej Gałaś - pollux@geol.agh.edu.pl

Use of Unmanned Aerial Vehicles for 3D topographic Mapping and Monitoring the Air Quality of Open-pit Mines

BUI Xuan Nam[1)], LEE Changwoo[2)], NGUYEN Quoc Long[1,*)], ADEEL Ahmad[3)], CAO Xuan Cuong[1)], NGUYEN Viet Nghia[1)], LE Van Canh[1)], NGUYEN Hoang[1)], LE Qui Thao[1)], DUONG Thuy Huong, NGUYEN Van Duc[2)]

[1)] Hanoi University of Mining and Geology, Vietnam
[2)] Dong-A University, Busan, Korea
[3)] University of the Punjab, Lahore, Pakistan

Corresponding author: nguyenquoclong@humg.edu.vn

Abstract. Recently remarkable advancement development of unmanned aerial vehicles (UAVs) has been observed and their applications have been shown in many fields such as agriculture, industry, and environmental management. However, in the mining industry, the application of UAV technology remains potential. This paper presents a low-cost unmanned aerial vehicle technology-based system for 3D mapping and air quality monitoring at open-pit mine sites in Vietnam. The system includes several dust sensors that are mounted on a low-cost rotary-wing type UAV. The system collects a variety of data, mainly images and airborne pollutant concentrations. To evaluate the performance of the proposed system, field tests were carried out at the Coc Sau coal mine. Based on the images transmitted to the ground monitoring station, large scale 3D topographic maps were successfully modeled. In addition, sensors mounted on the UAV system were able to monitor the levels of environmental variables associated with the air quality within the pit such as temperature, dust, CO, CO_2, and NOx. The field test results in this study illustrate the applicability of the low-cost UAV for the 3D mapping and the air quality monitoring at large and deep coal pits with relatively high accuracy.

1. Introduction

As one of the most important economic activities, the mining industry of Vietnam has been developing at a great pace. Coal produced by the Vietnam national coal-mineral industries holding corporation limited (Vinacomin) increased significantly from 27.5 million tons in 2004 to 47.5 million tons in 2010 (Tran & Nguyen, 2011). This accomplishment was attributed to the continuous application of advanced technologies in producing activities. In addition, Tran and Nguyen (2011) pointed out that it is necessary to continuously enhance the technology of all producing stages in order to achieve all

Vinacomin's goals. Mine surveying and environmental management are two of those important activities which have received great attention from both mining managers and scientists.

Traditional methods such as total station, the global navigation satellite system (GNSS) have been widely used in mining surveying with an accuracy of under 5 cm (Barry & Coakley, 2013). However, their main disadvantages are high cost and time consuming (Bui et al., 2016). In addition, the two methods meet many difficulties in areas with complicated terrains, especially unsafety for surveyors.

The mining industry of Vietnam has made a great contribution to the country's economy. However, this industry also inevitably leads to many environmental problems. In Vietnam, larger-scale open pit mines are often situated close proximity to population centers. For example, two of the largest open-pit coal mines in Vietnam, Coc Sau, and Deo Nai, are just about 1 km far from the Cam Pha city, Quang Ninh province (Figure 1). While blasting is an integral part of large-scale open-pit mining, it normally causes the emission of particulate material and gases potentially hazardous to health (Alvarado, Gonzalez, Fletcher, & Doshi, 2015). These activities generate particles and gases such as methane (CH_4), carbon dioxide (CO_2), nitrogen oxides (NO_x), and sulfur oxides (SO_x) that have potentially dangerous environmental and health impacts. It is noted that airblast, ground vibration, flyrock, toxic fumes, and particulate matter are the result of the blasting activity (Raj, 2005). All blasting events in mining areas emit the primary residue of Particulate matter, aerosols, ammonia, carbon dioxide (CO_2), nitrogen, nitrogen oxides (NO_x), and sulfur oxides (SO_x) (Alvarado et al., 2015). Although the exothermic reaction generates CO_2, water vapor, and Nitrogen (N_2) in a special case, other toxic fumes are proved to be produced in a range of concentrations as a result of environmental and technical factors (Attalla, Day, Lange, Lilley, & Morgan, 2007). In order to have proper management of air quality in mining areas, it is important to establish an effective monitoring system of air quality.

Recently, a rapid development in the unmanned aerial vehicle (UAV) technology has brought many benefits to not only military but also a wide range of civil fields such as logistics (Haidari et al., 2016; Olivares, Cordova, Sepúlveda, & Derpich, 2015), precise agriculture (Puri, Nayyar, & Raja, 2017; Rokhmana, 2015), forestry (Paneque-Gálvez, McCall, Napoletano, Wich, & Koh, 2014), urban management (Khan, Ectors, Bellemans, Janssens, & Wets, 2017; Salvo, Caruso, & Scordo, 2014; Spanogianopoulos, Zhang, & Spurgeon, 2017), hazardous and environmental management (Mourato, Fernandez, Pereira, & Moreira, 2017; Oleire-Oltmanns, Marzolff, Peter, & Ries, 2012), and mining industry. The preliminary successes of UAV applications have proved that this technology could be a promising technology and likely to be employed in a wider field. While the world has witnessed many excellent examples of using the UAV technology in the mining industry for topographical survey, safety investigation and other works (Sungjae Lee & Choi, 2016), this technology is still relatively new to Vietnam (Bui et al., 2016). For instance, the UAV technology was utilized to carry out a topographic survey of areas on the slope of an open-pit mine (McLeod et al., 2013). Another UAV based performance of topographic survey of an ore stockpile was given by Cryderman, Mah, and Shufletoski (2014). These authors used topographic data to estimate ore carrying capacity. S. Lee and Choi (2015) have proved that fixed-wing and rotary-wing UAVs, the most popular ones, can be used effectively in both small-scale and large-scale open-pit mines as a topographic surveying tool (S. Lee & Choi, 2015). For air quality monitoring in open-pit mine sites, results of the laboratory and field tests conducted by Alvarado et al., (2015) demonstrated the feasibility of coupling an opto-electronical dust sensor with UAVs.

As mentioned above, the application of UAVs has been proved as an alternative tool for both 3D mapping and the air quality monitoring. In this study, a low-cost UAV-based

system was employed to perform two-fold purposes at Coc Sau open-pit coal mine, one of the largest coal pit in Vietnam. This low-cost UAV system named as UMS-AM is designed to collect the varieties of data which can be used for optimizing mining operations and also control the atmospheric environment.

2. Description of the UMS-AM system

2.1 UAV platforms

The type of UAV is classified based on different but interrelated characteristics such as size and payload, wing types, flight endurance, flight range, altitude and capabilities (Berie & Burud, 2018). Based on wing types, there are two main types of UAV, namely the rotary-wing and fixed-wing UAVs. The latter is suitable for the applications that demand longer flight endurance, but large space is needed for take-off and landing. Although the former uses batteries and has shorter flight times (Paneque-Gálvez et al., 2014), it has been increasingly common because of its ability to take off and land vertically in the small space and to maintain position. Therefore, in this study, a rotary-wing UAV was considered as a feasible platform for the system. Specifically, its characteristics are in the following table 1.

Table 1. Specifications of major private UAV equipment

Name of UAV	Inspire 2
Weight	4000 g
Battery	4280 mAh
Camera	Multi: CMOS, 1" 20 MP
Max flight time	Approx. 27 min
Cruise speed	- P mode/A-mode: 16.4 ft/s (5 m/s) - S-mode: 19.7 ft/s (6 m/s)
Radio link range	7 km
Payload	Approx. 1.9 kg

The variety of UAV equipment allows users to have many different options. One of the major advantages of this UAV type is their low prices. However, the payload has to be taken into consi**d**eration as there are several air quality sensors and accessories mounted on the UAV. In this study, the DIJ Inspire 2 was utilized for the investigation as shown in figure 1.

Fig. 1. DJI Inspire 2 UAV (https://www.dji.com)

2.2 Sensors

2.2.1 Optical sensor (Inspire 2's camera parameters)

The Zenmuse X4S is a powerful camera featuring a 20 megapixel 1-inch sensor and a maximum ISO of 12,800. Dynamic range is increased from the Zenmuse X3 by 1 stop, with the signal to noise ratio and color sensitivity increased by 1.5 stops for next-level image quality. The Zenmuse X4S uses a DJI-designed compact lens with low dispersion and low distortion 24mm equivalent prime lens. This 84° FOV, high resolution lens makes the Zenmuse X4S as powerful during aerial imaging as it is on the ground. Combined with CineCore 2.0, the Inspire 2's powerful image processing system, it can record 4K/60 H.264 and 4K/30 H.265 videos at a 100Mbps bitrate, and oversample 5.2K video into 4K video in real-time, capturing fine image details. In Burst Mode, the Zenmuse X4S supports 14fps shooting at 20 megapixels in both JPEG and DNG formats. It is able to make the difficult balance between agility and image quality (https://www.dji.com/zenmuse-x4s).

2.2.2 Air quality monitoring system

To evaluate mine pit the air quality within the atmosphere of a deep pit mine, the levels of four major pollutants including PM_{10}, CO, NO, and NO_2 were measured by UAV. Several sensors described in Table 2 were attached to UAV for monitoring. Due to the load limitation of UAV, light and compact sensors were packed in a perforated box and mounted on the vehicle. Figure 3 shows the monitoring box installation and a picture of UAV flight.

The communication link played an important role between the data collection and transmission. The data transmission should satisfy the requirements of stability and reliability when the UAV equipped with the monitoring sensor box reach high altitude. Thus, a smartphone or a tablet was attached into the monitoring box as a relay station and also transceiver to store the measurement data. The structure of the UAV air quality monitoring platform and the system concept are illustrated in Figure 2. In this study, prior to flying the UAV, all the sensors were calibrated.

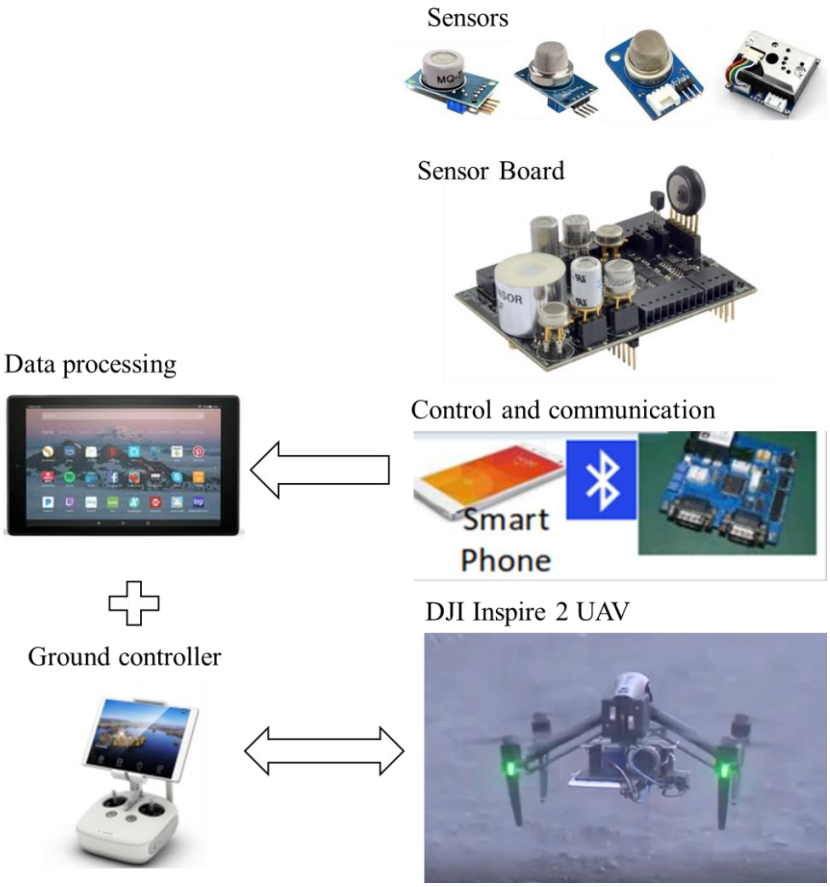

Fig. 2. Structure of the UAV air quality monitoring platform and system concept for collecting a drone mounted air quality sensor

In addition, two ground monitoring stations were installed on the top of the pit mainly to monitor the atmospheric condition of the free stream including the barometric pressure, temperature and wind velocity along with the direction.

Table 2. Specifications of the air quality monitoring sensors

Monitoring Target	Sensor category	Range	Precision	Resolution
PM_{10}	Laser dust sensor	0-500 µg/m^3	± 10%	0.3 µg/m3
CO	Electrochemistry sensor	0-750ppm	± 5% ppm	1 ppm
NO	Electrochemistry sensor	0-250ppm	± 5% ppm	1 ppm
NO_2	Electrochemistry sensor	0-20ppm	± 5% ppm	0.1 ppm

Fig. 3. Air quality monitoring components of the UMS-AS system

3. Study site

Coc Sau, as shown in Figure 4, was the second largest and the deepest open-pit mine in Vietnam at the time of the study. Coal produced at the Coc Sau mine contributed over 2 million tons to the VINACOMIN's production.

4. Operation and data processing

4.1 3D mapping section

Flight plans for aerial photography are established using the Pix4DCapture software installing in an Ipad tablet. Considering the maximum flight time during battery charge, one of the flight routes is shown in Fig 5a, and the flight altitude is calculated by considering the topographic altitude of the surrounding areas. In addition, the lateral vertical overlaps of the aerial photographs to be photographed were set to 80%.

In order to improve the accuracy of terrain survey results using UAVs, it is necessary to correct the data using ground control points. In this study, 35 GCPs were installed in the study area using markers (Fig 5b). We used GNSS CORs to measure the coordinates of these GCPs. We measured the X, Y and Z coordinates of the GCPs by receiving the satellite signals for about one minute after vertically positioning the CORs rover at the center of the markers.

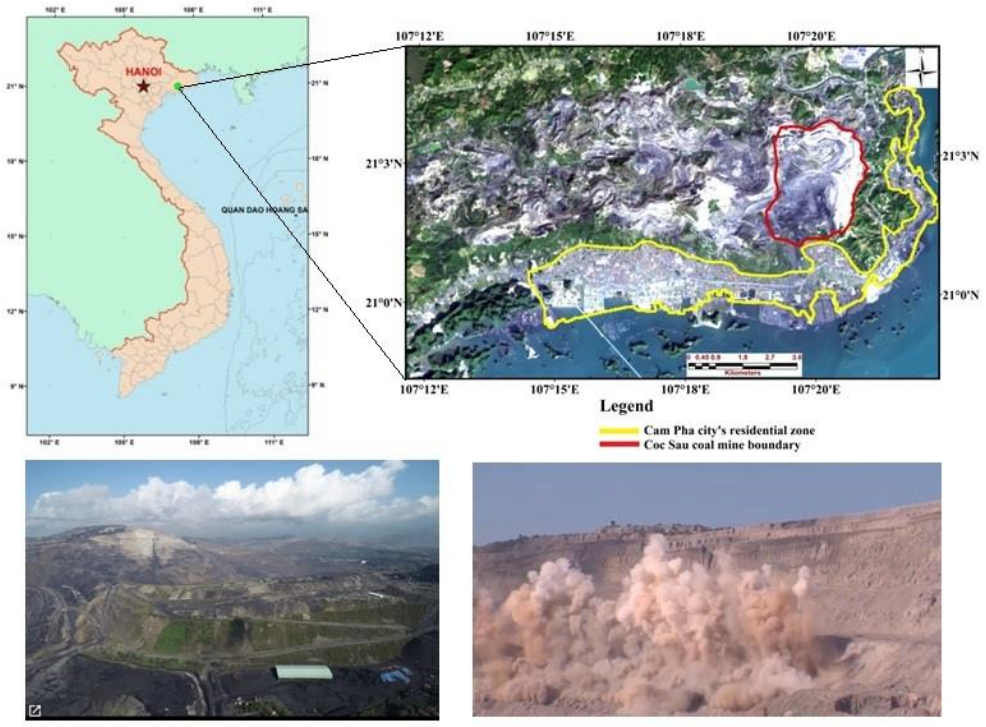

Fig. 4. Location of the study area in Cam Pha city, Quang Ninh province, Vietnam

There is a variety of software for processing aerial photographs such as Pix4D, Autodesk 123D Catch, DroneMapper, Acute3D, TBC, Agisoft Photoscan, and PhotoModeler. However, Agisoft Photoscan has been approved to be the best one (Sona, Pinto, Pagliari, Passoni, & Gini, 2014). Therefore, in this study, Agisoft Photoscan (ver 1.3.1) was used to process aerial photographs captured at the site (Fig 5d). When these photos are entered into Agisoft Photoscan, key points that can be identified simultaneously from multiple images are automatically extracted. With GNSS GCPs, 3D point clouds are built for automatic photo matching process. In the next stage, the automatic aerial triangulation (AAT) procedure is undertaken including the three following steps: (i) calculate both external and internal orientation parameters; (ii) perform the least squares block adjustment; and (iii) build mesh, digital surface model, and orthophoto.

4.2 Air quality monitoring measurement

This study had two-fold purposes for monitoring the atmospheric environment and understanding the pollutants dispersion mechanism. Investigation of the air quality was carried out within a large and deep pit mine. Pollutants dispersion in a deep pit depends on the surface wind and the air density differences between the in and outside of the pit.

However, it is well known that strong nocturnal inversions occur in valleys and mountain basins on calm, clear night (e.g. Hibberd 2003, Clements et al 2003) but there was almost no data related to the existence of the inversion layer at the deep pits. Thus, this

study measured vertical temperature profiles to identify the temperature gradient to determine the airflow stability during the study.

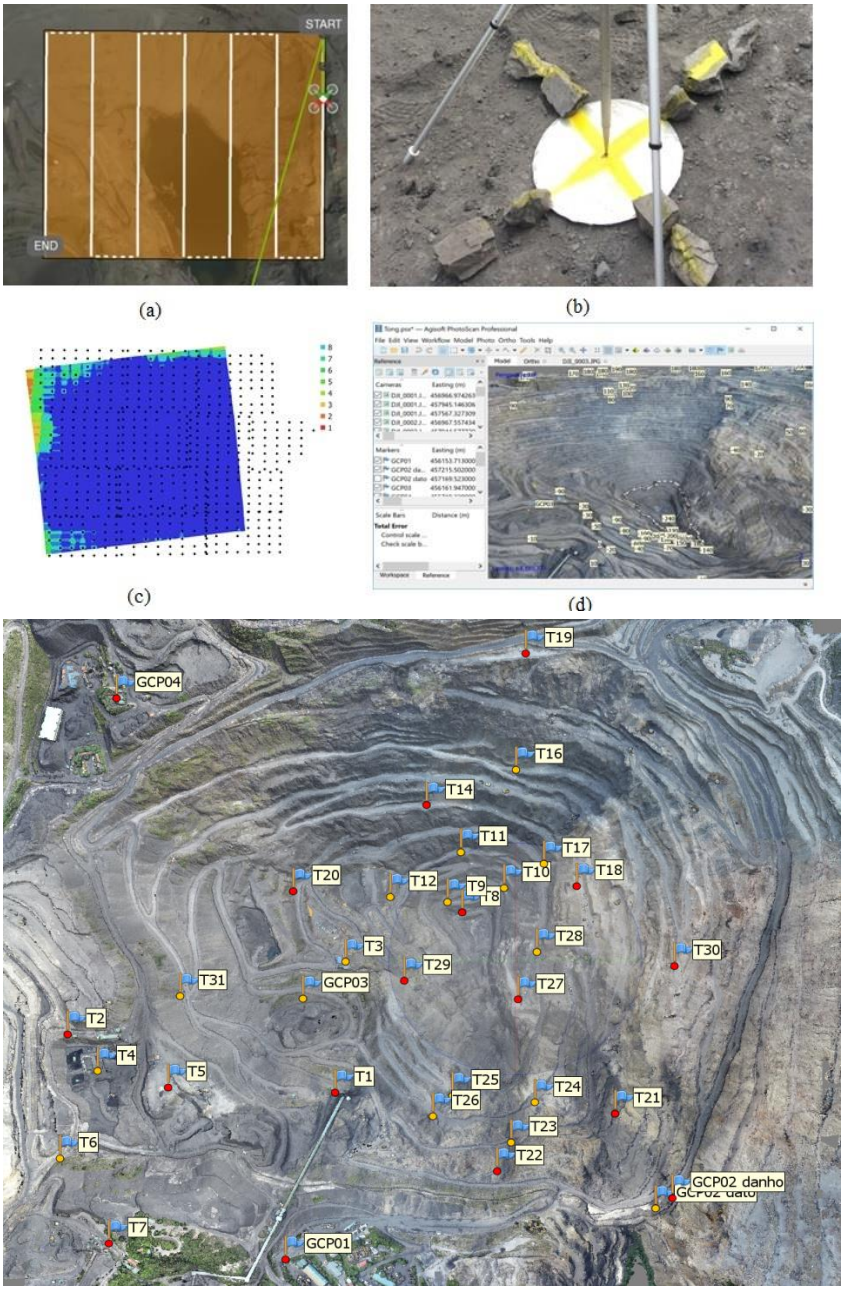

Fig. 5. 3D mapping steps in Coc Sau coal mine (a) Flight route and shooting points designed for the study area; (b) The designed marker and Ground control points (GCPs) measured by GNSS CORs; (c) Camera locations and image overlap; (d) Processing UAV photos with Agisoft Photoscan software; (f) distribution of calibrated and checked points

Due to the limited battery capacity of UAV, the UAV has less hover time with more load. The total load including sensors and other accessories was 1.0 kg, the hover time was about 25 minutes. However, by excluding the time for starting and landing, it was necessary to shorten the hover time to 15 minutes. Figure 6 shows the UAV flight paths to measure the atmospheric environment problems within the pit. The space within the pit was divided into two sections; H1 at -140m and H2 at 120m as shown in Figure 6. UAV flew through these zones in a systematical way. The data collected were utilized to make 3D environment maps.

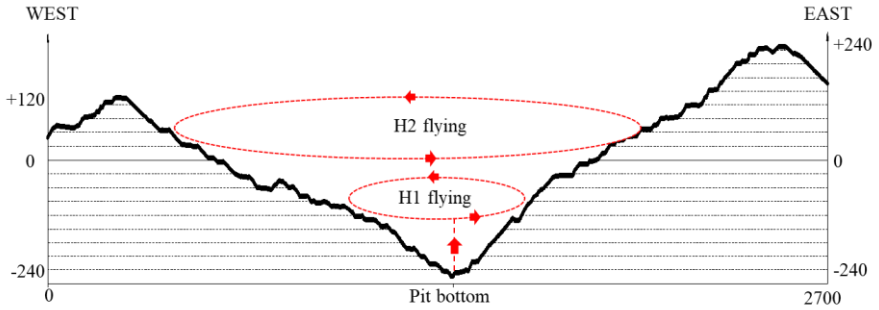

Fig. 6. UAV flight paths to measure the atmospheric environment at pit

For the second purpose to measure the vertical temperature profiles within the pit, the UAV was flown along the flight paths shown in Figure 7. UAV started at the center of the pit bottom and flew along the vertical line to 250m above the sea level. The flight was made twice a day, before the sunrise and after the sunset.

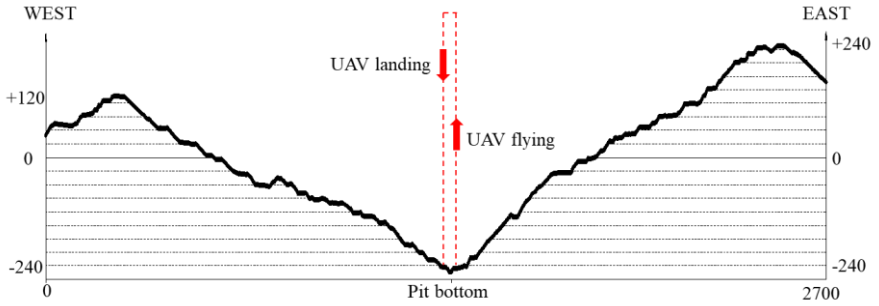

Fig. 7. UAV flight to measure the vertical temperature profiles

4.3 Accuracy assessment of the digital surface model

Accuracy assessment of the Digital Surface Model (DSM) is an important task, and without this task, the DSM is useless. In this project, both the horizontal and vertical assessments were carried out by comparing DSM with the GCPs measured by a Leica total station in term of Root Mean Square Error (RMSE). More specifically, assessments in easting ($RMSE_X$), northing ($RMSE_Y$), vertical ($RMSE_Z$), and all components ($RMSE_{XYZ}$)

were used, as suggested in Agüera-Vega (Agüera-Vega, Carvajal-Ramírez, & Martínez-Carricondo, 2016), using equations as follows:

$$\Delta X = \mathrm{X_{DSM}} - \mathrm{X_{GCP}} \quad (1)$$

$$\Delta Y = \mathrm{Y_{DSM}} - \mathrm{Y_{GCP}} \quad (2)$$

$$\Delta Z = \mathrm{Z_{DSM}} - \mathrm{Z_{GCP}} \quad (3)$$

$$\Delta XYZ = \mathrm{XYZ_{DSM}} - \mathrm{XYZ_{GCP}} \quad (4)$$

$$RMSE_{\mathrm{X}} = \mathrm{SQRT}\left[(1/n) \sum_{i=1}^{n} (\mathrm{X_{DSM}} - \mathrm{X_{GCPi}})^2 \right] \quad (5)$$

$$RMSE_{\mathrm{Y}} = \mathrm{SQRT}\left[(1/n) \sum_{i=1}^{n} (\mathrm{Y_{DSM}} - \mathrm{Y_{GCPi}})^2 \right] \quad (6)$$

$$RMSE_{\mathrm{Z}} = \mathrm{SQRT}\left[(1/n) \sum_{i=1}^{n} (\mathrm{Z_{DSM}} - \mathrm{Z_{GCPi}})^2 \right] \quad (7)$$

$$RMSE_{\mathrm{XYZ}} = \mathrm{SQRT}\left[(1/n) \sum_{i=1}^{n} ((X_{\mathrm{DSM}} - X_{\mathrm{GCPi}})^2 + (Y_{\mathrm{DSM}} - Y_{\mathrm{GCPi}})^2 + (Z_{\mathrm{DSM}} - Z_{\mathrm{GCPi}})^2) \right] \quad (8)$$

where $\mathrm{X_{GCPi}}$ and $\mathrm{X_{DSM}}$ are the X-coordinate component of GCP and corresponding coordinate in DSM, respectively; $\mathrm{Y_{GCPi}}$ and $\mathrm{Y_{DSM}}$ are the Y-coordinate component of GCP and corresponding coordinate in DSM, respectively; $\mathrm{Z_{GCPi}}$ and $\mathrm{Z_{DSM}}$ are the Z-coordinate component of GCP and corresponding coordinate in DSM, respectively.

5. Some of the field test results

5.1 3D mapping

Table 3 shows the aerial photographs of the study area using our designed system. 687 aerial photographs were shot according to the flight plan (Fig 5c). However, for the area where air quality was monitored, there were 56 photos. The average spatial resolution of the aerial photographs was about 8.55 cm/pixel. It took about 6 hours to process 687 aerial images using Agisoft Photoscan.

Table 3. Data acquisition

Number of images	687	Camera stations	680
Flying attitude	327 m	Tie points	527,464
Ground resolution	8.55 cm/pixel	Projections	2280976

To determine the best camera-lens parameters in this research, an optimization process was carried out. For this task, the 35 GCPs were split into two subsets: (i) the first one is a calibrating dataset that accounts for 17 GCPs of the total GCPs and was used for the calibration of the camera-lens model and the bundle adjustment; (ii) the second one is a checking dataset that consists of the remaining GCPs. 18 GCPs were used for checking the final model and confirming its accuracy. Distribution of these GCPs in this study area is

shown in Fig. 5e. This is because these were unsafe areas to reach due to the coal seams still were exploiting.

After the following steps: photo align, camera calibration, bundle adjustment, cloud point building, and mesh creation, the digital surface model of the mine was produced (Fig. 8c). For the model calibration, RMSE for X, Y, Z, XYZ is 1.1 cm, 1.7 cm, 4.9 cm, and 5.1 cm, respectively. The largest error for X is 2.0 cm and for Y is 5.4 cm whereas the largest error for Z is 9.5 cm. The largest error for XYZ is 9.5 cm (Table 4). These indicate that the close fit of the DSM model with the calibrating dataset.

Table 4. RMSE in X, Y, Z, XY and XYZ of GCPs used for the model calibration.

Calibration Points	ΔX (m)	ΔY (m)	ΔXY (m)	ΔZ (m)	Δ XYZ (m)
GCP01	0.003	0.002	0.004	0.011	0.012
GCP02 danho	-0.004	-0.014	0.015	-0.02	0.058
GCP04	-0.012	0.001	0.012	0.021	0.016
T2	-0.004	0.013	0.014	0.013	0.019
T5	0.007	0.007	0.010	-0.016	0.019
T7	0.005	-0.002	0.005	-0.054	0.054
T8	-0.02	-0.028	0.034	-0.063	0.072
T14	0.015	-0.012	0.019	-0.054	0.057
T18	0.004	-0.007	0.008	-0.025	0.026
T19	-0.008	0.001	0.008	0.095	0.095
T20	-0.007	-0.003	0.008	-0.014	0.016
T21	-0.007	-0.011	0.013	0.091	0.092
T22	0.006	-0.008	0.010	0.004	0.011
T27	-0.025	-0.017	0.030	0.063	0.07
T29	-0.016	0.012	0.020	0.079	0.081
T30	-0.007	-0.013	0.015	-0.028	0.032
T1	-0.004	-0.008	0.009	-0.017	0.019
Total	0.011	0.017	0.016	0.049	0.051

Table 5. RMSE in X, Y, Z, and XYZ of check points in this project.

Check points	ΔX (m)	ΔY (m)	ΔXY (m)	ΔZ (m)	Δ XYZ (m)
GCP03	0.120	0.166	0.205	-0.195	0.283
T3	-0.060	-0.020	0.063	-0.080	0.102
T4	-0.098	0.000	0.098	0.128	0.161
T6	-0.005	-0.032	0.032	-0.207	0.210
T9	0.053	-0.003	0.053	-0.204	0.309
T10	0.069	0.037	0.078	0.255	0.267

T11	0.094	-0.094	0.133	0.148	0.199
T12	0.022	0.003	0.022	-0.148	0.150
T15	0.035	-0.011	0.037	0.090	0.097
T16	0.044	-0.032	0.054	-0.035	0.065
T17	0.033	-0.089	0.095	-0.081	0.125
T23	-0.016	-0.064	0.066	-0.075	0.068
T24	0.006	-0.058	0.058	-0.071	0.059
T25	0.070	0.077	0.136	0.085	0.144
T26	-0.079	0.002	0.079	-0.071	0.079
T28	-0.108	-0.017	0.169	0.159	0.232
T31	0.082	-0.062	0.128	0.068	0.145
GCP02 dato	0.006	0.015	0.016	0.138	0.139
Total	0.066	0.061	0.090	0.138	0.164

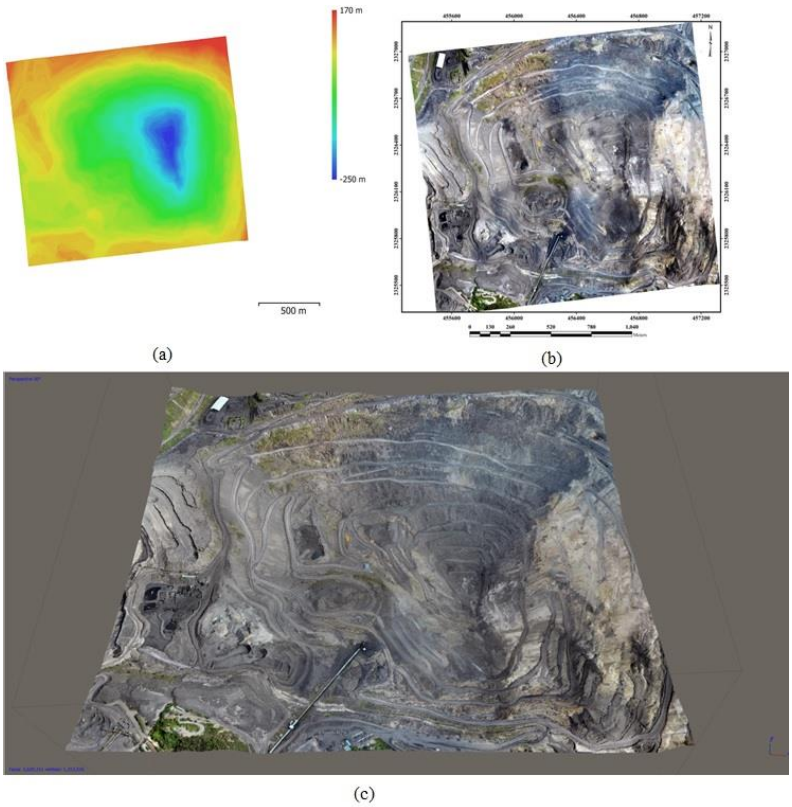

Fig. 8. Results of 3D mapping using the UMS-AM system (a) Digital Elevation Model (DEM); (b) Othorphoto; (c) The 3D model of the Coc Sau coal mine.

Fig. 8a shows the DEM and orthoimage produced using the proposed system with a resolution of 34 cm/pixel and 8.5 cm/pixel, respectively. In addition, Fig. 8c shows the topographical results of the study area in three dimensions. For the accuracy assessment of the results, the root mean square error (RMSE) for the position coordinates of the GCPs in the X, Y, and Z directions is used.

Since the calibrating dataset was used for both the optimization process and the goodness-of-fit, the result may be too positive. Therefore, the checking dataset that was not used in the calibration phase was used to assess the accuracy of the DSM model. The result is shown in Table 5. It could be seen that the RMSE of X, Y, Z, XYZ are 6.6 cm, 6.1 cm, 13.8 cm, and 16.4 cm, respectively. The highest error for X is 12.0 cm and for Y is 16.6 cm whereas the highest error for Z is 25.5 cm and the highest error for XYZ is 28.3 cm (Table 5). These indicate that the accuracy of the DSM model is appropriate with the accuracy requirement for mine surveying missions.

5.2 Air monitoring

Figure 9 shows the environment maps plotted in terms of CO, Dust (PM_{10}), NO and temperature. These maps were generated by ArcGIS (version 10.2). In addition, in order to complete the 3D contours, the Inverse Distance Weighted (IDW) interpolation method was employed. These maps show the environmental pollution profiles at the altitude of +120m.

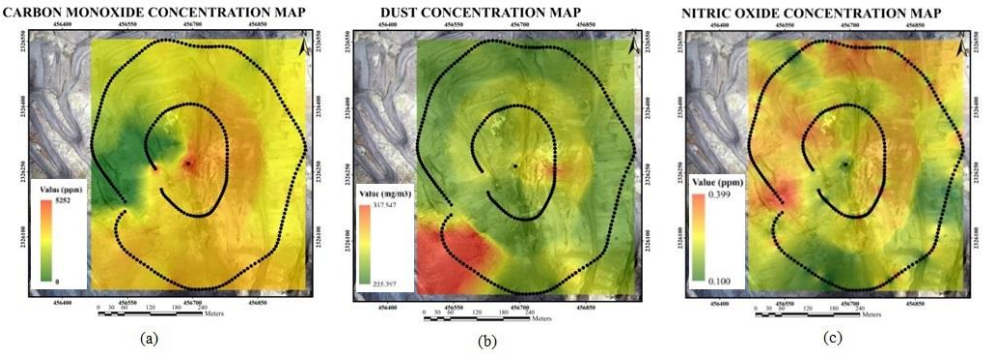

Fig. 9. Concentration maps of air components (a) CO; (b) Dust (PM10); (c) NO

The dispersion mechanism within a deep open pit mine is complicated due to the effect of topographic, thermal and meteorological factors. The meteorological conditions within the deep open pit coal mine are significantly affected by temperature (stability) and roughness conditions which ultimately generate complex dispersion phenomenon including separation of the atmospheric boundary layer, recirculation, re-suspension, and settling of PM_{10} (Bitkolov, 1969; Grainger & Meroney, 1993). Based on the site measurement, Figure 10 shows the vertical temperature profiles.

The possible temperature inversion effect was observed in Figure 10 (a) which was based on the the first day measurement before the sunrise. However, this phenomenon was not detected clearly in the other days. Further, the dispersion of air pollutants is dependent on the Pasquill stability of the atmosphere classes in Table 6.

Table 6. Pasquill stability classes by the vertical temperature gradient

Stability class	Vertical temp gradient, ΔT/ΔZ (DegC/100m)	Definition
A	-1.9	very unstable
B	-1.9 to -1.7	unstable
C	-1.7 to -1.5	slightly unstable
D	-1.5 to -0.5	neutral
E	-0.5 to 1.5	slightly unstable
F	1.5 to 4.0	stable
G	> 4.0	very stable

Table 7 shows the vertical temperature gradients for three days' experiments. The temperature gradient was in the range of 0.64-1.53 ^{o}C/100 m and the atmosphere can be classified as E and F. This implies "slightly unstable" and "stable" which indicate the dispersion of pollutants generated within the pit is hardly dispersed out of the deep pit. This resulted in high dust concentrations observed during the study in Figure 9 (b).

Table 7. Vertical temperature gradients during the study

Category	Before sunrise		After sunset	
	Upward flight	Downward flight	Upward flight	Downward flight
1st day measurement	1.17	1.53	0.64	0.68
2nd day measurement	0.68	0.84	1.53	1.28
3rd day measurement	1.21	1.12	1.13	1.23

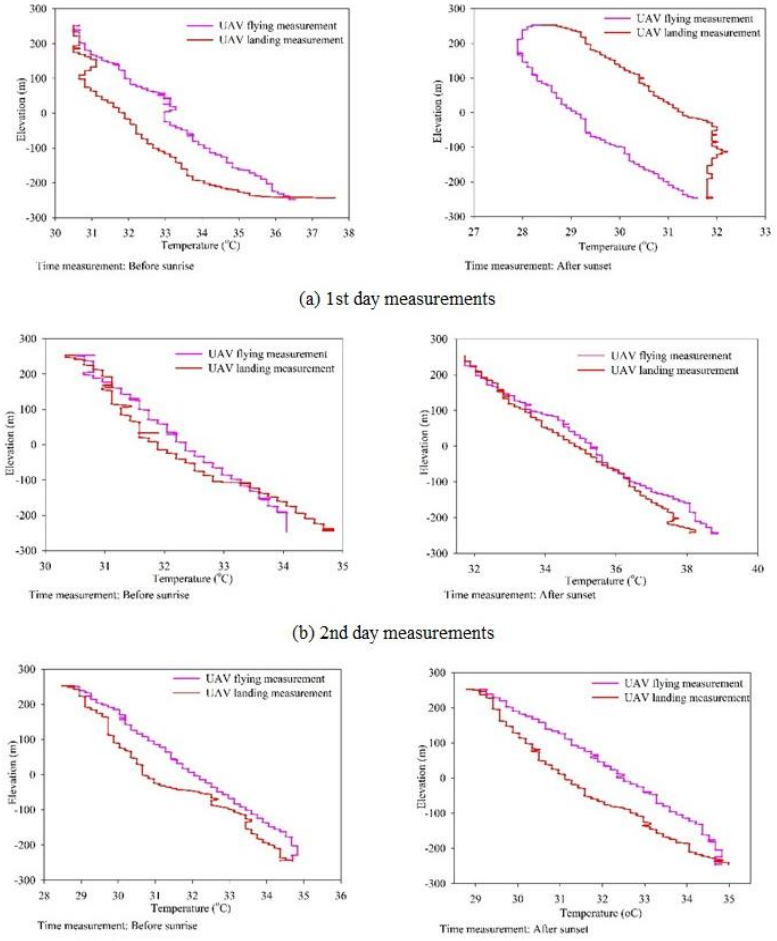

Fig. 10. Vertical temperature profiles by UAV measurement

6. Conclusion

In this study, a UAV-based system has been developed ultimately for the topographical survey and the air quality management in the mining industry. The UAV system includes a DJI Inspire 2 equipped by the RGB Zenmuse X4S camera, air quality monitoring sensors and data logging system. Through the site study, the system proved to be a safe, effective and economical tool for environmental management. Some of the limitations experienced during the study were closely related to the UAV system itself; the limitation on UAV allowable load was the most significant problem for the monitoring purposes. One of the advantages of the low-cost UAV system is that 3D models can be generated easily without additional efforts, while the system equipped with low-cost reliable sensors clearly show the applicability of the mine environment monitoring system within the large and deep pit mines.

For the accuracy of 3D models, the result showed that the DSM model has high accuracy; RMSE in the calibrating dataset is 2 cm and 4.9 cm for vertical and horizontal, respectively indicating high success-rate of fit, whereas RMSE in the checking dataset is 13.8 cm and 9 cm for vertical and horizontal, indicating high accuracy. These indicate that the processes of capturing images, establishment of GCPs, and photogrammetric processing were carried out successfully.

Ultimately, pollutant control measures can be derived by the system, since the air pollution profiles are visible in the 3D maps and the main causes of the pollution can be easily verified based on the 3D maps.

7. Acknowledgements

Paper was presented during the 5th POL – VIET International Conference Scientific-Research Cooperation between Vietnam and Poland, 08-10.07.2019, AGH UST, Krakow, Poland. This research was supported by the Ministry of Education and Training of Vietnam (MOET) under grant number B2018-MDA-03SP and by the Research Institute for Mining Electro-Mechanics of Hanoi University of Mining and Geology.

8. References

1. Agüera-Vega, F., Carvajal-Ramírez, F., & Martínez-Carricondo, P. (2016). Accuracy of Digital Surface Models and Orthophotos Derived from Unmanned Aerial Vehicle Photogrammetry. *Journal of Surveying Engineering*, 04016025.
2. Alvarado, M., Gonzalez, F., Fletcher, A., & Doshi, A. (2015). Towards the Development of a Low Cost Airborne Sensing System to Monitor Dust Particles after Blasting at Open-Pit Mine Sites. *Sensors, 15*(8), 19667. Retrieved from http://www.mdpi.com/1424-8220/15/8/19667
3. Attalla, M., Day, S., Lange, T., Lilley, W., & Morgan, S. (2007). *NOx Emissions from Blasting in Open Cut Coal Mining in the Hunter Valley*. Retrieved from ACARP: Newcastle, Australia,:
4. Barry, P., & Coakley, R. (2013). Accuracy of UAV photogrammetry compared with network RTK GPS. *Int. Arch. Photogramm. Remote Sens, XL-1 W*, 27-31.
5. Berie, H. T., & Burud, I. (2018). Application of unmanned aerial vehicles in earth resources monitoring: focus on evaluating potentials for forest monitoring in Ethiopia. *European Journal of Remote Sensing, 51*(1), 326-335. doi:10.1080/22797254.2018.1432993
6. Bitkolov, N. Z. (1969). Wind and Temperature of quarry atmospheres. *Fiziko-Tekhnicheskie Problemy Razrabotki Poleznykh Iskopaemykh*(5), 66-73.
7. Bui, T. D., Nguyen, C. V., Hoang, M. H., Dong, B. P., Nhu, V. H., Tran, T. A., & Nguyen, Q. M. (2016). *Xây dựng mô hình số bề mặt và bản đồ trực ảnh sử dụng công nghệ đo ảnh máy bay không người lái.* Paper presented at the Hội nghị khoa học: Đo đạc bản đồ với ứng phó biến đổi khí hậu, Hà Nội.
8. Cryderman, C., Mah, S. B., & Shufletoski, A. (2014). Evaluation of UAV Photogrammetric Accuracy for Mapping and Earthworks Computations. *GEOMATICA, 68*(4), 309-317. doi:10.5623/cig2014-405
9. Grainger, C., & Meroney, R. N. (1993). *Boundary-Layer Meteorol*: Kluwer Academic Publishers.
10. Haidari, L. A., Brown, S. T., Ferguson, M., Bancroft, E., Spiker, M., Wilcox, A., . . . Lee, B. Y. (2016). The economic and operational value of using drones to

transport vaccines. *Vaccine, 34*(34), 4062-4067. doi:10.1016/j.vaccine.2016.06.022

11. Khan, M. A., Ectors, W., Bellemans, T., Janssens, D., & Wets, G. (2017). UAV-Based Traffic Analysis: A Universal Guiding Framework Based on Literature Survey. *Transportation Research Procedia, 22*, 541-550. doi:https://doi.org/10.1016/j.trpro.2017.03.043
12. Lee, S., & Choi, Y. (2015). On-site demonstration of topographic surveying techniques at open-pit mines using a fixed-wing unmanned aerial vehicle (drone). *Tunnel & Underground Space, 25*, 527–533.
13. Lee, S., & Choi, Y. (2016). Reviews of unmanned aerial vehicle (drone) technology trends and its applications in the mining industry. *Geosystem Engineering, 19*(4), 197-204. doi:10.1080/12269328.2016.1162115
14. McLeod, T., Samson, C., Labrie, M., Shehata, K., Mah, J., Lai, P., . . . Elder, J. H. (2013). Using Video Acquired from an Unmanned Aerial Vehicle (UAV) to Measure Fracture Orientation in an Open-Pit Mine. *GEOMATICA, 67*(3), 173-180. doi:10.5623/cig2013-036
15. Mourato, S., Fernandez, P., Pereira, L., & Moreira, M. (2017). *Improving a DSM Obtained by Unmanned Aerial Vehicles for Flood Modelling*. Paper presented at the IOP Conf. Series: Earth and Environmental Science.
16. Oleire-Oltmanns, S., Marzolff, I., Peter, K., & Ries, J. (2012). Unmanned Aerial Vehicle (UAV) for Monitoring Soil Erosion in Morocco. *Remote Sens., 4*(11), 3390-3416. doi:10.3390/rs4113390
17. Olivares, V., Cordova, F., Sepúlveda, J. M., & Derpich, I. (2015). Modeling Internal Logistics by Using Drones on the Stage of Assembly of Products. *Procedia Computer Science, 55*, 1240-1249. doi:https://doi.org/10.1016/j.procs.2015.07.132
18. Paneque-Gálvez, J., McCall, M. K., Napoletano, B. M., Wich, S. A., & Koh, L. P. (2014). Small drones for community-based forest monitoring: An assessment of their feasibility and potential in tropical areas. *Forests, 5(6)*, 1481–1507.
19. Puri, V., Nayyar, A., & Raja, L. (2017). Agriculture drones: A modern breakthrough in precision agriculture. *Journal of Statistics and Management Systems, 20*(4), 507-518. doi:10.1080/09720510.2017.1395171
20. Raj, R. (2005). *Sustainable mining systems and technologies in Sustainable Mining Practices*. USA: Taylor & Francis: Oak Brook.
21. Rokhmana, C. A. (2015). The Potential of UAV-based Remote Sensing for Supporting Precision Agriculture in Indonesia. *Procedia Environmental Sciences, 24*(Supplement C), 245-253. doi:https://doi.org/10.1016/j.proenv.2015.03.032
22. Salvo, G., Caruso, L., & Scordo, A. (2014). Urban Traffic Analysis through an UAV. *Procedia - Social and Behavioral Sciences, 111*, 1083-1091. doi:https://doi.org/10.1016/j.sbspro.2014.01.143
23. Sona, G., Pinto, L., Pagliari, D., Passoni, D., & Gini, R. (2014). Experimental analysis of different software packages for orientation and digital surface modelling from UAV images. *Earth Science Informatics, 7*(2), 97-107. doi:10.1007/s12145-013-0142-2
24. Spanogianopoulos, S., Zhang, Q., & Spurgeon, S. (2017). Fast Formation of Swarm of UAVs in Congested Urban Environment. *IFAC-PapersOnLine, 50*(1), 8031-8036. doi:https://doi.org/10.1016/j.ifacol.2017.08.1228
25. Tran, X. H., & Nguyen, A. T. (2011). *Đổi mới, hiện đại hóa, khai thác và tuyển, chế biến nhằm phát triển bền vững ngành than - khoáng sản.* Paper presented at the Hội nghị khoa học kỹ thuật mỏ toàn quốc - 2011, Nha Trang.

Comparison of the Resampling Methods for Gridded DEM Downscaling

Nguyen Quang Minh[1*], Nguyen Thi Thu Huong[1], La Phu Hien[1], Duong Thi Tuyet Nhung[1], Nguyen Thi Minh Hong[1], Vu Van Anh[2]

[1] Hanoi University of Mining and Geology, 18 Vien St, Duc Thang, Bac Tuliem, Hanoi

[2] General Department of Remote Sensing, Ministry of Natural Resources and Environment

Abstract. In this paper, a comparison and evaluation of three resampling methods for gridded DEM is implemented. The evaluation was based on the results of bilinear resampling, bi-cubic and Kriging resampling methods for an experiment using both degraded and sampled datasets at 20 m and 60 m spatial resolutions. The evaluation of the algorithms was accomplished comprehensively with visual and quantitative assessments. The visual assessment process was based on direct comparison of the same topographic features in different downscaled images, scatterplots and profiles. The quantitative assessment was based on the most commonly used parameters for DEM accuracy assessment such as root mean square errors (RMSEs), linear regression parameters m and b, and correlation coefficient R. Both visual and quantitative assessment revealed greater accuracy of the Kriging over the other two conventional methods.

1. Introduction

The spatial resolution of a gridded DEM affects both the information content and the accuracy of the data and, potentially, of many other secondary data products [1]. Examples include the well-known effects of spatial resolution on the spatial properties of DEM and other spatial data [2], on slope and aspect [3], watershed boundary delineation and the accuracy of SWAT schemes [4], water run-off models [5], three dimensional modelling of landscapes [6], local slope, plan curvature, drainage area [7], soil survey results and soil moisture [8]. All of the above-mentioned studies showed that DEMs with a finer spatial resolution can produce more informative and more accurate results.

Gridded DEMs with fine spatial resolution and high accuracy can be acquired using remote sensing and airborne LiDAR technology, ground surveying or photogrammetry [9]. Airborne LiDAR enables the acquisition of data with a very high density of 3-dimensional coordinate points and, therefore, production of a DEM with sub-meter spatial resolution. Although being capable of generating a fine spatial resolution DEM, airborne LiDAR technology has some challenges such as the very large amount of data storage required and high computing capacity for data processing. Compared with airborne LiDAR, other methods for fine spatial resolution DEM acquisition such as ground surveying and photogrammetry are more time consuming and labour intensive [10].

Sometimes, it is necessary to resample the raster DEM to a higher resolution using the common algorithms such as nearest neighbour, bilinear and bi-cubic interpolation.

Potentially, these algorithms can downscale the raster DEM data [11]. That means the resolution or the accuracy of raster DEM were slightly improved through resampling using these approaches [12]. Another method for resampling gridded DEM data to a finer resolution Kriging interpolation [13]. Dixon and Earls [14] used the simple nearest neighbour resampling to increase the resolution of DEMs and compare the effects of results to the DEM's products such as stream flow, watershed, delineations, number of sub-basins and slopes. It was showed that the simple resampling of DEM did not increase the accuracy of DEMs greatly, or, the resampling methods did not create new significant information that is not available at the original resolution of DEM [15]. The experiments by Rees [16] and Shi et. al. [12] showed that bilinear, bicubic and Kriging resampling increased the accuracy of DEMs in term of root mean square error (RMSE) with a suitable value of re-sampling ratio *r*. Comparing three resampling methods, Kriging performed better than the other two methods for smooth terrain. However, for terrain with high roughness, the performance of three methods were similar and further assessment of these three methods is necessary [16]. Therefore, in this paper, the evaluation of the algorithms was accomplished comprehensively with visual and quantitative assessments. The visual assessment process was based on direct comparison of the same topographic features in different resampled images, scatterplots and profiles. The quantitative assessment was based on the most commonly used parameters for DEM accuracy assessment such as root mean square errors (RMSEs), linear regression parameters *m* and *b*, and correlation coefficient *R*.

2. Method

To test the three algorithms for resampling, the DEMs with coarser spatial resolution were used as an input to produce DEMs at the same resolution of reference data using the bilinear, bi-cubic resampling, and Kriging interpolation. In the experiment with Kriging interpolation, several Kriging parameters such as semivariogam models, number of samples and range of searching for samples were tested. The most accurate results were selected with Kriging interpolation using exponential variogram model with 8 samples.

The assessment was implemented based on both visual comparison of the resulting DEMs from the three different methods and quantitative evaluation using the parameters which were usually used for DEMs' accuracy assessment such as RMSE [17], coefficient of determination, linear regression parameters, and the elevation profiles [18].

Visual assessment of the results was carried out by several approaches. The first approach is direct visual comparison of the DEM images, especially comparison of the same topographical features in different images. The second approach is to analyse the scatterplots between the elevation values the pixels of reference DEMs and the elevation values of the corresponding pixels of the bilinear and bi-cubic resampled DEMs, and Kriging interpolated DEM. Another approach which was used in many previous research on DEM evaluation is comparing the profiles of the resulted downscaled DEMs [17]. These profiles present the match between the surfaces formed by the reference DEM and the surfaces formed by DEM at coarse spatial resolution, bilinear, bi-cubic and Kriging resampling algorithms and therefore enable the evaluation of the effects of the algorithms on different forms of terrain and topographical features.

The quantitative assessment was implemented mainly based on the RMSEs for whole images and profiles. Together with the RMSEs, the linear regression coefficients such as slope *m*, intercept *b*, and correlation *R* were used to assess the match between the downscaled DEMs from the bilinear and bi-cubic resampling methods, Kriging interpolation and the reference DEMs.

3 Reference and Testing Data

Two types of data were used to evaluate the proposed algorithm. The first type of data was *degraded* coarse DEMs which were calculated from the reference DEMs at fine resolution using nearest neighbour (or averaging method) to make a source of error-free data for algorithm testing. Error-free means the elevation values of pixels in DEM do not contain interpolation and measurement errors. The second type of data is real DEMs which are mostly sampled from point elevation or contour data. Actually, the elevation of a pixel of the DEM represents the elevation of the surface covered by this pixel so it must be the averaged elevation of this surface. The interpolation algorithms are used to estimate this representing elevation from point or contour data so the elevation of a pixel in the real grid DEMs is actually the averaged elevation of all points within the footprint of this pixel with some estimation errors.

The spatial resolution for testing DEM datasets in this paper was selected between 5 m and 60 m and, accordingly, the zoom factor values are 3 or 4. There are two reasons for this selection the spatial resolution. The first reason is because most of currently available sources of grid DEM data are at this range of resolution. The second and more important reason is that the increasing in accuracy of the data at these spatial resolutions is useful for many applications.

The first DEM dataset covered an area of about 3.5 km by 3.5 km and were acquired at Yen Thanh District, Nghe An Province, in North Central Vietnam. The area is located at 18^{o} 58' 57.03" N, 105^{o} 22' 44.87" E, about 45 km from Vinh City. This DEM was produced from topographic maps at the scale of 1:10000. The spatial resolution of the original DEM is 20 m (Fig. 1(a)) and this was degraded to 60 m by averaging the elevation value of 20 m pixels within the footprint of the degraded 60 m (Fig. 1.(b)).

The second dataset was acquired using ground surveying in Lang Son Province of Vietnam. The area of the test field is about 200 m by 200 m in Mai Pha Ward, Lang Son City which is about 150 km from Hanoi. A set of 533 measured elevation points were used with Kriging interpolation to generate a gridded DEM dataset at 5 m spatial resolution for use as a reference, as can be seen in Figure 3(a). The accuracy of reference DEM was assessed based on the ASPRS Accuracy Standard for Digital Geospatial Data [19,20] with a set of 234 validation points. The results of assessment (Table 1) showed that the quality of the reference DEM is slightly better than that of 66.7-cm ASPRS DEM Class and Class VIII of ASPRS 1990 Standards [20] with RMSEz of 48.3 cm and the Appropriate Contourinterval of 1.449-meter. The coarse DEM at 20 m spatial resolution was created using the same interpolation algorithm from the point data (Figure 3(b)). This coarse 20 m DEM was used as input for the algorithms to make 5 m DEM and this result was compared with 5 m DEM reference data.

4. Assessment

Visual comparison showed that the resulting DEMs generated by the bilinear and bi-cubic resampling methods, and Kriging interpolation are visually more similar to the reference DEM than the coarse spatial resolution DEMs for both degraded and sampled datasets. The improvement in visual similarity between the resampled DEMs and reference DEM is seen clearly when comparing between the 20 m DEMs in degraded datasets in Nghe An (Fig. 1) and 5 m and 20 m DEMs resampled datasets with reference DEMs (Fig. 2). While the images of original coarse resolution DEMs and the DEMs by resampling methods, especially the images created by bi-cubic resampling, were blurred with noises and the shapes of terrain features in these images look distorted, the images of Kriging interpolation downscaled DEMs in Fig. 1(e), Fig. 2(e) look less noise and very similar to

the reference DEMs in Fig. 1(a), Fig. 2(a). The most clearly improvement of reconstruction of the shapes of terrains can be seen in the marked areas in Fig. 1.

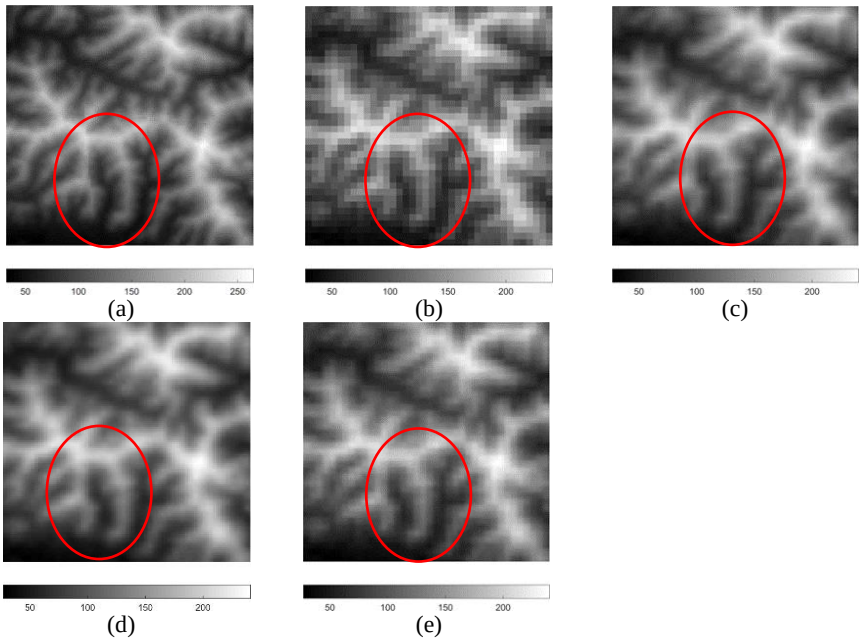

Fig. 1 Downscaling of DEM from 60 m to 20 m spatial resolution. (a) Reference DEM at 20 m resolution; (b) Degraded DEM at 60 m resolution (note: this forms the only input to the algorithms); (c) DEM at 20 m using bilinear resampling; (d) DEM at 20 m resolution using bi-cubic resampling; (e) DEM at 20 m resolution using Kriging interpolation.

The comparison of the surfaces of the resulting DEMs using profiles reveals a clearer advantage of the resampling methods over the original coarse resolution DEM. In

Fig. 3, the elevation profiles of the Kriging interpolated DEMs are closer to the profiles of reference DEMs than those of the bilinear and bi-cubic resampled DEM for both two datasets. This is most clearly seen in the 5 m Lang Son dataset in

Fig. 3(c) (a column profile) and

Fig. 3(d) (a row profile) in places such as tops of hills or bottoms of valleys. In these images, it is possible to observe that the surface formed by the Kriging interpolation DEM are closer to the 5 m reference surface.

The visual comparison of scatterplots in Fig. 4 also showed the better match between the results of the resampling methods and the reference DEM data in comparison with the original coarse DEM. In these scatterplots, the two DEM data are considered to be closer if the data points are located closer to the regression line. That means the slope coefficient m is closer to the value of 1 and the intercept coefficient b is closer to the value of 0. The scatterplots of the resampling results in Fig. 4 showed a closer match between the reference DEM and the Kriging interpolation DEM data in comparison with the original coarse DEM data, the bilinear and bi-cubic resampling,. The data points in the scatterplots in Fig. 4 showed that it is very close to and (sometime exactly on) the best fit line and the best fit line's coefficients in these scatterplots are closer to the value of 1 and 0.

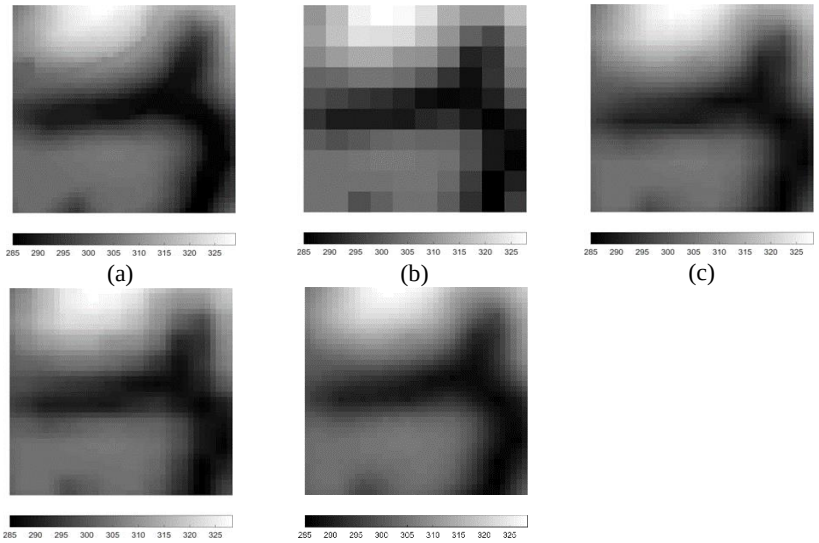

Fig. 2 Downscaling of DEM data from 20 m to 5 m spatial resolution. (a) Reference DEM data at 5 m resolution; (b) Degraded DEM data at 20 m resolution (note: this forms the only input to the algorithms); (c) DEM at 5 m resolution resulted from bilinear resampling; (d) DEM at 5 m resolution resulted from bi-cubic resampling; (e) DEM at 5 m resolution resulted from Kriging interpolation.

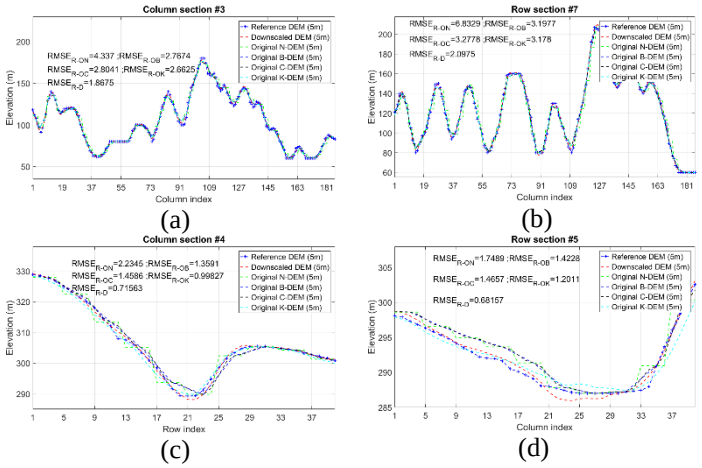

Fig. 3 Comparison of reference surface (reference DEM), original coarse resolution surface (original N-DEM), bilinear (original B-DEM) and bi-cubic (original C-DEM) resampled surfaces based on profiles: (a) a column profile for 20 m degraded dataset in Nghe An; (b) a row profile for 20 m degraded dataset in Nghe An; (c) a column profile for 5 m sampled dataset in Lang Son; (d) a row profile for 5 m sampled Lang Son dataset.

Coinciding with the result of visual observation, quantitative assessment based on the RMSE (Table 1) reveals a greater accuracy for the resampling and Kriging interpolation methods. The RMSEs for the bilinear, bi-cubic resampling and Kriging interpolation methods are 3.3716 m, 3.3716 m and 2.8874 m, respectively. Comparing with the RMSE of the original 60 m data, the RMSE of the resampled DEMs at 20 m reduced significantly for all three methods. The improvement in accuracy for sampled dataset is similar to that of the

degraded dataset. The RMSE of 5 m Lang Son data decreased sharply for the resampling algorithms DEM with the values of 1.5139 m for bilinear resampling, 1.6 m for bi-cubic resampling, and 1.2092 m for the Kriging interpolation. These statistics demonstrate that the resampling methods can increase the accuracy of the gridded DEM when it is used to downscale DEM to a finer spatial resolution.

The increase in accuracy in term of RMSE, along with the profiles, demonstrated the effects of the terrain features on the algorithm. For the Nghe An dataset, the increase in accuracy between the original and downscaled DEMs was relatively constant. The similarity of the two DEMs can also be evaluated quantitatively using the linear regression coefficients (*m*, *b*) and the correlation coefficient *R* (Table 2). Comparing two DEMs, if the elevation of a pixel in the reference dataset is *x* and the elevation of the corresponding pixel in the comparing dataset is *y*, the expected perfect fit line should be $y = x$ such that $m = 1$ and $b = 0$. Because the value of *m* may be greater or smaller than 1 and the value of *b* may be greater or smaller than 0, comparison between different values of *m* and *b* to define the closeness of them to 1 and 0, respectively, sometimes it is not easy to evaluate. To make it easier for this evaluation, the sub-parameters such as were calculated. The third parameter for evaluating the fitting of the two datasets is the correlation coefficient *R*. The correlation coefficient measures the association between two datasets and, thus, captures the distribution of the data points in the scatterplots around the best fit line. The closer value of R^2 to 1, the more data points are located close to the best fit line. A perfect match between two DEM datasets means that all the data points are located on the identity line ($y = x$) and the coefficient of determination $R^2 = 1$. That means the two datasets are exactly the same if the value of *m* is equal to 1, *b* is equal to 0 and R^2 is equal to 1, simultaneously.

To evaluate the results of the different methods, linear regression models were fitted to the relation between the reference data and the bilinear and bi-cubic resampled, and Kriging interpolated data. The coefficient values show the better fitting of the Kriging interpolated DEMs with the reference DEMs than those of the original DEMs, bilinear and bi-cubic resampled DEMs. For all four datasets, the values of parameters *m*, *b* and R^2 of Kriging interpolated DEMs are much closer to the values of 1, 0, and 1, respectively, than those of the original, bilinear and bi-cubic resampled DEMs. In case of the Lang Son 5 m resampled dataset, the values |1 - m| = 0.0550, |b| = 16.3717 and R2 = 0.9884 for the Kriging interpolated DEM showed greater similarity to the reference DEM than those of the original coarse DEM (|1 - m| = 0.0310, |b| = 9.3306 and R2 = 0.9425), bilinear resampled DEM (|1 - m| = 0.0399, |b| = 12.3782 and R2 = 0.9793), bi-cubic resampled DEM (|1 - m| = 0.0342, |b| = 10.6432 and R2 = 0.9763.

Linear regression coefficients for the 20 m Nghe An degraded dataset showed that the resampled DEM matches very closely to the reference DEM. Surprisingly, the comparison also showed that the original coarse DEM with parameters of |1-m| = 0.0178 and |b| = 2.1147 is generally more matched (less bias) to the reference DEM than the resampled

Table 1. Root mean squared error for bilinear, bi-cubic, Kriging resampling methods

	Input coarse DEM (m)	**Bilinear (m)**	**Bi-cubic (m)**	**Kriging (m)**	**Accuracy improvement over input DEM (%)**
RMSE for D1 dataset (20 m resolution)					
Overall RMSE	6.9326	3.3026	3.3716	2.8874	71.4
Min CP	3.8029	2.5245	2.5619	2.6330	49.7
Max CP	5.1846	2.9851	3.0731	2.7065	61.1
Min RP	4.5824	2.8843	2.9332	2.8899	57.2
Max RP	6.4972	2.9903	3.0293	2.8799	73.0
RMSE for S1 dataset (5m resolution)					
Overall RMSE	2.4571	1.5139	1.6000	1.2092	65.4
Min CP	1.4960	1.2419	1.2912	0.8727	34.9

Max CP	1.6962	1.1635	1.1821	1.1771	69.8
Min RP	1.7289	1.4081	1.4297	1.4138	35.6
Max RP	1.9510	1.4361	1.5174	1.6807	69.8
RMSE for S2 dataset (30m resolution)					

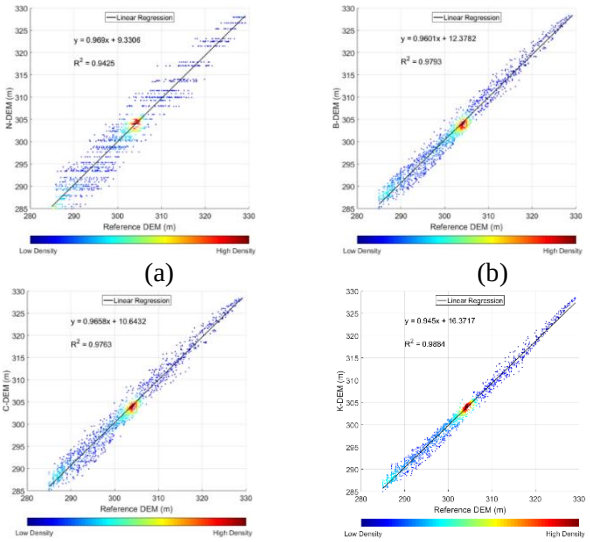

Fig. 4 Scatterplots of the reference fine spatial resolution DEM against the downscaled DEM for the sampled 5 m Lang Son dataset test: (a) the reference DEM and coarse degraded DEM (N-DEM), (b) the reference DEM and the bilinear resampled DEM (B-DEM), (c) the reference DEM and the bi-cubic resampled DEM (C-DEM), (d) the reference DEM and Kriging interpolated DEM (K-DEM).

DEMs with |1 - m| = 0.0235 and |b| = 2.5368, and |1 - m| = 0.0219 and |b| = 2.3680 for bilinear and bi-cubic resampled DEMs, respectively. However, more data points of the bilinear (R^2 = 0.9951) and bi-cubic (R^2 = 0.9948) resampled DEMs are distributed close to the best fit line than those of the original 20 m DEM (R^2 = 0.9770).

Comparing the slope parameter *m* and intercept parameter *b* of the best fit lines of all four datasets, it is clear that all the slope parameters m of the resampled DEMs are smaller than 1 and the intercept parameters *b* are larger than 0. This means that for locally-low places (usually the bottom of valleys) the pixels of the DEM data produced by these methods are likely to be higher than the corresponding pixels in the reference DEM. Conversely, for locally-high places such as the top of hills or mountain ridges, the elevation of the pixels in the resampled DEM data is likely lower than that of the corresponding pixels in the reference image. This is due to the smoothing effect (referred to as conditional bias where highs are under-predicted and lows are over-predicted).

5. Conclusions

A test for resampling algorithms to increase the spatial resolution and accuracy of gridded DEMs was implemented and demonstrated comprehensively using data with different DEM spatial resolutions and characteristics. Tests of the resampling algorithms were implemented on two types of elevation datasets; 20 m DEMs in Nghe An province, Vietnam and a 5 m sampled DEM in Lang Son province. The test results revealed a sharp

increase in accuracy for the Kriging interpolated gridded DEMs in comparison with the original (coarse) gridded DEM, and the bilinear and bi-cubic resampling. Visual assessment

revealed the greater similarity of the Kriging interpolated DEMs with the reference DEM than the DEMs generated by bilinear and bi-cubic resampling methods. Quantitative accuracy assessment based on the RMSE revealed an increase in DEM accuracy for the Kriging algorithm over the bilinear and bi-cubic resampling methods. The RMSE of the Kriging interpolated DEMs decreased by approximately 58% and 50%for the 20 m DEMs in Nghe An province and 5 m sampled DEM in Lang son province, respectively.

Table 2. Linear regression coefficients for Nghe An 20 m dataset, and the Lang Son 5 m

Datasets		**Linear Regression Coefficients**		
		m	*b*	R^2
20 m Nghe An dataset	60 m degraded DEM	0.9822	2.1147	0.9770
	20 m bilinear resampled DEM	0.9765	2.5368	0.9951
	20 m bi-cubic resampled DEM	0.9781	2.3680	0.9948
	20 m Kriging interpolated DEM	0.9832	1.8217	0.9962
Lang Son dataset	20 m coarse DEM	0.9690	9.3306	0.9425
	5 m bilinear resampled DEM	0.9601	12.3782	0.9793
	5 m bi-cubic resampled DEM	0.9658	10.6432	0.9763
	5 m Kriging interpolated DEM	0.9450	16.3717	0.9884

Further evaluation was also implemented using linear regression of the original fine spatial resolution DEM against the original, the bilinear and bi-cubic resampled, and Kriging interpolated DEMs, particularly focusing on the coefficients *m*, *b* and *R2*. Analysis of these parameters showed that the Kriging interpolated DEMs was closer to the reference DEMs than the original DEM and those produced using the bilinear and bi-cubic resampling methods.

References

1. S. Saksena and V. Merwade, J. Hydrol. **530**, 180 (2015).
2. Z. Zhao, G. Benoy, T. L. Chow, H. W. Rees, J. L. Daigle, and F. R. Meng, Water Resour. Manag. **24**, 1363 (2010).
3. T. Bolstad, Paul V. & Stowe, ISPRS J. Photogrametric Eng. Remote Sens. **60**, 1327 (1994).
4. K. S. Rawat, G. Krishna, A. Mishra, J. Singh, and S. V. Mishra, J. Appl. Nat. Sci. **6**, (2018).
5. R. F. Vázquez and J. Feyen, J. Hydrol. **334**, 73 (2007).
6. J. M. Schoorl, M. P. W. Sonneveld, and A. Veldkamp, Earth Surf. Process. Landforms (2000).
7. M. P. Smith, A. X. Zhu, J. E. Burt, and C. Stiles, Geoderma **137**, 58 (2006).
8. W. L. Kuo, T. S. Steenhuis, C. E. McCulloch, C. L. Mohler, D. A. Weinstein, S. D. DeGloria, and D. P. Swaney, Water Resour. Res. **35**, 3419 (1999).
9. Q. Guo, W. Li, H. Yu, and O. Alvarez, Photogramm. Eng. Remote Sens. **76**, 701 (2013).
10. X. Liu, Prog. Phys. Geogr. (2008).
11. D. Kidner, M. Dorey, and D. Smith, in *GeoComputation.Org* (1999).
12. W. Shi, B. Wang, and Y. Tian, Math. Geosci. **46**, 445 (2014).
13. C. H. Grohmann and S. S. Steiner, Int. J. Geogr. Inf. Sci. **22**, 895 (2008).
14. B. Dixon and J. Earls, Hydrol. Process. (2009).
15. L. E. Band and I. D. Moore, Hydrol. Process. **9**, 401 (1995).
16. W. G. Rees, Int. J. Remote Sens. **21**, 7 (2000).
17. U. Alganci, B. Besol, and E. Sertel, ISPRS Int. J. Geo-Information **7**, (2018).

18. S. Kienzle, Trans. GIS **8**, 83 (2003).
19. K. Whitehead and C. H. Hugenholtz, Photogramm. Eng. Remote Sens. **81**, 787 (2015).
20. ASPRS, Photogramm. Eng. Remote Sens. **81**, (2015).

An approach of mapping quarries in Vietnam using low-cost Unmanned Aerial Vehicles

NGUYEN Quoc Long [11*], BUI Xuan Nam[2], CAO Xuan Cuong[1], LE Van Canh[1]

[1] Hanoi University of Mining and Geology, Department of Mine Surveying, Hanoi, Vietnam
[2] Hanoi University of Mining and Geology, Department of Surface Mining, Hanoi, Vietnam
and Mine Surveying, Krakow, Poland

Abstract. In Vietnam, there are a huge number of quarries that are exploited and mainly provide materials to the construction sector of the country. However, most of the quarries are operating without topographic plans due to a lack of surveying activities. This paper introduces an approach of using low-cost UAVs to produce digital surface models which in turn are used to draw topographic maps of quarries in Vietnam. For assessments of accuracy, safety, and working efficiency, four quarries different in terrain conditions, namely Luong Son, Long Son, Nui Nho, and Nui Dai were selected as the study areas. Ground control points were established in each area by using GNSS/RTK for camera calibration and accuracy assessment. The accuracy of DSM was assessed using the root-mean-square error (RMSE) in X, Y, Z, XY, and XYZ components. Capturing images from each site were processed by using Agisoft®PhotoScan Professional 1.5.2. The results showed that all the DSM models of the four areas have high accuracy, RMSE on the checked GCPs ranges from 1.0 to 9.0 cm, from 1.2 to 5.0 cm, from 4.4 to 13.4 cm, from 1.6 to 10.3 cm, and from 4.9 to 16.9 cm for X, Y, Z, XY, XYZ components, respectively. We concluded that the low-cost UAV based mapping technology can guarantee the accuracy of DSMs, the safety of UAV flying, and the efficiency of surveying working simultaneously when using in quarries.

Introduction

Vietnam's mining industry was started by French in the late 19th century before being taken by Vietnamese in 1954 [1]. As one of the most important economic activities, the mining industry of Vietnam has been developing at a great pace. There have been approximately 1100 mines under excavation in which nearly two-third are open-pit ones [1]. There are several large size open-pit mines such as Coc Sau, Cao Son, Deo Nai, Nui Beo (coal mines), Sin Quyen (copper mine), the remain of open-pit mines are in small and medium sizes. These mines include quarries that mainly provide materials to the cement production industry and construction in Vietnam.

It is undeniable that topographic documents play an important role in the mining operation. However, while several large coal open-pit mines have frequently topographic surveys, almost every medium and small – sized ones do not. Therefore, these open-pit mines rely on experience to carry out mining operations without topographical maps and accurate mine drawings. There are several possible reasons including relatively lacking capital and skills due to the conditions of one small business which in turn lead to not

[1] *Corresponding author: nguyenquoclong@humg.edu.vn*

acquired surveying equipment and professional surveyors [2]. Recently, the rapid development of geospatial technologies has brought many benefits to the mining surveying. Among the most widely used surveying techniques such as Electronic Distance Measurement (EDM) surveys or Total Station (TS) and RTK Global Navigation Satellite System (GNSS) which are able to obtain observations with millimeter accuracy but cost and time consuming, there have been new alternative techniques for topographic surveying such as Terrestrial Laser Scanning (TLS) and airborne Light Detection and Ranging (LiDAR) or airborne laser scanning (ALS) [3]. However, for these new ones, the cost and survey time are still a critical issue to open-pit mines. For example, as the observation distance of TLS is normally short, many scanning stations are required for the complex terrain of open-pit mines. For LiDAR, it is noted that large uncertainties could be found in vertical values while measuring such complicated open-cast mine environment [4].

In Vietnam, small and medium sized open-pit mines such as quarries are often located in areas with complicated terrains and a variety of geological conditions. Many of them are high limestone mountains, others are at a level of 100 meters below the sea level. The changes of terrain elevation at these mines are significant. These lead to many challenges for surveying services which are conducted by using traditional methods.

Recent advancements in robots and GNSS technologies have provided various Unmanned Aerial Vehicles (UAVs) and UAV photogrammetry is recognized as a technology that can replace or complement existing surveying equipment [5]. Especially, small and low-cost UAVs with nonmetric digital cameras are becoming a valid and effective alternative surveying technique for topographic reconnaissance and volumetric computation [5-7], Civil Engineering ([8], disaster prevention [9, 10], agriculture [11]. In addition, with the possibility of measuring a large area quickly, the UAV technology could be observation solutions for small and medium open-air mine sites in Vietnam.

In this study, we perform investigations on the accuracy of 3D mapping several complex terrain open-pit mines by using the UAV technology. These quarries are with a variety of size and terrain and located in different regions of Vietnam, namely Nui Nho, Long Son, Luong Son, and Nui Dai. In all cases, a DJI Phantom 4 Professional was used to capture images, at different flight heights, whereas ground control points were measured by using GNSS RTK. The image processing was carried out using Agisoft®PhotoScan Professional 1.3. Finally, accuracy assessment for each case was performed and conclusions are given.

Study areas

The study areas are four quarries with specific characteristics of terrain in the Northern and Southern Vietnam, namely Luong Son, Long Son, Nui Nho, and Nui Dai. While Luong Son and Long Son are located in the northern mountainous region of Vietnam, Nui Nho and Nui Dai are situated in the southern of Vietnam (Fig. 1a). Long Son is a limestone quarry and provides materials for the production of cement, whereas other three mines mainly provide materials for civil construction such as air stations, roads, dams, etc. The area of Long Son quarry is about 12 hectares with the highest point of 110m. The largest difference between the mine and the surrounding area in altitude is about 100 m (Fig. 1b). Luong Son is a mine of construction material stone, with an exploiting area of about 13 hectares with steep rocky topography and the biggest difference in elevation is 110 m. Both Long Son and Luong Son mines are exploited by cutting down from the top.

Nui Dai and Nui Nho are two quarries located in the southern part of Vietnam (Fig. 1a). Nui Dai is one of the biggest quarries in Vietnam with the exploiting area of about 70

hectares. The highest peak of the mining area is 145 m, the lowest point is at 1 m above sea level. Nui Nho is with an area of 27 ha, and down to the level of -110 m below sea level.

Materials and Methods

Principle of UAV based mapping technology

Unmanned aerial vehicles (UAVs) are a generic aircraft design which are intended to operate without a human pilot on board [12]. It has been known with other terms such as remote piloted aircraft or unmanned aerial system. Actually, according to ICAO [13], there are a difference in the two terms. While the latter refers to UAVs that do not allow pilot interventions during the flight and are mainly used in military contexts, the former one refers to unmanned aircraft which are remotely controlled by a pilot [14]. To classify UAVs, one can base on a wide range of different platforms which, due to their physical size, structures and power, differ in terms of their capability and simplicity of operation. These factors impact the payload carrying capacity, speed, altitude, and range of flight, which determines the different applications that can be performed by each type of UAV.

In the field of surveying and mapping, the UAV is classified and summarized based on its structure and type of taking-off and landing operation. There are two main UAVs including fixed-wing and rotary-wing. Fixed-wing unmanned airplanes are flying with air lift and are energy-efficient and can fly for a long time so that a large area can be shot at one time. On the other hand, rotor blades are relatively inefficient. Although the short flight time is short, vertical takeoff and landing are possible, so it can be used in small and medium-sized open-pit mines where it is difficult to secure landings.

(a)

(b)

(c)

(d)

Fig. 1. Location of investigating open-cast mines
(a) Luong Son; (b) Long Son; (c) Nui Nho; (d) Nui Dai

UAV and Camera

In small surveying projects, rotary-wing UAVs such as DJI Phantom 3, or 4 professional are often utilized widely. In this work, the study sites are small so we use a phantom 4 professional to capture images. The Phantom 4 professional is a quadcopter drone with four powerful rotors (Fig 2). Its airframe carries the GPS/IMU that enables it to have posture control, stop flight, and automatically take off and land with high stability [15]. The drone is capable of both manual flight mode using the controller and automatic flight mode using the Android or IOS smartphone applications. If you use the automatic mode, you can set the flight path, flight speed, flight altitude, shooting range and overlapping of the photographs, so you can take more aerial photographs. The drone is equipped with a 20 megapixel RGB camera with a focal length of 8.8 mm and sensor a size of 13.2 x 8.8 mm that allows high-resolution aerial photography [16].

Fig 2. Description of components of a DJI Phantom 4 Professional [16]

Establishment of ground control points

Ground control points (GCPs) play an important role in geo-referencing and evaluating the accuracy of the DSM model. Therefore, GCPs need to be placed on the ground before carrying out image acquisition. In the condition that all quarries were still operating, field reconnaissance was conducted to select safe areas for placing these GCPs with a help of a handhold GPS (Mapping v3.8 installed in a Samsung A7 smartphone). The GCPs were

distributed in each study area as much as possible, and they were assigned to positions accessible from the field. The number of GCPs was also different from site to site as it depends on the requirement of accuracy and size of each area (Fig 4).

Fig. 3 GCP marks and their coordinates measured by GNSS/RTK

In order to easily detect GCPs in acquiring images, the GCPs were marked with highly reflective material for enhancing the contrast. The size of the printed marks was 60 x 60 cm (Fig. 3). In the next step, coordinates (x, y, z) (VN2000/UTM Zone 48 N) for these GCPs were determined using GNSS/RTK and the available horizontal and vertical surveying networks at the mine areas.

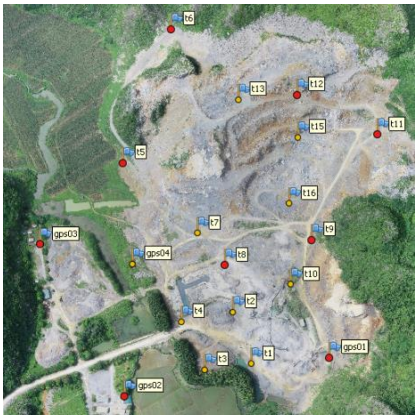

(a) Luong Son quarry

(b) Long Son quarry

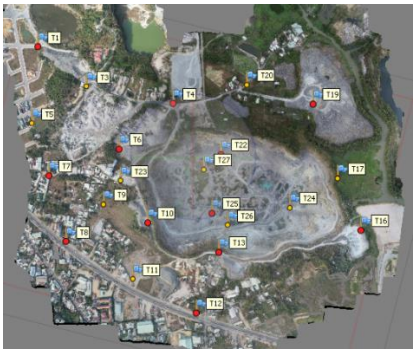

(c) Nui Nho quarry (d) Nui Dai quarry

GCP for calibrating the model

GCP for checking the accuracy of digital surface model

Fig 4. Distribution of calibrated and checked points in the four study areas

UAV image acquisition

For the aerial photography of the study area, the automatic mode flight plan of the Phantom 4 Pro was established using the Pix4D Capture application installed in an IOS smartphone. In the automatic mode, several important parameters are upload to the drone including the size of mapping areas, flight height, as well as end-lap and side-lap of images. As the limitation of flight time, each study area requires several missions to capture enough images for mapping purpose. Table 1 illustrates flying missions of four study areas. In all cases, both forward and side overlaps were set to 80%, but the flight altitudes changed site by site as the change of the study areas‘ terrain (Table 1). Based on these settings, automatic flight plans were developed to capture aerial photographs in the study areas.

Table 1. Flying missions

Name of mine	Flight Altitude (m)	No of mission	No of images	Image resolution (cm/pix)	Area (hectare)
Luong Son	331	6	372	5.36	114
Long Son	303	1	80	5.95	15
Nui Nho	265	7	414	7.48	197
Nui Dai	365	3	215	7.76	121

Processing and accuracy assessment

In this study, Agisoft Photoscan Professional (ver 1.3) was used to process UAV acquired images taken at the field. The data processing procedure of Agisoft Photoscan includes five steps: (i) photo-alignment; (ii) bundle block adjustment; (iii) optimization, (iv) 3D surface reconstruction, (v) generation of Digital Surface Model (DSM). Firstly, when images are input, key points that can be identified from each image are automatically extracted, and then the singularities extracted from each image are linked with each other through mutual comparison among a plurality of images, this process is called “photo-alignment”. When geometric corrections of singularities are completed in each image, the singularities representing the same points in several images are automatically matched through comparison between consecutive UAV images. When the singularities are extracted, 3D point cloud and the DSM model are generated. Also, an orthophoto can be produced through the combination of UAV images.

Accuracy assessment of the Digital Surface Model (DSM) is an important task, and without this task, the DSM is useless. In this project, both the horizontal and vertical assessments were carried out by comparing DSM with the GCPs measured by a Leica total station in term of Root Mean Square Error (RMSE). More specifically, assessments in

easting ($RMSE_X$), northing ($RMSE_Y$), vertical ($RMSE_Z$), and all components ($RMSE_{XYZ}$) were used, as suggested in Agüera-Vega [17], using equations as follows:

$$\Delta X = X_{DSM} - X_{GCP} \quad (1)$$

$$\Delta Y = Y_{DSM} - Y_{GCP} \quad (2)$$

$$\Delta Z = Z_{DSM} - Z_{GCP} \quad (3)$$

$$\Delta XYZ = XYZ_{DSM} - XYZ_{GCP} \quad (4)$$

$$RMSE_X = SQRT\left[(1/n)\sum_{i=1}^{n}(\Delta X)^2\right] \quad (4)$$

$$RMSE_Y = SQRT\left[(1/n)\sum_{i=1}^{n}(\Delta Y)^2\right] \quad (5)$$

$$RMSE_Z = SQRT\left[(1/n)\sum_{i=1}^{n}(\Delta Z)^2\right] \quad (6)$$

$$RMSE_{XYZ} = SQRT\left[(1/n)\sum_{i=1}^{n}((\Delta X)^2 + (\Delta Y)^2 + (\Delta Z)^2))\right] \quad (7)$$

where X_{GCPi} and X_{DSM} are the X-coordinate component of GCP and corresponding coordinate in DSM, respectively; Y_{GCPi} and Y_{DSM} are the Y-coordinate component of GCP and corresponding coordinate in DSM, respectively; Z_{GCPi} and Z_{DSM} are the Z-coordinate component of GCP and corresponding coordinate in DSM, respectively.

Results and discussions

In term of processing time, an average of 8 hours was spent to process orthographic images and DSMs on a computer with Windows 10 64-bit operating system, 2.93 GHz × 4 CPU, and 32G RAM.

Luong Son case

For the case of Luong Son quarry a total of 372 images were acquired through six missions. The point cloud of the quarry with around 20 million 3D points, was extracted according to the data processing method described above, and an orthographic image and a DSM were generated with resolutions of 5.3 and 43.7 cm, respectively. In addition, topographic contours at 1 m intervals could be extracted from the DSM. The results are shown in Fig 5c. The results are shown in Table 2 and 3. The root mean square error (RMSE) of the position coordinates was analyzed to be about 2.0 cm in the horizontal direction and 4.4 cm in the vertical direction

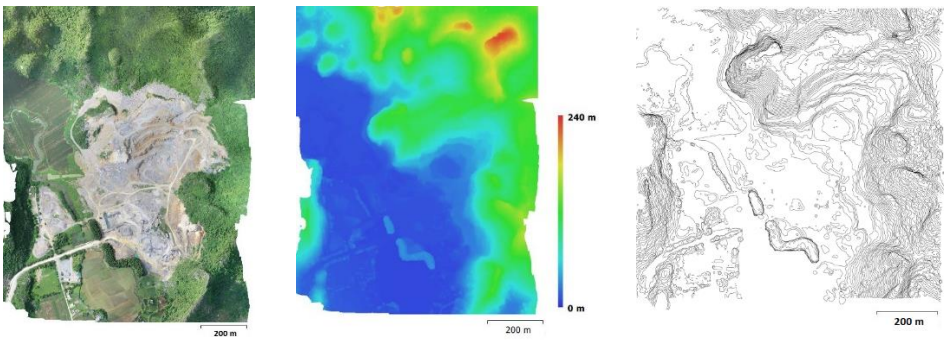

(a) (b) (c)

Fig 5. Processing results for Luong Son site
(a) Orthophoto (b) DSM, (c) Contour plan (an interval of 1 m)

Table 2. Error and RMSE in X, Y, Z, XY and XYZ of GCPs used for the model calibration

Calibration points	X error (m)	Y error (m)	Z error (m)	XY error (m)	XYZ error (m)
T5	0.007	-0.019	-0.014	0.020	0.024
T6	0.013	0.006	0.001	0.014	0.014
T8	-0.008	-0.020	-0.019	0.022	0.029
T11	0.024	0.010	0.000	0.026	0.026
T12	0.016	0.011	0.091	0.019	0.093
GPS02	0.007	-0.003	0.017	0.008	0.019
GPS03	0.015	0.019	-0.019	0.024	0.031
GPS01	0.013	0.052	0.028	0.053	0.060
T9	-0.019	0.009	0.022	0.021	0.031
RMSE	**0.015**	**0.022**	**0.035**	**0.026**	**0.043**

Table 3. Error and RMSE in X, Y, Z, XY and XYZ of GCPs used for the checking DSM

Checking points	X error (m)	Y error (m)	Z error (m)	XY error (m)	XYZ error (m)
T1	-0.004	-0.018	-0.072	0.018	0.074
T2	-0.004	-0.006	-0.034	0.007	0.034
T3	-0.032	-0.003	0.026	0.032	0.042
T4	0.006	-0.006	0.022	0.009	0.024
T7	0.000	-0.022	0.012	0.022	0.025
T10	-0.004	-0.009	0.040	0.010	0.041
T13	0.002	0.008	0.012	0.008	0.015
T15	0.019	0.003	0.049	0.019	0.052
T16	-0.025	0.029	-0.078	0.038	0.086
GPS04	-0.002	-0.016	0.041	0.016	0.044
RMSE	**0.014**	**0.015**	**0.044**	**0.020**	**0.049**

Long Son case

For the case of Long Son quarry, with an area of 15 hectares, a total of 80 images were acquired through one mission. The point cloud of the quarry with approximately 3.77 million 3D points, was extracted according to the data processing method described above, and an orthographic image and a DSM were generated with resolutions of 5.9 cm and 23.8 cm/pix, respectively. In addition, topographic contours at 1 m intervals could be extracted from the DSM. The results are shown in Fig 6. The results are shown in Table 4 and 5. The root mean square error (RMSE) of the position coordinates was analyzed to be about 2.6 cm in the horizontal direction and 5.3 cm in the vertical direction.

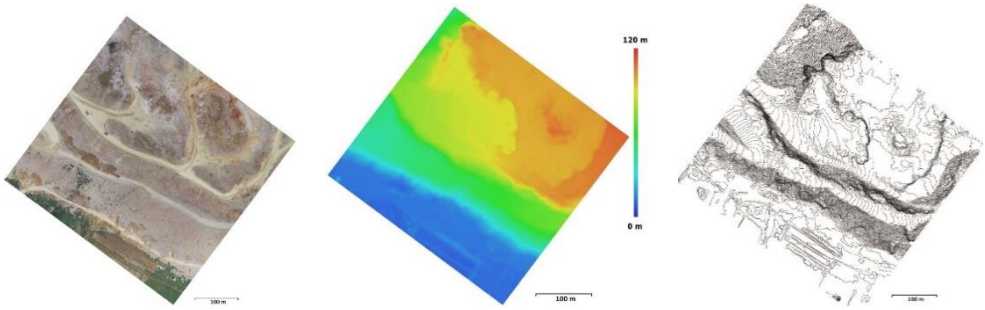

(a) (b) (c)

Fig 6. Processing results for Long Son site
(a) Orthophoto (b) DSM, (c) Contour plan (an interval of 1 m)

Table 4. Error and RMSE in X, Y, Z, XY and XYZ of GCPs used for the model calibration

Calibration points	X error (m)	Y error (m)	Z error (m)	XY error (m)	XYZ error (m)
A2	-0.006	-0.001	-0.002	0.007	0.007
A3	-0.002	-0.002	0.013	0.002	0.013
A4	0.006	0.005	-0.030	0.008	0.031
A6	0.007	-0.001	0.024	0.007	0.025
A9	-0.007	0.001	-0.008	0.007	0.011
BS1	-0.007	0.005	-0.003	0.009	0.009
BS4	0.005	-0.003	-0.001	0.006	0.006
RMSE	**0.007**	**0.003**	**0.016**	**0.007**	**0.017**

Table 5. Error and RMSE in X, Y, Z, XY and XYZ of GCPs used for the checking DSM

Checking points	X error (m)	Y error (m)	Z error (m)	XY error (m)	XYZ error (m)
12	0.012	-0.001	0.060	0.012	0.061
23	0.003	0.055	0.011	0.055	0.056
A 5	-0.014	0.003	-0.008	0.014	0.016
A 7	-0.005	0.001	-0.081	0.005	0.081
A 8	-0.010	-0.007	-0.061	0.012	0.062
RMSE	**0.010**	**0.025**	**0.053**	**0.026**	**0.059**

Nui Nho case

For the case of Nui Nho quarry, the largest study area (197 hectares), a total of 414 images were acquired through seven missions. The point cloud of the quarry with 30.818 million 3D points, was extracted according to the data processing method described above, and an orthographic image and a DSM were generated with resolutions of 7.4 and 29.9 cm/pix, respectively. In addition, topographic contours at 1 m intervals could be extracted from the DSM. The results are shown in Fig 7. The results are shown in Table 6 and 7. The root mean square error (RMSE) of the position coordinates was analyzed to be about 10.3 cm in the horizontal direction and 13.4 cm in the vertical direction.

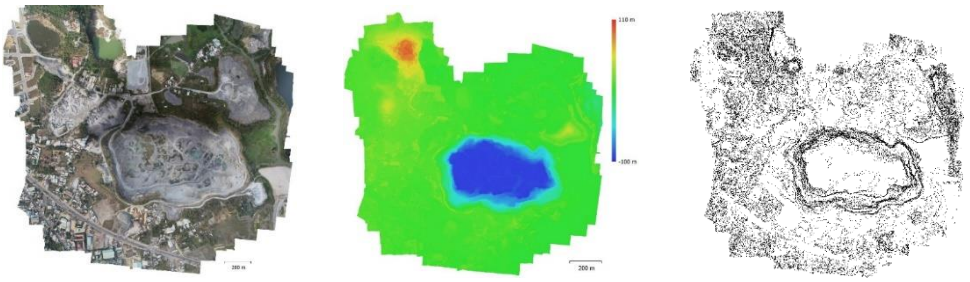

(a) (b) (c)

Fig 7. Processing results for Nui Nho site
(a) Orthophoto (b) DSM, (c) Contour plan (an interval of 1 m)

Table 6. Error and RMSE in X, Y, Z, XY and XYZ of GCPs used for the model calibration

Calibration points	X error (m)	Y error (m)	Z error (m)	XY error (m)	XYZ error (m)
T4	0.000	-0.001	0.000	0.001	0.002
T1	-0.001	-0.001	0.000	0.001	0.001
T6	-0.003	-0.003	0.001	0.005	0.005
T7	-0.004	0.002	0.000	0.005	0.005
T8	-0.002	0.003	-0.001	0.004	0.004
T10	0.002	0.005	0.000	0.005	0.005
T13	0.007	0.002	0.002	0.007	0.008
T12	-0.002	0.007	-0.004	0.007	0.008
T16	0.003	-0.001	0.001	0.003	0.003
T19	-0.001	-0.005	-0.002	0.005	0.006
T24	0.009	-0.005	0.001	0.010	0.010
T25	0.009	0.002	-0.001	0.009	0.009
T22	-0.017	-0.004	0.001	0.018	0.018
RMSE	**0.007**	**0.004**	**0.002**	**0.007**	**0.008**

Table 7. Error and RMSE in X, Y, Z, XY and XYZ of GCPs used for the checking DSM

Checking points	X error (m)	Y error (m)	Z error (m)	XY error (m)	XYZ error (m)
T3	-0.086	0.013	-0.005	0.087	0.087
T23	0.004	-0.001	0.038	0.004	0.038

T5	-0.241	-0.010	-0.396	0.241	0.464
T9	-0.019	0.008	0.041	0.020	0.045
T11	-0.007	0.054	0.018	0.055	0.058
T17	0.062	-0.126	0.013	0.141	0.141
T20	-0.044	-0.052	0.017	0.068	0.070
T26	0.000	-0.004	0.035	0.004	0.035
T27	-0.047	0.017	0.004	0.050	0.050
RMSE	**0.090**	**0.050**	**0.134**	**0.103**	**0.169**

Nui Dai case

For the case of Luong Son quarry, with an area of 121 hectares, a total of 215 images were acquired through six missions. The point cloud of the quarry with 16.37 million 3D points, was extracted according to the data processing method described above, and an orthographic image and a DSM were generated with resolutions of 7.7 and 31 cm/pix, respectively. In addition, topographic contours at 1 m intervals could be extracted from the DSM. The results are shown in Fig 8. The results are shown in Table 9 and 10. The root mean square error (RMSE) of the position coordinates was analyzed to be about 1.6 cm in the horizontal direction and 8.4 cm in the vertical direction

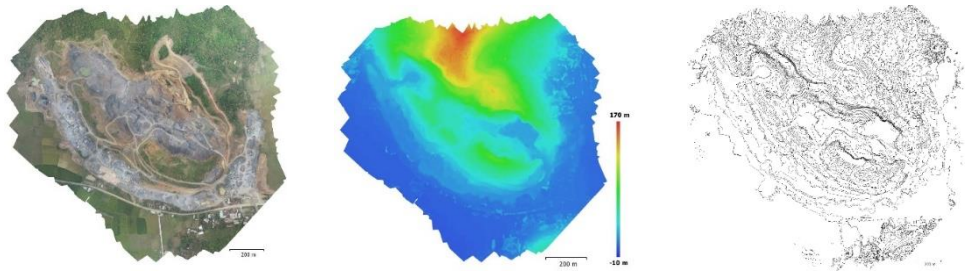

(a) (b) (c)

Fig 8. Processing results for Nui Dai site
(a) Orthophoto (b) DSM, (c) Contour plan (an interval of 1 m)

Table 9. Error and RMSE in X, Y, Z, XY and XYZ of GCPs used for the model calibration

Calibration points	X error (m)	Y error (m)	Z error (m)	XY error (m)	XYZ error (m)
G5	-0.028	-0.015	0.012	0.031	0.034
G3	-0.019	0.003	0.074	0.019	0.076
G9	-0.011	-0.004	-0.005	0.011	0.012
G8	-0.006	-0.008	-0.047	0.010	0.048
G1	0.024	0.000	-0.024	0.024	0.034
G4	0.015	0.022	-0.016	0.027	0.031
G7	-0.028	0.010	0.004	0.030	0.030
G11	-0.030	0.016	-0.083	0.034	0.089
G12	0.019	-0.007	0.099	0.020	0.101
G18	0.011	-0.023	-0.004	0.026	0.026

G20	0.008	-0.009	0.038	0.012	0.040
G14	0.000	0.007	0.000	0.007	0.007
G15	0.000	0.000	-0.001	0.000	0.001
G16	0.000	0.000	0.000	0.000	0.000
RMSE	**0.018**	**0.012**	**0.044**	**0.021**	**0.049**

Table 10. Error and RMSE in X, Y, Z, XY and XYZ of GCPs used for the checking DSM

Checking points	X error (m)	Y error (m)	Z error (m)	XY error (m)	XYZ error (m)
GPS_01	0.013	-0.001	-0.026	0.013	0.029
G2	0.008	0.023	0.040	0.024	0.047
G6	-0.004	0.006	-0.034	0.007	0.035
G10	-0.020	0.012	-0.084	0.023	0.087
G13	-0.001	-0.001	-0.179	0.002	0.179
G17	-0.009	-0.019	-0.081	0.021	0.083
G19	-0.006	-0.007	0.018	0.009	0.020
RMSE	**0.010**	**0.012**	**0.084**	**0.016**	**0.086**

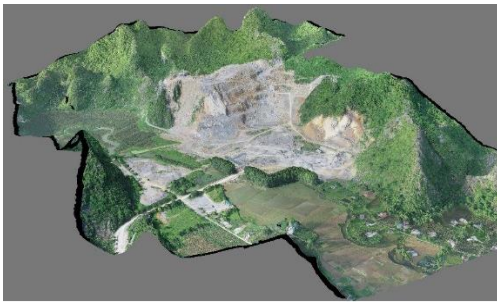

(a) Luong Son quarry

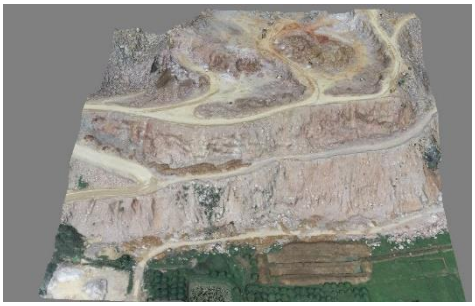

(b) Long Son quarry

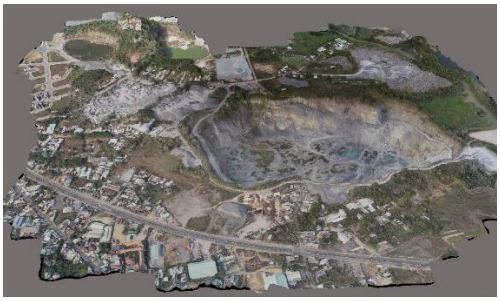

(c) Nui Nho quarry

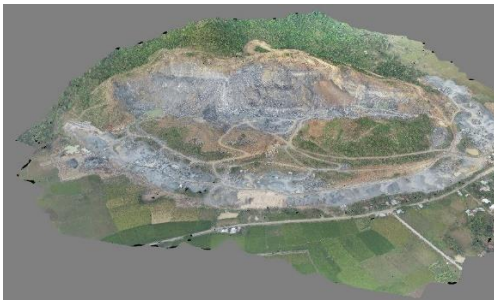

(d) Nui Dai quarry

Fig 9. 3D visualization of the four study areas using the orthophotos and DSMs

Discussions

One of important input parameters that needs to be set while developing flight plans is the flight height. It is undeniable that this factor should be seriously considered as it influences on several important issues such as DSM's accuracy, the safety of UAV flying

and the efficiency of UAV mapping. In the four study cases, the flight height ranging from 150 m to 250 m ensures the safety of flying, the accuracy of final topographic plans, and the working efficiency. Specifically, the case of Luong Son quarry which is the most complicated terrain among the four study sites. With the flight altitude was set to 331 m, the drone's safety was ensured. While one may question the accuracy, the results show that the MRSEs of XY and X are 2.1 and 4.6 cm, respectively. In other words, this completely meets the accuracy requirement of the detailed survey. In addition, with an average of 15 minutes per mission, the flying time of Luong Son case was only 1.5 hours. Another complex terrain quarry is Nui Dai, with the maximum and minimum elevations are +145m m and +1 m, respectively. However, with the flight elevation of 365 m, a total of 45 minutes spent on flying, the RMSEs of XY and Z (in checking dataset) are 1.6 and 8.4 cm, respectively, indicating the success of field work. For the case of Long Son quarry, as the smallest area of 12 hectares, only one flight mission was carried out to capture images. The accuracy of its DSM is high, and RMSE in checking dataset is 5.3 cm and 2.6 cm for vertical and horizontal, respectively. The lowest accuracy was seen in the DSM of Nui Nho quarry, RMSE in checking dataset is 10.3 cm and 13.4 cm for vertical and horizontal. From the above analysis, the UAV technology shows its efficiency in mapping small sized open-pit mines.

Conclusions

In this research, an assessment of potential application of low cost UAVs for producing DSM and topographic plans at small and medium sized mine areas with four case studies at Luong Son, Long Son, Nui Nho, and Nui Dai quarries, in Vietnam. Accordingly, a lightweight and small DJI Phantom 4 Professional equipped by the nonmetric RGB Sony EXMOR camera was used. For calibration of the camera and accuracy assessment of DSMs, GCPs were established and determined XYZ coordination (VN2000/UTM Zone 48 N) using a GNSS/RTK CHC X20 with the horizontal accuracy of 5 mm + 1 ppm and the vertical accuracy of 10 mm + 2 ppm.

In order to guarantee the accuracy of DSMs, the safety of UAV flying, and the efficiency of surveying working simultaneously, the flight height for missions was set to from 150 to 250 m with taking terrain conditions into account.

The result showed that the DSM model of Luong Son, the most complicated terrain quarry, has high accuracy though the flight elevation was set to 331 m; the high success-rate of fit was confirmed through RMSEs in the calibrating dataset, 2.6 cm and 3.5 cm for vertical and horizontal, respectively, whereas RMSE in the checking dataset is 4.6 cm and 2.1 cm for vertical and horizontal, indicating high accuracy.

These indicate that the processes of capturing images, establishment of GCPs, and photogrammetric processing were carried out successfully. In addition, in this study, the low-cost rotary-wing drone can be used to survey a small scale and complex terrain quarry quickly. Also, it can be operated by a small number of surveyors, about two people. Therefore, it is considered that this small drone can replace or supplement existing surveying equipment and can be practically used at quarries.

Acknowledgements

Paper was presented during the 5th POL – VIET International Conference Scientific-Research Cooperation between Vietnam and Poland, 08-10.07.2019, AGH UST, Krakow,

Poland. And this research was supported by the Research Center for Mining Electro-Mechanics of Hanoi University of Mining and Geology.

1. References

1. Tran, X.H. and A.T. Nguyen. *Innovation, Modernization, exploitation, screening, production in order to achieve the sustainable development of Coal and Minerals Industry*. in *Vietnam National Mining Science and Technology Congress*. 2011. Nha Trang, Vietnam.

2. Lee Sungjae and C. Yosoon, *opographic survey at small-scale open-pit mines using a popular rotary-wing unmanned aerial vehicle (drone).* Tunnel & Underground Space, 2015. **25**.

3. Tien Bui, D., et al. *Lightweight Unmanned Aerial Vehicle and Structure-from-Motion Photogrammetry for Generating Digital Surface Model for Open-Pit Coal Mine Area and Its Accuracy Assessment*. 2018. Cham: Springer International Publishing.

4. Jonathan L. Carrivick, Mark W. Smith, and D.J. Quincey, *Structure from Motion in the Geosciences*. 2016: Wiley.

5. Siebert, S. and J. Teizer, *Mobile 3D mapping for surveying earthwork projects using an Unmanned Aerial Vehicle (UAV) system.* Automation in Construction, 2014. **41**: p. 1-14.

6. Cryderman, C., S.B. Mah, and A. Shufletoski, *Evaluation of UAV Photogrammetric Accuracy for Mapping and Earthworks Computations.* GEOMATICA, 2014. **68**(4): p. 309-317.

7. Clapuyt, F., V. Vanacker, and K. Van Oost, *Reproducibility of UAV-based earth topography reconstructions based on Structure-from-Motion algorithms.* Geomorphology, 2016. **260**: p. 4-15.

8. Park, M.H., S.G. Kim, and S.Y. Choi, *The study about building method of geospatial informations at construction sites by unmanned aircraft system (UAS).* Journal of the Korean Cadastre Information, 2013. **15**(1): p. 145-156.

9. Birk, A., et al.

10. Niethammer, U., et al., *UAV-based remote sensing of the Super-Sauze landslide: Evaluation and results.* Engineering Geology, 2012. **128**: p. 2-11.

11. Zarco-Tejada, P.J., et al., *Tree height quantification using very high resolution imagery acquired from an unmanned aerial vehicle (UAV) and automatic 3D photo-reconstruction methods.* European Journal of Agronomy, 2014. **55**(C): p. 89-99.

12. ICAO, *Unmanned Aircraft Systems (UAS)*, I.C.A. Organization, Editor. 2011: ICAO: Montreal, QC, Canada.

13. ICAO, *Manual on Remotely Piloted Aircraft Systems (RPAS)*, I.C.A. Organization, Editor. 2015: ICAO: Montreal, QC, Canada.

14. Stöcker, E.C., et al., *Review of the current state of UAV regulations.* Remote sensing, 2017. **9**(5): p. urn:issn:2072-4292.

15. Ajayi, O.G., et al., *Generation of accurate digital elevation models from UAV acquired low percentage overlapping images.* International Journal of Remote Sensing, 2017. **38**(8-10): p. 3113-3134.

16. DJI, *Phantom 4 Pro Visionary intelligence and elevated imagination, https://www.dji.com/phantom-4-pro.* 2017.

17. Agüera-Vega, F., F. Carvajal-Ramírez, and P. Martínez-Carricondo, *Accuracy of Digital Surface Models and Orthophotos Derived from Unmanned Aerial Vehicle Photogrammetry.* Journal of Surveying Engineering, 2016: p. 04016025.

Dr Paweł ĆWIĄKAŁA AGH

Prof. Hana Stankowa VSB Ostrava

Miscellaneous

Application of uncertainty analysis based on Monte Carlo (MC) simulation for life cycle inventory (LCI)

Dariusz Sala[1,*], Bogusław Bieda[1]

[1]AGH University of Science and Technology, Faculty of Management, Krakow, Poland

Abstract. You The use of Monte Carlo (MC) simulation was presented in order to assess uncertainty in life cycle inventory (LCI) studies. The MC method is finded as an important tool in environmental science and can be considered the most effective quantification approach for uncertainties. Uncertainty of data can be expressed through a definition of probability distribution of that data (e.g. through standard deviation or variance). The presented case in this study is based on the example of the emission of SO2, generated during energy production in Integrated Steel Power Plant (ISPP) in Kraków, Poland. MC simulation using software Crystal Ball® (CB), software, associated with Microsoft® Excel, was used for the uncertainties analysis. The MC approach for assessing parameter uncertainty is described. Analysed parameter (SO2,) performed in MC simulation were assigned with log-normal distribution. Finally, the results obtained using MC simulation, after 10,000 runs, more reliable than the deterministic approach, is presented in form of the frequency charts and summary statistics. Thanks to uncertainty analysis, a final result is obtained in the form of value range. The results of this study will encourage other researchers to consider this approach in their projects, and the results of this study will encourage other LCA researchers to consider the uncertainty in their projects and bring closer to industrial application.

1 Introduction

1.1 Uncertainty analysis of LCI

By definition, statistic and uncertainty are inexorably linked [1]. Definition of uncertainty given by Huijbregts [2] is the following: "Uncertainty is defined as incomplete or imprecise knowledge, which can arise from uncertainty in the data regarding the system, the choice of models used to calculate emissions and the choice of scenarions with which to define system boundaries, respectively", and uncertainty defined by Walker et al. [3] as „any deviation from the unachievable ideal of completely deterministic knowledge of the relevant system" was quoted in . According to [4] uncertainty analysis is another important issue in LCA, as average data is usually used without considering the associated variability, and the results can be misleading when comparing systems [4]. Deterministic approaches and the description of processes in the studies of ecological life cycle assessment do not properly reflect the reality [5]. The analysis of uncertainty, a pervasive topic in LCA studies

* Corresponding author: Dsala@zarz.agh.edu.pl

[6], has been a subject for more than 10 years, and many LCA software tools (e.g. SimaPro, GaBi) facilitate uncertainty propagation by means of sampling methods, most often used Monte Carlo (MC) simulation [7,8,4]. Following the categorization of the US-EPA, quoted in [9], tree types of uncertainty can be distinguished: parameter uncertainty, model uncertainty, and scenario uncertainty. Also in this work [9] has been presented the main sources of uncertainty (e.g. data inaccuracy and gaps, unrepresentative data, model uncertainty, estimation of uncertainty). Detailed description of the combination of sources of uncertainty (parameter, model and scenario uncertainties) and combination of source of uncertainty and methods to address them (deterministic, probabilistic, possibilistic, and simple methods) is discussed in the [10].

2. Monte Carlo Simulation

2.1 Parametr uncertainty – Data quality

One of the difficulties encountered in constructing a representative LCA is data availability [11]. The quality of the data collected in the inventory is crucial to the outcome of the LCA [12]. McCarthy [13] quoted many excellent texts on probability and probability distributions used for uncertainty modelling. Analysis of this literature [e.g. 7, 8, 14] indicated that majority of the data in environmental as well as ecological estimations and in the description of chemical parameters have most often a log-normal followed by normal or uniform shapes to use.

Parametr uncertainty of an LCA study is discussed in several studies [e.g. 8, 15, 16]. In this study uncertainty analysis at the LCI level is conducted using Oracle Crystal Ball® (CB) associated with Excel spreadsheet models for performing MC simulation. The CB software helps analyse the risks and uncertainties associated with Microsoft Excel spreadsheet models. LCI data were defined as probability distributions instead of deterministic values.

The MC approach for assessing parameter uncertainty involves the following steps [17]:

1/ select a distribution to describe possible values of each parameter;

2/ specify properties of each parameters;

3/ generate data from the distribution;

4/ use the generated data as possible values of the parameter in the model to produce output.

In fact, data uncertainty is often mentioned as a crucial limitation for a clear interpretation of LCA results. However, uncertainty analysis is not commonly performed in LCAs [2, 9, 18], although great efforts have been made on classification, definition, and sources of uncertainty as well as methodological aspects for expressing uncertainty [19].

The knowledge of geometric mean, μ_g, and geometric standard deviation, σ_g, of probability distributions of input data, may prove useful during the process of defining the confidence intervals. Effective formula for the multiplicative confidence interval is provided in the work of other researchers [e.g. 7, 14], and take the following form:

$$[\mu_g / \sigma_g, \mu_g * \sigma_g] \text{ for confidence interval of 68\%} \quad (1)$$

where:

μ_g – mean geometric value

σ_g – standard geometric deviation.

Detailed classification of methods for uncertainty characterization, uncertainty analysis, and sensitivity analysis, according to the amount of information they provide, their availability in LCA software, etc. is presented and discussed in [20]. Types of random variables in uncertainty analysis in LCA studies is

2.2 Case study

Thecas study used the MCsimulation approach is illustrated below, based on the example of the emission of SO_2, generated during energy production in in Integrated Steel Power Plant (ISPP) in Kraków, Poland, based on the data obtained in 2005. By approximating the SO_2 emissions with log-normal distribution, with a range of zero to infinity and its parameters set to the levels shown in Fig. 1, where the mean value corresponds to an annual deterministic SO_2 emission level amounting to 916.64 Mg. Simulation, with geometric standard deviation, σ_g =1.5, for the emission of SO_2, is suggested in literature (Sonneman et al., 2004).

The results of the MC simulation, with a 10 000-step randomisation cycle, are shown in Fig. 2, and in the form of statistical reports in Fig. 3 and 4.

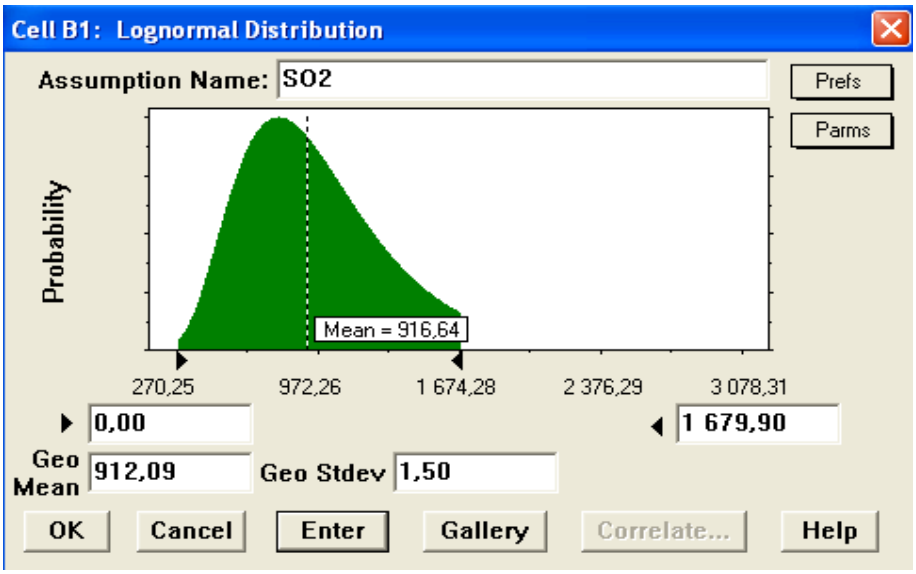

Fig. 1. Parameters of log-normal distribution approximating SO_2 emissions.

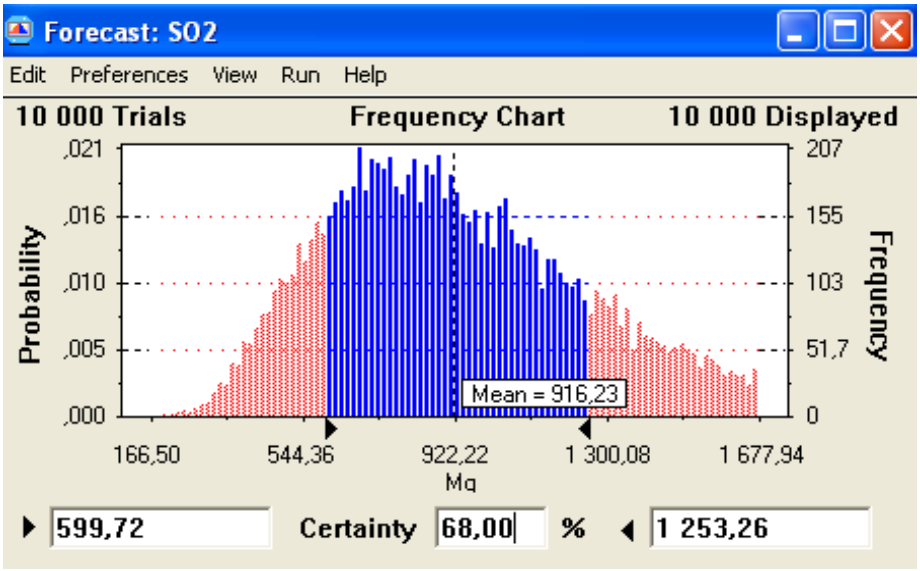

Fig. 2. Frequency chart of the SO_2 emissions forecast, with 68% confidence interval

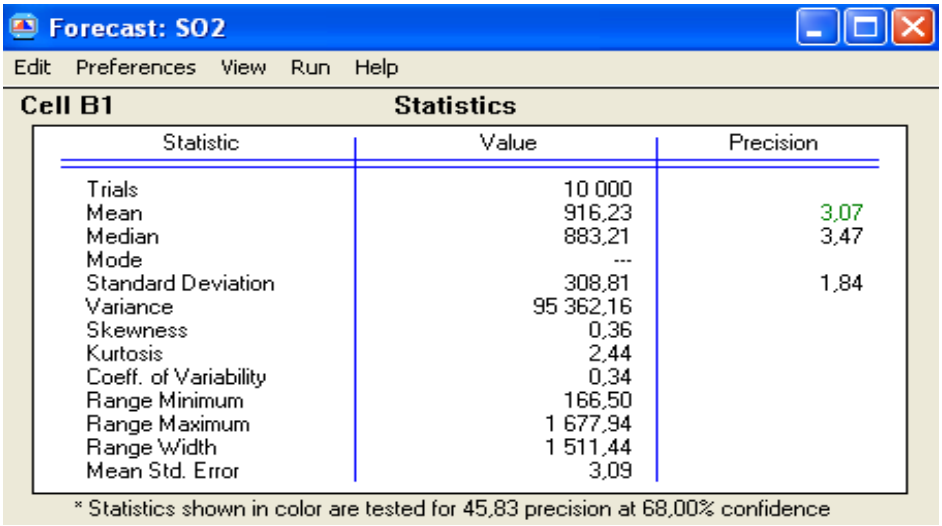

Fig. 3. SO_2 emissions report – Statistics

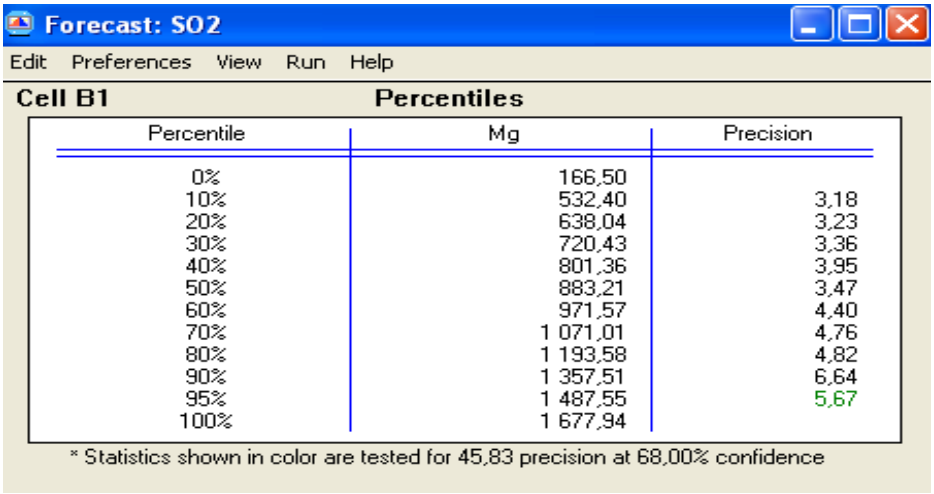

Fig. 4.. SO_2 emissions report – Percentiles

The intervals corresponding to the 68% confidence level, calculated with the help of suggested geometric standard deviation, σ_g =1.5, for the emission of SO_2 is equal to: [599.72; 1253.26]

Conclusion

Thanks to uncertainty analysis, a final result is obtained in the form of value range. As a result, the results in this study based on the real data and obtained using MC simulation are more reliable than the deterministic approach and has the advantage that no normality is presumed**.**

Acknowledgements

Paper was presented during the 5th POL – VIET International Conference Scientific-Research Cooperation between Vietnam and Poland, 08-10.07.2019, AGH UST, Krakow, Poland.

This publication and research was funded from subvention for the maintenance and development ofresearch potential granted to AGH University of Science and Technology, Management Department, Kraków, Poland.

References

Online references will be linked to their original source, only if possible. To enable this linking extra care should be taken when preparing reference lists.

References should be cited in the text by placing sequential numbers in brackets (for example, [1], [2, 5, 7], [8-10]).

1. E.P. Smith, K. Ye. *A statistical , of uncertainty*.(Society of Environmental Toxicology and Chemistry/SETAC, Pellston, Michigan, Pensacola, FL, 1998)
2. M.A.J. Huijbregts. Int. J. Life Cycle Assess. **3**, 5, (1998)
3. W.E. Walker, P. Harremoës, J. Rotmans, J.P. van der Sluijs, M.B.A. van Asselt, P. Janssen, M.P. Krayer von Krauss. Integr. Assess. **4**, 1 (2003)
4. N. Escobar, J. Ribal, G. Clemente, N. Sanjuán. J. Clean. Prod. **79** (2014)

5. Canarache, C. Simota, C. *Databases and Simulation Modelling in Compaction and Erosion Studies.* (Sustainable Land Management-Environmental Protection, A soil Physical Approach, Advances in Geoecology 35. Catena Verlag GmbH, Reiskirchen, Germany, 2002)
6. R. Heijungs, M. Lenzen, M. Int. J. Life Cycle Assess. **19** 2014)
7. G. Sonnemann, F. Castells, M. Schumache. *Integrated Life-Cycle And Risk Assessment For Industrial Processes*.(Lewis Publishers Boca Raton, London, New York, Washington, DC, 2004)
8. B. Bieda. *Stochastic Analysis in Production Process and Ecology under Uncertainty*. (Springer-Verlag, Heidelberg Berlin, 2012)
9. A.E. Bjorklund. Int. J. Life Cycle Assess.**7** (2002)
10. C. Scope, P. Ilg, S. Muench, E.J. Guenthe. Int. J. Life Cycle Assess. **21** (2016)
11. B. Sprecher, Y. Xiao, A. Walton, J. Speight, R. Harris, R. Kleijn, G. Visser, G.J. Kramer. Environ. Sci. Technol. **48**, 7 (2014)
12. M.Z. Hauschild, M.A. Barlaz.A., 2011. *LCA in Waste Management Introduction to Principle and Method*. (Solid Waste Technology & Management. Chapter 3.1. 1st edn. vol 1. Wiley, Chichester, 2011)
13. M.A. McCarthy. *Bayesian Methods. for Ecology*. (Cambridge University Press, 2007)
14. J.V. Spadaro, A. Rabl. Environ. Impact Asses. **28** (2008)
15. Ciroth, M. Srocka. Int. J. Life Cycle Assess. **13,** 3 (2008)
16. Grant, R. Ries, C. Thompson. Int. J. Life Cycle Assess. **21**, (2016)
17. W.J. Warren-Hicks, D.R. Moore. *Uncertainty analysis in ecological risk assessment.* (Society of Environmental Toxicology and Chemistry/SETAC, Pellston, Michigan, Pensacola, FL, 1998)
18. S. Ross, D. Evans, W. Webber. Int. J. Life Cycle Assess. **7** (2002)
19. M. Guo, R.J. Murphy. Sci. Total Environ. 435-436 (2012)
20. E. Igos, E. Benetto, R. Meyer, P. Baustert, B. Othoniel. Int J Life Cycle Assess. **4** (2018)

ISBN: 978-83-943772-4-3